NONLINEAR EFFECTS IN INTERFACIAL FRACTURE

Thesis by

Philippe H. Geubelle

In Partial Fulfillment of the Requirements

for the Degree of

Doctor of Philosophy

California Institute of Technology

Pasadena, California

1993

(Submitted March 4, 1993)

A mes parents, pour la patience qu'ils ont manifestée et les encouragements qu'ils m'ont prodigués au cours de près d'un quart de siècle d'apprentissage.

Acknowledgments.

As the time has come for me to summarize the work performed through these years of graduate school, I would like to express my thanks to all the people who have made it possible. First of all, I would like to acknowledge my advisor Professor W.G. Knauss for his constant supervision and precious guidance throughout my Ph.D. thesis. I also would like to thank Professor J.K. Knowles, not only for some useful discussions regarding the analytical part of the dissertation, but also for arousing in me through his lectures the enthusiasm and the rigor indispensable in the asymptotic investigation presented hereafter. I am also grateful to Professor G. Ravichandran for sharing some of his "numerical expertise" in the computational aspects of this work. My thanks also go to the other members of my thesis committee, Professors T. Christman and J. Hall, for taking the time to review the dissertation.

I would like to acknowledge repeated discussions with Dr. C.T. Liu, technical director of the AFOSR program F04611-88-K-0024 which supported the present work. Additional support was provided by ONR (grant N00014-91-J-1427) under the supervision of Dr. P. Schmidt. The computational part of the dissertation has been performed on the Cray-YMP of the San Diego Supercomputing Center, the access of which has been made possible through a grant by the NSF to the Galcit Solid Mechanics Group.

Finally, I am most appreciative of all the students of the Caltech Aeronautics Department with whom I had the chance to work during these past few years, and especially of my roommate John Lambros : the numerous technical and non-technical conversations we have had have helped me greatly throughout my years here.

Abstract.

The issue of the non-coplanar quasi-static propagation of a crack in homogeneous and bimaterial sheets is investigated. Through a preliminary linear analysis, it is shown that the interface crack kinking problem is confronted, in most practical cases, with difficulties which do not arise in the homogeneous situation : the crack path as predicted by the maximum energy release rate criterion cannot be determined uniquely and an additional length parameter, absent in the homogeneous case, needs to be specified to assure uniqueness. Following that development, the assumption of small deformations is relinquished and it is shown how the size of the nonlinear zone imparts possibly the physical significance of the additional length parameter. The analysis is performed numerically in the homogeneous and bimaterial cases within the framework of the nonlinearly elastic theory of plane stress and using a "boundary-layer" approach. Material and geometrical nonlinearities are combined through the use of the Generalized Neo-Hookean (GNH) model. As the length of the crack extension becomes comparable to the size of the nonlinear zone, a transition is observed between the value of the energetically most favorable kink angle predicted by the linear theory and a unique "nonlinear" value which is found to be independent of the crack extension length and the far-field loading conditions.

The results of the crack propagation analysis are related to those of a detailed asymptotic analysis of the structure of the near-tip stress and deformation fields for the GNH class of hyperelastic materials. The investigation addresses a) the symmetric (mode I) and non-symmetric (mixed-mode) homogeneous situations, b) the rigid substrate case and c) the general bimaterial problem which allows for an arbitrary choice, on both sides of the interface, of the three material parameters characterizing the

GNH model. The asymptotic analysis allows to quantify the effect of the "hardening" characteristics on the blunting of the crack and the associated stress and strain singularities, and shows that the near-tip fields corresponding to a general non-symmetric loading are, in the homogeneous situation, related to those of the symmetric (mode I) case through a rotation which depends on the material characteristics and the far-field loading conditions. A somewhat similar property is obtained in the bimaterial problem, where the existence of a non-oscillatory and "contact-free" solution is confirmed for all material combinations.

Table of contents.

Finite strains at the tip of a crack in a sheet of hyperelastic material : I. Homogeneous case.

Introductory remark.

This doctoral dissertation is organized in five complementary papers, each containing its own abstract, introduction and conclusion. The first chapter is concerned with the preliminary analysis of the interfacial crack propagation problem. The inconsistencies inherent in the linearized analysis presented there motivated the investigation of the nonlinear effects in interface fracture discussed throughout the thesis. The second chapter summarizes the results of the nonlinear analysis of the non-coplanar crack propagation problem in homogeneous and bimaterial sheets of Generalized Neo-Hookean material. It is shown there by using the finite element method that the size of the large deformation (or nonlinear) zone constitutes a restriction in the limiting process associated with the concept of "infinitesimal crack extension" suggested by the energy release rate criterion, commonly used in crack path prediction analyses. The results of the nonlinear crack propagation study are explained by those of an asymptotic analysis of the structure of the strain and stress fields in the vicinity of a crack in Generalized Neo-Hookean sheets.

The asymptotic results, which are consistent with the finite strain theory of plane stress, are summarized in the last three chapters. The homogeneous situation is discussed in chapter 3 for the symmetric (mode I) and non-symmetric (mixed-mode) cases. The next chapter describes two special bimaterial situations : in the first one, the two components of the bimaterial specimen have the same "hardening" characteristics while the second problem deals with the rigid substrate case. These preliminary steps yield somewhat simpler solutions which allow an easier understanding of the structure of the near-tip fields. Also presented in the forth paper is a numerical investigation of the transition process between the two aforementioned interface fracture problems. Finally, the general bimaterial situation, in which the material parameters characterizing

the two Generalized Neo-Hookean sheets are chosen arbitrarily, is presented in the fifth chapter.

Crack propagation at and near bimaterial interfaces : linear analysis[1].

Abstract.

The problem of the growth of a crack located at the interface between two linearly elastic solids is considered when conditions promoting propagation along and/or away from the interface prevail. Both a stress and a maximum energy release rate criterion are examined. It is found that in contrast to the corresponding problem for crack growth in homogeneous solids no unique propagation direction results when continuum considerations alone prevail. Uniqueness is established only upon invoking a presumably material dictated minimum crack extension size. The result for this linearized analysis are compared with experimental observations on kink fracture involving two elastomers with small strain capabilities.

1.- Introduction.

Although long standing problems of adhesion mechanics have required consideration of failure and fracture at and near interfaces, it was only the advent of composite materials and the improved understanding of fracture in non-monolithic solids which motivated a widespread interest in interfacial fracture studies. In addition, the need to better understand the failure characteristics of layered systems such as epitaxial layers of semiconductors in the electronics industry and electronic packaging in general require the same technology base for failure prediction and prevention. The

[1] This is the written version of an identically titled presentation given in March of 1991 at a symposium at the California Institute of Technology in honor of J.K. Knowles's 60th birthday.

early, geology-prompted discovery by Williams (1959) of the general differences between the stress field at the tip of a crack in a homogeneous, linearly elastic solid and that at an interface between two elastic solids established the oscillatory character of the stress field. Although this local crack tip stress field has been confirmed repeatedly in the sequel (Rice and Sih (1965), England (1965), Erdogan (1965)), the physical reason for this behavior or its non-physical aspects of material interpenetration along the crack plane have not been explained satisfactorily to this day. Various ways have been proposed to resolve this problem : some have eliminated the oscillatory term by postulating a frictionless contact zone (Comninou (1977a, 1977b), Gautesen and Dundurs (1987, 1988)), by relinquishing the hypotheses of infinitesimal deformations (Knowles and Sternberg (1983), Ravichandran and Knauss (1989), Herrmann (1989)) or by introducing a transition layer (Yang and Shih (1990)). Others (Shih and Asaro (1988, 1989), Shih (1991)) have used a plasticity model to compute the detailed stress and deformation fields at the crack tip : the mere addition of nonlinear material response apparently did not eliminate the inconsistency although the region in which the oscillations occurred was now reduced still more, below physically acceptable (atomic) dimensions. But the more widely used approach to deal with this problem for some engineering applications is the concept of small-scale contact (Rice, 1988) which essentially ignores its presence on the basis of its usually very small size.

The linearly elastic bimaterial asymptotic solution has other features which distinguish it from its homogeneous counterpart, most of which have been outlined by Rice (1988). Among these is the lack of self-similarity of the singular crack tip expansion field. As illustrated by Symington (1987), the bimaterial situation leads to "rotational stress and deformation fields" at the crack tip, which not only result in the stress and displacement oscillations extremely close to the crack tip, but also extend to a region far outside of the contact zone.

In the past, we have favored the viewpoint that the small zone of mechanical inconsistency may be simply ignored on the basis of the small physical extent and that the major role of the special stress field for interfacial cracks is characterized by the general mixity of stress intensity. We feel now that this is not strictly admissible as an approximation unless one provides also a suitable reasoning to do so, especially when such an "approximation" leads to inconsistency in terms of what is accepted as normal in the fracture of homogeneous bodies. The implication of this statement will become clear below.

It is the purpose of this paper to outline the effect of the stress field rotation at the crack tip on criteria to determine the orientation of crack propagation when the latter moves along or kinks away from the interface, thus amplifying on the results of He and Hutchinson (1989). We show below that, in contrast to the case of fracture in a homogeneous body, the determination of kink direction from an interface cannot be accomplished uniquely without also specifying a fixed crack extension length, in agreement with the results of Mukai *et al.* (1990) who studied the effect of the kink length in the centered interfacial crack case. In the absence of such a length specification -such as is the case in the homogeneous fracture case- the criteria of maximum circumferential stress (Erdogan and Sih (1963)) or the maximum energy release rate criterion (Palaniswamy and Knauss (1978), Wu (1978)) cannot yield unique values for the kink angle.

The work is carried out numerically when closed form analytical methods are too difficult. We make use of the available analytical results to certify the requisite numerical precision. In the next section, we provide a brief description of the Erdogan-Sih criterion and then deal in section 3 with the energy release rate for the interface crack, followed in section 4 by a condensed comparison of the results with some experimental data for this problem.

But before proceeding to further developments we summarize first the concepts and major notational conventions for later use. Following established notation, we use Dundurs' mismatch parameters (Dundurs (1969)) defined as

$$\alpha = \frac{\mu_1(\kappa_2+1)-\mu_2(\kappa_1+1)}{\mu_1(\kappa_2+1)+\mu_2(\kappa_1+1)} = \frac{E_1^{'}-E_2^{'}}{E_1^{'}+E_2^{'}}, \qquad \beta = \frac{\mu_1(\kappa_2-1)-\mu_2(\kappa_1-1)}{\mu_1(\kappa_2+1)+\mu_2(\kappa_1+1)}, \tag{1.1}$$

where subscripts *1* and *2* refer to the materials above and below the interface respectively (see figure 3)[2], E_ρ, ν_ρ and μ_ρ are Young's modulus, Poisson's ratio and shear modulus of material ρ respectively, $E^{'} = E$ in plane stress and $E/(1-\nu^2)$ in plane strain, $\kappa = (3-\nu)/(1+\nu)$ in plane stress and $3-4\nu$ in plane strain.

The full field expansion of the stresses at the tip of the interface crack as in Sun and Jih (1987) yields ahead of the crack tip (along the interface)

$$\sigma_{22} + i\sigma_{12}\big|_{\theta=0} = \frac{K_1 + iK_2}{\sqrt{2\pi r}}(r/l)^{i\varepsilon}, \tag{1.2}$$

where K_α are the stress intensity factors, l is a characteristic length of the problem (e.g., the crack length) and $\varepsilon = \frac{1}{2\pi} ln[(1-\beta)/(1+\beta)]$ which is referred to as the oscillatory parameter.

2.- The maximum opening stress criterion.

The problem of crack path prediction in a homogeneous linearly elastic solid has been extensively studied and its results are widely accepted. Several criteria have been introduced to relate the local loading conditions (characterized by the homogeneous stress intensity factors K_I and K_{II}) to the value of the crack kink angle; the primary criteria among these are most readily understood in terms of physical phenomenology,

---

[2] Greek indices take the values *1* and *2*. Summation on repeated indices is implied.

namely the maximum opening stress criterion (Erdogan and Sih (1963)) and the maximum energy release rate criterion (Palaniswamy and Knauss (1978), Wu (1978)). Since these criteria provide fairly similar results in the homogeneous case, experimental work has not allowed to clearly distinguish between them, although the energy criterion is physically somewhat more appealing. This similarity in results for the two criteria does not hold for bimaterial interfaces between linearly elastic solids. Furthermore, as it will be shown here later, the two approaches must be used with much caution -if they can be used at all- in most nonhomogeneous cases.

In this section, we examine first the case of the maximum opening stress criterion. The basic postulate behind this criterion is that the crack will propagate in that radial direction along which the opening (or circumferential) stress $\sigma_{\theta\theta}$ is maximized. It can thus be simply expressed as follows :

$$\lim_{r\to 0}\frac{\partial\sigma_{\theta\theta}}{\partial\theta}\bigg|_{\theta=\omega} = 0 \quad \text{and} \quad \lim_{r\to 0}\frac{\partial^2\sigma_{\theta\theta}}{\partial\theta^2}\bigg|_{\theta=\omega} < 0, \qquad (-\pi < \omega < \pi). \tag{2.1}$$

As mentioned in the introduction, the linearly elastic asymptotic stress field has a rotating character in those bimaterial cases where $\varepsilon \neq 0$; for the circumferential stress $\sigma_{\theta\theta}$, this character is illustrated in figure 1. Recall that for the homogeneous problem the value of $\sigma_{\theta\theta}\sqrt{r/l}$ (for $r/l \to 0$) is independent of the radius (i.e., all the curves in fig.1 are superposed). It is clear then that, in the present case, the value of the potential kink angle as determined by the stress criterion depends on the radius of the circle along which the "opening stress" is computed. This relationship between the local loading conditions (characterized by $\gamma = tan^{-1}(K_2/K_1)$) and the corresponding kink angle ω is given by the following implicit relation, which is illustrated in figure 2

$$tan(\gamma - \varepsilon ln\frac{r}{l}) = \frac{A(\omega;\varepsilon)}{B(\omega;\varepsilon)}, \tag{2.2}$$

where

$$A(\omega;\varepsilon) = \varepsilon\cosh(\pi-\omega)\cos\frac{3\omega}{2} + \frac{3}{2}\sinh\varepsilon(\pi-\omega)\sin\frac{3\omega}{2}$$
$$+ e^{\varepsilon(\omega-\pi)}\sin\frac{\omega}{2}\cos\frac{\omega}{2}\left(\frac{3}{2}\cos\frac{\omega}{2} - 2\varepsilon\sin\frac{\omega}{2} + 2\varepsilon^2\cos\frac{\omega}{2}\right),$$
$$B(\omega;\varepsilon) = \varepsilon\sinh(\pi-\omega)\sin\frac{3\omega}{2} - \frac{3}{2}\cosh\varepsilon(\pi-\omega)\cos\frac{3\omega}{2} \qquad (2.3)$$
$$- e^{\varepsilon(\omega-\pi)}\sin\frac{\omega}{2}\cos\frac{\omega}{2}\left(\frac{3}{2}\sin\frac{\omega}{2} + 2\varepsilon\cos\frac{\omega}{2} + 2\varepsilon^2\sin\frac{\omega}{2}\right).$$

This solution is valid for $0 < \omega < \pi$; π has to be replaced by $-\pi$ for $-\pi < \omega < 0$.

We note first that the curve for $\varepsilon = 0$ corresponds to that obtained for the corresponding homogeneous fracture problem. The radial dependence of the kink angle ω appears then through a shift $\varepsilon ln(r/l)$ of the corresponding "master curve" described in figure 2. It would therefore appear that, in contrast to fracture in homogeneous solids, the maximum opening stress criterion does not produce a unique kink angle in the bimaterial case, unless an additional characteristic length is introduced; this length scale might be considered as a material parameter and would correspond to the value of the shift to be applied. We emphasize, however, that such a length scale is not an integral part of the fracture or kinking model, but constitutes a kind of "retrofit" to the linearized theory.

3.- The maximum energy release rate criterion.

The application of the maximum energy release rate criterion to the bimaterial case will be discussed in terms of analytical and numerical methods. We start with a brief review of the analytical results available to date.

Analytical results.

The maximum energy release rate criterion is based on the postulate that the crack will propagate along that path which maximizes the release of energy. If $G(\omega)$ is the energy release rate defined as the variation of potential energy Π corresponding to a virtual crack advance Δl in the direction ω, i.e.,

$$G = -\lim_{\Delta l \to 0} \frac{\Delta \Pi}{\Delta l}, \tag{3.1}$$

then this value is maximized for a kink angle ω^* satisfying the relations

$$\left.\frac{\partial G}{\partial \omega}\right|_{\omega=\omega^*} = 0 \quad \text{and} \quad \left.\frac{\partial^2 G}{\partial \omega^2}\right|_{\omega=\omega^*} < 0, \qquad (-\pi < \omega^* < \pi). \tag{3.2}$$

The application of this criterion to the interfacial problem has been first documented by He and Hutchinson (1989) who used a method based on the superposition of dislocations which has been proven successful in the homogeneous case (Hayashi and Nemat-Nasser (1981)). Through an integral representation of the crack extension and a dimensional analysis, they were able to relate the local loading conditions at the tip of the extended crack to the stress intensity factors describing the asymptotic field at the tip of the semi-infinite interfacial crack prior to the extension. From this numerically obtained complex relationship, they compared the energy release rate of the kinked crack $G(\omega)$ to the variation of energy G_0 corresponding to an extension along the interface, the analytic expression of which has been derived by Malyshev and Salganik (1965) as

$$G_0 = \frac{(c_1 + c_2)(K_1^2 + K_2^2)}{16 \cosh^2 \pi\varepsilon}, \tag{3.3}$$

where the material constants $c_\rho = (\kappa_\rho + 1)/\mu_\rho$ (ρ not summed) and κ_ρ have been defined in section 1.

He and Hutchinson (1989) first considered the case $\beta = \varepsilon = 0$, then studied the effect of a non-zero β. The implicit assumption behind their investigation is that the energy release rate of the kinked crack is independent of the crack extension length Δl, except in a region very close to the crack tip where the strong oscillations and the crack face interpenetration mentioned in the introduction take place. They invoked a weak influence of the second mismatch parameter β which ostensibly only affects in a mild manner the relationship between the energetically most favorable kink angle ω^* and the local loading parameter $\gamma (= tan^{-1}(K_2/K_1))$. Some typical curves they obtained are shown in figure 3.

One notes that, in contrast to the maximum opening stress criterion, the maximum energy release rate criterion predicts that the relation between the kink angle ω^* and the local loading angle γ is not one-to-one : for a certain range of loading conditions, the crack will propagate along the interface, which seems to be more in accord with experimental observations (see section 4). This result could be exploited to experimentally determine the interfacial fracture toughness. If the latter is of the same order as the fracture energies of the two materials, a curve similar to that shown in figure 3 is expected. If the interface is much weaker than either material, the crack will tend to propagate along the interface for a much wider range of load mixity conditions.

In the next section, we use the finite element technique to study the effect of β on the kinking behavior of the interface crack in more detail, using He and Hutchinson's special results to verify the numerical analysis.

Numerical analysis.

The finite element technique has been extensively used in the field of linearly elastic interfacial fracture mechanics, especially in order to relate the local loading

parameters (i.e., the interface stress intensity factors K_1 and K_2) to the remote loading conditions, the geometry and the material properties. In this analysis, the semi-energetic numerical scheme proposed by Matos *et al.* (1989) is used, which combines the values of the nodal crack opening displacements with the values of the J-integral (obtained through the domain-integration technique) to extract the two stress intensity factors. This method, which is relatively easy to implement, was shown in Matos *et al.* (1989) to provide an accuracy comparable to the more complex and fully energy-based methods.

The determination of the angular and radial variation of the energy release rate was carefully investigated in order to analyze the effect on the computed value of $G(\omega;\alpha,\beta,\Delta l)$ of the mesh refinement and distribution, which has been shown by Maiti (1990) to be of prime importance in the homogeneous case, especially when the kink angle is large. Since it was not possible, due to the presence of the interface, to adopt the doubly focussed mesh as suggested by Maiti, we chose the simpler mesh illustrated in figure 4.

The mesh is composed of approximately 2500 four-node bilinear elements concentrically focussed at the tip of the crack, the initial length of which was taken to be unity. The global geometry that was adopted is close to that of the bimaterial specimen used in the experiments (see figure 7). The problem was also solved by using a "boundary-layer" approach in which a circular mesh is constructed around the crack tip and boundary conditions corresponding to a bimaterial K-field are applied along the outer circle. The second approach, which is applicable as long as the crack extension remains a small portion of the outer radius, allows to avoid the numerical error associated with the determination of the stress intensity factors (through the method described above) and to improve the mesh refinement around the crack tip without increasing the number of elements. Both approaches yielded identical results. The

number of nodes and their distribution was slightly varied depending on the length of the extension Δl. The number of released nodes was determined by a preliminary analysis of the homogeneous situation to allow comparison with analytic results. It was ascertained that a minimum number of 5 released nodes is needed to guarantee an acceptable accuracy of the finite element scheme. We therefore selected 6 release nodes, equally spaced along the crack extension.The smallest element size was of the order of a tenth of the crack extension length. The question arises as to whether this type of meshing which suppresses the detail of the oscillation zone has serious consequences on the numerical results. This possible influence of the oscillation zone on the computed value of the energy release rate is examined analytically in the appendix for the special case of interfacial separation. Using the relations developed there, it is possible to show that the maximum contribution of the contact zone (which is of the order of $5 * 10^{-8} l$) to the total energy release rate G is of the order of 2% in the present analysis summarized in figure 6b.

Two independent methods were used to compute the energy release rate : the first corresponds to the "potential energy" definition of G described by equation (3.1) and the second is related to the crack closure work

$$G = \lim_{\Delta l \to 0} \frac{1}{2\,\Delta l} \int_0^{\Delta l} T_\alpha^{(1)} \Delta u_\alpha^{(2)} ds, \tag{3.4}$$

where $T_\alpha^{(1)}$ are the tractions existing along the crack extension prior to its opening and $\Delta u_\alpha^{(2)}$ are the opening displacements across the unloaded extension. Both methods gave almost identical values (within 0.01%) for the energy release rate G.

An idea of the accuracy of the computed value of G may be obtained by comparing the value of $G(\omega = 0) = G_0$ (extension along the interface) with the value of the J-integral. The effect of the crack extension length on the obtained precision is summarized in table 1. As expected, the error on the absolute value of G_0 increases

with decreasing crack extension length due to the imprecision associated with higher crack tip gradients. This problem can be solved by further refining the mesh but such studies showed that an increase in the number of elements can affect the absolute value of G, but does not change the ratio $G(\omega)/G_0$ nor the value of the kink angle corresponding to the maximum energy release rate.

$\frac{\Delta l}{l}$	G_0/J	error
10^{-2}	1.011	1.1%
10^{-3}	1.021	2.1%
10^{-4}	1.042	4.2%

Table 1.- Details on the precision of the computed values of the energy release rate as a function of Δl.

Results and discussion.

A comparison between numerical and analytical results is presented in figure 5 for the case $\alpha = 0.5\ \beta = 0$ and for three different crack extension lengths. The agreement with He and Hutchinson's analytical results is very satisfactory, except in the region near $\omega = 0$, were both analyses show some imprecision due to the flatness of the (G,ω) curve which makes the computation of the maximum relatively difficult. The independence of the energy release rate G, and therefore of the energetically most favorable kink angle ω^*, on the crack extension length Δl is obvious for the special case $\beta = 0$.

The more general case of $\beta \neq 0$ is illustrated in figures 6a and b. In figure 6a, the angular variation of the energy release rate normalized by the value of the applied J-

integral is presented for the loading conditions $\gamma = -45.0°$ and for three values of Δl. Except in the self-similar case of an extension along the interface ($\omega = 0$)[3] , the energy release rate shows a definite dependence on the crack extension length Δl.

The complete relationship between the energetically most favorable kink angle ω^* and the local loading parameter $\gamma$is given in figure 6b. If the individual curves are shifted by $\varepsilon ln(\Delta l/l)$, one obtains a unique "master" curve, also shown in figure 6b, which is compared with He and Hutchinson's analytic solution obtained for the same value of α and β[4] . The difference that is apparent in figure 6b could not be explained by the coarseness of the finite element mesh since a much refined mesh (with close to 4000 elements and up to 15 released nodes) yields identical results[5] to that obtained with the coarser mesh. Thus, as was the case for the stress criterion and unlike for the homogeneous situation, the maximum energy release rate criterion does not provide a unique value of the kink angle in bimaterial cases when $\beta \neq 0$, but again, an additional length scale is necessary to make this criterion unique. This characteristic length Δl^*, which would most likely be considered as a property of the bimaterial combination, would be determined experimentally by computing the horizontal shift of the master curve necessary to fit the experimental (ω^*, γ) curve. Thus, as in section 2, this length parameter is not part of the fracture model, but a retrofit parameter used "to make the linearized analysis work." The physical significance of the characteristic length Δl^* is still unknown at this point : it could, for example, correspond to a flaw size or an indicator of flaw distribution. It is also undetermined whether there is a unique characteristic length for each bimaterial combination or whether each component of the

---

[3] The slight dependence of G_0 on the length of the extension is associated with the numerical imprecision described in table 1.

[4] The error bars are associated with the imprecision of the determination of the maxima in figure 8 of He and Hutchinson (1989).

[5] marked by asterisks in figure 6b.

bimaterial combination has its own Δl^* -though that latter case could lead to non-unique values of the kink angle ω^* for every loading condition γ.

We note that the dependence of the energy release rate G on the crack extension length Δl has been suggested by Mukai *et al.* (1990) who studied the kinking behavior of a bimaterial crack of finite length; they concluded that a crack extension of a length which is at least equal to the (initial) length l of the crack was necessary to make ω^* appear to converge to a unique value. In the present context of small crack extension during the kink process, that configurational change is, however, inappropriate. The effect of Δl on the energy release rate has been acknowledged by Hutchinson in a private communication and in a recent publication by him and Suo (1991).

4.- Information from experiments.

The issue of interfacial crack propagation has also been studied experimentally in our laboratories. Here, some of the experimental results are extracted for comparison with the results of the linear analysis described above. A more complete description of the experimental procedure is given by Bowen and Knauss (1991a).

The fracture specimen, the geometry of which is given in figure 7, is composed of two co-cured sheets of Solithane 113, a polyurethane of small strain capabilities which has also been used previously to study the problem of crack propagation and kinking for the homogeneous case (Palaniswamy and Knauss (1978)). By adjusting the relative proportions of the base polymer and its crosslinking agent, the mechanical properties of the polyurethane are modified : the Young's modulus and Poisson's ratio of the two components used in the experiment, together with the corresponding plane

stress[6] values of the mismatch parameters α, β and ε, are listed in table 2. Excellent bond strength was achieved between the two sheets of Solithane by curing the two compositions almost simultaneously; as shown by Bowen and Knauss (1991b), the interface toughness was comparable to at least the toughness of the weaker of the two components.

	material 1	material 2
composition	Solithane 55/45	Solithane 45/55
$E\,(N/cm^2)$	*319*	*123*
ν	*0.499*	*0.499*
$\alpha = 0.44 \quad \beta = 0.11 \quad \varepsilon = -0.036$		

Table 2.- Material properties of the components used in the experiment and corresponding mismatch parameters. The composition is given in terms of the weight ratio "resin/crosslinking agent"

The effect of the far-field loading conditions on the propagation behavior of the interfacial crack has been examined by rotating the bimaterial fracture specimen with respect to the loading axis. The relation between the far-field loading angle ψ (see figure 7) and the crack tip local loading angle $\gamma\,(= tan^{-1}(K_2/K_1))$ has been obtained numerically using the displacement-based semi-energetic method described in section 3.2 assuming plane stress conditions. It has to be noted that the reference length l used in the definition of K_1, K_2 (and therefore γ) in (1.2) has been chosen as $l = 1\,cm$, which is approximately half of the initial crack length.

The comparison between the experimental and analytical results is presented in figure 8 which shows the variation of the kink angle ω with respect to the local mixity

[6] Due to the near-incompressibility of the polymer, the plane strain values of the mismatch parameters are $\alpha = 0.44$ $\beta \approx \varepsilon \approx 0$.

parameter γ. The solid curve corresponds to the numerical solution (corresponding to $\Delta l/l = 1$) and the dashed curve is the shifted analytical curve "fitted to the experimental points."

The shift was chosen to match the range of loading conditions for which the crack propagates along the interface ($\omega = 0$). The comparison with the experimental results shows good agreement also for negative values of the kink angle (i.e., when the crack propagates into the soft (lower modulus) material) but the agreement is less satisfactory when the crack propagates into the hard (higher modulus) material. The characteristic length Δl^*, determined from the value of the shift ($= \varepsilon \ ln(\Delta l^*/l)$) is approximately *1.1 mm*. As mentioned earlier, the physical significance of this value is not clear at this time. It is however worth pointing out that there are at least two size scales that could be considered relative to this value : one is the plate thickness while the other is a measure of the zone in which deformations are nonlinear. Based on a finite strain analysis which matches Generalized Neo-Hookean material behavior to the mechanical response of the two components (Geubelle and Knauss (1992)), one finds that, in the experiments, the size of the nonlinear zone should be of the order of *0.5 mm* in the softer material and less than *0.1 mm* in the harder one. By comparison, the plate thickness was about *3 mm*. The examination of the effects of large deformations on the propagation behavior of an interface crack is still ongoing and represents a problem that is too large to warrant inclusion in this presentation.

It might be appropriate at this point to discuss which of the plane stress or plane strain assumptions are more adequate to study the problem of crack propagation in the present experimental conditions. We understand that, although the specimen geometry suggests the use of the plane stress assumption, the stress and strain fields at the tip of the interface crack are three-dimensional, with conditions more akin to plane strain prevailing in the immediate vicinity of the crack tip. A three-dimensional numerical

investigation by Nakamura (1991) has analysed the respective extent of the plane stress, plane strain and three-dimensional regions. It was shown there that, while the thickness-averaged value of the energy release rate is very close to the plane stress solution, a plane strain K-field exists within a radius of approximately *0.5* percent of the plate thickness near the midplane, for plates having a thickness to crack length ratio smaller than one. Let K_α^σ and K_α^ε $(\alpha = 1,2)$ represent the components of the plane stress and plane strain stress intensity factors respectively. The relationship between the plane stress phase angle $\gamma^\sigma (= tan^{-1}(K_2^\sigma / K_1^\sigma))$ and the plane strain phase angle $\gamma^\varepsilon (= tan^{-1}(K_2^\varepsilon / K_1^\varepsilon))$ has been recently investigated numerically by Lee and Rosakis (1991). By assuming, as we will do here, the existence of a plane stress asymptotic field throughout the plate at a certain distance from the crack tip, they obtained

$$\gamma^\sigma + \varepsilon^\sigma \ln h/l \approx \gamma^\varepsilon + \varepsilon^\varepsilon \ln h/l, \tag{4.1}$$

where h is the plate thickness, l is the characteristic length used to define the two phase angles (1.2), and ε^σ and ε^ε are the plane stress and plane strain values of the oscillation index. This relation suggests that the "master" (ω^*, γ) curve corresponding to the plane strain values of the mismatch parameters $(\alpha^\varepsilon = 0.44\,\varepsilon^\varepsilon \approx 0)$ has to be shifted by $(\varepsilon^\varepsilon - \varepsilon^\sigma)\ln(h/l)$ $(\approx 2.4^\circ)$ to allow comparison with the experimental results. The shifted "local plane strain" curve is also presented in figure 8. Note also that, if fully plane strain conditions are assumed, no adjustment of the analytical results are possible through shifting $(= \varepsilon^\varepsilon \ln \Delta l/l)$ at all since the oscillation index is then almost zero due to the high incompressibility of the two components. Although it seems likely that the phenomena dictating the propagation behavior of the interfacial crack involve distances that are much smaller than the thickness of the specimen, the agreement between the experimental results and the analytical curve obtained by assuming local plane strain conditions is less satisfactory than for the fully plane stress situation.

5.- Conclusion.

The propagation of a crack along and away from a bimaterial interface has been investigated analytically, using the linear theory of elasticity. Some major differences with the homogeneous situation have been noted : firstly, the maximum opening stress criterion and the maximum energy release rate criterion provide very different results in the bimaterial case, the energy criterion being more in accord with experimental observations; secondly, unlike in the homogeneous situation, the linear analysis of the kinking behavior of an interfacial crack necessitates an additional length parameter corresponding to the initial crack extension to bring the analysis into closer accord with measurements. This parameter, which constitutes a "retrofit to the theory", is not part of the fracture model but should probably be considered to be a property byproduct of the bimaterial combination. However, the experimentally obtained value of the additional length scale for the bimaterial specimen investigated in the present work is found to be orders of magnitude larger than any physically dictated characteristic length.

Acknowledgments.

The authors are indebted to Dr. C.T. Liu, technical monitor on contract F04611-88-K-0024; additional support came from ONR Grant N00014-91-J-1427 under the direction of Dr. P. Schmidt. The computing facilities of the San Diego Supercomputing Center assisted materially in this work. We also wish to acknowledge repeated discussions with Professor J.W. Hutchinson of Harvard University and with Dr. Noel O'Dowd, research fellow at Caltech.

Appendix : A note related to energy release rate computations for kinking interface cracks.

With the growing importance of composite materials and structures, including packaged electronic (chip) devices, the need to better understand and control failure behavior at and near interfaces has taken on also increased engineering significance. In comparison with fracture of homogeneous solids, the (linearly) elastic analysis of "brittle" interfacial fracture problems suffers from complications associated with the appearance of a contact zone very close to the tip of the interface crack and with the "oscillatory" character of the near-tip stress distribution. In contrast to homogeneous solids, this stress and deformation field behavior complicates the fracture analysis of the kinking behavior of an interface crack since it makes the usually so useful quantity of the energy release rate non-unique when the crack kinks away from the interface.

The question arises then as to whether the dependence of the energy release rate G on the length Δl of the (virtual) crack extension is related to the presence of a contact or interpenetration zone adjacent to the tip of the interface crack. The objective of the present note is to somewhat quantify the influence of the small contact zone on the Δl-dependence of the energy release rate. This analysis can, for example, be used in finite element investigations of the interface crack kinking behavior to determine whether the discretization of the crack tip region eliminates sufficient detail so as to introduce a sizable error in the numerical computation of the energy release rate.

At least a partial answer to this question may be provided if one could determine the contribution to the energy release rate that derives from the immediate vicinity of the crack tip relative to that for a larger distance along the crack extension. Thus, if the total advance of the crack is Δl, one would be interested in determining what contribution to

G derives from an arbitrary fraction δ of that length, but located immediately adjacent to the crack tip (figure A.1). We provide an answer to this question in closed form when the crack propagates along the interface. While we recognize that propagation of a crack along an interface yields unique energy release rates, while the kink problem does not, we believe that the present contribution establishes a size scale relation that allows an estimate of the influence of the contact zone on the computed value of G.

The size r_c of the oscillation zone can be expressed as (Rice (1988))

$$\frac{r_c}{l} = exp\left[\frac{1}{\varepsilon}\left(tan^{-1}(2\varepsilon) - \gamma - sign(\varepsilon)\pi\right)\right], \tag{A.1}$$

where $\gamma = tan^{-1}(K_2/K_1)$ and the stress intensity factors K_α are defined by relation (1.2). Assuming that the contact zone represents a fraction $\delta = r_c/\Delta l$ of the crack extension length Δl, it is of interest to know how much of the computed energy release rate corresponds to this fraction of the extension length. In other words, one tries to compute the ratio

$$h(\delta;\varepsilon) = G_\delta/G, \tag{A.2}$$

where G is the total energy release rate corresponding to the extension Δl, and G_δ is the fraction of G corresponding to a fraction $\delta_*\Delta l$ of the crack extension.

A relatively simple analytical expression for $h(\delta;\varepsilon)$ can be derived when the crack extension is along the interface ($\omega = 0^\circ$). In this case, one writes

$$\begin{aligned} G &= \lim_{\Delta l\to 0}\frac{1}{2\Delta l}\int_0^{\Delta l}[\sigma_{\alpha 2}(x_1)\,\Delta u_\alpha(\Delta l - x_1)]dx_1, \\ G_\delta &= \lim_{\Delta l\to 0}\frac{1}{2\Delta l}\int_0^{\delta_*\Delta l}[\sigma_{\alpha 2}(x_1)\,\Delta u_\alpha(\Delta l - x_1)]dx_1, \qquad (0\le\delta\le 1) \end{aligned} \tag{A.3}$$

where Δu_α are the displacement jumps across the crack and $\sigma_{\alpha\beta}$ are the stresses ahead of the crack tip. The analytical expression of G has been derived by Malyshev and Salganik (1965) as

$$G = \frac{\pi c_{12}(1+4\varepsilon^2)}{2\cosh(\pi\varepsilon)}, \tag{A.4}$$

where

$$c_{12} = \frac{(c_1+c_2)(K_1^2+K_2^2)}{8\pi(1+4\varepsilon^2)\cosh(\pi\varepsilon)}, \tag{A.5}$$

with the material constants c_α defined in section 3. Combining the expressions of the stresses along the interface and the displacement jumps behind the crack tip with (A.3b), one obtains

$$G_\delta = \lim_{\Delta l\to 0}\frac{c_{12}}{\Delta l}\left[\int_0^{\Delta l}\sqrt{\frac{\Delta l - x_1}{x_1}}\cos\left(\varepsilon \ln\frac{\Delta l - x_1}{x_1}\right)dx_1 + 2\varepsilon\int_0^{\Delta l}\sqrt{\frac{\Delta l - x_1}{x_1}}\sin\left(\varepsilon \ln\frac{\Delta l - x_1}{x_1}\right)dx_1\right] \tag{A.6}$$

The transformation

$$y = \frac{\Delta l - x_1}{x_1} \tag{A.7}$$

leads to

$$h(\delta;\varepsilon) = \frac{2\cosh(\pi\varepsilon)}{\pi(1+4\varepsilon^2)}\{\Re[I] + 2\varepsilon\Im[I]\}, \tag{A.8}$$

where

$$I = \int_{\frac{1-\delta}{\delta}}^{\infty}\frac{y^{\frac{1}{2}+i\varepsilon}}{(y+1)^2}dy, \tag{A.9}$$

and $\Re[I]$ and $\Im[I]$ denote the real and imaginary parts of I respectively. After integration by parts, (A.9) can be rewritten as

$$I = \delta^{\frac{1}{2}-i\varepsilon}(1-\delta)^{\frac{1}{2}+i\varepsilon} + \left(\frac{1}{2}+i\varepsilon\right) B\left(\frac{1}{2}+i\varepsilon, \frac{1}{2}-i\varepsilon\right) \left\{1 - I_{1-\delta}\left(\frac{1}{2}+i\varepsilon, \frac{1}{2}-i\varepsilon\right)\right\}, \quad \text{(A.10)}$$

where $B(a,b)$ is the Beta function and $I_x(a,b)$ is the incomplete normalized Beta function (Abramowitz and Stegun (1972)) defined as

$$I_x(a,b) = \frac{B_x(a,b)}{B(a,b)}, \quad \text{(A.11)}$$

where

$$B_x(a,b) = \int_0^x t^{a-1}(1-t)^{b-1}dt. \quad \text{(A.12)}$$

Using the properties

$$I_x(a,b) = 1 - I_{1-x}(b,a), \quad \text{(A.13)}$$

$$B\left(\frac{1}{2}+i\varepsilon, \frac{1}{2}-i\varepsilon\right) = \frac{\pi}{\cosh(\pi\varepsilon)}, \quad \text{(A.14)}$$

the final expression of the integral I is obtained as

$$I = \delta^{\frac{1}{2}-i\varepsilon}(1-\delta)^{\frac{1}{2}+i\varepsilon} + \left(\frac{1}{2}+i\varepsilon\right)\frac{\pi}{\cosh(\pi\varepsilon)} I_\delta\left(\frac{1}{2}-i\varepsilon, \frac{1}{2}+i\varepsilon\right). \quad \text{(A.15)}$$

The value of $h(\delta;\varepsilon)$ is then computed by combining (A.8) and the following series representation of I

$$I = \frac{\delta^{\frac{1}{2}-i\varepsilon}(1-\delta)^{\frac{1}{2}+i\varepsilon}}{\frac{1}{2}-i\varepsilon}\left[1 + \frac{1+2i\varepsilon}{3-2i\varepsilon}\sum_{n=1}^{\infty}\rho_n\right], \quad \text{(A.16)}$$

where the coefficients ρ_n of the infinite sum are determined recursively by

$$\begin{cases} \rho_1 = \delta, \\ \rho_n = \dfrac{n\delta}{\left(\frac{1}{2}+n-i\varepsilon\right)}\rho_{n-1}. \end{cases} \quad \text{(A.17)}$$

The δ-variation of $h(\delta;\varepsilon)$ is illustrated in figure A.2 for various values of ε, showing very little effect of the oscillation parameter. Furthermore, the result indicates that the contribution to the value of the total energy release rate over the contact zone is limited to less then *10%* for values of $r_c/\Delta l$ of up to *0.01*.

References.

Abramowitz, M. and Stegun, I.A., 1972, "Handbook of mathematical functions," Dover, New-York.

Bowen, J.M. and Knauss, W.G., 1991a, "An experimental study of interfacial crack kinking," *Galcit SM Report 91-15*, Caltech.

Bowen, J.M. and Knauss, W.G., 1991b, "The characterization of the energy of fracture at and near interfaces between viscoelastic solids," *Galcit SM Report 91-14*, Caltech, submitted to the *Journal of Adhesion.*

Comninou, M., 1977a, "The interface crack," *ASME J. Appl. Mech.*, Vol.44, pp.631-636.

Comninou, M., 1977b, "Interface crack with friction in the contact zone," *ASME J. Appl. Mech.*, Vol.44, pp.780-781.

Dundurs, J., 1969, "Edge-bonded dissimilar orthogonal elastic wedges under normal and shear loading," *ASME J. Appl. Mech.*, Vol.36, pp.650-652.

England, A.H., 1965, "A crack between dissimilar media," *ASME J. Appl. Mech.*, Vol.32, pp.400-402.

Erdogan, F., and Sih, G.E., 1963, "On the crack extension in plates under plane loading and transverse shear," *J. Basic Engng.*, Vol.85, pp.519-527.

Erdogan, F., 1965, "Stress distribution in bonded dissimilar materials with cracks," *ASME J. Appl. Mech.*, Vol.32, pp.403-410.

Gautesen, A.K., and Dundurs, J., 1987, "The interface crack in a tension field," *ASME J. Appl. Mech.*, Vol.54, pp.93-98.

Gautesen, A.K., and Dundurs, J., 1988, "The interface crack under combined loading," *ASME J. Appl. Mech.*, Vol.55, pp.580-586.

Geubelle, P.H. and Knauss, W.G., 1992, "A note on a finite deformation analysis of the nonlinear zone size in the bimaterial fracture experiment," *Galcit SM Report 92-34,* Caltech.

Hayashi, K., and Nemat-Nasser, S., 1981, "Energy release rate and crack kinking under combined loading," *ASME J. Appl. Mech.*, Vol.48, pp.520-524.

He, M.-Y., and Hutchinson, J.W., 1989, "Kinking of a crack out of an interface," *ASME J. Appl. Mech.*, Vol.56, pp.270-278.

Herrmann, J.M., 1989, "An asymptotic analysis of finite deformations near the tip of an interface crack," *J. Elast.*, Vol.21, pp.227-269.

Hutchinson, J.W., and Suo, Z., 1991, "Mixed mode cracking in layered materials," *Advances in Applied Mechanics*, Vol.28, edited by J.W. Hutchinson and T.Y. Wu, Academic Press.

Knowles, J.K., and Sternberg, E., 1983, "Large deformations near a tip of an interface-crack between two Neo-Hookean sheets," *J. Elast.*, Vol.13, pp.257-293.

Lee, Y.-J. and Rosakis, A.J., 1991, "Interfacial cracks in plates : part I. A three-dimensional numerical investigation," to be submitted to *Int. J. Solids Struct.*

Maiti, S.K., 1990, "Finite element computation of the strain energy release rate for kinking of a crack," *Int. J. Fract.*, Vol.43, pp.161-170.

Malyshev, B.M., and Salganik, R.L., 1965, "The strength of adhesive joints using the theory of crack," *Int. J. Fract. Mech.*, Vol.1, pp.114-128.

Matos, P.P.L., McMeeking, R.M., Charalambides, P.G., and Drory, M.D., 1989, "A method for calculating stress intensities in bimaterial fracture," *Int. J. Fract.*, Vol.40, pp.235-254.

Mukai, D.J., Ballarini, R., and Miller, G.R., 1990, "Analysis of branched interface cracks," *ASME J. Appl. Mech.*, Vol.57, pp.887-893.

Nakamura, T., 1991, "Three-dimensional stress field of elastic interface cracks," presented at the 1991 Annual Winter ASME Meeting in Atlanta, to appear in *ASME J. Appl. Mech.*

Palaniswamy, K., and Knauss, W.G., 1978, "On the problem of crack extension in brittle solids under general loading," *Mechanics Today*, Vol.4, edited by S. Nemat-Nasser, Pergamon Press, pp.87-148.

Ravichandran, G., and Knauss, W.G., 1989, "A finite elastostatic analysis of bimaterial interface cracks," *Int. J. Fract.*, Vol.39, pp.235-253.

Rice, J.R., and Sih, G.C., 1965, "Plane problems of cracks in dissimilar media," *ASME J. Appl. Mech.*, Vol.32, pp.418-423.

Rice, J.R., 1988, "Elastic fracture mechanics concepts for interfacial cracks," *ASME J. Appl. Mech.*, Vol.55, pp.98-103.

Shih, C.F., and Asaro, R.J., 1988, "Elastic-plastic analysis of cracks on bimaterial interfaces : part I - small-scale yielding," *ASME J. Appl. Mech.*, Vol.55, pp.299-316.

Shih, C.F., and Asaro, R.J., 1989, "Elastic-plastic analysis of cracks on bimaterial interfaces : part II - structure of small-scale yielding fields," *ASME J. Appl. Mech.*, Vol.56, pp.763-779.

Shih, C.F., 1991, "Cracks on bimaterial interfaces : elasticity and plasticity aspects," *Mat. Sc. Engng.*, Vol.A 143, pp.77-90.

Sun, C.T., and Jih, C.J., 1987, "On strain energy release rates for interfacial cracks in bi-material media," *Engng. Fract. Mech.*, Vol.28 No.1, pp.13-20.

Symington, M.F., 1987, "A review of some aspects of the linear elastic analysis of bimaterial cracks," *Master Thesis*, Division of Engineering, Brown University, Providence.

Williams, M.L., 1959, "The stress around a fault or crack in dissimilar media," *Bull. Seismol. Soc. Am.*, Vol.49, pp.199-204.

Wu, C.H., 1978, "Maximum energy release rate criterion applied to a tension-compression specimen with crack," *J. Elast.*, Vol.8, pp.235-257.

Yang, Y., and Shih, C.F., 1990, "Fracture along an interlayer," *Technical report,* Division of Engineering, Brown University, Providence.

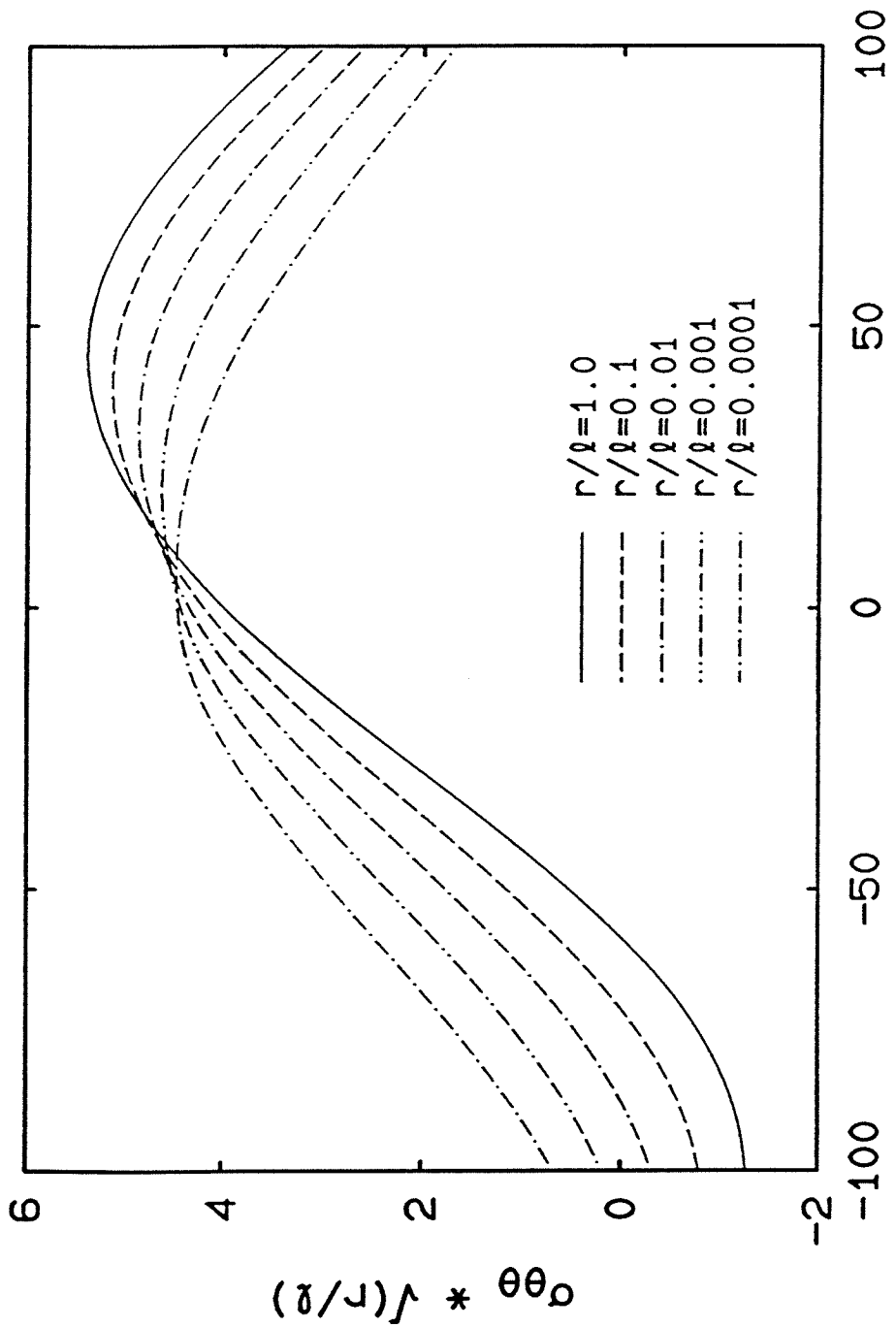

Figure 1. Angular variation of the circumferential stress at various radii about the crack tip ($\varepsilon = -0.05$, $K_1 = 10$, $K_2 = -5$).

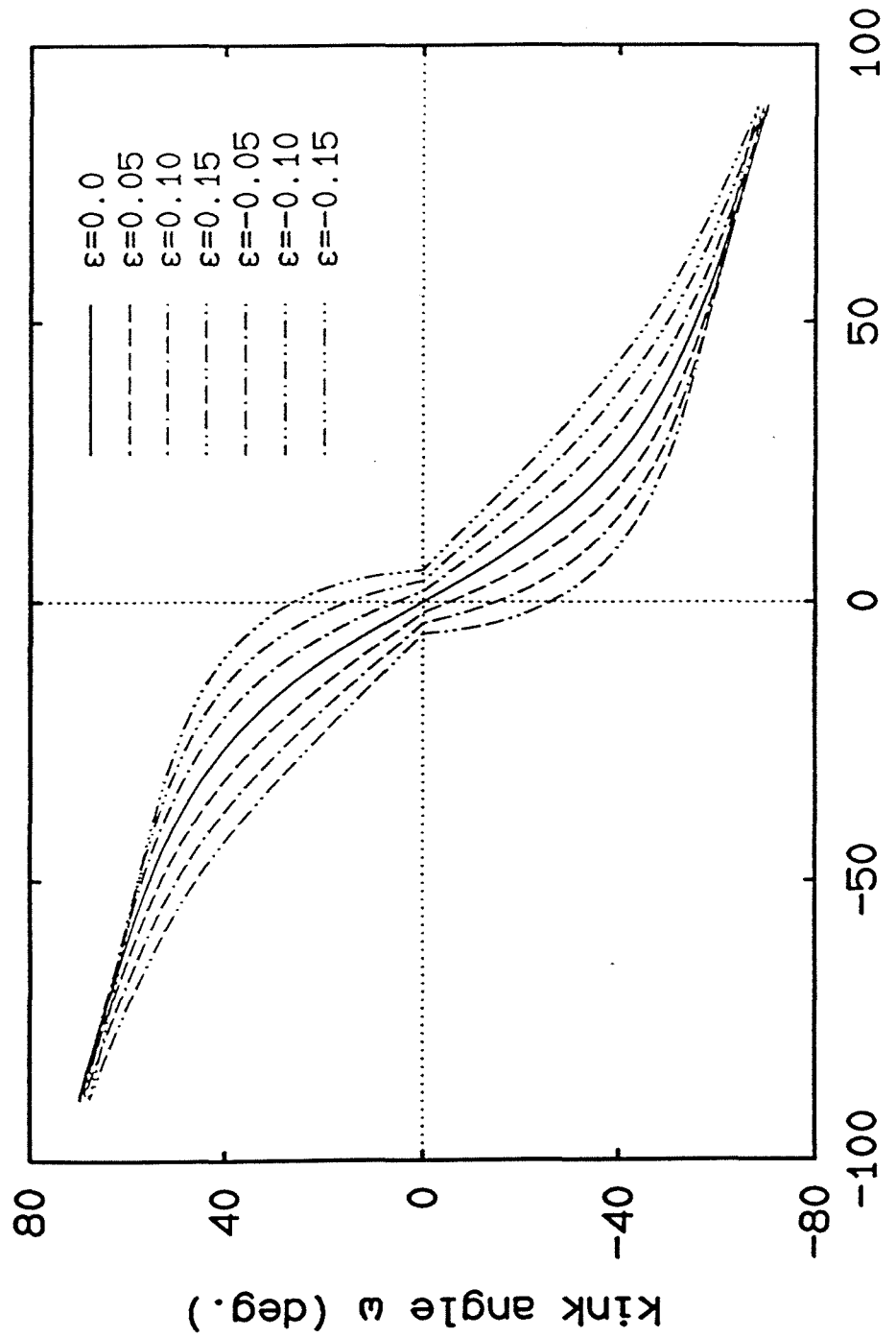

Figure 2. Kink angle as predicted by the maximum circumferential stress criterion ($\gamma = tan^{-1}(K_2/K_1)$).

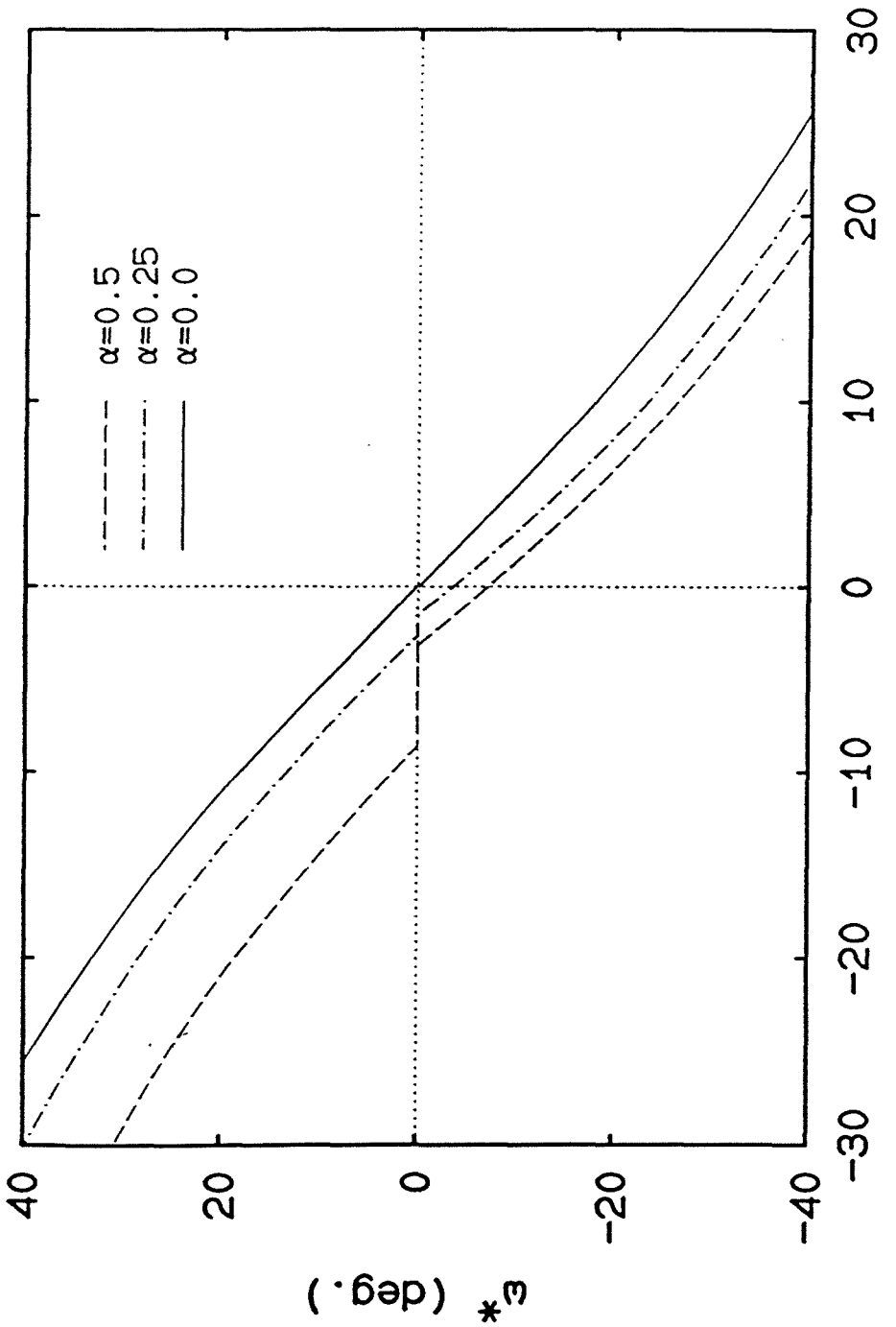

Figure 3. Kink angle ω^* vs local loading parameter γ for various values of α (from He and Hutchinson (1989), $\beta = 0$).

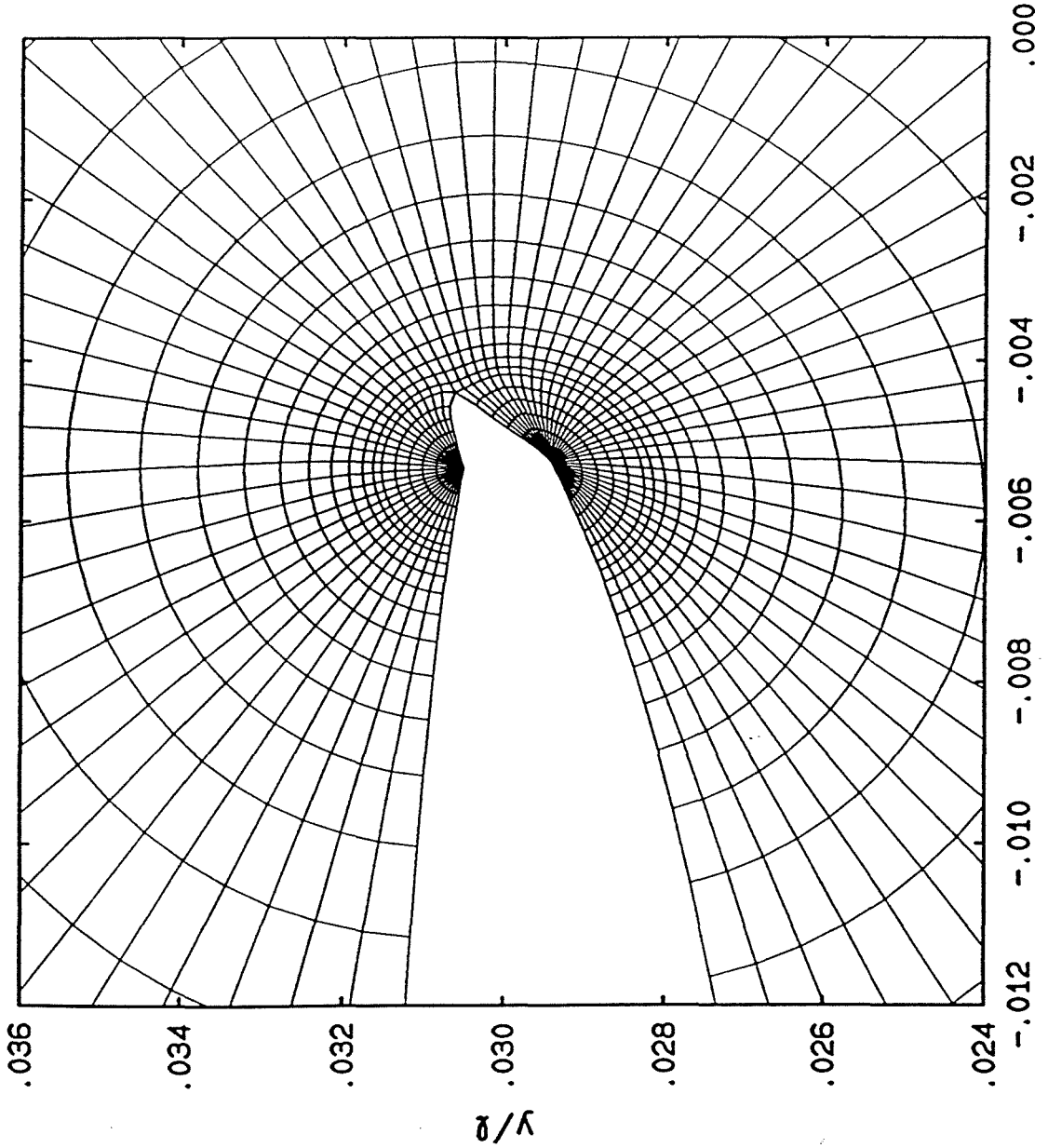

Figure 4. Details of the deformed finite element mesh after crack extension.

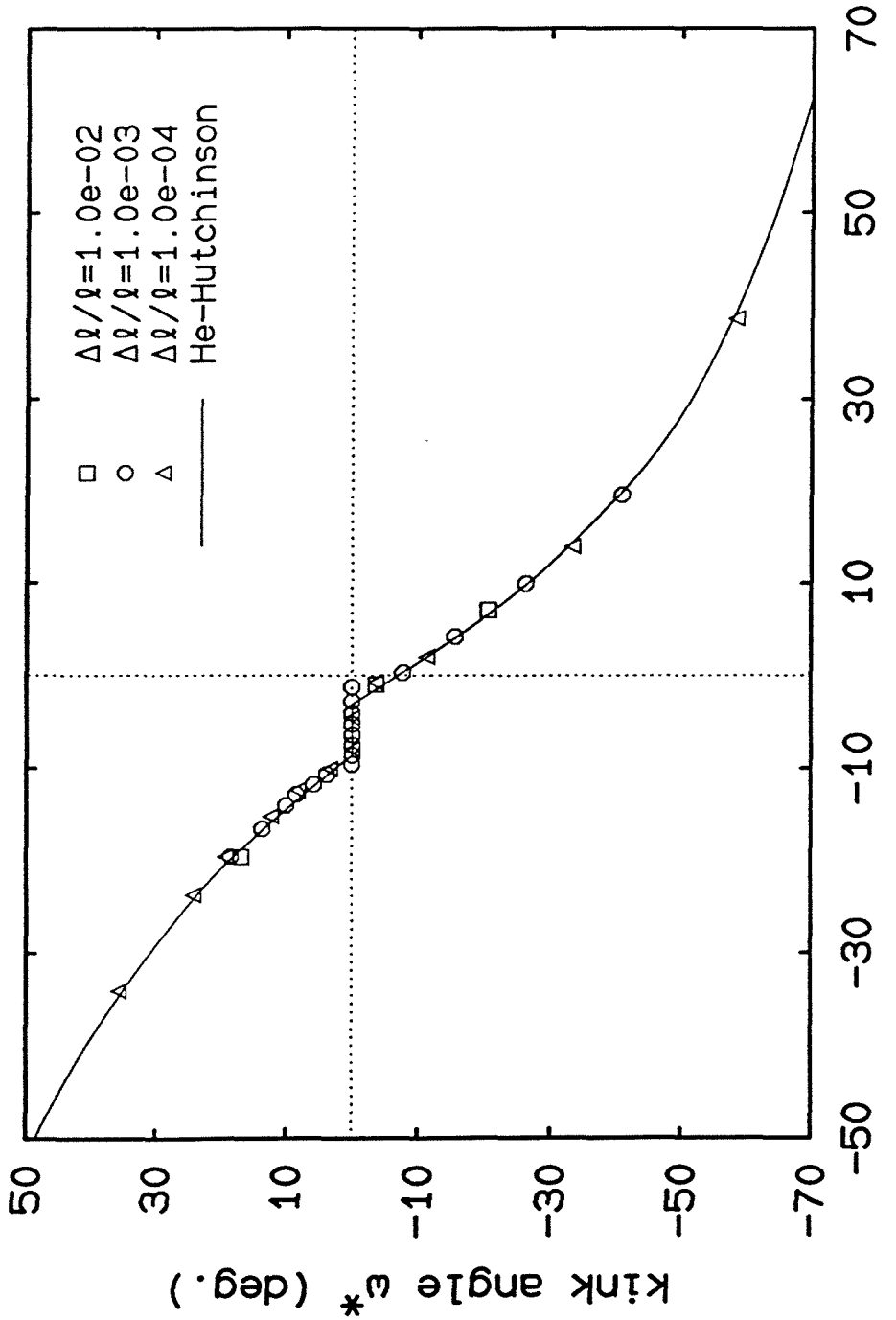

Figure 5. Kink angle ω^* vs loading angle γ for $\alpha = 0.5$ $\beta = \varepsilon = 0.0$.

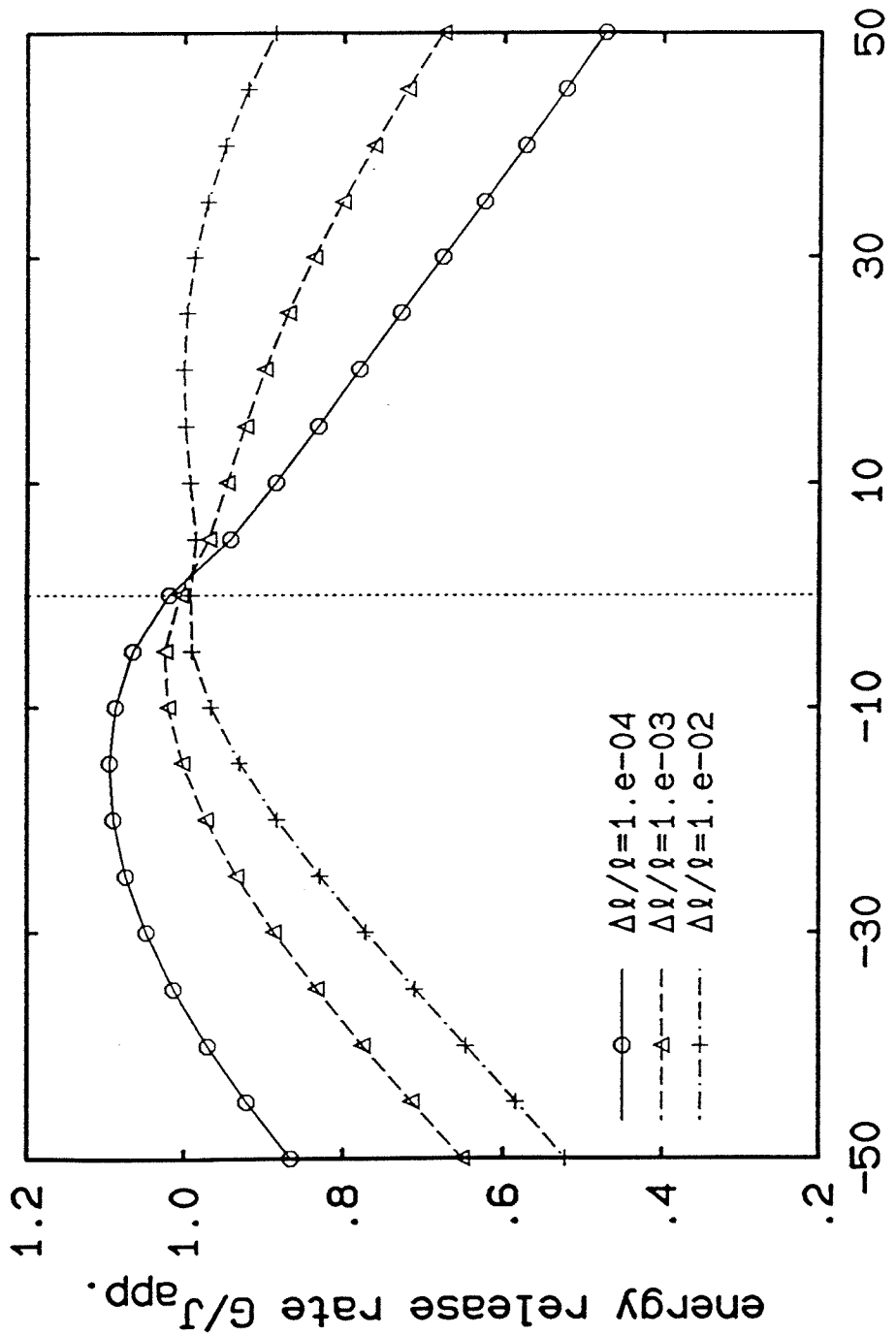

Figure 6a. Angular variation of the energy release rate for three different crack extension lengths Δl ($\alpha = 0.5$ $\beta = 0.25$ $\varepsilon = -0.08$).

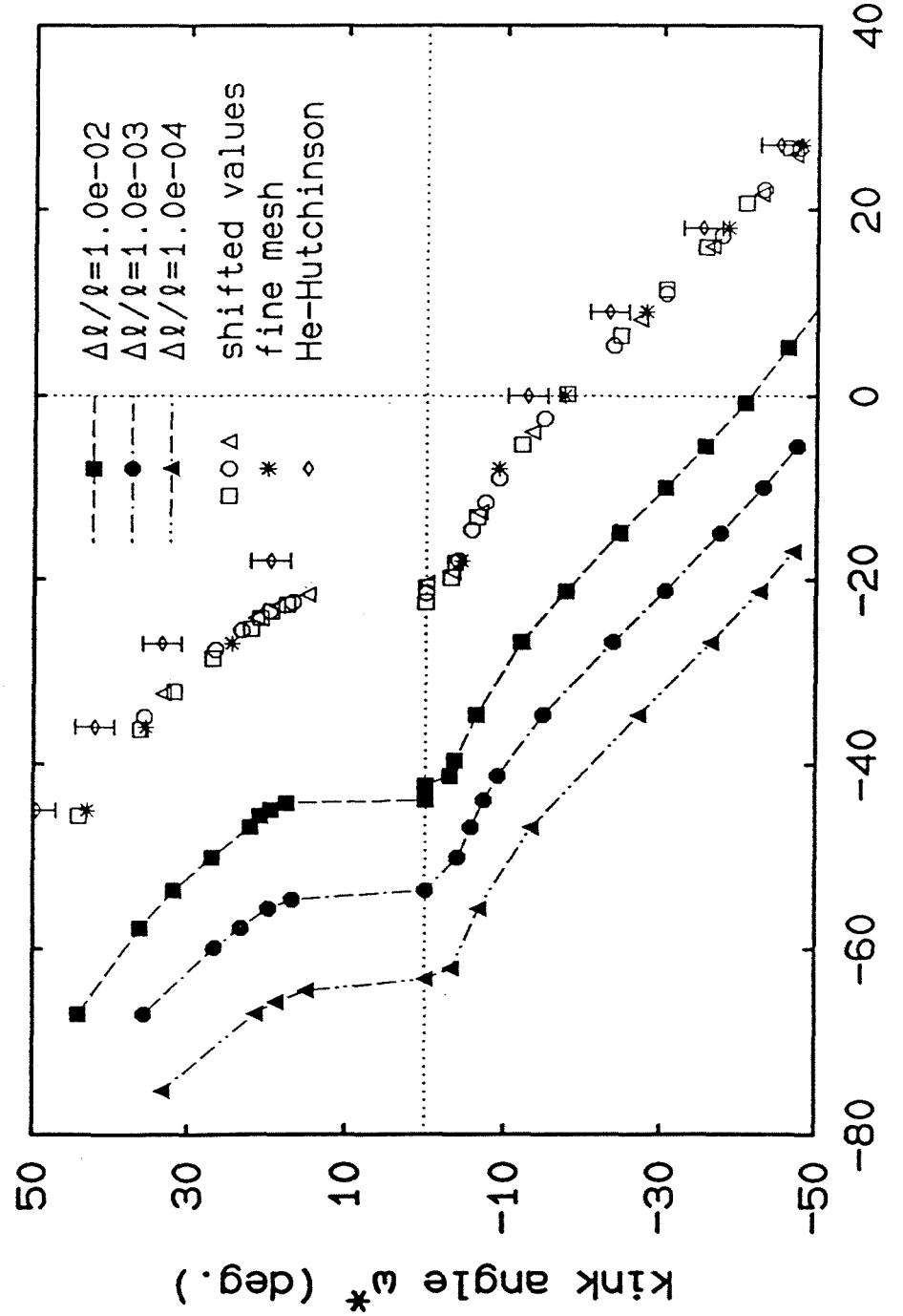

Figure 6b. Kink angle ω^* vs loading angle γ for $\alpha = 0.5$ $\beta = 0.25$: comparison of the numerical analysis with He and Hutchinson's results.

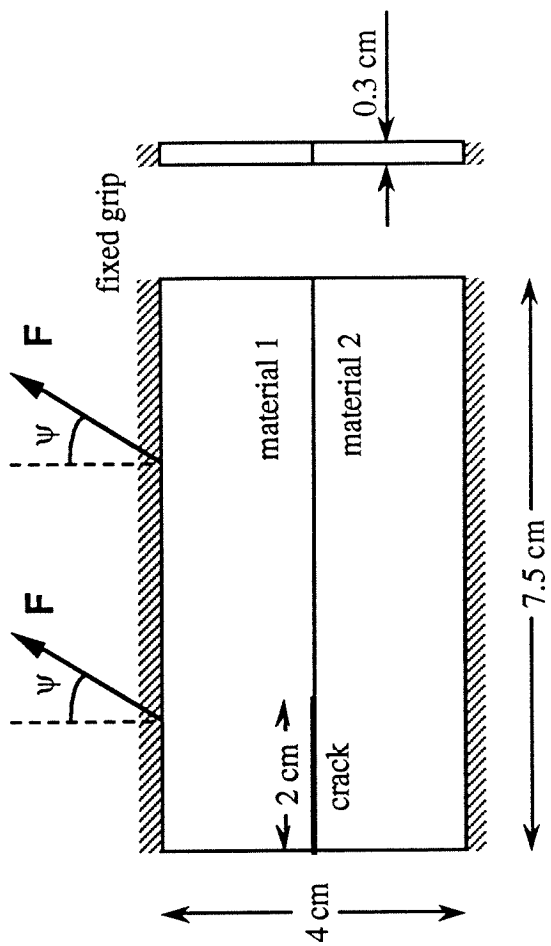

Figure 7. Dimensions of the interfacial fracture specimen.

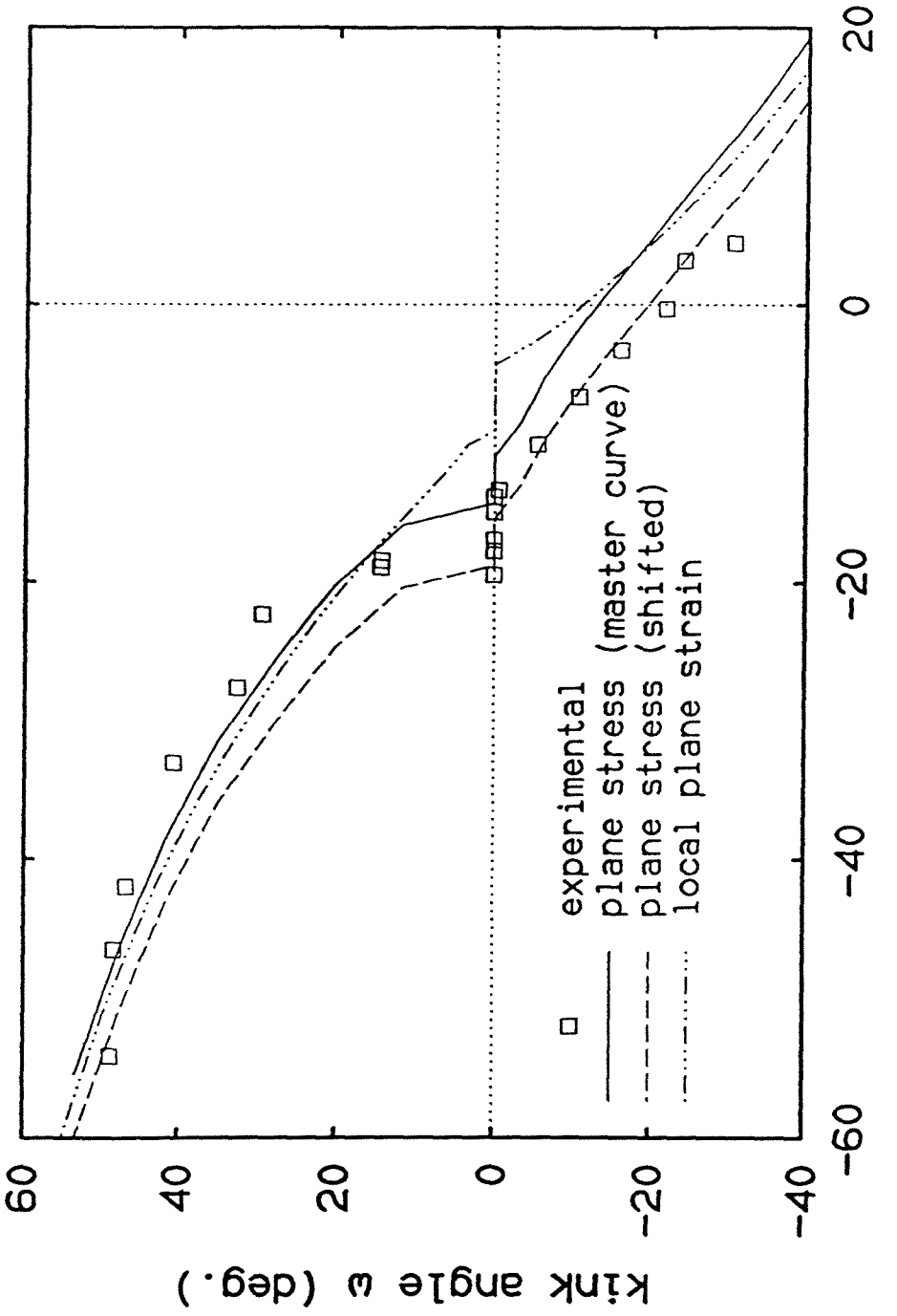

Figure 8. Comparison of experimental and analytical results.

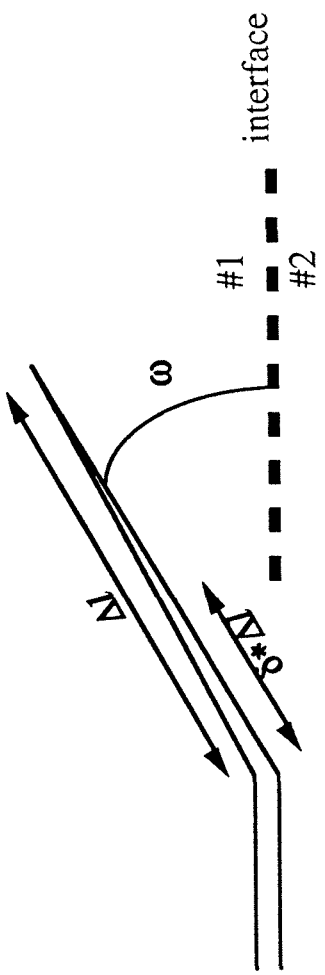

Figure A.1. Geometry of the interface crack kinking problem.

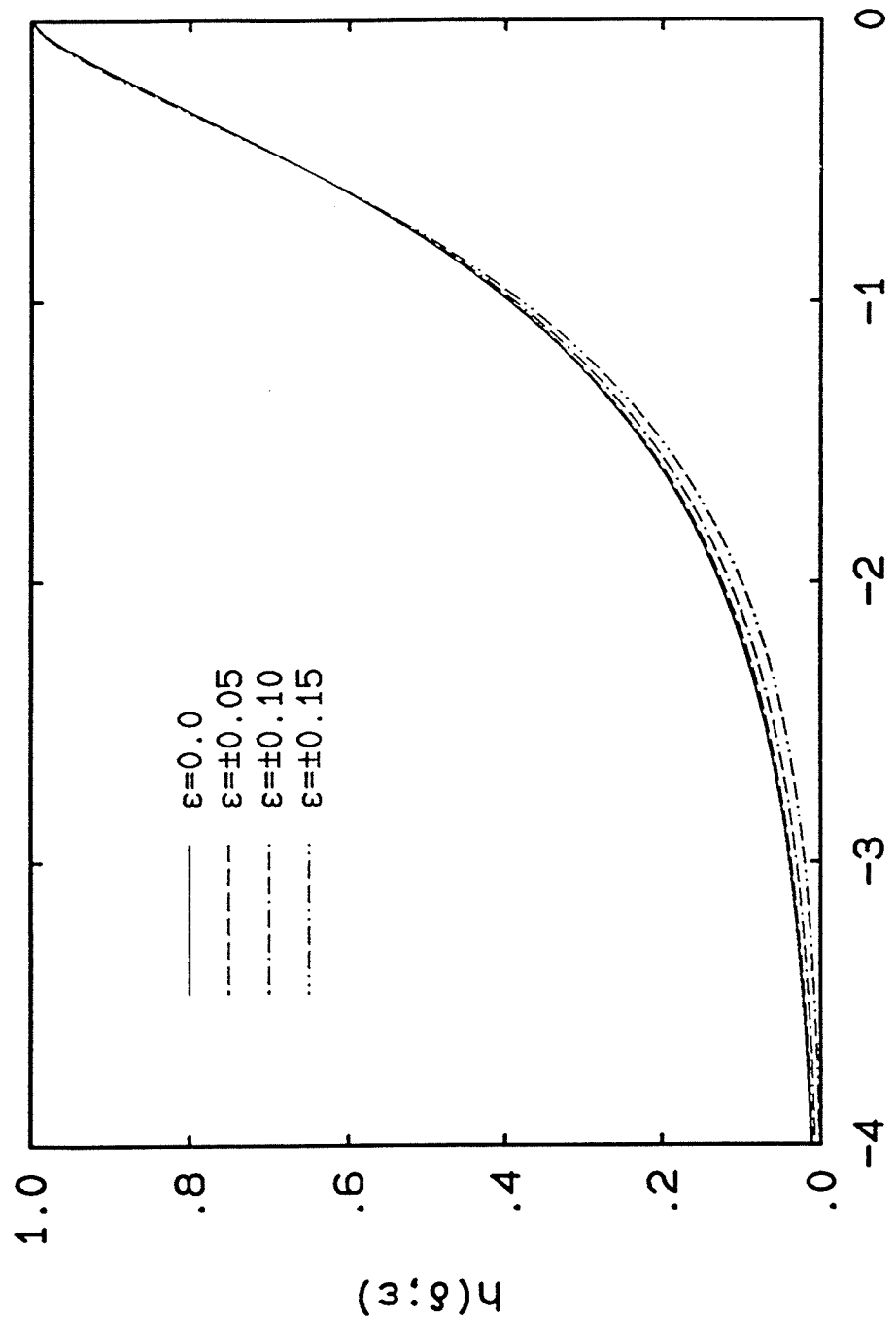

Figure A.2. $h(\delta;\varepsilon)$ versus crack extension fraction δ for various values of ε.

Crack propagation in homogeneous and bimaterial sheets under general in-plane loading : Nonlinear analysis.

Abstract.

The problem of non-coplanar crack propagation in homogeneous and bimaterial sheets is investigated within the framework of the nonlinear theory of plane stress and for the Generalized Neo-Hookean class of hyperelastic solids. The analysis is performed numerically using a boundary-layer approach and the maximum energy release rate criterion. The influence of the large deformation effect on the limiting process associated with the concept of "infinitesimal virtual crack extension" is examined, together with the possible relation between the size of the nonlinear zone and the additional length parameter appearing in the linearized analysis of the interfacial crack propagation problem. As the virtual crack extension is gradually shortened to a size comparable to that of the nonlinear zone, a transition is observed between the non-unique value predicted by the linearized theory and a single "nonlinear" value, which is independent of the crack extension length but also independent of the far-field loading conditions.

1.- Introduction.

The propagation path taken by a crack subjected to loading that is not symmetric with respect to the crack plane has been investigated extensively since the early work by Erdogan and Sih [1] in two-dimensional geometries. Various criteria have been

proposed to determine the kink angle of the crack : some, such as the maximum (opening) stress criterion, suggest that the fracture process be dictated by the conditions existing at the crack-tip prior to its propagation; others, such as the criterion of local symmetry and the maximum energy release rate criterion [2-6], require the knowledge of the near-tip conditions during crack propagation. The latter criterion is a generalization of Griffith energy-balance argument to the non-coplanar situation and consists in comparing the energy stored in the solid before and after the kinking process, for a vanishingly small "virtual" extension of the crack. The predicted propagation angle corresponds thus to that which maximizes the reduction in potential energy between the two states. Due to its attractive relationship to the fundamental minimum potential energy principle, the maximum energy release rate criterion is today the most commonly used principle. Various investigation methods have been proposed in combination with this criterion such as the use of Muskhelishvili's complex potentials and conformal mapping [2,3] or dislocation (Green's) method [4,5]. More recently, Maiti [7] examined the crack kinking problem numerically using the finite element method.

As pointed out by Shih [8], mode-mixity is one of the main characteristics of the near-tip stress and deformation fields for an interfacial crack. It is therefore natural that the issue of crack kinking away from an interface has received special attention in the past few years as substantial progress was made in the mechanics of bimaterial interface fracture. Almost all investigations [9-13] involve the dislocation method employed successfully in the homogeneous case under the precepts of linear elasticity theory. However, as was underlined in [14], the bimaterial situation presents a major difficulty absent in the homogeneous situation : while, in the monolithic case, it is possible to compute the energetically most favorable kink angle as the length of the extension tends to zero, such a limiting process is not possible in general within the linearized theory for bimaterial cases and a unique kink angle cannot be computed. In

order to resolve the non-uniqueness issue, an additional length parameter corresponding to the length of the extension has to be introduced. Note once again that such a length scale does not appear in the homogeneous case. It has been suggested that the additional length scale is associated with physical size scales present in the components of the bimaterial specimen such as the size of the microstructure or of the fracture process domain. This approach does not seem, however, compatible with the experimentally deduced additional length parameter[1] obtained for the particular material combination used in [14].

In the present paper, we examine whether the length parameter can be somehow associated with the size of the nonlinear large deformation zone present around the crack-tip. We thus investigate how the limiting process mentioned above is affected by relinquishing the assumption of infinitesimal strains and allowing for large deformations and rotations along with non-linear constitutive behavior. The motivation behind the present analysis comes from the fact that the length parameter appearing in the linearized bimaterial situation has been shown to be associated with the inconsistencies inherent in the linear analysis of the interface crack problem (contact and overlapping of the crack faces, oscillatory near-tip fields, ...). However, as was first shown in [15], these difficulties disappear if finite strain effects are taken into account. We show here that, even in the homogeneous situation, the size of the large deformation zone introduces a length scale which restricts the limiting process associated with the maximum energy release rate criterion.

The analysis is conducted within the framework of the nonlinearly elastic theory of plane stress. Material and geometrical nonlinearities are combined through the use of the Generalized Neo-Hookean model. Due to the complexity of the field equations and of the problem geometry, the analysis is performed numerically with the aid of the finite

[1] See discussion in section 4 of [14].

element method. The details of the computational analysis are described in the next section. Then, the results corresponding to the homogeneous case are discussed in section 3 while section 4 is dedicated to a survey of the bimaterial situation.

2.- Numerical investigation.

We present next the details of the numerical analysis, within the nonlinear theory of elasticity, of the maximum energy release rate criterion, and, in particular, of the spatial discretization and the computation of the energy release rate.

Finite element mesh.

Throughout the present numerical investigation, we are concerned with the boundary value problem symbolically represented in figure 1. It consists of a circular domain of radius l, along the outer boundary of which displacement boundary conditions corresponding to a "linear K-field" are applied. The crack, initially of length l, is extended by an amount Δl in a direction ω relative to the crack axis[2]. The ratio of the crack extension length to the original length is varied between 10^{-6} and 10^{-2}. The lower limit is justified by the numerical imprecision associated with very high gradients close to the crack-tip while a ratio of 10^{-2} is the maximum allowable value to keep the "boundary layer" approach meaningful. The latter approach has been chosen instead of the more conventional "global problem," such as, for example, the centered crack problem, for the following three reasons : first, it has been shown to provide similar results as long as the length of the crack extension Δl is small compared to the original length l; second, because it allows a direct control through the applied K-field boundary

[2] Note that, throughout the present analysis, dimensions and angles are defined with respect to the undeformed coordinates.

conditions over the loading conditions prevailing at the crack-tip before its extension; and finally, because the more compact geometry associated with such a boundary layer approach allows for a better spatial discretization than the global approach for an equivalent computational cost.

As pointed out by Maiti [7], the design of the finite element mesh is of prime importance, especially in the crack-corner and branch-tip region, to ensure precision of the predicted energetically most favorable kink angle. It was suggested there to use a doubly focused mesh (i.e., focused at the kink corner and at the branch tip) in order to capture the interaction between the two singularities arising in the post-extension problem. Since the analysis of the bimaterial situation, for which such a discretization is not possible for most kink angles, constitutes one of the main objectives of the present investigation, we have opted for a simpler mesh focused at the original crack-tip only, as described in figure 2. Numerical precision has however been achieved by increasing the mesh refinement : the crack extension is represented by *10* equally spaced elements and the inner annuli are divided into *72* 5-degree-sectors. Outside of the inner circle of radius Δl, *25* to *35* elements are distributed geometrically along a radial line, with the progression factor chosen such that the first "outside" element has a size similar to that of the *10* "inner" ones. The total number of *4*-node bilinear elements was thus *3240* for $\Delta l/l = 10^{-6}$ and *2520* for $\Delta l/l = 10^{-2}$.

The precision of the numerical scheme was assessed by performing a preliminary linearly elastic analysis of the homogeneous situation for which generally accepted results exist. The results are shown in figure 3 which presents the variation of the kink angle ω^* as predicted by the maximum energy release rate criterion with respect to the phase angle γ characterizing the local mode mixity at the unextended crack-tip, defined by

$$\gamma = tan^{-1}(K_2/K_1). \qquad (2.1)$$

The numerical values, denoted by symbols and corresponding to 5 values of $\Delta l/l$, are compared with the analytical solution (dashed curve). Also shown is the prediction corresponding to the maximum opening stress criterion which, in the homogeneous case, gives results very similar to those of the energy-based criterion, especially for small values of γ. The agreement between the numerical and analytical results is quite satisfactory, differing in all cases by at most *1.0 degree*.

Computation of the energy release rate.

As mentioned before, the nonlinear analysis of the crack propagation problem is performed within the framework of the finite strain theory of plane stress, the main relations of which have been summarized in [15]. The material model used throughout the present investigation is the so-called Generalized Neo-Hookean (GNH) model described in detail in [16]. It is characterized by three parameters μ, b and n which determine, respectively, the linearly elastic, "yielding" and "hardening" behaviors of the incompressible hyperelastic material through the plane stress elastic potential

$$U(I,J)=\frac{\mu}{2b}\left\{\left[1+\frac{b}{n}\left(I+J^{-2}-3\right)\right]^{n}-1\right\}, \tag{2.2}$$

with I and J being the two scalar invariants associated with the two-dimensional deformation.[3] The GNH model has been implemented, together with a fully Lagrangian scheme, in a modified version of the finite element program FEAP [17]. The initial crack problem is first solved by applying nodal tractions along the crack extension to keep it closed. Then, these tractions are progressively relaxed until the stress-free kink is fully open and the associated unloading work is computed. This process is repeated for various crack extensions to obtain the variation of the energy release rate with

[3] See section 2 of [16] for more details.

respect to the kink angle, and, thereby, to compute the energetically most favorable crack path.

As mentioned in [14], two methods are used to calculate the energy release rate G: the first one is based on the potential energy definition

$$G_W = -\lim_{\Delta l \to 0} \frac{\Delta \Pi}{\Delta l}, \tag{2.3}$$

where Π is the potential energy contained in the body and, in the present case, is the integral over the domain of the strain energy density $U(I,J)$ defined in (2.2). For hyperelastic solids, the energy release rate can be equivalently determined by computing the closure work of the extended crack

$$G_{cc} = \lim_{\Delta l \to 0} \frac{1}{\Delta l} \int_0^{\Delta l} \int_0^{\Delta \boldsymbol{u}} \boldsymbol{T}.\, d\Delta \boldsymbol{u}\; ds, \tag{2.4}$$

where $\boldsymbol{T}$ and $\Delta \boldsymbol{u}$ denote the traction and displacement jump vectors along the crack extension respectively. By monitoring the nodal tractions and displacements of the M nodes distributed along the kink during the N unloading steps of the extension process, and using a simple trapezoidal integration rule, (2.4) is approximated by

$$G_{cc} \approx \frac{1}{2\,\Delta l} \sum_{I=1}^{M} \sum_{J=1}^{N} \sum_{\alpha=1}^{2} (T_\alpha^{I,J-1} + T_\alpha^{I,J})(\Delta u_\alpha^{I,J} - \Delta u_\alpha^{I,J-1}), \tag{2.5}$$

with $T_\alpha^{I,J}$ and $\Delta u_\alpha^{I,J}$ representing the α-component at node I and unloading step J of the tractions and displacements respectively. The two approaches yield very similar results (within 0.1%) if a sufficient number of unloading steps are used (5 to 50 depending on the load level).

3.- Homogeneous case.

Confident of the precision of the numerical scheme, we first investigate the homogeneous Neo-Hookean situation for which the hardening parameter of the hyperelastic sheet is unity. Seven values of the local mixity parameter have been considered (γ=*0, 10, 20, 30, 40, 50* and *60°*). The amplitude of the far-field loading has also been varied as $\overline{K} = |K|/\mu\sqrt{l} = 10^{-4}$, 10^{-3}, 10^{-2}, 10^{-1} and *1*, where $|K| = \sqrt{K_I^2 + K_2^2}$, μ is the shear modulus and l is the radius of the circular domain on which the boundary-layer analysis is performed. For each far-field loading condition, *5* values of the crack extension length Δl have been investigated, as mentioned earlier ($\Delta l/l = 10^{-6}$, 10^{-5}, 10^{-4}, 10^{-3} and 10^{-2}). The results of the *175* cases thus defined are summarized in figure 4 which presents the variation, with respect to $\Delta l/l$, of the ratio ω^*/ω_L^*, where ω^* and ω_L^* are the kink angles predicted by the nonlinear and linear theory respectively.[4] It is observed that, except in the particular case $\gamma = 0°$ (mode I) for which, by symmetry, the maximum energy release rate criterion always predicts a coplanar crack growth, the nonlinear analysis suggests a dependence of the energetically most favorable kink angle ω^* on the length of the extension Δl. As the size of the nonlinear zone increases with $\overline{K}$, a transition is observed between the γ-dependent linear value ω^* and a unique γ-independent value $\omega^* = 0°$. One can better visualize the transition process by comparing the length of the extension Δl with a "measure" of the size of nonlinear zone. The length scale characterizing the zone of dominance of the nonlinear effects that is adopted here is derived from the results of an asymptotic analysis of the near-tip stress and deformation fields for a crack in a homogeneous sheet of GNH material under general (mixed-mode) loading conditions [16]. It was shown there that, in the large deformation region, the stress singularity is stronger than that predicted by the linearized theory (the norm of the Cauchy stress

[4] Recall that, as shown in figure 3, ω_L^* is independent of the crack extension length Δl.

tensor varies as the inverse of the distance to the crack-tip instead of the inverse square root singularity suggested by the linearized theory), and that, under "small-scale nonlinear yielding" conditions such as those considered in the present boundary-layer type analysis, a fairly sharp transition is observed between the two asymptotic behaviors, as symbolically represented in figure 5. The size r_{NL} of the nonlinear zone has been shown in [16] to be

$$\frac{r_{NL}}{l} = \frac{1}{3\pi n^2}\frac{\mathcal{J}}{\mu l}, \tag{3.1}$$

where $\mathcal{J}$ is the value of the conservation integral. It is interesting to note that if the individual curves in figure 4 are shifted by normalizing the crack extension length Δl with respect to the nonlinear zone size r_{NL}, one obtains the single set of transition curves presented in figure 6. It seems therefore that the load-dependent measure (3.1) of the nonlinear zone size, which is, in the present analysis, the only length scale characterizing the large deformation effects on the near-tip fields, unifies all the transition curves surprisingly well despite its relative simplicity.

Although the transition curves are slightly different for each value of the local mixity parameter γ, the six "mixed-mode" curves ($\gamma \neq 0^\circ$) show a fairly sharp transition between the two limiting values ($\omega^* = 0^\circ$ and $\omega^* = \omega_L^*$). This somewhat surprising result can be explained by the structure of the large deformation strain and stress fields existing near the crack-tip under non-symmetric loading conditions. It has been shown, through the asymptotic analysis summarized in [16], that, within the nonlinear theory of plane stress and for the GNH class of hyperelastic materials, the near-tip fields corresponding to mixed-mode cases consist of mere rotations of the symmetric (mode I) approximations, the rotation depending on the "linear mixity parameter" γ through a one-to-one relation which is itself a function of the "hardening"

exponent[5] n. It is therefore natural that, when the length of the crack extension is chosen well within the zone of dominance of the nonlinear effects, the predicted kink angle ω^*, which is "measured" in terms of the undeformed coordinates, tends to zero for all mixity ratios.

The size of the nonlinear zone may thus become a "geometrical lower-bound" to the concept of virtual crack extension inherent in the maximum energy release rate criterion : the limit $\Delta l \to 0$ appearing in the definitions (2.3) and (2.4) of G exists even if the nonlinear effects are taken into account but the value of the predicted path angle corresponding to such a limiting process is at variance with experimental observations [2], although the latter have been obtained in situations in which finite strain effects are not dominant. To our knowledge, no comparable data addressing the large deformation companion problem are available at this time. Although we grant that the special GNH model may represent the physical phenomena in the nonlinear zone imperfectly, the present analysis indicates that the propagation behavior of the crack is probably dictated by conditions prevailing outside of the nonlinear zone.

The case $n = 0.7$ has also been investigated for $\gamma = 40^\circ$, showing a very similar transition curve (figure 6). Although the analysis has been performed within the framework of the nonlinearly elastic theory of plane stress for the particular class of GNH materials, we believe that such a behavior should also occur for other classes of materials, as well as under plane strain conditions where the rotation property of the near-tip fields has been shown to be valid, too [18].

---

[5] See figure 19 in [16].

4.- Interface crack problem.

We turn next to the large deformation investigation of the interface crack propagation problem. Let $(\mu^{(1)}, b^{(1)}, n^{(1)})$ and $(\mu^{(2)}, b^{(2)}, n^{(2)})$ be the material parameters characterizing the upper and lower Generalized Neo-Hookean sheets, respectively. Detailed asymptotic analyses of various bimaterial problems [19,20] have shown that, as was the case in the homogeneous situation, the deformation fields existing near the tip of an interface crack between two sheets of GNH materials consist in the rotation of a "canonical bimaterial field," the rotation being a function of the far-field conditions and the geometrical and mechanical characteristics of the bimaterial specimen. For example, in the particular case where both components have similar "hardening" behaviors (i.e., $n^{(1)}=n^{(2)}=n$), the near-tip field is given by [19]

$$\boldsymbol{y} = \boldsymbol{Q}\, \boldsymbol{y}^{*}, \tag{4.1}$$

where $\boldsymbol{y}$ is the deformed coordinate vector field, $\boldsymbol{Q}$ is an orthonormal tensor and $\boldsymbol{y}^{*}$ is the "canonical" deformation field

$$\begin{cases} y_1^{*} \sim c\, r^{p} g(\theta;n), \\ y_2^{*} \sim a\, r^{m} j(\theta)\, f(\theta;n) + k\, r^{t} l(\theta;n) + d\, r^{q} j(\theta)\, h(\theta;n), \end{cases} \tag{4.2}$$

in which the asymptotic exponents m, p, t and q are a function of n and have been given in figure 2 of [19]; the angular functions $f(\theta;n)$, $g(\theta;n)$, $h(\theta;n)$ and $l(\theta;n)$ are continuous on $[-\pi,\pi]$; a, c, d and k are scalars and $j(\theta)$ is the step function characterizing the concentration of the deformations in the weaker component as

$$j(\theta) = \begin{cases} 1 & (0 \le \theta \le \pi), \\ \xi = \left[\dfrac{\mu^{(1)}}{\mu^{(2)}} \left(\dfrac{b^{(1)}}{b^{(2)}} \right)^{n-1} \right]^{1/(2n-1)} & (-\pi \le \theta < 0). \end{cases} \tag{4.3}$$

It is therefore expected that, due to the structure (4.1)-(4.3) of the near-tip fields, the nonlinear analysis of the maximum energy release rate criterion yields results similar to the homogeneous situation : when the crack extension length Δl is chosen within the zone where the near-tip approximation is valid, one obtains an energetically most favorable kink angle which does not depend on Δl but also on the far-field loading conditions. In the "boundary-layer" analysis adopted here, the latter are characterized by the complex stress intensity factor $K = K_1 + iK_2$ associated with the linearized bimaterial asymptotic solution.[6]

The numerical investigation described in section 3 for the homogeneous case has been repeated for exemplary purposes in the bimaterial situation with $\mu^{(1)}/\mu^{(2)} = 2$, $b^{(1)}/b^{(2)} = 1$ and $n^{(1)} = n^{(2)} = n = 0.8$. The corresponding values of the "linear" moduli mismatch parameters[7] are $\alpha = 0.333$, $\beta = 0.083$ and $\varepsilon = -0.027$. The nonlinear mismatch parameter ξ introduced in (4.3) is equal to 3.175. Ten loading conditions have been considered ($\overline{K} = |K|/\mu^{(2)}\sqrt{l} = 10^{-4}$, 10^{-3}, 10^{-2}, 10^{-1} and 1, and $\gamma = 0°$ and $-30°$) with, for each case, the same values of $\Delta l/l$ as in section 3. The results are summarized in figures 8a (for $\gamma = -30°$) and 8b (for $\gamma = 0°$), showing, as was the case in the monolithic situation, a transition between the linear values of ω^* (obtained for small $\overline{K}$) and the unique nonlinear value[8] which is found to be $\omega^* \approx -30°$. Note that since the value predicted by the linear theory depends on Δl, a transition curve similar to that presented in figures 6 and 7 does not exist. Although the "unique kink angle" associated with the large deformation zone depends on the material

---

[6] The definition of the bimaterial stress intensity factor used here is similar to that described in section 1 of [14] : the length scale that needs to be introduced in order to determine the phase angle γ has been chosen as the radius l of the circular domain represented in figure 1.

[7] See section 1 of [14].

[8] Note that, in the case $\Delta l/l = 10^{-2}$, the size of the nonlinear zone corresponding to the largest value of $\overline{K}$ is of the order of the length of the crack extension. This explains why the transition between the "linear" and the "nonlinear" values of ω^* is not completely shown in figures 8a and 8b.

combination, the trend observed in the present problem is applicable to other bimaterial situations because of the aforementioned "rotation property" of the near-tip fields.

The nonlinear analysis of the crack extension problem thus seems to restrict the limiting process ($\Delta l \rightarrow 0$) which, in the linearized analysis, did not provide a unique value of the energetically most favorable kink angle. But the independence of the (large deformation) kink angle on the far-field loading conditions seems to indicate also that conditions prevailing outside of the nonlinear zone determine the propagation behavior of the interface crack. It is therefore possible that the size of the nonlinear zone might provide an indication for the additional length scale necessary to obtain an agreement between analytical and experimental results, for situations where the large deformation effects are not negligible. The values deduced from the experimental observations described in section 4 of [14] do not contradict this possibility.

Acknowledgments.

This work has been sponsored by AFOSR (contract F044611-88-K-0024) under the technical monitoring of Dr. C.T. Liu. Additional support has been provided by ONR (grant N00014-91-J-1427) under the patronage of Dr. Peter Schmidt. The accesss to the Cray YMP of the San Diego Super-computing Center was made possible through a grant by the National Science Foundation.

References.

1. Erdogan, F. and Sih, G.C., *On the crack extension in plates under plane loading and transverse shear.* J. Basic Engng., 1963. **85**: pp. 519-527.

2. Palaniswamy, K. and Knauss, W.G., *On the problem of crack extension in brittle solids under general loading,* in *Mechanics Today,* S. Nemat-Nasser, Editor. 1978, Pergamon Press: pp. 87-148.

3. Wu, C.H., *Maximum energy release rate criterion applied to a tension-compression specimen with crack.* J. Elast., 1978. **8**: pp. 235-257.

4. Lo, K.K., *Analysis of branched cracks.* J. Appl. Mech., 1978. **45**: pp. 797-802.

5. Hayashi, K. and Nemat-Nasser, S., *Energy release rate and crack kinking under combined loading.* J. Appl. Mech., 1981. **48**: pp. 520-524.

6. Karihaloo, B.L., *On crack kinking and curving.* Mech. of Materials, 1982. **1**: pp. 189-201.

7. Maiti, S.K., *Finite element computation of the strain energy release rate for kinking of a crack.* Int. J. Fract. Mech., 1990. **43**: pp. 161-170.

8. Shih, C.F., *Cracks on bimaterial interfaces : elasticity and plasticity aspects.* Mat. Sc. Engng., 1991. **A 143**: pp. 77-90.

9. Hayashi, K. and Nemat-Nasser, S., *On branched interface cracks.* J. Appl. Mech., 1981. **48**: pp. 529-533.

10. He, M.-Y. and Hutchinson, J.W., *Kinking of a crack out of an interface.* J. Appl. Mech., 1989. **56**: pp. 270-278.

11. Miller, G.R. and Stock, W.L., *Analysis of branched interface cracks between dissimilar anisotropic media.* J. Appl. Mech., 1989. : p. 844.

12. Mukai, D.J., Ballarini, R., and Miller, G.R., *Analysis of branched interface cracks.* J. Appl. Mech., 1990. **57**: pp. 887-893.

13. Wang, T.C., Shih, C.F., and Suo, Z., *Crack extension and kinking in laminates and bicrystals.* Int. J. Solids Struct., 1992. **29**(3): pp. 327-344.

14. Geubelle, P.H. and Knauss, W.G., *Crack propagation at and near bimaterial interfaces : Linear analysis.* Galcit SM Report 91-16, Caltech, 1991. To appear in J. Appl. Mech.

15. Knowles, J.K. and Sternberg, E., *Large deformations near the tip of an interface crack between two Neo-Hookean sheets.* J. Elasticity, 1983. **13**: pp. 257-293.

16. Geubelle, P.H. and Knauss, W.G., *Finite strains at the tip of a crack in a sheet of hyperelastic material : I. Homogeneous case.* Galcit SM Report 92-42, Caltech, 1992. Submitted to J. Elasticity.

17. Zienkiewicz, O.C., *The finite element method.* 3rd ed. 1977, McGraw-Hill.

18. Le, K.C., *On the singular elastostatic field induced by a crack in a Hadamard material.* Q. J. Mech. Appl. Math, 1992. **45**(1): pp. 101-117.

19. Geubelle, P.H. and Knauss, W.G., *Finite strains at the tip of a crack in a sheet of hyperelastic material : II. Special bimaterial cases.* Galcit SM Report 92-43, Caltech, 1992. Submitted to J. Elasticity.

20. Geubelle, P.H. and Knauss, W.G., *Finite strains at the tip of a crack in a sheet of hyperelastic material : III. General bimaterial case.* Galcit SM Report 92-44, Caltech, 1992. Submitted to J. Elasticity.

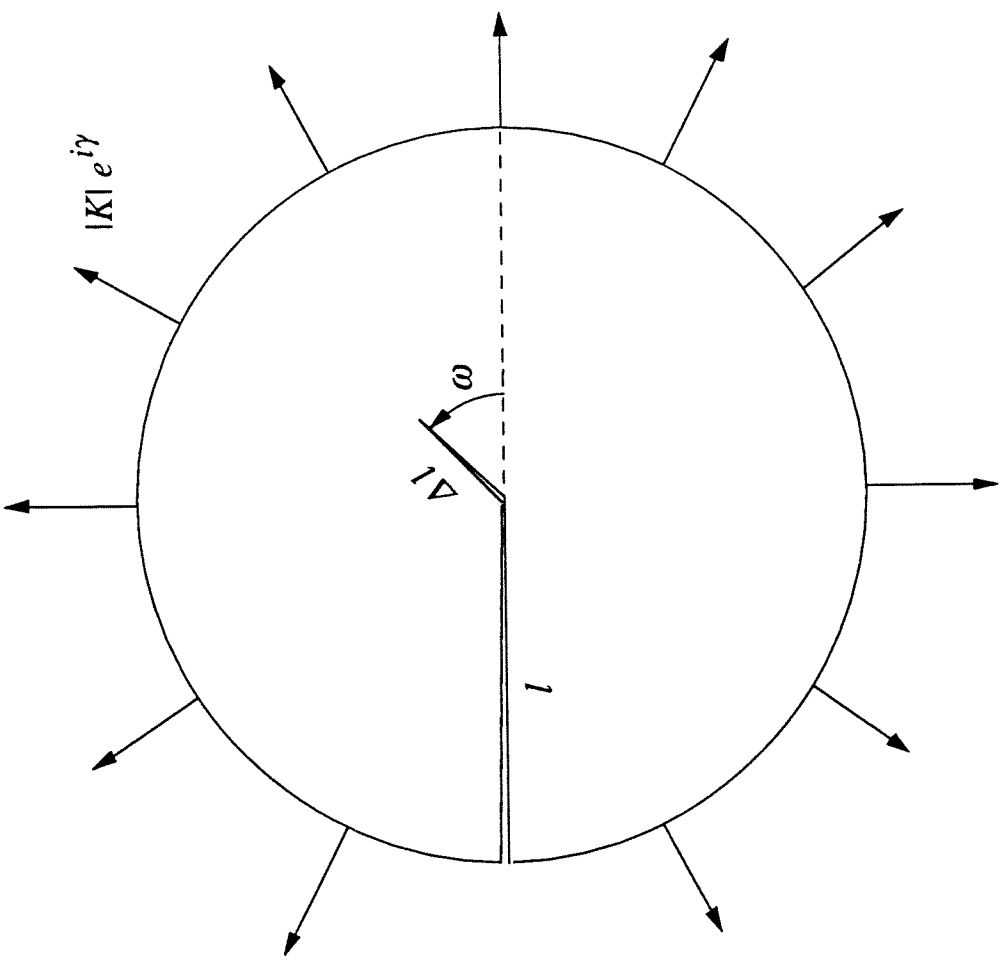

Figure 1. Geometry of the boundary-layer analysis of the crack propagation problem.

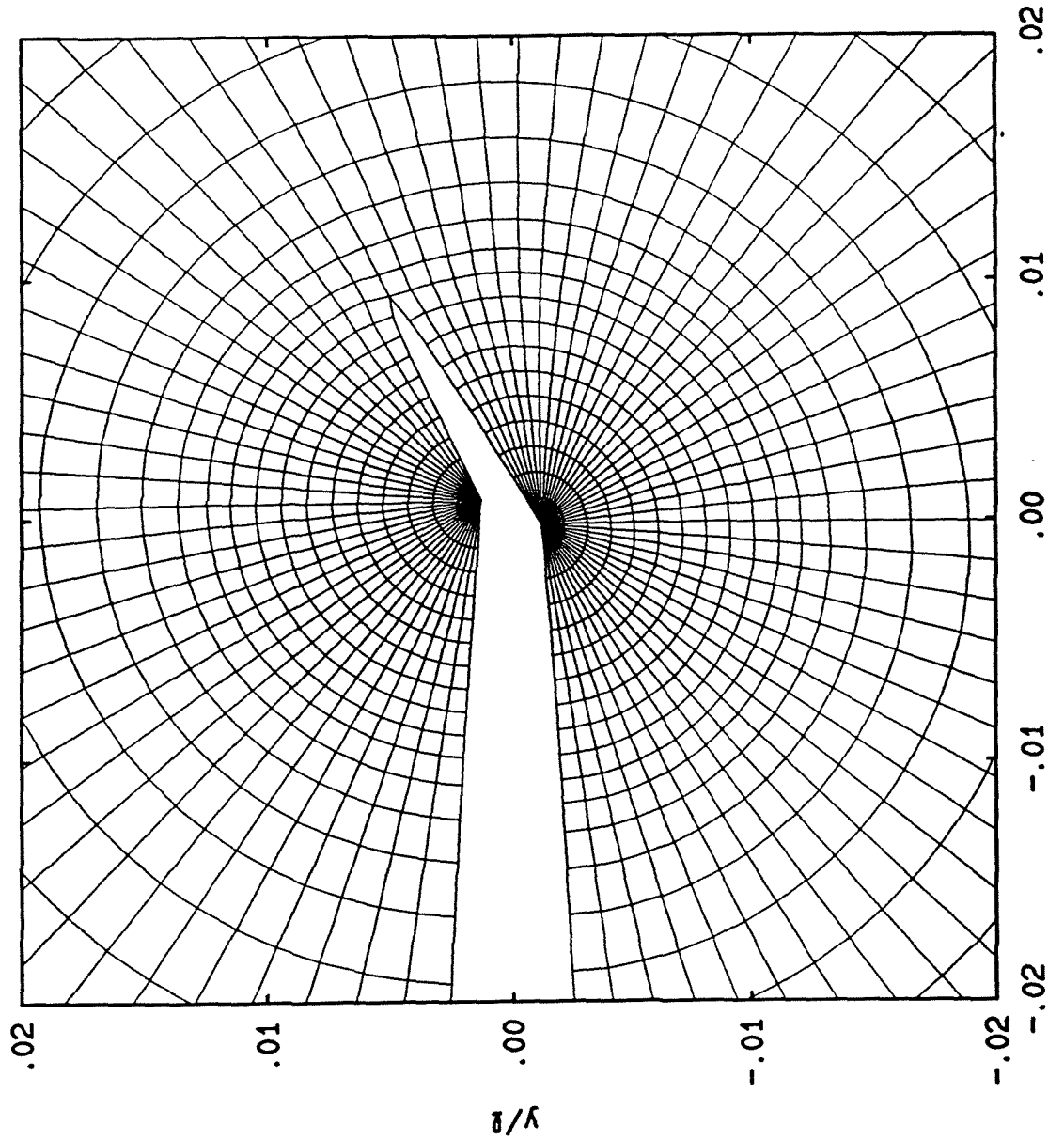

Figure 2. Details of the deformed finite element mesh after crack extension in the case $\Delta l/l = 10^{-2}$.

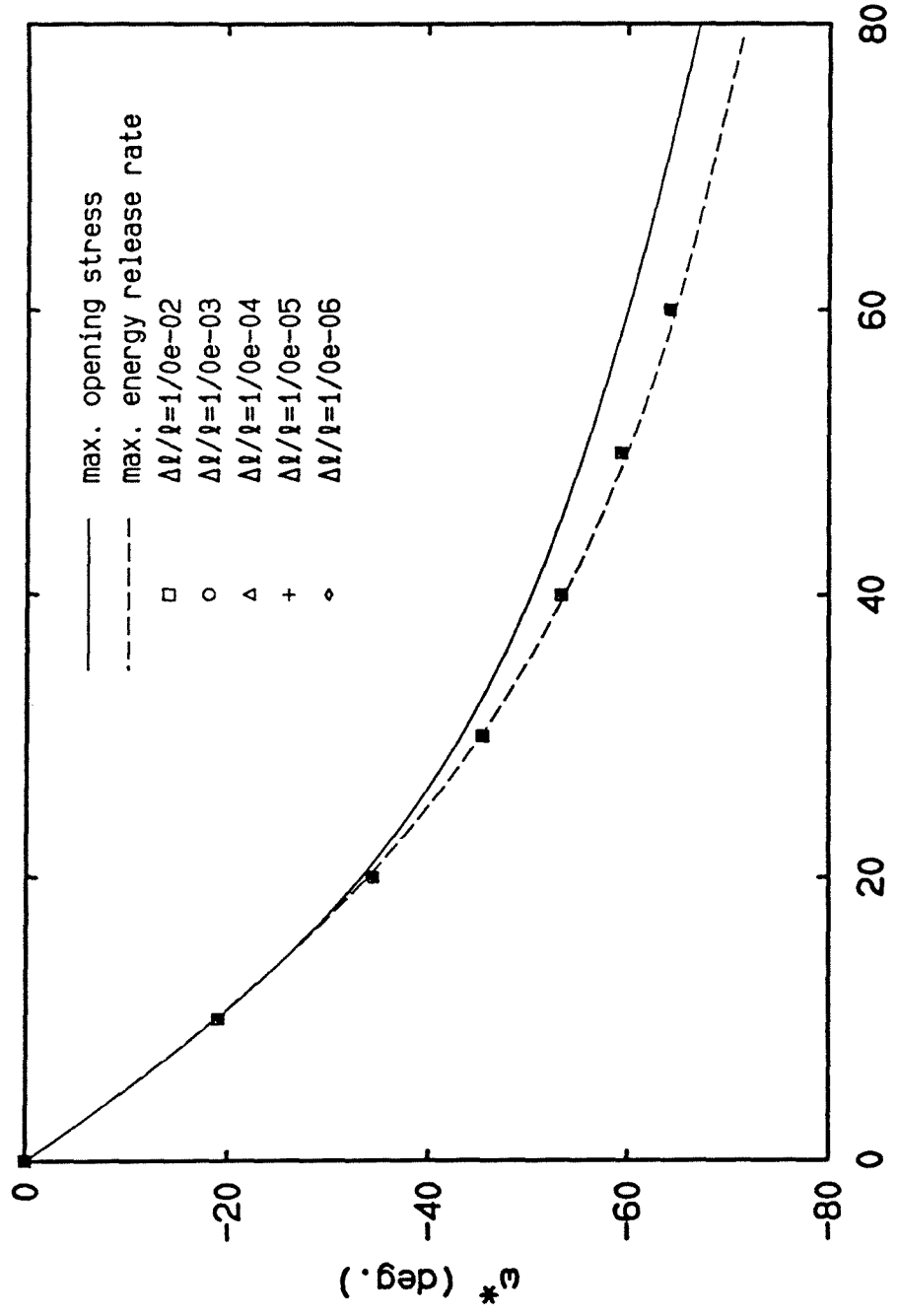

Figure 3. Results of the preliminary linear analysis of the homogeneous situation : variation of the energetically most favorable kink angle ω^* with respect to the mode-mixity parameter γ for various values of the ratio $\Delta l/l$.

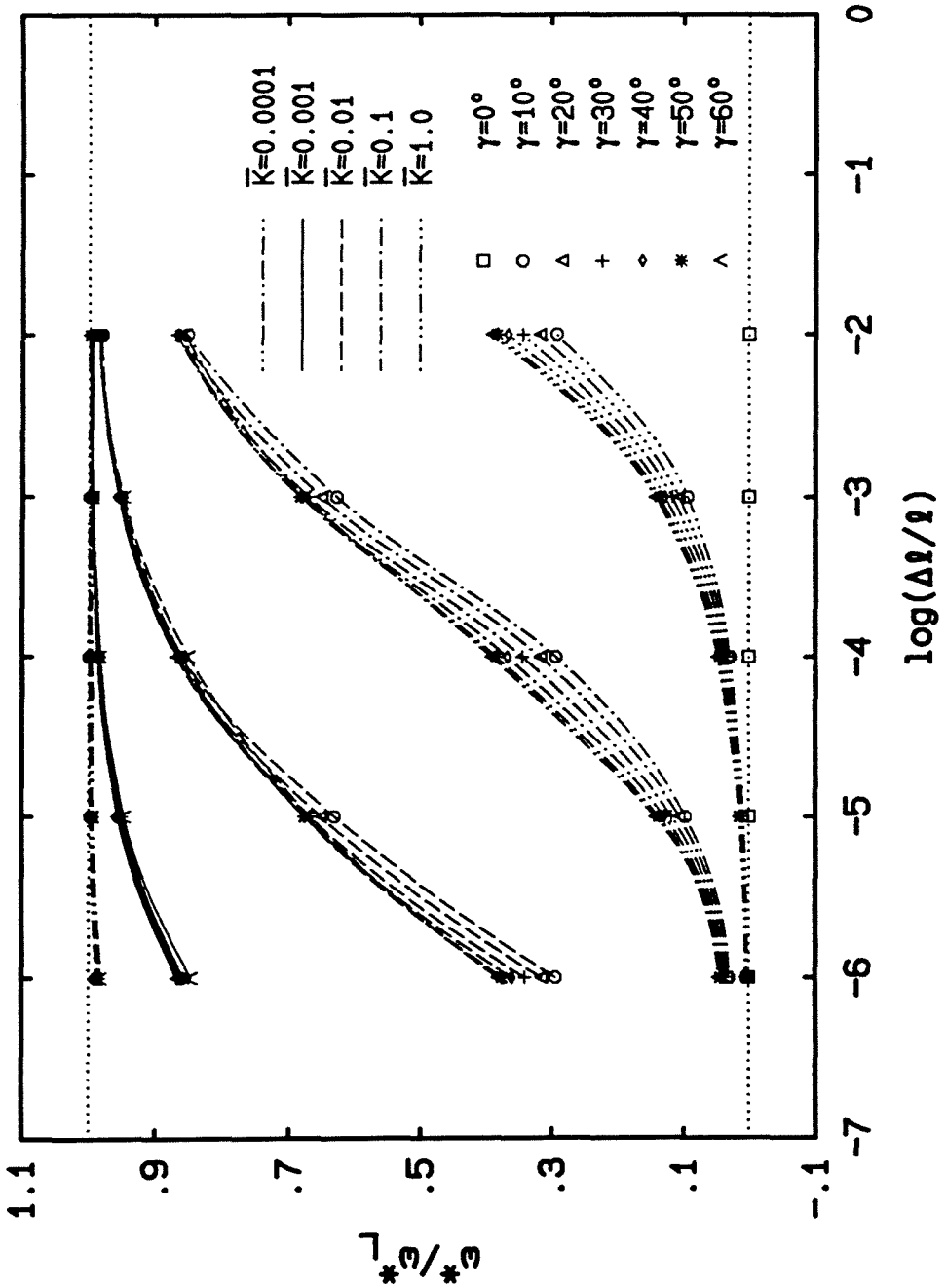

Figure 4. Ratio of the "nonlinear" to the "linear" kink angle versus $\Delta l/l$ for various values of the mode-mixity parameter γ and amplitude $\bar{K}$ characterizing the crack tip loading conditions before extension in a homogeneous sheet.

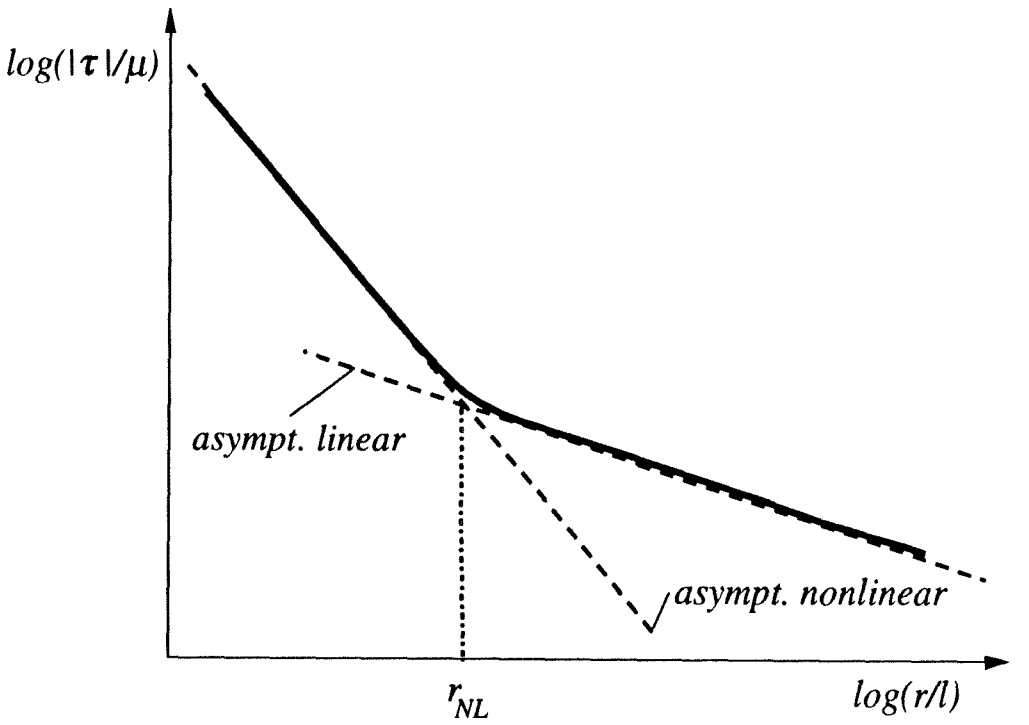

Figure 5. Radial variation of the norm of the true (Cauchy) stress tensor and determination of the size of the zone of dominance of the nonlinear effects by comparison with the linear and nonlinear asymptotic predictions (see, e.g., figure 18 of [16]).

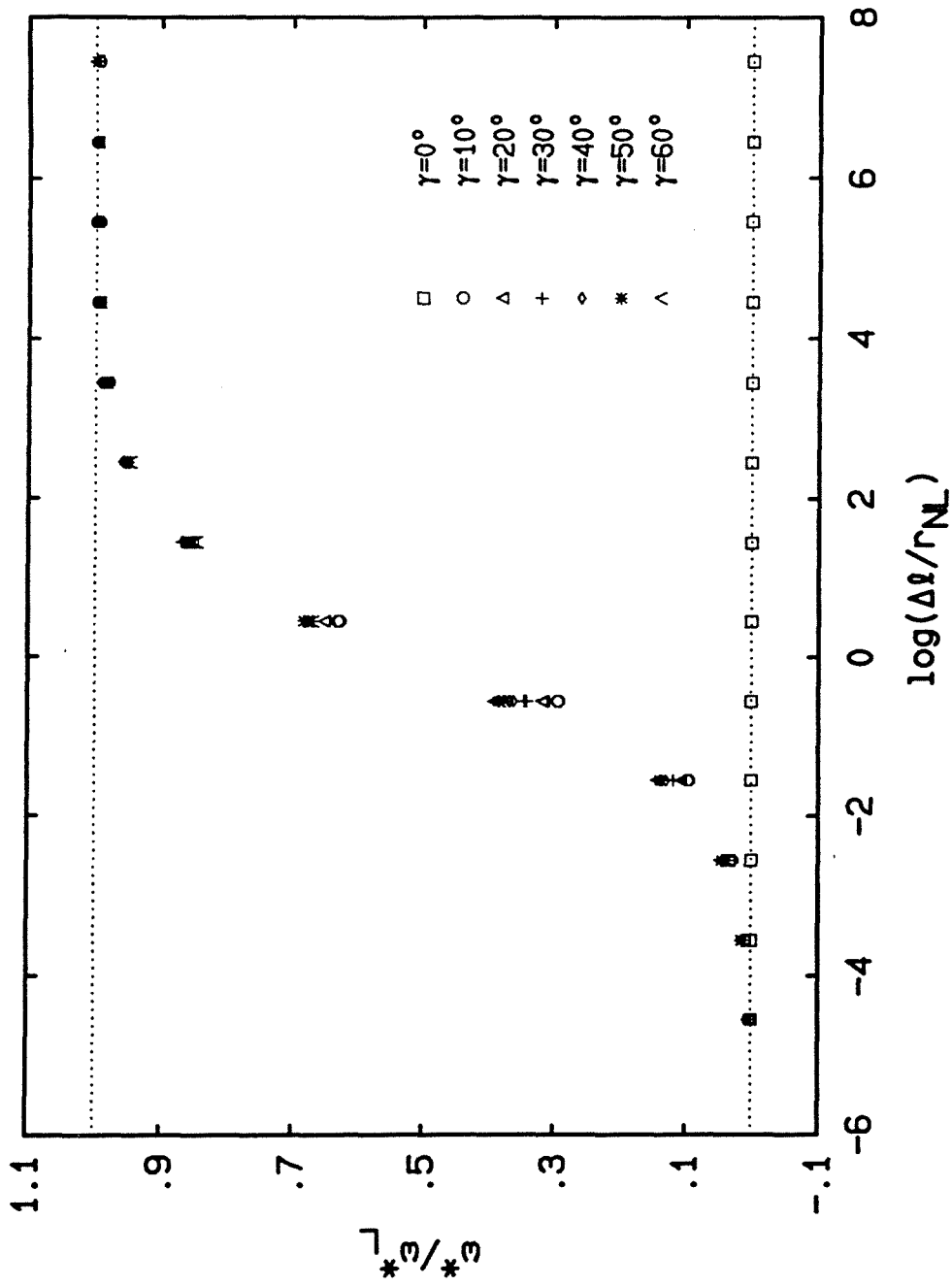

Figure 6. Variation of ω^* (normalized by the linear value ω_L^*) with respect to the crack extension length Δl (normalized by the size of the nonlinear zone r_{NL} defined in (3.1)).

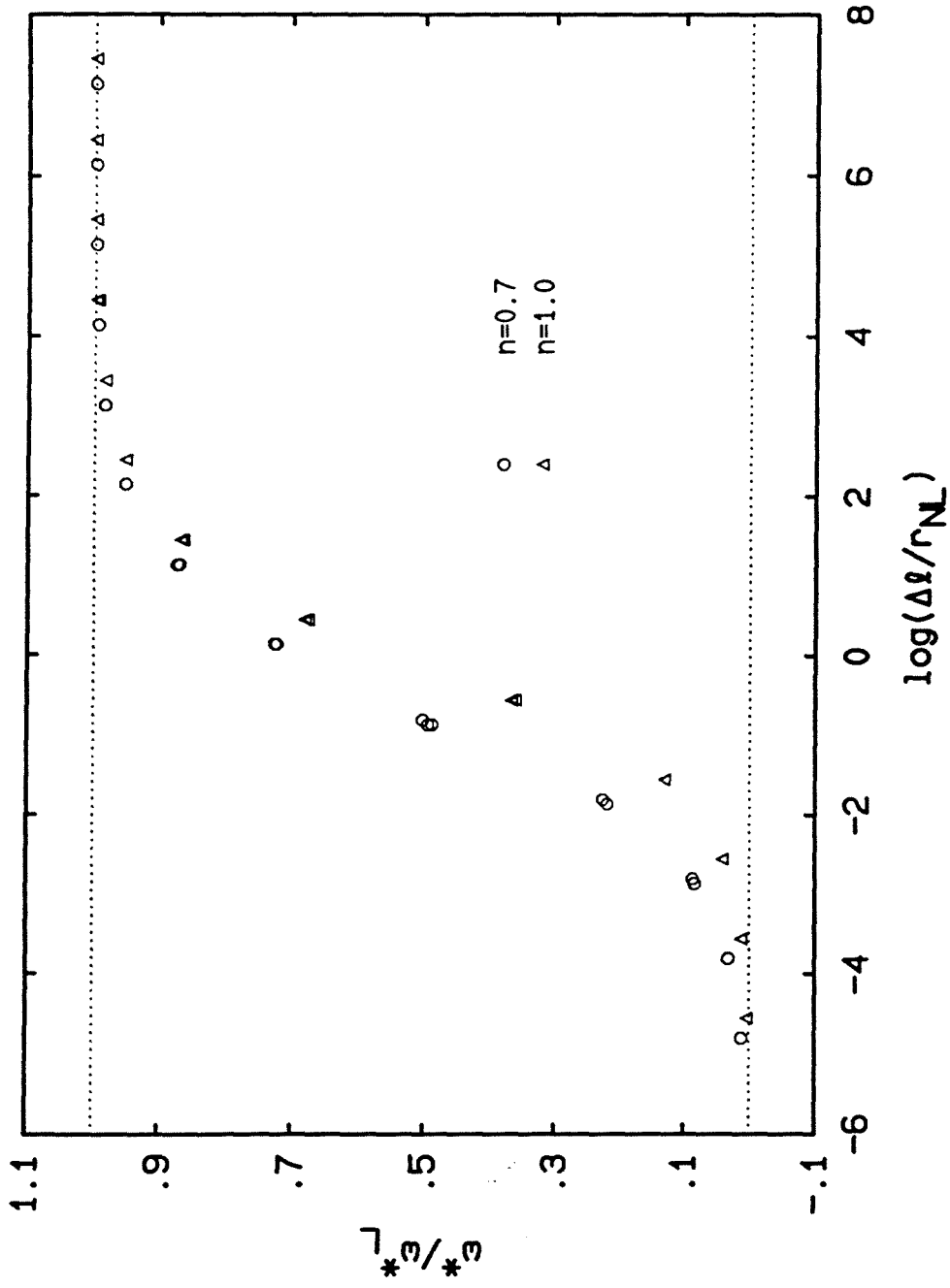

Figure 7. Kink angle ω^* versus $\Delta l/r_{NL}$ for $\gamma = 40^\circ$ and for two values of the "hardening" exponent $n = 0.7$ and 1.0.

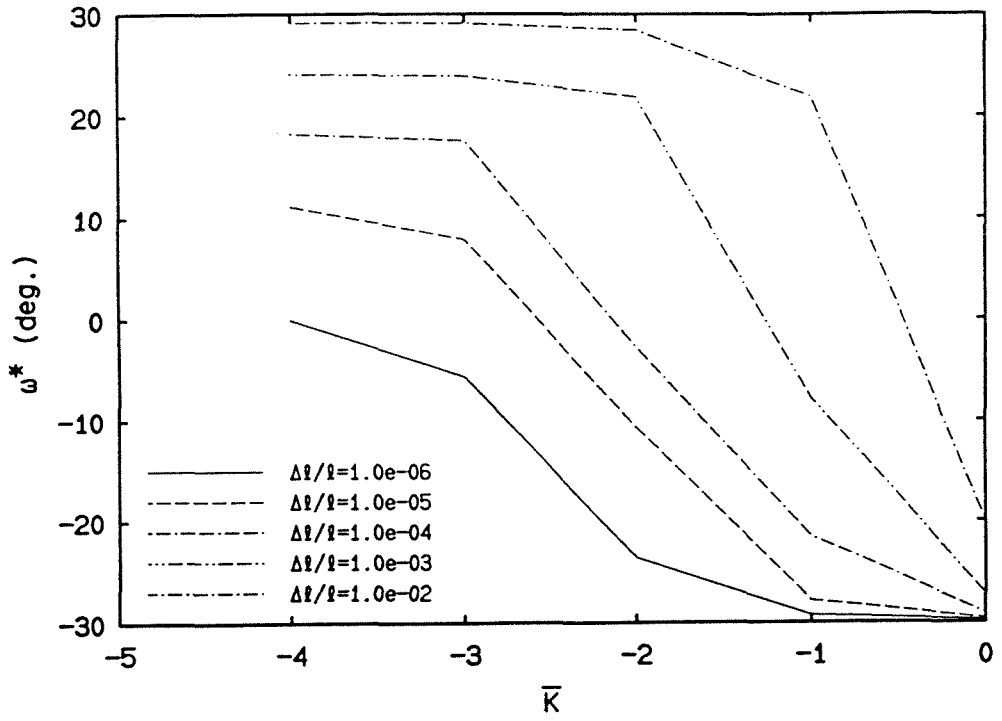

(a)

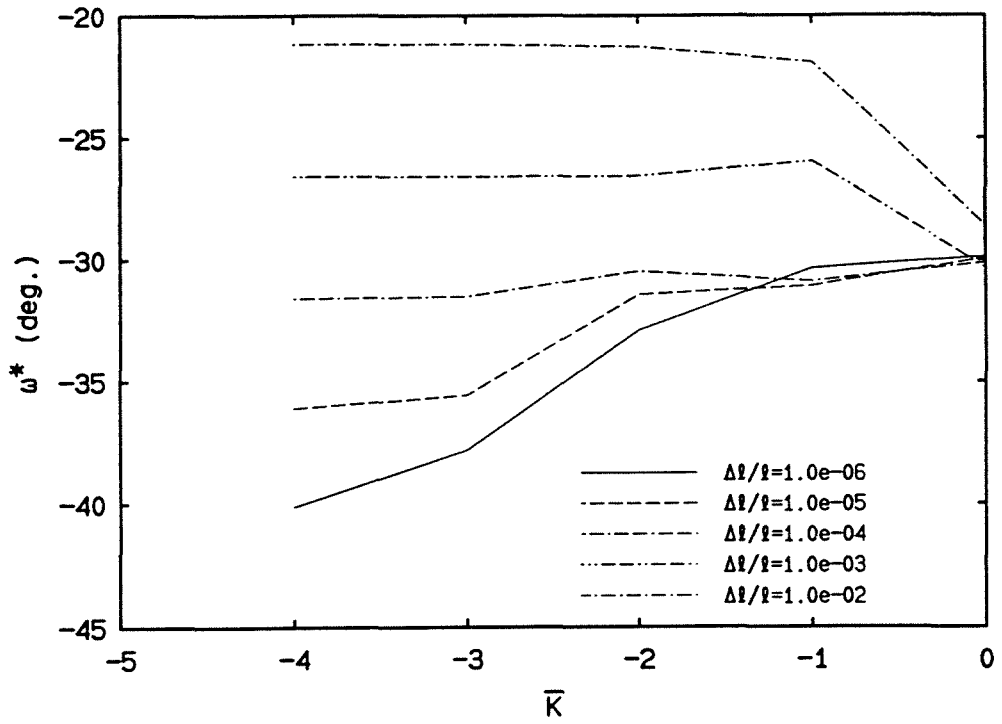

(b)

Figure 8. Variation of ω^* with respect to the amplitude $\overline{K}$ of the applied far-field loading in the bimaterial situation for various values of the crack extension length $\Delta l/l$ showing a transition between the "linear" value (obtained for $\overline{K} \leq 10^{-4}$) and the unique "nonlinear" value which is independent of γ: (a) $\gamma = -30^\circ$, (b) $\gamma = 0^\circ$.

Finite strains at the tip of a crack in a sheet of hyperelastic material : I. Homogeneous case.

Abstract.

This paper describes an asymptotic analysis of the strain and stress fields at the tip of a crack in a sheet of incompressible hyperelastic material. The investigations are carried out within the framework of finite elastostatics and for the class of Generalized Neo-Hookean materials. Both the symmetric (mode I) and non-symmetric (mixed-mode) cases are considered. It is shown that the latter situation corresponds locally to a rigid body rotation of the symmetric fields. The effect of the "hardening" parameter on crack tip blunting is investigated analytically and numerically.

1.- Introduction.

Most fracture mechanics investigations beyond the scope of the linearized theory of elasticity involve modifications of the linear constitutive relation in favor of more complex and realistic material models, while retaining the kinematic assumption of infinitesimal deformations (see, e.g., [1-4]). But these analyses often yield strain fields which are locally unbounded, in contradiction to the underlying assumption that justify the kinematic linearization.

In the past two decades, several analytical investigations have been documented which study the effect of relinquishing the small deformation assumption on the near-tip fields. The first of these analyses, by Wong and Shield [5], investigated the case of

a crack in a biaxially loaded sheet of Neo-Hookean material, in the framework of finite strain plane stress theory of elasticity. The method of successive approximations employed there required however that the deformations be large across the whole sheet. In two successive papers, Knowles and Sternberg [6,7] conducted an asymptotic plane strain analysis of a symmetrically loaded traction free crack in a slab of compressible hyperelastic material. The constitutive model adopted in their investigation was dictated by the large strain behavior of the material and allowed for a wide range of "hardening" (and "softening") characteristics. An additional indication of the finite strain effect on the near-tip fields was given by Knowles [8] in his investigation of the large antiplane shear deformations at the tip of a crack in a homogeneous slab of Generalized Neo-Hookean incompressible material. These pioneering works are summarized in two survey papers [9,10].

More recently, the general plane strain problem (mixed-mode loading) was studied by Stephenson [11] and by Le [12] for the incompressible and compressible cases respectively. The impossibility of an antisymmetric (mode II) solution within the framework of nonlinear elasticity, as was first observed in [11], was further analyzed by Knowles [13] who showed that, due to the nonlinear effects, crack opening is to be expected when mode II loading is applied away from the crack tip, even if the amount of loading is small.

Finally, motivated by the recent resurgent interest in bimaterial fracture, two asymptotic analyses of the near-tip stress and strain fields for an interface crack between two hyperelastic materials were produced. In [14], Knowles and Sternberg studied the case of a bimaterial sheet made of two Neo-Hookean materials. They showed that, in this case, the oscillatory singularities appearing in the linear asymptotic solution are not present when the infinitesimal strain assumption is relinquished and that a smooth opening of the crack is obtained regardless of the far-field loading

conditions. Similar conclusions were obtained by Herrmann [15] in his finite plane strain investigation of an interface crack between two slabs of compressible material. The material model used in [15] is more general than the Neo-Hookean model used in [14] and allows for a difference in the hardening behaviors of the components of the bimaterial combination.

Our objective in this series of papers is to perform an in-depth study of the problem of a crack in a homogeneous and bimaterial sheet made of a class of incompressible hyperelastic materials. The constitutive model used throughout this work is the so-called Generalized Neo-Hookean (GNH) model, introduced by Knowles [8] in his investigation of the finite strain antiplane shear case. This material model presents enough complexity to capture a fairly wide range of material behaviors but, at the same time, its simplicity makes it accessible to an asymptotic analysis. Furthermore, it includes, as a special case, the Neo-Hookean model previously used by Knowles and Sternberg [14] in their bimaterial asymptotic solution which has been confirmed numerically by Ravichandran and Knauss [16] and which can be used as a reference for later comparison purposes.

In this first paper, we consider the situation of a crack in a homogeneous sheet of GNH material. This preliminary analysis, which deals with both the symmetric (mode I) and non-symmetric (mixed-mode) cases and contains information relevant to subsequent papers on bimaterial fracture problems, starts with a review of the relations governing the plane stress nonlinearly elastic theory and a brief presentation of the GNH model in section 2. The asymptotic analysis for the symmetrically loaded crack will be summarized in section 3 while the mixed-mode situation will be delineated in section 4. The fifth section will contain a discussion of the results and their implications on the crack blunting and propagation behavior; that section concludes with the results of a "small-scale yielding" boundary-layer type numerical analysis.

The next paper [17] covers some special cases of the bimaterial situation : in the first of these, both components are assumed to possess the same "hardening" characteristics; in the second problem, one of the components is considered as rigid. These "intermediate steps" of analysis allow us to better understand the effect of blunting and elastic modulus mismatch on the interface crack-tip fields. In the third and final paper [18], the general (and more complex) case of two bonded GNH sheets is considered. In all cases, at least the first two terms of the asymptotic expansion are obtained and a full-field numerical investigation using the finite element method is performed in order to connect the resulting asymptotic solution to the far-field loading conditions.

2.- Finite plane stress elastostatics - Generalized Neo-Hookean model.

Throughout this work, we shall deal with finite plane stress deformations in a sheet made of a class of homogeneous, isotropic, incompressible, hyperelastic materials, in the absence of body forces. As a preliminary to the asymptotic analysis, the present section contains a brief review of the basic relations governing the nonlinear theory of plane stress elastostatics and a presentation of the material model. A more complete description of the nonlinear equilibrium theory of plane stress can be found in [14].

Consider a body $\mathcal{B}$ which, in an undeformed configuration, occupies a thin cylindrical region $\mathcal{D}$, the mid-plane of which is denoted by Π. By introducing a Cartesian coordinate system on Π, one can associate with every point of the plane a two-dimensional position vector[1] $\boldsymbol{x}$ characterized by the material (or undeformed)

[1] Throughout this paper, letters in boldface denote two-dimensional vectors and second-order tensors.

coordinates $(x_1,\ x_2)$. Let[2] y_α denote the spatial (deformed) coordinates of the mid-plane points, defined by the mapping

$$\boldsymbol{y} = \hat{\boldsymbol{y}}(\boldsymbol{x}) = \boldsymbol{x} + \boldsymbol{u}(\boldsymbol{x}), \qquad (\boldsymbol{x} \in \Pi), \tag{2.1}$$

where $\boldsymbol{y}$ represents the deformed position vector and $\boldsymbol{u}$ the displacement vector. We assume that the mapping $\boldsymbol{y}$ is twice continuously differentiable and has a unique inverse on Π. The deformation-gradient field $\boldsymbol{F}$ associated with $\boldsymbol{y}$ is given by

$$\boldsymbol{F} = \nabla \boldsymbol{y} = \boldsymbol{1} + \nabla \boldsymbol{u}, \tag{2.2}$$

where $\boldsymbol{1}$ is the unit tensor and the gradient is computed with respect to the undeformed configuration. Let $\boldsymbol{G}$ denote the corresponding left Cauchy-Green deformation tensor and I and J, the associated scalar invariants defined as

$$\begin{aligned} &\boldsymbol{G} = \boldsymbol{F}\,\boldsymbol{F}^T, \\ &I = tr\,\boldsymbol{G} = y_{\alpha,\beta}\,y_{\alpha,\beta} = \lambda_1^2 + \lambda_2^2, \qquad \text{on } \Pi, \\ &J = det\,\boldsymbol{F} = y_{1,1}y_{2,2} - y_{1,2}y_{2,1} = \lambda_1\lambda_2 = 1/\lambda, \end{aligned} \tag{2.3}$$

where λ_α are the in-plane principal stretches and λ is the transverse stretch. The relation between the in-plane and out-of-plane stretches is motivated by the isochoric property of the deformations associated with the incompressibility of the material.[3]

Let $\boldsymbol{\tau}$ denote the true (Cauchy) stress field accompanying the deformation. The equilibrium equations in the absence of body forces are

$$div\ \boldsymbol{\tau} = \boldsymbol{0}, \qquad \boldsymbol{\tau} = \boldsymbol{\tau}^T, \qquad \text{on } \Pi^*, \tag{2.4}$$

---

[2] Greek indices range over the values (1,2). Summation on repeated indices is implied, unless specified otherwise.

[3] See [14] for more details.

where Π^* is the image of Π under the deformation $\boldsymbol{y}$. In terms of the nominal (Piola) stress field $\boldsymbol{\sigma}$ related to $\boldsymbol{\tau}$ through

$$\boldsymbol{\sigma} = \boldsymbol{\tau}\, \boldsymbol{F}^{-T}, \qquad \text{on } \Pi, \tag{2.5}$$

the equilibrium equations (2.4) can be written as

$$div\, \boldsymbol{\sigma} = \boldsymbol{0}, \qquad \boldsymbol{\sigma}\boldsymbol{F}^T = \boldsymbol{F}\, \boldsymbol{\sigma}^T, \qquad \text{on } \Pi. \tag{2.6}$$[4]

The relationship between nominal and true stresses is also the subject of the following results : let Γ be a regular arc in Π and $\Gamma^*=\boldsymbol{y}(\Gamma)$ its deformation image in Π^*, and let $\boldsymbol{n}$ and $\boldsymbol{n}^*$ be the oriented unit normal vectors on Γ and Γ^* respectively, then (2.5) implies

$$\boldsymbol{\tau}\boldsymbol{n}^* = \boldsymbol{0} \quad on\ \Gamma^* \quad \Leftrightarrow \quad \boldsymbol{\sigma}\boldsymbol{n} = \boldsymbol{0} \quad on\ \Gamma. \tag{2.7}$$

This fundamental result indicates that traction-free boundary conditions can equivalently be applied on the undeformed geometry without *a priori* knowledge of the deformation.

To conclude this presentation of the basic relations governing the nonlinear plane stress theory for incompressible homogeneous hyperelastic material, we introduce the plane stress elastic potential U, a function of the two scalar invariants I and J such that

$$\boldsymbol{\sigma} = 2U_I\boldsymbol{F} + JU_J\boldsymbol{F}^{-T}, \qquad \text{on } \Pi, \tag{2.8}$$

where U_I and U_J designate the partial derivatives of $U(I,J)$ with respect to I and J respectively. The choice of the elastic potential will strongly influence the form of the

[4] Unlike $\boldsymbol{\tau}$, $\boldsymbol{\sigma}$ is not, in general, symmetric.

solution. Throughout this analysis, we are concerned with the Generalized Neo-Hookean (GNH) model, the three-dimensional elastic potential of which is given by

$$W(I_1, I_2) = \frac{\mu}{2b}\left\{\left[1+\frac{b}{n}(I_1-3)\right]^n - 1\right\}, \tag{2.9}$$

where I_1 and I_2 are the three-dimensional scalar invariants associated with the deformation (see section 2 of [14] for more details on the transition between the three-dimensional and the plane stress equations). In (2.9), μ (the shear modulus), b and n are the three material parameters which determine the linearly elastic, "yielding" and "hardening" behaviors of the material, respectively, as shown later in this section. The corresponding plane stress elastic potential is given by

$$U(I, J) = \frac{\mu}{2b}\left\{\left[1+\frac{b}{n}\left(I+J^{-2}-3\right)\right]^n - 1\right\}. \tag{2.10}$$

As mentioned before, this material model has been introduced by Knowles in his asymptotic analysis of the antiplane shear (mode III) case [8]. It has also been used by Rosakis and Rosakis [19] in the finite elastic analysis of the screw dislocation problem and by Rajagopal and Tao [20] in their investigation of the inhomogeneous deformation of a GNH wedge. Note that the Generalized Neo-Hookean formulation reduces to the Neo-Hookean one when $n=1$. Combining (2.8) and (2.10), the nominal stresses become

$$\sigma_{\alpha\beta} = \mu A^{n-1}\{y_{\alpha,\beta} - \lambda^3 \varepsilon_{\alpha\mu}\varepsilon_{\beta\nu}y_{\mu,\nu}\}, \tag{2.11}$$

where $A = 1+b(I+\lambda^2-3)/n$ and $\varepsilon_{\alpha\beta}$ is the two-dimensional alternator ($\varepsilon_{11}=\varepsilon_{22}=0$, $\varepsilon_{12}=-\varepsilon_{21}=1$). The Cauchy stresses are given by (2.5) and (2.11) as

$$\tau_{\alpha\beta} = \mu A^{n-1}\{y_{\alpha,\gamma}y_{\beta,\gamma} - \lambda^2\delta_{\alpha\beta}\}. \tag{2.12}$$

Finally, the equilibrium equations (2.6), written in terms of the deformed coordinates, yield, for this class of materials,

$$A^{n-2}\left\{\frac{b(n-1)}{n}\left(\frac{\partial I}{\partial x_\beta}+\frac{\partial \lambda^2}{\partial x_\beta}\right)\left(y_{\alpha,\beta}-\lambda^3\varepsilon_{\alpha\mu}\varepsilon_{\beta\nu}y_{\mu,\nu}\right)+A\left(\nabla^2 y_\alpha-\frac{\partial \lambda^3}{\partial x_\beta}\varepsilon_{\alpha\mu}\varepsilon_{\beta\nu}y_{\mu,\nu}\right)\right\}=0, \quad (2.13)$$

where A, I and λ have been defined in (2.3) and (2.11).

In order to understand the physical significance of the material parameters introduced in the GNH model, it is instructive to examine the response in a three-dimensional homogeneous deformation corresponding to a uniaxial stress parallel to the x_2-axis. In such a case, the deformations are

$$y_1 = x_1/\sqrt{\lambda}, \qquad y_2 = \lambda\, x_2, \qquad y_3 = x_3/\sqrt{\lambda}, \qquad (2.14)$$

where λ is the uniaxial elongation in the x_2-direction. The engineering (nominal) uniaxial stress is readily found to be

$$\sigma_{22} = \mu\left[1+\frac{b}{n}\left(\lambda^2+\frac{2}{\lambda}-3\right)\right]^{n-1}\left(\lambda-\frac{1}{\lambda^2}\right). \qquad (2.15)$$

The effect of the "hardening" exponent n is illustrated in figure 1. The stress-strain curve will keep a positive slope as long as $n \geq 1/2$. It can be shown that the equations of equilibrium lose their ellipticity when $n < 1/2$. Throughout this analysis, we will consider only the elliptic situation $(n > 1/2)$, excluding thereby the appearance of shocks and discontinuities usually associated with hyperbolic problems [21, 22].

The effect of the parameter b on the uniaxial stress-strain curve of GNH materials is demonstrated in figure 2 for $n=0.6$, showing that b controls the "extent of linearity," or, equivalently, the "yielding level" of the material.

3.- Local analysis of the symmetric (mode I) crack problem.

Problem formulation.

The global crack problem, illustrated in figure 3, consists of a crack of length $2l$ embedded in an infinite sheet of GNH material under uniaxial tension. The coordinate system is chosen on the mid-plane such that the crack line $\mathcal{L}$ is

$$\mathcal{L} = \{\boldsymbol{x} \mid -l \le x_1 \le l,\ x_2 = 0\}, \tag{3.1}$$

and the (undeformed) domain Π is the whole $(x_1,\ x_2)$ plane exterior to $\mathcal{L}$.

The determination of the full-field solution to the global crack problem consists of finding a deformation field $\hat{\boldsymbol{y}}(\boldsymbol{x})$ which is twice continuously differentiable on Π, continuous up to $\mathcal{L}$ and continuously differentiable up to the interior of the segment $\mathcal{L}$ and satisfying the equilibrium equations (2.13). Furthermore, the associated nominal stress field has to conform to the traction-free boundary conditions along $\mathcal{L}$, i.e.,

$$\sigma_{\alpha 2}(|x_1| < l\ ,\ x_2 = 0^{\pm}) = 0. \tag{3.2}$$

In addition, the deformation has to satisfy the kinematic loading conditions at infinity

$$\hat{\boldsymbol{y}}(\boldsymbol{x}) = \overset{\infty}{\boldsymbol{F}}\boldsymbol{x} + O(1), \qquad \text{as } x_1^2 + x_2^2 \to \infty, \tag{3.3}$$

where

$$\left[\overset{\infty}{F}_{\alpha\beta}\right] = \begin{bmatrix} \overset{\infty}{\lambda}_1 & 0 \\ 0 & \overset{\infty}{\lambda}_2 \end{bmatrix}, \qquad \overset{\infty}{\lambda}_2 > 1, \tag{3.4}$$

with $\overset{\infty}{\lambda}_\alpha$ denoting the principal stretches at infinity. This particular choice of $\overset{\infty}{\boldsymbol{F}}$ insures a symmetric (mode I) loading of the sheet. The more general mixed-mode loading situation will be considered in section 4.

The full-field solution to the global crack problem described above is too complex to be expressed in analytical form. However, taking for granted the existence of a solution to the global crack problem, it is possible to perform an asymptotic analysis of the stress and strain fields in the immediate vicinity of the crack tips. As will be shown later in this section, the only length scale appearing in this purely local analysis is associated with an energy parameter (the $\mathcal{J}$-integral) which is itself related to the amplitude of the far-field loading, the specimen geometry and the material characteristics of the GNH sheet. We can therefore define a generic geometry that will be used throughout this asymptotic investigation and which could be applied in various "global" situations : it consists of a semi-infinite crack embedded in an infinite sheet of GNH material as shown in figure 4. The crack line $\mathcal{L}$ is now expressed as

$$\mathcal{L} = \{\boldsymbol{x} \mid \quad x_1 \leq 0, \quad x_2 = 0\}. \tag{3.5}$$

In the local analysis that follows, it is more convenient to replace the Cartesian coordinates (x_1, x_2) by the corresponding polar coordinates (r, θ) defined in figure 4.

The "redefined" local crack problem consists thus in determining a deformation $\hat{\boldsymbol{y}}(\boldsymbol{x})$ satisfying the same continuity requirements and equilibrium equations as in the global problem, but with somewhat different boundary conditions : the stress-free conditions along the crack faces become

$$\sigma_{\alpha 2}(r, \theta = \pm\pi) = 0, \qquad (r > 0), \tag{3.6}$$

while the far-field loading conditions can be expressed locally as the symmetry requirements

$$\begin{aligned} y_1(r,\theta) &= y_1(r,-\theta), \\ y_2(r,\theta) &= -y_2(r,-\theta). \end{aligned} \tag{3.7}$$

Asymptotic analysis - first term.

The existence of a solution to the local problem is conditioned by the choice of asymptotic representation of the deformation field; we assume that, in the vicinity of the crack-tip, the deformation $\hat{y}(x)$ has the form

$$\begin{cases} y_1(r,\theta) = r^p v_1(\theta) + o(r^p), \\ y_2(r,\theta) = r^m v_2(\theta) + o(r^m), \end{cases} \qquad (r \to 0, -\pi \le \theta \le \pi), \qquad (3.8)$$

where the angular functions $v_\alpha(\theta) \in C^2([-\pi,\pi])$. We also require that the exponents m and p satisfy

$$m \text{ and } p > 0, \qquad m \text{ and/or } p < 1. \qquad (3.9)$$

The inequalities (3.9) are motivated by the anticipated fact that not all deformation gradients remain bounded as $r \to 0$, while the displacements have to be finite at the crack tip.

It is possible to proceed directly to the asymptotic analysis without further restriction on the value of the exponents m and p. However, one can simplify the analysis greatly by considering the following two arguments : first, we can adopt the heuristic considerations introduced by Knowles and Sternberg [6] leading to the inequality

$$p > m, \qquad (3.10)$$

motivated by an examination of the shape of the deformed crack boundaries. The case $p<m$ corresponds to a cusp-like opening of the crack while the deformed crack would be wedge-shaped in the vicinity of the tip if $p=m$. The only physically acceptable situation, reinforced by various experimental observations, is such that the crack opens smoothly, as predicted by (3.10). The second simplifying argument involves the a

priori estimation of the exponent of the lower order term *(m)* through the use of the conservation integral $\mathcal{J}$, introduced by Rice [23] and generalized by Knowles and Sternberg [24]. The reasoning is based on the fact that the asymptotic solution must satisfy the path-independence of $\mathcal{J}$ defined by

$$\mathcal{J} = \int_{\Gamma} (W n_1 - \sigma_{\alpha\beta} n_\beta y_{\alpha,1}) ds, \tag{3.11}$$

where W is the elastic potential defined in (2.9) and Γ is any smooth contour with outward normal $\boldsymbol{n}$ surrounding the crack tip, starting from the lower crack face and ending on the upper one (figure 4). By choosing a vanishingly small contour and examining the radial dependence of the lower order terms of (3.11) after substituting the asymptotic representation (3.8), one must impose

$$m = 1 - 1/2n \tag{3.12}$$

in order to ensure a finite limit to the $\mathcal{J}$-integral which is consistent with the assumed existence of a solution to the global problem described earlier. This reasoning allows us to transform the eigenvalue problem associated with the lower order term (in $r^m v_2(\theta)$) into a mere differential equation. The same argument was used by Rice and Rosengren [2] in their investigation of the elasto-plastic (HRR) asymptotic field and was examined by Knowles and Sternberg [6].[5]

We can now proceed to the determination of the other asymptotic quantities p, $v_1(\theta)$ and $v_2(\theta)$. By examining the order of every term appearing in the equilibrium equations (2.13) with the aid of (3.10), it can be shown that (2.13) can be reduced to

$$(n-1)\frac{\partial I}{\partial x_\beta} y_{\alpha,\beta} + I \nabla^2 y_\alpha = 0, \qquad (r \to 0, -\pi \le \theta \le \pi), \tag{3.13}$$

[5] See discussion at the end of section 5 in [6].

where $I = y_{\gamma,\delta}\, y_{\gamma,\delta}$. Substituting (3.8) into (3.13), the equilibrium equations yield the following differential equations

$$\begin{aligned} &B_{v_2} D_{v_1} + (n-1)[2p(m-1)B_{v_2} v_1 + \dot{B}_{v_2} \dot{v}_1] = 0, \\ &B_{v_2} D_{v_2} + (n-1)[2m(m-1)B_{v_2} v_2 + \dot{B}_{v_2} \dot{v}_2] = 0, \end{aligned} \tag{3.14}$$

where $(\dot{})$ denotes $d(\,)/d\theta$ and

$$\begin{aligned} B_{v_2}(\theta) &= m^2 v_2^2(\theta) + \dot{v}_2^2(\theta), \\ D_{v_1}(\theta) &= p^2 v_1(\theta) + \ddot{v}_1(\theta), \\ D_{v_2}(\theta) &= m^2 v_2(\theta) + \ddot{v}_2(\theta). \end{aligned} \tag{3.15}$$

The boundary conditions are asymptotically satisfied by

$$\dot{v}_\alpha(\pm\pi) = 0, \tag{3.16}$$

while the symmetry of the deformations requires that

$$\begin{aligned} &\dot{v}_1(0) = 0 \qquad (v_1(\theta) \text{ is even}), \\ &v_2(0) = 0 \qquad (v_2(\theta) \text{ is odd}). \end{aligned} \tag{3.17}$$

As mentioned above, the second of (3.14), together with (3.16) and the second of (3.17) form an eigenvalue problem in $(m, v_2(\theta))$ which has been reduced through (3.12) to a nonlinear differential equation which seems to be common to various finite strain situations : it was first solved by Knowles and Sternberg [6] in the compressible plane strain case for a quite different material model; the same equation was then encountered by Knowles [8] and Stephenson [11] in the incompressible anti-plane shear and plane strain situations. Its solution is given by

$$v_2(\theta) = a\, f(\theta; n), \qquad (-\pi \le \theta \le \pi), \tag{3.18}[6]$$

where a is an undetermined constant and

---

[6] For normalization purpose, we choose $f(\pi;n)=1$.

$$f(\theta;n)=\left[n(\omega+k\cos\theta)\right]^{\frac{n-1}{2n}}\sin\frac{\theta}{2}\left[1-\frac{2k^2\cos^2\theta/2}{1+\omega}\right]^{1/2}, \qquad (3.19)$$

with

$$k=1-1/n, \qquad (3.20)$$

$$\omega=(1-k^2\sin^2\theta)^{1/2}. \qquad (3.21)$$

The angular function $f(\theta;n)$ is represented in figure 5.

Substitution of (3.18)-(3.21) into the first of (3.14) results in the second-order linear differential equation

$$\ddot{v}_1+\frac{k^2\sin\theta}{(1-k^2\sin^2\theta)^{1/2}}\dot{v}_1+p(p-k)v_1=0, \qquad (3.22)$$

which, with (3.16) and the first of (3.17), forms an eigenvalue problem for $(p, v_1(\theta))$. Our efforts to obtain a closed-form solution to this eigenvalue problem have been unsuccessful so far. However, the WKB theory [25] can be used to obtain a fairly good approximation of p and $v_1(\theta)$ for $n\geq 0.55$. The details of the computation are summarized in the appendix.

The eigenvalue problem (3.22) can also be readily solved numerically. The variation of p and m with respect to n is shown in figure 6, while the angular variation of $v_1(\theta)$ is presented in figure 7 in the form

$$v_1(\theta)=c\,g(\theta;n), \qquad (3.23)$$

where $g(\theta;n)$ has been normalized such that $g(0;n)=1$ and c is a scalar. Note that, for $0.5<n<1$, the first asymptotic term for both y_1 and y_2 generates unbounded gradients as the crack tip is approached, since both m and p are less than unity.

Domain of validity of the asymptotic solution.

It is appropriate at this point of the analysis to discuss the domain of validity of the asymptotic solution described above. As mentioned in the preliminary presentation of the GNH material model, the hardening exponent n must be strictly greater than $1/2$ to ensure the ellipticity of the equilibrium equations (2.13).

But an examination of the order of the terms constituting (2.13) which led to the asymptotic form (3.13) of the equilibrium equations introduces an additional restriction on the values of n for which the asymptotic solution (3.8), (3.12), (3.18)-(3.21) and (3.23) is valid. The lower-order term for the second deformed coordinate $y_2(r,\theta)$ is valid for all values of $n>1/2$. But the most restrictive assumption

$$y_{1,\beta} = O(r^{p-1}) >> \lambda^3 \varepsilon_{1\mu}\varepsilon_{\beta\nu} y_{\mu,\nu} = O(r^{5-3p-2m}), \tag{3.24}$$

used in the derivation of (3.13), requires that

$$p<1+1/4n. \tag{3.25}$$

This condition is represented by a dotted line in figure 6. The acceptable range for the hardening exponent for the approximation of $y_1(r,\theta)$ to be valid is thus

$$1/2 < n \lesssim 7/5. \tag{3.26}$$

For higher values of n, the nature of the first asymptotic equilibrium equation changes drastically and the separable form (3.8) of the near-tip solution is not expected to be applicable.

Additional terms.

The linearized theory of elasticity suggests the appearance of only one singular term $(O(r^{-1/2}))$ in the asymptotic expansion of the near-tip stress and strain fields. In this section, we examine whether higher-order terms in the asymptotic expression of the deformations cannot also lead to singular values of the strains in the nonlinear situation.

Let us write the additional terms as

$$\begin{cases} y_1(r,\theta) \sim c\, r^p g(\theta;n) + r^s w_1(\theta), \\ y_2(r,\theta) \sim a\, r^m f(\theta;n) + r^q w_2(\theta), \end{cases} \tag{3.27}$$

where m, p, f and g have been given analytically or numerically before, a and c are scalars, $s>p$, $q>m$ and $w_1(\theta)$ is even while $w_2(\theta)$ is odd. After lengthy but elementary computations, one finds that the only term capable of generating singular terms[7] is the term of order r^q which can be written as

$$w_2(\theta) = d\, h(\theta;n), \tag{3.28}$$

where d is an undetermined constant and $h(\theta;n)$ satisfies

$$B_f D_h + 2D_f E_2 + (n-1)(2q(m-1)B_f h + \dot{B}_f \dot{h} + 2m(m+q-2) f E_2 + 2\dot{f}\dot{E}_2) = 0, \tag{3.29}$$

with the boundary conditions $h(0) = \dot{h}(\pi) = 0$ and where

$$B_f = \dot{f}^2 + m^2 f, \qquad D_f = \ddot{f} + m^2 f, \qquad E_2 = mqfh + \dot{f}\dot{h}. \tag{3.30}$$

The eigenvalue problem (3.29)-(3.30) has been solved analytically by Knowles and Sternberg [6] who introduced the following transformation

---

[7] i.e., such that its order is at most unity.

$$\cos\zeta = \frac{1-k}{\sqrt{2}}\frac{\sqrt{1+k\sin^2\theta-\omega\cos\theta}}{\omega+k\cos\theta}, \qquad (3.31)$$
$$V(\zeta) = [\omega+k\cos\theta]^{-q}h(\theta),$$

where k and ω are given by (3.20) and (3.21) respectively. Note that $\zeta(\theta=0)=\pi/2$ and $\zeta(\theta=\pi)=0$.

By using (3.31), (3.29) becomes

$$V''(\zeta)+\frac{4nq(nq-n+1)}{2n-1}V(\zeta)=0, \qquad (3.32)$$

which, with the transformed boundary conditions

$$V'(0)=V(\pi/2)=0, \qquad (3.33)$$

readily yields

$$q=(n-1+\sqrt{n^2+16n-8})/2n, \qquad (3.34)$$
$$h(\theta;n)=n^q(\omega+k\cos\theta)^q(4\cos^3\zeta-3\cos\zeta), \qquad (3.35)$$

where the multiplicative constant term in (3.35) has been added to obtain $h(\pi;n)=1$ (figure 8) and where the relation between θ and ζ is given by (3.31). A visualization of the variation of q with respect to the hardening exponent n is given in figure 6, showing that, for $n<9/14$, the second term also generates unbounded strains at the crack tip. It can be shown that, as n approaches $1/2$, additional singular terms appear in the asymptotic expansion of the second deformed coordinates y_2. The condition for validity of this higher-order term is identical to that of the first asymptotic exponent, i.e.,

$$q<1+1/4n. \qquad (3.36)$$

A discussion of the stress and strain fields associated with the derived asymptotic solution together with a numerical verification of the results is presented in the fifth section of this paper. In the next section, we summarize first the investigation of the non-symmetric (mixed-mode) case.

4.- Local analysis of the mixed-mode crack problem.

Introduction - problem formulation.

As mentioned in the introduction, two investigations of the general mixed-mode case, within the framework of finite elasticity have been produced so far, both concerning the plane strain case : the first one by Stephenson [11] for the incompressible situation and the last one by Le [12] who solved the compressible case. Both analyses yielded the somewhat surprising result that the near-tip deformation field is obtained through a mere rotation of the canonical symmetric (mode I) asymptotic field, the amplitude of the rotation being dictated by the far-field loading conditions. In both cases, this result was obtained through an argument based on the plane strain assumption which rules out any deformation normal to the plane of investigation. In this section, we examine whether a similar result is to be expected in the plane stress situation, in which a stretch transverse to the mid-plane is possible.

Let us first recall a result obtained by Stephenson [11] who showed, by investigating the effect of an antisymmetric displacement field

$$u_1(x_1, x_2) = u_1(x_1, -x_2), \qquad u_2(x_1, x_2) = -u_2(x_1, -x_2) \tag{4.1}$$

on the equilibrium equations, that the mode II crack problem fails to admit an antisymmetric solution about the plane of the crack under the nonlinear theory of finite plane strain. Although this important property was proven in the particular case of a

Mooney-Rivlin material, the author conjectured that it would be valid for "every legitimate choice of the plane-strain elastic potential" ([11], p.74). A numerical confirmation of this property in the GNH situation is presented in section 5.

The formulation of the global mixed-mode crack problem is similar to the symmetric situation described in section 3, except that the far-field deformation tensor $\overset{\infty}{\boldsymbol{F}}$ does not possess the diagonal form (3.4) but allows for loading in shear. The local crack problem is also identical to the mode I situation except that the symmetry requirements (3.7) do not apply.

First asymptotic term.

We start again from the general expression of the first asymptotic term in separable form

$$y_\alpha(r,\theta) \sim r^{m_\alpha} v_\alpha(\theta), \qquad \text{(no sum on } \alpha\text{)}, \tag{4.2}$$

where $m_\alpha > 0$ and at least one $m_\alpha < 1$ and where $v_\alpha \in C^2([-\pi,\pi])$. One can simplify the analysis of this term somewhat by noting that (4.2) may be replaced, without loss of generality, by

$$y_\alpha(r,\theta) \sim r^{m} v_\alpha(\theta). \tag{4.3}$$

This simplification, suggested in [11], is justified by the fact that if $\{\boldsymbol{y}, \boldsymbol{\sigma}\}$ is solution of the problem, so is $\{\boldsymbol{Q}\boldsymbol{y}, \boldsymbol{Q}\boldsymbol{\sigma}\}$ for all proper orthogonal tensors $\boldsymbol{Q}$.

As was the case for the symmetric case, the conservation of the $\mathcal{J}$-integral defined by (3.11) yields

$$m = 1 - 1/2n. \tag{4.4}$$

After substituting (4.3) into the asymptotic equilibrium equations (3.13), one obtains a system of coupled second-order differential equations

$$B\ddot{v}_\alpha + (n-1)\dot{B}\dot{v}_\alpha + mB\{2(n-1)(m-1)+m\}v_\alpha = 0, \tag{4.5}$$

where

$$B(\theta) = m^2 v_\gamma(\theta)v_\gamma(\theta) + \dot{v}_\gamma(\theta)\dot{v}_\gamma(\theta). \tag{4.6}$$

The boundary conditions along the crack faces remain

$$\dot{v}_\alpha(\pm\pi) = 0. \tag{4.7}$$

The solution to (4.5)-(4.7) can be written as

$$v_\alpha(\theta) = a_\alpha f(\theta;n), \qquad (-\pi \le \theta \le \pi), \tag{4.8}$$

where a_α are two scalars left undetermined by the present local analysis[8] and $f(\theta;n)$ is given by (3.19)-(3.21) and is shown in figure 5.

This first asymptotic term, however, yields an identically vanishing Jacobian and thus does not constitute a one-to-one mapping. Furthermore, it does not define the near-tip variation of the transverse stretch. These reasons motivate the search for a two-term expansion of the elastostatic crack-tip field.

Higher-order terms.

Motivated by the same argument that led to (4.3), we will seek a two-term approximation of the form

$$y_\alpha(r,\theta) \sim a_\alpha r^m f(\theta;n) + r^s w_\alpha(\theta), \tag{4.9}$$

[8] See discussion in section 5.

where $s>m$ and $w_\alpha(\theta) \in C^2([-\pi,\pi])$. An examination of the respective orders of the various terms constituting the equilibrium equations (2.13) shows that the same asymptotic form (3.13) can be used for the second term in (4.9) provided that the exponent s satisfies

$$m < s < \frac{3-m}{2} = 1 + \frac{1}{4n}. \tag{4.10}$$

Under these restrictions, (3.13) yields the following system of coupled linear second-order differential equations

$$\begin{aligned} &(a_1^2 + a_2^2)H_1^s(w_1) + 2a_1^2 H_2^s(w_1) + 2a_1 a_2 H_2^s(w_2) = 0, \\ &(a_1^2 + a_2^2)H_1^s(w_2) + 2a_1 a_2 H_2^s(w_1) + 2a_2^2 H_2^s(w_2) = 0, \end{aligned} \tag{4.11}$$

where a_α are the multiplicative constants of the first term and $H_\alpha^s(w)$ are two linear differential operators given by

$$\begin{aligned} H_1^s(w) &= B_f D_w + (n-1)(2s(m-1)B_f w + \dot{B}_f \dot{w}), \\ H_1^s(w) &= D_f E_w + (n-1)(m(m+s-2)f E_w + \dot{f}\dot{E}_w), \end{aligned} \tag{4.12}$$

with

$$\begin{aligned} B_f &= \dot{f}^2 + m^2 f^2, \qquad & E_w &= ms f w + \dot{f}\dot{w}, \\ D_f &= \ddot{f} + m^2 f, & D_w &= \ddot{w} + s^2 w. \end{aligned} \tag{4.13}$$

Together with the asymptotic boundary conditions

$$\dot{w}_\alpha(\pm\pi) = 0, \tag{4.14}$$

(4.11)-(4.13) constitutes an eigenvalue problem for s and $w_\alpha(\theta)$, under the restrictions (4.10).

Without any loss of generality and motivated by the introductory remark concerning the impossibility of a purely antisymmetric solution, we assume that $a_2 \neq 0$ so as to define

$$a_{12} = a_1/a_2 \tag{4.15}$$

and use the linearity of the operators $H^s_\alpha(w)$ to rewrite (4.11) as

$$\begin{aligned} &(1+a_{12}^2)H^s_1(w_1) + 2a_{12}H^s_2(a_{12}w_1 + w_2) = 0, \\ &(1+a_{12}^2)H^s_1(w_2) + 2H^s_2(a_{12}w_1 + w_2) = 0. \end{aligned} \tag{4.16}$$

Combining the relations (4.16), the asymptotic equilibrium equations can be uncoupled as

$$\begin{aligned} &(1+a_{12}^2)\, H^s_1(w_1 - a_{12}w_2) = 0, \\ &(1+a_{12}^2)\, H^s_3(a_{12}w_1 + w_2) = 0, \end{aligned} \tag{4.17}$$

where $H^s_3(w) = (H^s_1 + 2H^s_2)(w)$. Noting that $H^s_1(w)$ and $H^s_3(w)$ are the same differential operators as the ones encountered in the symmetric (mode I) case in the determination of the first term of y_1 (3.14a) and the second term of y_2 (3.29), we can write the asymptotic expansion as

$$\begin{cases} y_1(r,\theta) \sim a_1 r^m f(\theta;n) + a_1 k r^t l(\theta;n) + a_2 c r^p g(\theta;n) + a_1 d r^q h(\theta;n), \\ y_2(r,\theta) \sim a_2 r^m f(\theta;n) + a_2 k r^t l(\theta;n) - a_1 c r^p g(\theta;n) + a_2 d r^q h(\theta;n), \end{cases} \tag{4.18}$$

where a_α, k, c and d are undetermined constants. In (4.18), $(t, l(\theta;n))$ and $(q, h(\theta;n))$ are the first two solutions of the eigenvalue problem

$$H^s_3(w) = 0, \qquad (-\pi \leq \theta \leq \pi), \tag{4.19}$$

with

$$\dot{w}(\pm\pi) = 0, \tag{4.20}$$

which satisfy the restriction (4.10). The latter can be solved by using Knowles and Sternberg's transformation (3.31) : q and $h(\theta;n)$ have been given by (3.34) and (3.35) while t and $l(\theta;n)$ are similarly obtained as

$$t = (n - 1 + \sqrt{n^2 + 6n - 3})/2n, \tag{4.21}$$

$$l(\theta;n) = n^t(\omega + k\cos\theta)^t(2\cos^2\zeta - 1), \tag{4.22}$$

where the expression for $\zeta(\theta)$ is given by (3.31). The variation of t with respect to n is illustrated in figure 6 and $l(\theta;n)$ is shown in figure 9.

Finally, p and $g(\theta;n)$, which are solutions of

$$H_1^s(w) = 0, \qquad (-\pi \le \theta \le \pi), \tag{4.23}$$

together with (4.20), have been computed numerically in the previous section and are shown in figures 6 and 7 respectively.

5.- Discussion of the asymptotic results - Numerical investigations.

The section contains first a discussion of the asymptotic deformation field described by (4.18), together with a study of the structure of the associated near-tip stress fields. We then present the results of a numerical investigation of the symmetric and non-symmetric cases.

Structure of the deformation field.

A major result of the analysis of the mixed-mode situation is that, like in the plane strain case, the general (non-symmetric) solution is obtained by a rotation of the symmetric (mode I) field. Let $\boldsymbol{y}^*$ denote the latter, i.e.,

$$\begin{cases} y_1^* \sim c_* r^p g(\theta; n), \\ y_2^* \sim a_* r^m f(\theta; n) + k_* r^t l(\theta; n) + d_* r^q h(\theta; n), \end{cases} \tag{5.1}$$

where a_*, c_*, k_* and d_* are constants which depend on the far-field loading conditions, the geometry and the material properties.[9] The general field is given by

$$\boldsymbol{y} = \boldsymbol{Q}\,\boldsymbol{y}^*, \tag{5.2}$$

where the orthogonal tensor $\boldsymbol{Q}$ corresponds to a rotation angle θ given by the mode mixity of the first asymptotic term

$$\tan\theta = -a_{12}, \tag{5.3}$$

where $a_{12} = a_1/a_2$, i.e.,

$$\boldsymbol{Q} = \frac{1}{a}\begin{pmatrix} a_2 & a_1 \\ -a_1 & a_2 \end{pmatrix}, \qquad a^2 = a_1^2 + a_2^2 = a_2^2(1 + a_{12}^2). \tag{5.4}$$

The relation between the nonlinear mode mixity parameter a_{12} and the far-field mode mixity will be examined numerically later in this section, using a "small-scale yielding boundary- layer" approach.

The result (5.2) has an important implication for the nonlinearly elastic analysis of the propagation behavior of a crack under general loading conditions [26]. It has to be also noted that, unlike in the linearized analysis, the near-tip field contains more than

---

[9] Note that $k_* = 0$ in the mode I case since $l(\theta; n)$ is even in θ. But the term of order r^t appears in the mixed-mode solution.

one singular term, especially as n tends to $1/2$ where various asymptotic terms have comparable importance (m, t and q tend to 0 simultaneously as n approaches $1/2$).

Before we proceed further with the discussion of the structure of the stress and strain fields, we non-dimensionalize the asymptotic results (5.1) by normalizing the length quantities r and y_α as

$$\rho = r/l_c, \qquad \eta_\alpha = y_\alpha/l_c, \tag{5.5}$$

where l_c is a characteristic length defined as

$$l_c = a_*^{\frac{1}{1-m}}. \tag{5.6}$$

We then rewrite the symmetric asymptotic fields (5.1) as

$$\begin{cases} \eta_1^* \sim \bar{c}_* \rho^p g(\theta; n), \\ \eta_2^* \sim \rho^m f(\theta; n) + \bar{k}_* \rho^t l(\theta; n) + \bar{d}_* \rho^q h(\theta; n), \end{cases} \tag{5.7}$$

where $\bar{c}_*$, $\bar{k}_*$ and $\bar{d}_*$ are dimensionless constants defined by

$$\bar{c}_* = c_* a_*^{\frac{p-1}{1-m}}, \qquad \bar{k}_* = k_* a_*^{\frac{t-1}{1-m}}, \qquad \bar{d}_* = d_* a_*^{\frac{q-1}{1-m}}. \tag{5.8}$$

As mentioned before, the Jacobian of the transformation was left undetermined by the first asymptotic term in the non-symmetric case. It can be shown that the term of order r^t and r^q do not contribute either to the value of J to the first order. Using (5.2), one obtains

$$J = det[F_{\alpha\beta}] = det[F^*_{\alpha\beta}], \tag{5.9}$$

where $\boldsymbol{F}^* = \nabla \boldsymbol{y}^*$ is the mode I deformation gradient tensor. Combining (5.7) and (5.9), one obtains

$$J = \lambda^{-1} \sim \bar{c}_* \rho^{m+p-2} (p \dot{f} g - m f \dot{g}). \tag{5.10}$$

The angular variation of the Jacobian is shown in figure 10. Note that the Jacobian vanishes as θ approaches $\pm\pi$, which suggests that the approximations (5.1)-(5.2) deteriorate near the crack faces, along which the transverse stretch is left indeterminate by the present local analysis. It is nevertheless possible to obtain an estimate of the radial variation of λ along the crack faces through the approach used in [14], which is based on a modified form of the Cayleigh-Hamilton relation[10]

$$2U_I U_J M - (4U_I^2 + U_J^2)N + (4U_I^2 - U_J^2)J = 0, \tag{5.11}$$

where U_I and U_J are the partial derivatives of the elastic potential $U(I,J)$ defined in (2.10), $M = \sigma_{\alpha\beta}\sigma_{\alpha\beta}$ and $N = det[\sigma_{\alpha\beta}]$. Along the crack faces, (5.11) reduces to

$$2U_I U_J M + (4U_I^2 - U_J^2)J = 0, \qquad (\theta = \pm\pi), \tag{5.12}$$

where

$$M = \sigma_{11}^2 + \sigma_{21}^2 \sim \mu^2 A^{2n-2}(y_{1,1}^2 + y_{2,1}^2), \qquad (r \to 0), \tag{5.13}$$

in which

$$A = 1 + b(1 + \lambda^2 - 2)/n \sim bI/n, \qquad (r \to 0). \tag{5.14}$$

By substituting the expressions of U_I and U_J together with the symmetric asymptotic solution (5.7) into (5.12)-(5.14), there results

$$-\lambda^4 m^2 + (1 - \lambda^6)^2 \rho^{1/n} \sim 0, \qquad (r \to 0, \quad \theta = \pm\pi), \tag{5.15}$$

where $m = 1 - 1/2n$. Using the fact that in a tension field the transverse stretch vanishes as the crack tip is approached, (5.15) readily yields the following estimate along the crack faces

---

[10] See section 2 of [14] for the details of the computation leading to (5.11).

$$\lambda \sim \frac{\rho^{1/4n}}{\sqrt{m}}, \qquad (r \to 0, \quad \theta = \pm\pi). \tag{5.16}$$

As shown in [14], a more general estimate of λ that holds uniformly for $-\pi \le \theta \le \pi$ and includes (5.10) and (5.16) can be obtained using (5.11).[11]

Analysis of the near-tip stress field - characteristic length.

We turn next to the expression of the near-tip stress field. Since the general situation corresponds locally to a mere rotation of the "canonical" symmetric case, we focus on the latter. The nominal stresses are given asymptotically, with the aid of (2.11) and (5.7), by

$$\sigma_{\alpha\beta}/\mu \sim (b/n)^{n-1} I^{n-1} y_{\alpha,\beta}, \tag{5.17}$$

where

$$I = y_{\gamma,\delta} y_{\gamma,\delta} \sim \rho^{2m-2} B_f, \tag{5.18}$$

with

$$B_f(\theta) = m^2 f^2(\theta) + \dot{f}^2(\theta) = n^{-1/n} m^2 (k\cos\theta + \omega)^{-1/n}, \tag{5.19}$$

in which k and ω have been defined in (3.20) and (3.21) respectively. Combining (5.17)-(5.19) with (5.7), there results, finally

[11] See the discussion at the end of section 3 in [14] for more details.

$$\begin{cases} \sigma_{11}/\mu \sim b^{n-1}\,\bar{c}_*\,\rho^{p+\frac{1}{n}-2}\,B_f^{n-1}(p\cos\theta\, g - \sin\theta\,\dot{g}), \\ \sigma_{12}/\mu \sim b^{n-1}\,\bar{c}_*\,\rho^{p+\frac{1}{n}-2}\,B_f^{n-1}(p\sin\theta\, g + \cos\theta\,\dot{g}), \\ \sigma_{21}/\mu \sim b^{n-1}\,\rho^{\frac{1}{2n}-1}\,B_f^{n-1}(m\cos\theta\, f - \sin\theta\,\dot{f}), \\ \sigma_{22}/\mu \sim b^{n-1}\,\rho^{\frac{1}{2n}-1}\,B_f^{n-1}(m\sin\theta\, f + \cos\theta\,\dot{f}), \end{cases} \tag{5.20}$$

where $B_f(\theta)$ has been defined in (5.19) and $B_g(\theta) = \dot{g}^2(\theta) + p^2 g^2(\theta)$. The true stresses are given by

$$\begin{cases} \tau_{11}/\mu \sim (b/n)^{n-1}\bar{c}_*^{\,2}\,\rho^{2p+\frac{1}{n}-3}\,B_f^{n-1}\,B_g, \\ \tau_{22}/\mu \sim (b/n)^{n-1}\rho^{-1}\,B_f^{n}, \\ \tau_{12}/\mu = \tau_{12}/\mu \sim (b/n)^{n-1}\bar{c}_*\,\rho^{p+\frac{1}{2n}-2}\,B_f^{n-1}(m\,p\,f\,g + \dot{f}\,\dot{g}). \end{cases} \tag{5.21}$$

Figures 11 and 12 illustrate the angular variation of the nominal and Cauchy stresses respectively for $-\pi \le \theta \le \pi$. As the "hardening" exponent n decreases and the material approaches the "perfectly plastic" ("non-hardening") limit ($n \to 1/2$), the deformations and the stresses tend to concentrate into the first and fourth quadrants ($-\pi/2 \le \theta \le \pi/2$) as pointed out by figures 10 and 12. Note also that the stress singularities predicted by the nonlinear theory are stronger than the inverse square root singularity suggested by the linearized asymptotic elastic analysis. Furthermore, the radial dependence of the true stresses is different for each component $\tau_{\alpha\beta}$, the strongest singularity ($O(r^{-1})$) corresponding to the stress component perpendicular to the plane of the crack. The stress singularity is even stronger when the stress components are expressed in terms of the deformed coordinates. Let R be the dimensionless deformed distance to the crack tip. Along $\theta = 0$, (5.7) yields

$$R \sim \bar{c}_*\rho^{p}, \tag{5.22}$$

which suggests that

$$\tau_{22} = O(\rho^{-1}) = O(R^{-1/p}). \tag{5.23}$$

Along other rays $(\theta \neq 0)$, the singularity is even stronger since

$$R \sim \rho^m f(\theta; n) \qquad \text{and} \qquad m \leq p. \tag{5.24}$$

The characteristic length l_c defined in (5.6), which appeared in the nonlinear analysis and was used in the non-dimensionalization (5.5), can be related to the value of the conservation integral $\mathcal{J}$, defined in (3.11) and which can be, in turn, associated with the far-field loading conditions, the geometry of the global crack problem and the material characteristics. A substitution of (5.7) into (3.11) yields, after tedious but elementary integrations,

$$\mathcal{J} = 2\mu b^{n-1} l_c \bar{\mathcal{J}}(n), \tag{5.25}$$

where

$$\bar{\mathcal{J}}(n) = m^{2n-1} n^{1-n} \pi/4, \tag{5.26}$$

and μ, b and n are the material characteristics introduced in (2.9). The latter expression is illustrated in figure 13. The relation (5.25) allows, with the aid of (5.5), to express all the stresses in terms of the energy parameter $\mathcal{J}$. For example, the most singular true stress component becomes

$$\tau_{22} \sim \frac{\mathcal{J}}{\bar{\mathcal{J}}(n)} \frac{m^{2n}}{n^n} \frac{r^{-1}}{\omega + k\cos\theta}. \tag{5.27}$$

In addition to its effect on the various stress distributions, the hardening parameter n greatly influences the shape of the deformed crack near its tip. More precisely, it is possible, by varying the value of the hardening exponent, to study the phenomenon of crack blunting associated with a reduction of n. The shape of the upper face of the crack after deformation can be expressed as

$$\eta_2 \sim (\bar{c}_* g(\pi; n))^{-m/p} \eta_1^{m/p}. \tag{5.28}$$

The latter relation is symbolically represented in figure 14, showing that (5.28) is able to capture the blunting of the crack as the material behavior approaches the "perfectly plastic" characterization $(n \to 1/2)$.

Numerical investigation.

A detailed numerical investigation, using the finite element method, has been performed with the following two objectives : first, we examine whether a full-field numerical solution can capture the analytical asymptotic fields; next, we analyze the relation between the far-field loading conditions and the local nonlinear mixity parameter a_{12} introduced in (4.15).

A modified version of the finite element program FEAP [27] which included the GNH material description (2.9) and a fully-Lagrangian approach was used for the computations. A concentrically refined mesh with up to 3000 4-node bilinear elements was created around the crack tip. As mentioned before, the nonlinear asymptotic solution is characterized by the appearance of more that one singular term. A high mesh refinement is therefore sometimes necessary to capture the expected singular behavior. The ratio of the smallest element size to the largest has been chosen of the order of 10^{-8}.

The effect of the hardening exponent n on the blunting of the crack can be visualized in figure 15 by comparing the deformed shape of the crack for $n = 0.55$ and $n = 1.0$ in the mode I loading case.

A comparison between the numerical and asymptotic solutions is presented for the deformed coordinates y_1 (figure 16a) and y_2 (figure 16b) under mode I loading and

the in-plane transformation Jacobian $J(r,\theta)$ (figure 17) in the mixed-mode situation, showing good agreement in both cases.

The relationship between the far-field loading conditions and the near-tip mode mixity defined by $a_{12} = a_1/a_2$ has also been investigated numerically in the case of "small-scale finite yielding." The approach used here is similar to the method considered by Shih [3] in his analysis of the small-scale yielding mixed-mode HRR fields, in which a circular domain surrounding the crack tip is discretized into a concentric finite element mesh. The outer contour of the domain is then subjected to loading conditions corresponding to a plane stress K-field characterized by a mode-mixity parameter

$$\zeta_L = \frac{2}{\pi} tan^{-1}(K_{II}/K_I), \tag{5.29}$$

where K_I and K_{II} are, respectively, the mode I and mode II stress intensity factors relevant to linearized elastostatics. The material properties appearing in the computation of the latter are chosen as the linearized values of the GNH materials (shear modulus μ and Poisson's ratio $\nu = 0.5$). The size of the nonlinear zone can be estimated by the reasoning illustrated in figure 18. The radial dependence of the norm of the Cauchy stress tensor ahead of the crack tip (along $\theta = 0$) shows a fairly well defined transition between the nonlinear asymptotic solution

$$\frac{\sqrt{\tau_{\alpha\beta}\tau_{\alpha\beta}}}{\mu} \sim \frac{\mathcal{J}}{\mu l}\left(\frac{r}{l}\right)^{-1}\left(\frac{m^2}{n}\right)^n \frac{1}{4m\bar{\mathcal{J}}(n)} \tag{5.30}$$

and the value predicted by the linearized theory

$$\frac{\sqrt{\tau_{\alpha\beta}\tau_{\alpha\beta}}}{\mu} \sim \sqrt{\frac{3}{\pi}}\left(\frac{r}{l}\right)^{-1/2}\sqrt{\frac{\mathcal{J}}{\mu l}}, \tag{5.31}$$

in which the characteristic length l has been chosen as the radius of the circular domain on which the boundary layer analysis is performed and $\bar{J}(n)$ is given by (5.26). A good estimate of the size r_{NL} of the zone in which the nonlinear effects are preponderant is thus obtained by combining (5.30) and (5.31) to render, with the aid of (5.26),

$$\frac{r_{NL}}{l} = \frac{1}{3\pi n^2}\frac{J}{\mu l}. \tag{5.32}$$

The relation between the linear mode mixity parameter ζ_L and the nonlinear parameter defined as

$$\zeta_{NL} = \frac{2}{\pi}tan^{-1}(a_{12}) \tag{5.33}$$

is shown in figure 19, for various values of the hardening exponent n. Due to numerical instabilities, the "perfectly plastic" situation $(n \to 0.5)$ could not be investigated successfully so far. The "partial results" shown in figure 19 confirm however the trend observed in the small strain analysis (see figure 9 of [3][12]) : as the hardening exponent decreases, the nonlinear mode mixity increases for a given value of ζ_L. But, unlike in the infinitesimal strain investigation and, as was mentioned in the opening remark of section 4 concerning the impossibility of an antisymmetric deformation field, the nonlinear mode mixity parameter ζ_{NL} corresponding to a pure mode II far-field loading takes a value less than unity for all values of the hardening parameter n.

6.- Conclusion.

An asymptotic and numerical analysis of the near-tip finite deformation fields in a homogeneous sheet of Generalized Neo-Hookean material has been presented. Both

[12] Note that, in [3], the perfectly plastic situation corresponds to $n = \infty$.

the symmetric (mode I) and non-symmetric (mixed-mode) situations have been investigated. It was shown that the general case is asymptotically obtained by a mere rotation of the canonical symmetric fields, as it had been observed previously in the finite plane strain analysis. By varying the value of the hardening parameter appearing in the GNH material characterization, the phenomenon of crack blunting and its effect on the stress fields can be established. The nonlinear asymptotic analysis also reveals that there exists more than one singular term and that the leading singularity is stronger than that predicted by the linearized theory.

The asymptotic results have been captured numerically through a full-field nonlinear finite element investigation which also yielded, through a "boundary-layer small-scale yielding" analysis, the relation between the nonlinear and linear mode mixity parameters. The latter study confirms that the large deformation theory excludes the existence of an purely antisymmetric (mode II) deformation, at least for the class of materials considered here.

Acknowledgments.

The results presented in this paper have been obtained as part of a research program sponsored by AFOSR (contract F04611-88-K-0024) under the technical supervision of Dr. C.T. Liu. Additional support was provided by ONR (grant N00014-91-J-1427) with Dr. P. Schmidt as technical director. The computational part of this work has been performed on the Cray YMP of the San Diego Supercomputing Center. Helpful discussions with Professor J.K. Knowles are gratefully acknowledged.

Appendix.

In this section, an approximation of the solution of (3.22) is computed using the WKB method. The eigenvalue problem to be solved consists of finding $p > m = 1 - 1/2n$ (with $1/2 < n \leq 1$) and $g(\theta) \in C^2([0,\pi])$ satisfying

$$\ddot{g} + \frac{k^2 \sin\theta}{\omega}\dot{g} + p(p-k)g = 0, \tag{A.1}$$

with

$$\begin{aligned} &\dot{g}(0) = \dot{g}(\pi) = 0, \qquad && g(0) = 1, \\ &k = 1 - 1/n, \qquad && \omega = (1 - k^2 \sin^2\theta)^{1/2}. \end{aligned} \tag{A.2}$$

Using the transformation

$$g(\theta) = (\omega + k\cos\theta)^{k/2} v(\theta), \tag{A.3}$$

(A.1) can be rewritten in the more suitable form

$$\ddot{v} + Q(\theta; p)v = 0, \tag{A.4}$$

where

$$Q(\theta; p) = p(p-k) - \frac{k^2 \cos\theta}{2\omega^3} - \frac{k^4 \sin^2\theta}{4\omega^2}. \tag{A.5}$$

The boundary conditions (A.2) become

$$\dot{v}(0) = \dot{v}(\pi) = 0, \qquad v(0) = (1+k)^{-k/2}. \tag{A.6}$$

The general solution of (A.4) using the WKB approximation is

$$v(\theta) \sim A\, Q(\theta)^{-1/4} \cos\left[\int_0^\theta Q(t)^{1/2} dt\right] + B\, Q(\theta)^{-1/4} \sin\left[\int_0^\theta Q(t)^{1/2} dt\right]. \tag{A.7}$$

The application of the homogeneous boundary conditions (A.6a) yields the following relations for p

$$(Q(0))^{1/4}\,(Q(\pi))^{1/4}\,\sin\left[\int_0^{\pi}\sqrt{Q(t)}dt\right]=0, \tag{A.8}$$

from which results

$$\int_0^{\pi}\sqrt{Q(t)}\,dt = j\pi, \qquad (j=0,\pm 1,\pm 2,\ldots). \tag{A.9}$$

Various estimations of the integral on the left side of (A.9) yield different approximations of the eigenvalue p. As a first approximation, assuming that p is large, we can write

$$Q(\theta)\sim p(p-k), \tag{A.10}$$

which yields the first approximation of the first eigenvalue $(j=1)$

$$p_1=\frac{k+\sqrt{k^2+4}}{2}. \tag{A.11}$$

A comparison between this lower-order approximation and the numerically obtained values of p is presented in figure A.1, showing a good agreement for $n \geq 0.7$.

A better approximation of the eigenvalues can be obtained by developing $Q^{1/2}(\theta)$ in a two-term Taylor expansion

$$Q^{1/2}(\theta)\sim\sqrt{p(p-k)}\left\{1-\frac{k^2}{8p(p-k)\omega^2}\left(2\cos\theta+\omega-\omega^3\right)\right\}. \tag{A.12}$$

Then (A.9) is readily shown to provide the second approximation of the first eigenvalue

$$p_2=\frac{k+\sqrt{k^2+w^2(k)}}{2}, \tag{A.13}$$

where

$$w(k) = 1 + \sqrt{1 - \frac{k^2}{2}\left(1 - \frac{1}{\sqrt{1-k^2}}\right)}. \qquad (A.14)$$

As shown in figure A.1, a better agreement with the numerical values is achieved by using the latter approximation, except when n tends to 0.5 for which the WKB theory predicts an infinite value for p.

The WKB method also provides an estimation of the first eigenfunction. In order to satisfy (A.6), $v(\theta)$ must be chosen as

$$v(\theta) \sim A\ Q(\theta)^{-1/4} \cos\left[\int_0^\theta Q(t)^{1/2} dt\right], \qquad (A.15)$$

where

$$A = (1+k)^{-k/2}\{p(p-k) - k^2/2\}^{1/4}. \qquad (A.16)$$

Substituting (A.12) into (A.15), one gets, after integration and with the help of (A.3),

$$g(\theta) \sim (\omega + k\cos\theta)^{k/2} A\ Q(\theta)^{-1/4} \cos z(\theta), \qquad (0 \le \theta \le \pi), \qquad (A.17)$$

where

$$z(\theta) = \sqrt{p(p-k)}\left\{\theta - \frac{k^2}{8p(p-k)}\left[2\frac{\sin\theta}{\omega} + \frac{\tan^{-1}\left(\sqrt{1-k^2}\tan\theta\right)}{\sqrt{1-k^2}} - \theta\right]\right\}, \qquad (A.18)$$

in which k, ω, A, $Q(\theta)$ and p have been defined in (A.2), (A.5), (A.13), (A.14) and (A.16). A comparison between the WKB-approximated and the numerically computed values of $g(\theta)$ is shown in figure A.2 : an acceptable agreement is achieved for $n \ge 0.6$.

References.

1. Hutchinson, J.W., *Singular behavior at the end of a tensile crack in a hardening material.* J. Mech. Phys. Solids, 1968. **16**: pp. 13-31.

2. Rice, J.R. and Rosengren, G.F., *Plane strain deformation near a crack tip in a power law hardening material.* J. Mech. Phys. Solids, 1968. **16**: pp. 1-12.

3. Shih, C.F., *Small-scale yielding analysis of mixed-mode plane strain crack problems,* in *Fracture analysis.* 1974, ASTM STP 560: pp. 187-210.

4. Sharma, S.M. and Aravas, N., *Determination of higher-order terms in asymptotic elastoplastic crack tip solutions.* J. Mech. Phys. Solids, 1991. **39**(8): pp. 1043-1072.

5. Wong, F. and Shield, T., *Large plane deformations of thin elastic sheets of Neo-Hookean materials.* Z.A.M.P., 1969. **20**: pp. 176-199.

6. Knowles, J.K. and Sternberg, E., *An asymptotic finite-deformation analysis of the elastostatic field near the tip of a crack.* J. Elasticity, 1973. **3**: pp. 67-107.

7. Knowles, J.K. and Sternberg, E., *Finite-deformation analysis of the elastostatic field near the tip of a crack : reconsideration and higher-order results.* J. Elasticity, 1974. **4**: pp. 201-233.

8. Knowles, J.K., *The finite anti-plane shear field near the tip of a crack for a class of incompressible elastic solids.* Int. J. Fracture, 1977. **13**(5): pp. 611-639.

9. Knowles, J.K. *On some inherently nonlinear singular problems in finite elastostatics.* in *Eighth US National Congress of Applied Mechanics.* 1978. UCLA.

10. Sternberg, E. *Some recent advances in the application of nonlinear elastostatics to singular problems.* in *Symposium dedicated to the 65th birthday of W.T. Koiter.* 1979. Sijthoff and Noordhoff International Publishers.

11. Stephenson, R.A., *The equilibrium field near the tip of a crack for finite plane strain incompressible elastic materials.* J. Elasticity, 1982. **12**(1): pp. 65-99.

12. Le, K.C., *On the singular elastostatic field induced by a crack in a Hadamard material.* Q. J. Mech. Appl. Math, 1992. **45**(1): pp. 101-117.

13. Knowles, J.K., *A nonlinear effect in mode II crack problems.* Eng. Fract. Mech., 1981. **15**(3-4): pp. 469-476.

14. Knowles, J.K. and Sternberg, E., *Large deformations near the tip of an interface crack between two Neo-Hookean sheets.* J. Elasticity, 1983. **13**: pp. 257-293.

15. Herrmann, J.M., *An asymptotic analysis of finite deformation near the tip of an interface crack.* J. Elasticity, 1989. **21**: pp. 227-269.

16. Ravichandran, G. and Knauss, W.G., *A finite elastostatic analysis of bimaterial interface cracks.* Int. J. Fracture, 1989. **39**: pp. 235-253.

17. Geubelle, P.H. and Knauss, W.G., *Finite strains at the tip of a crack in a sheet of hyperelastic material : II. Special bimaterial cases.* Galcit SM Report 92-43, Caltech, 1992. Submitted to J. Elasticity.

18. Geubelle, P.H. and Knauss, W.G., *Finite strains at the tip of a crack in a sheet of hyperelastic material : III. General bimaterial case.* Galcit SM Report 92-44, Caltech, 1992. Submitted to J. Elasticity.

19. Rosakis, P. and Rosakis, A.J., *The screw dislocation problem in incompressible finite elastostatics : a discussion of non-linear effects.* J. Elasticity, 1988. **20**(1): pp. 3-40.

20. Rajagopal, K.R. and Tao, L., *On an inhomogeneous deformation of a Generalized Neo-Hookean material.* J. Elasticity, 1992. **28**: pp. 165-184.

21. Abeyaratne, R., *Discontinuous deformation gradients away from the tip of a crack in anti-plane shear.* J. Elasticity, 1981. **11**(4): pp. 373-393.

22. Silling, S.A., *Numerical studies of loss of ellipticity near singularities in an elastic material.* J. Elasticity, 1988. **19**(3): pp. 213-239.

23. Rice, J.R., *A path-independent integral and the approximate analysis of strain concentrations by notches and cracks.* J. App. Mech., 1968. **35**(2): p. 379.

24. Knowles, J.K. and Sternberg, E., *On a class of conservation laws in linearized and finite elastostatics.* Arch. Rat. Mech. Analysis, 1972. **44**: pp. 187-211.

25. Bender, C.M. and Orszag, S.A., *Advanced mathematical methods for scientists and engineers.* 1978. McGraw-Hill.

26. Geubelle, P.H. and Knauss, W.G., *Propagation of a crack in homogeneous and bimaterial sheets under general in-plane loading : Nonlinear analysis.* Galcit SM Report 93-1, Caltech, 1993. Submitted to J. Appl. Mech.

27. Zienkiewicz, O.C., *The finite element method.* 3rd ed., 1977. McGraw-Hill.

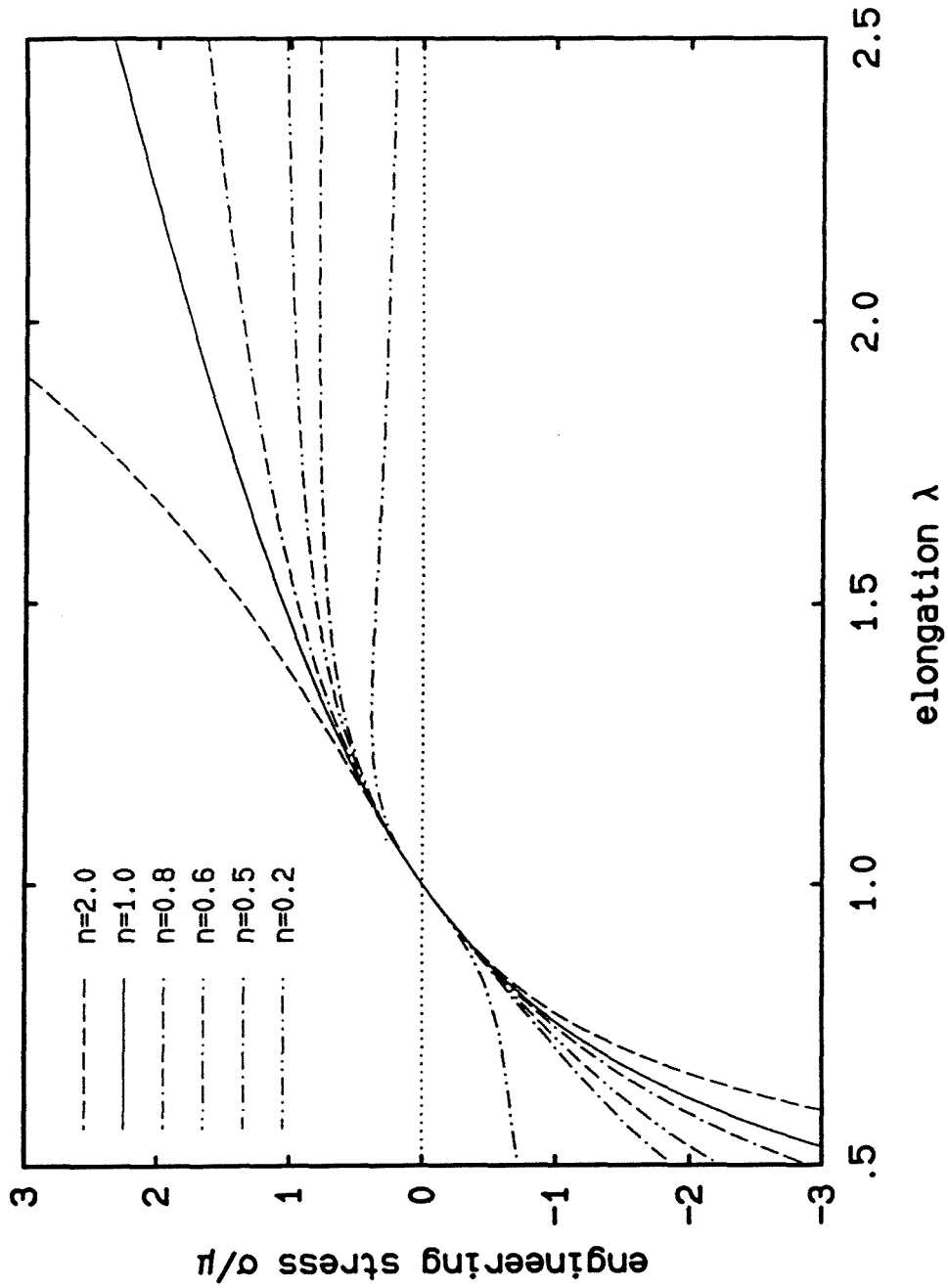

Figure 1. Uniaxial tension behavior of GNH materials - effect of the "hardening exponent" *n*.

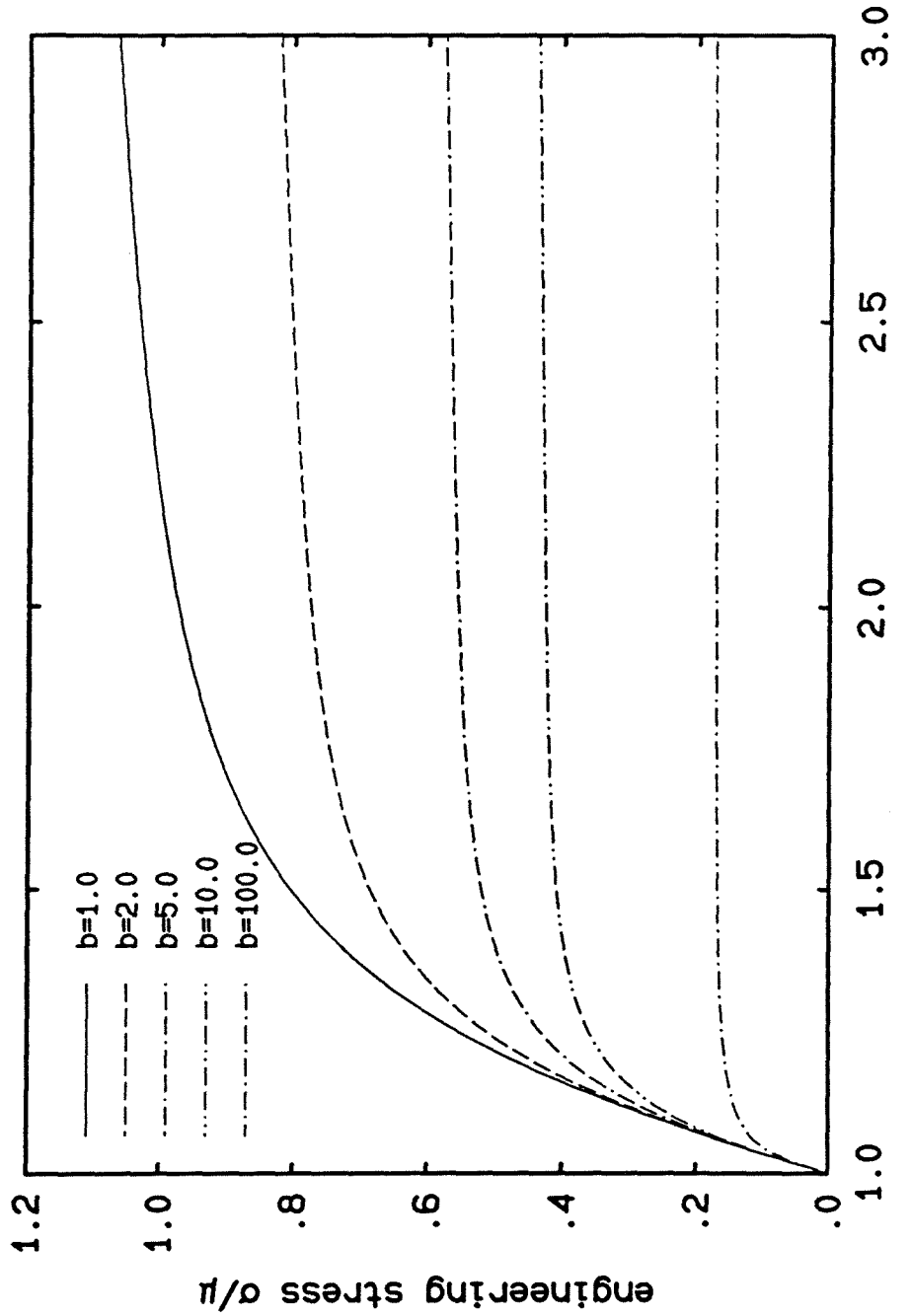

Figure 2. Uniaxial tension behavior of GNH materials - effect of the "yielding parameter" b.

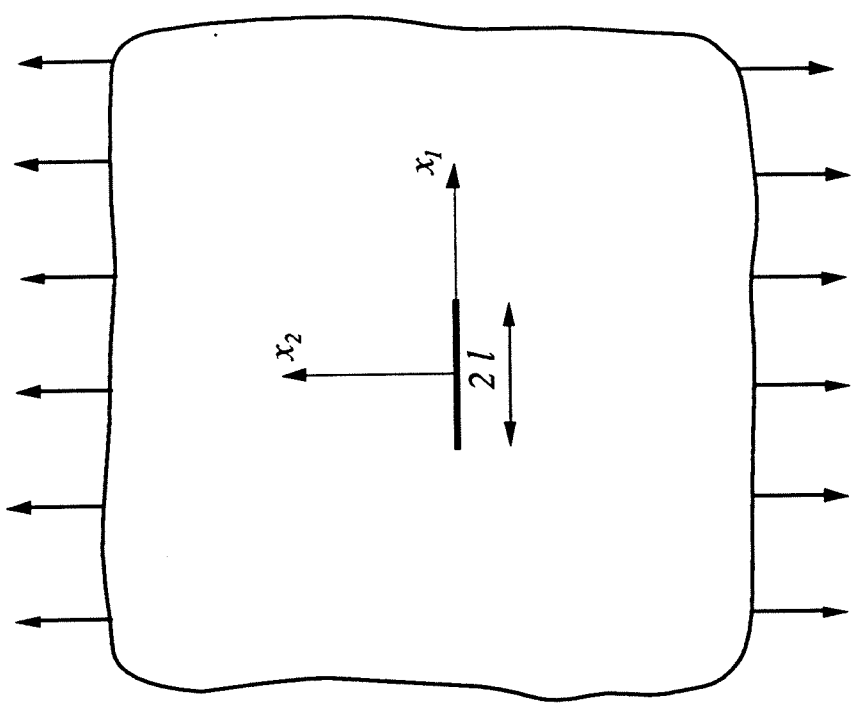

Figure 3. Geometry of the global crack problem.

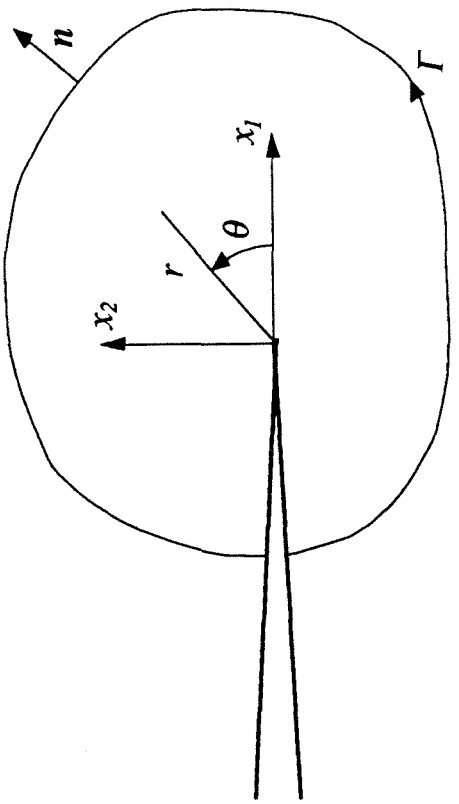

Figure 4. Geometry of the local crack problem.

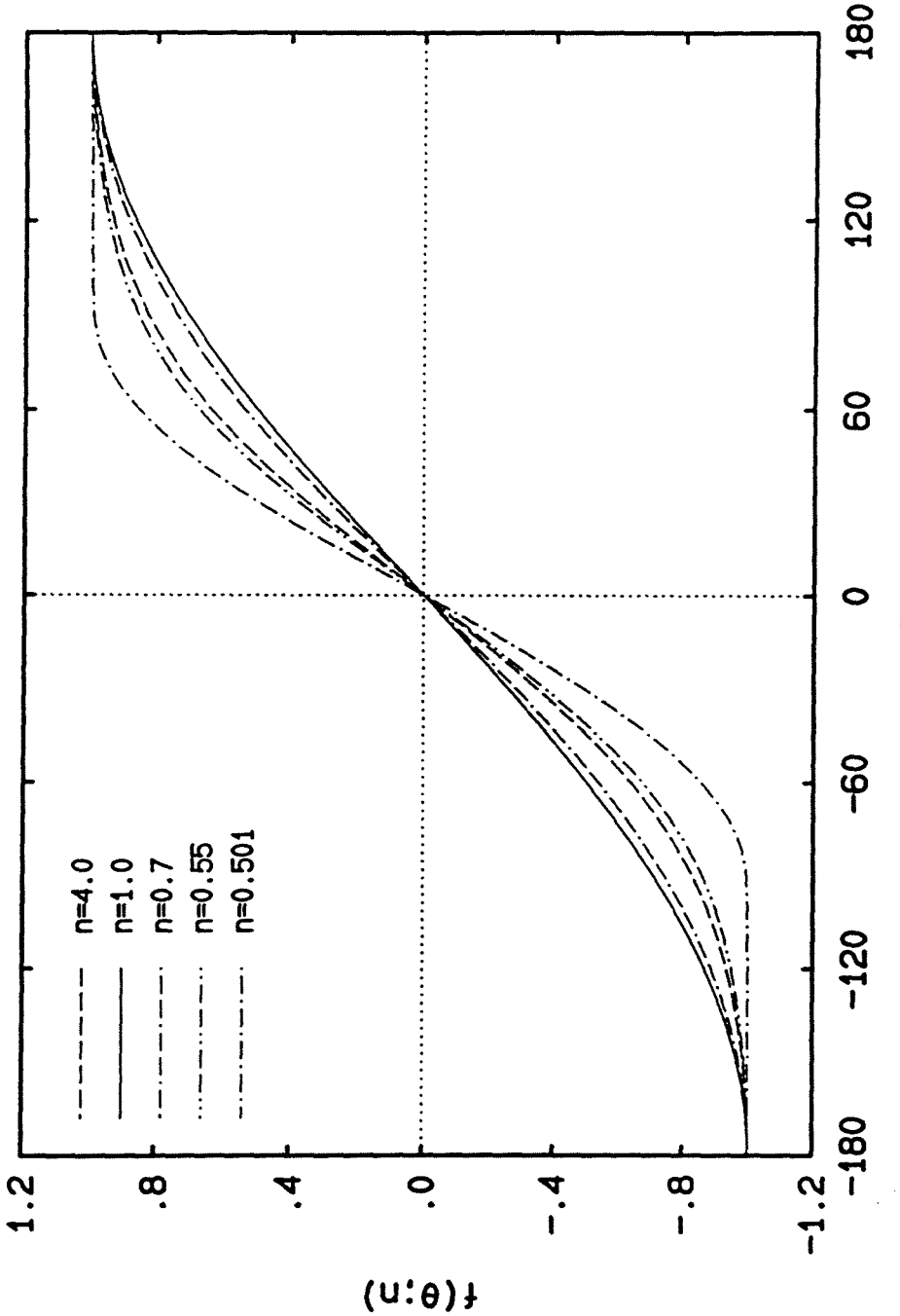

Figure 5. $f(\theta;n)$ for various values of n.

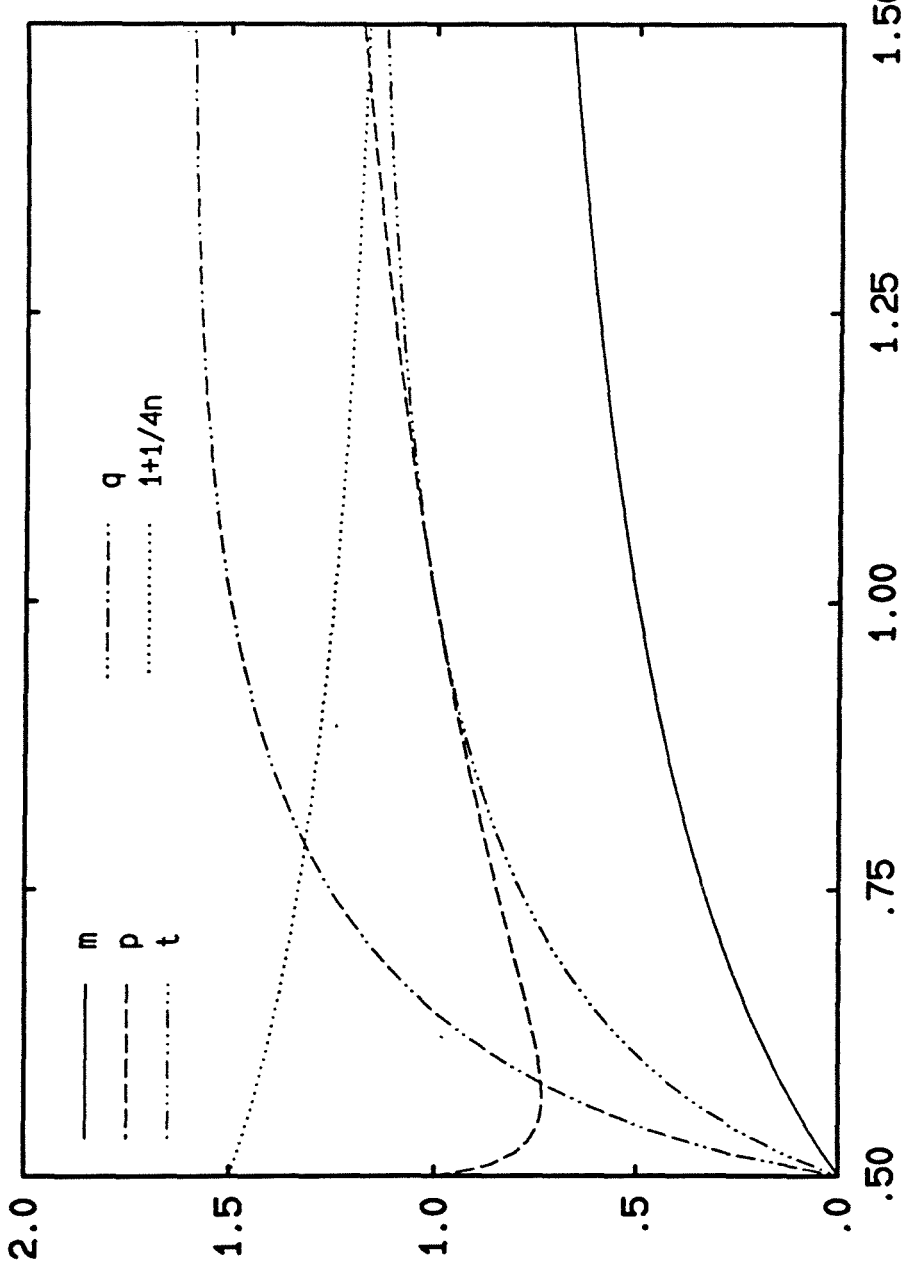

Figure 6. Various asymptotic exponents versus "hardening" parameter *n* and limit of validity.

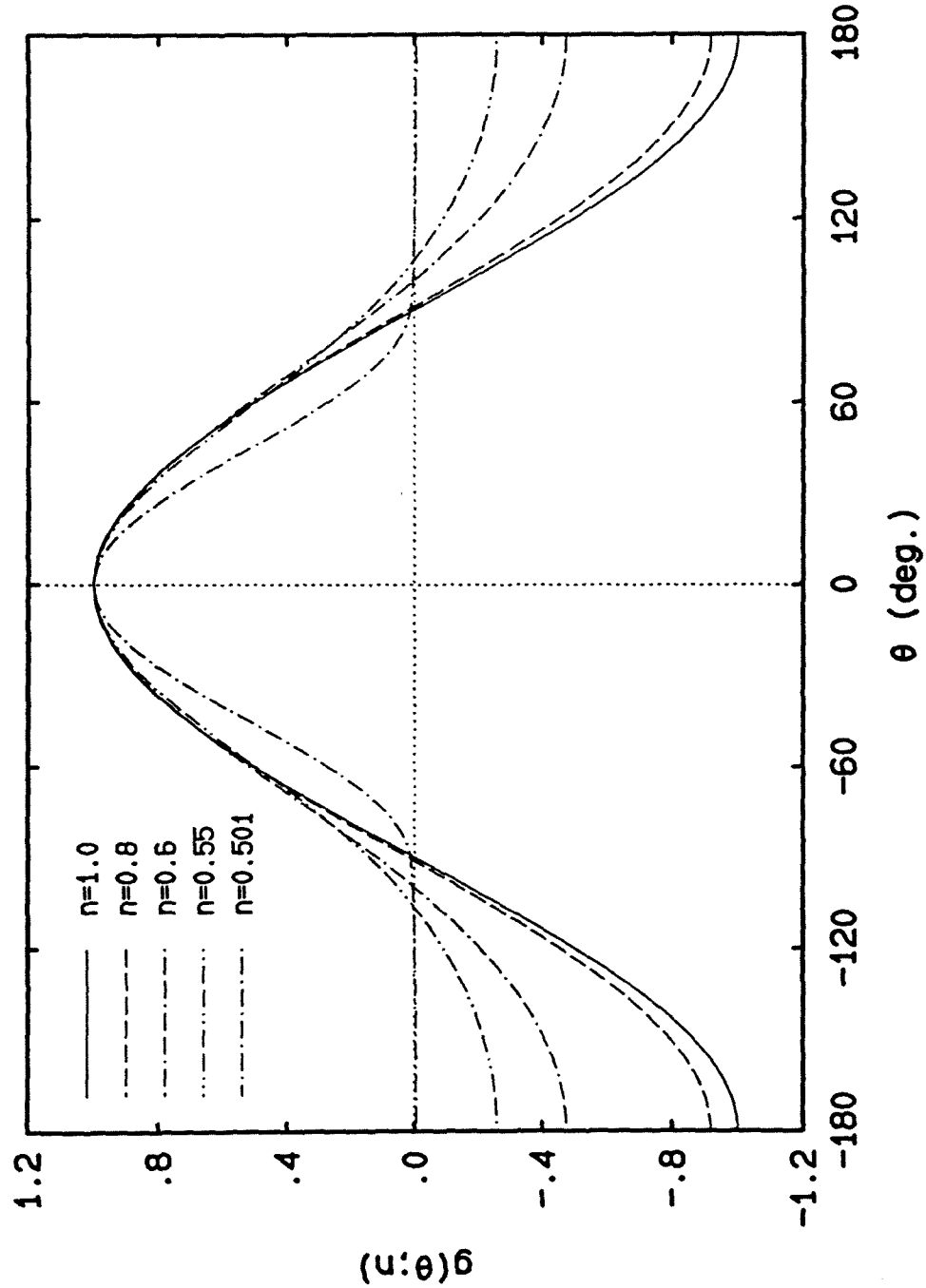

Figure 7. $g(\theta;n)$ for various values of n.

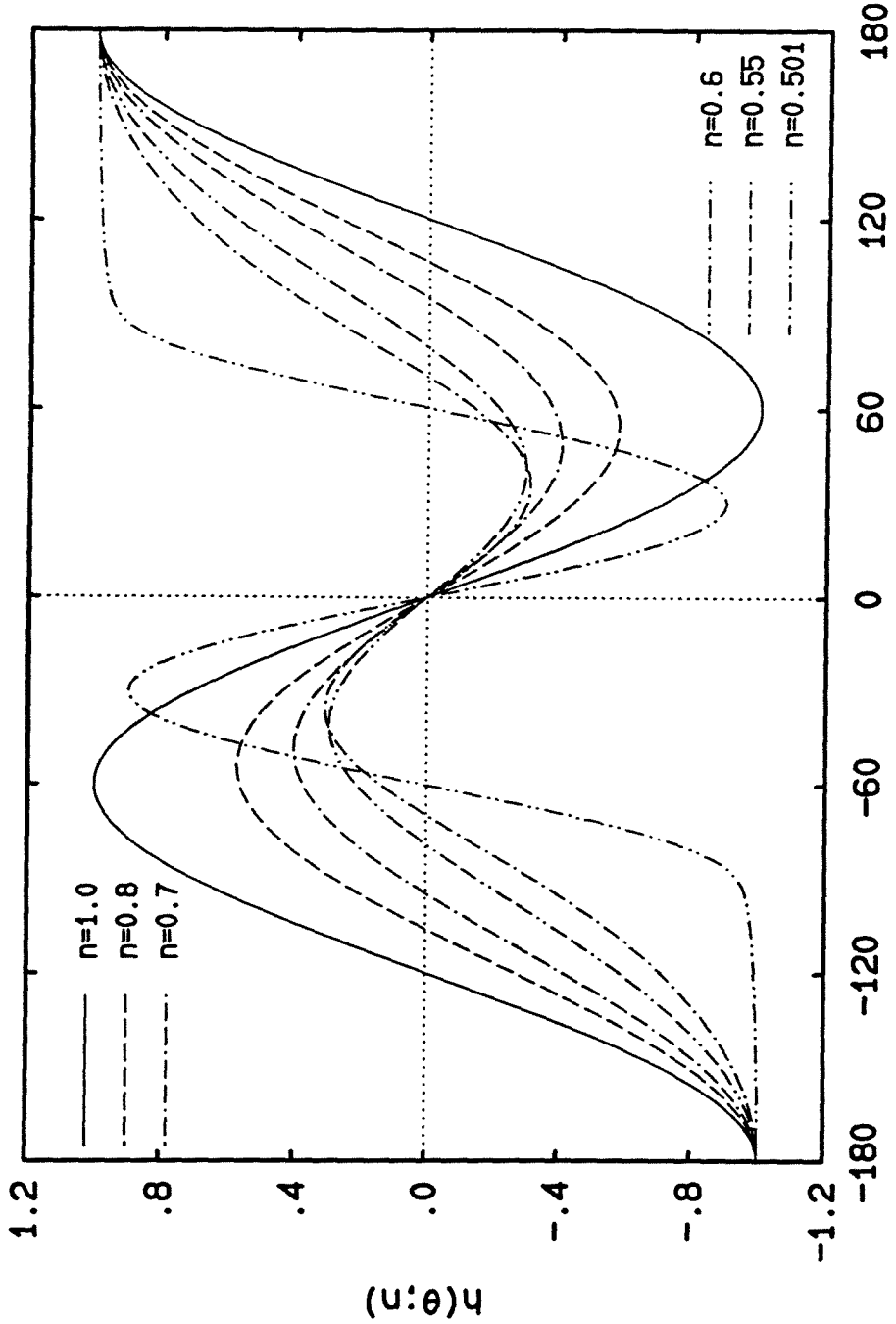

Figure 8. $h(\theta;n)$ for various values of n.

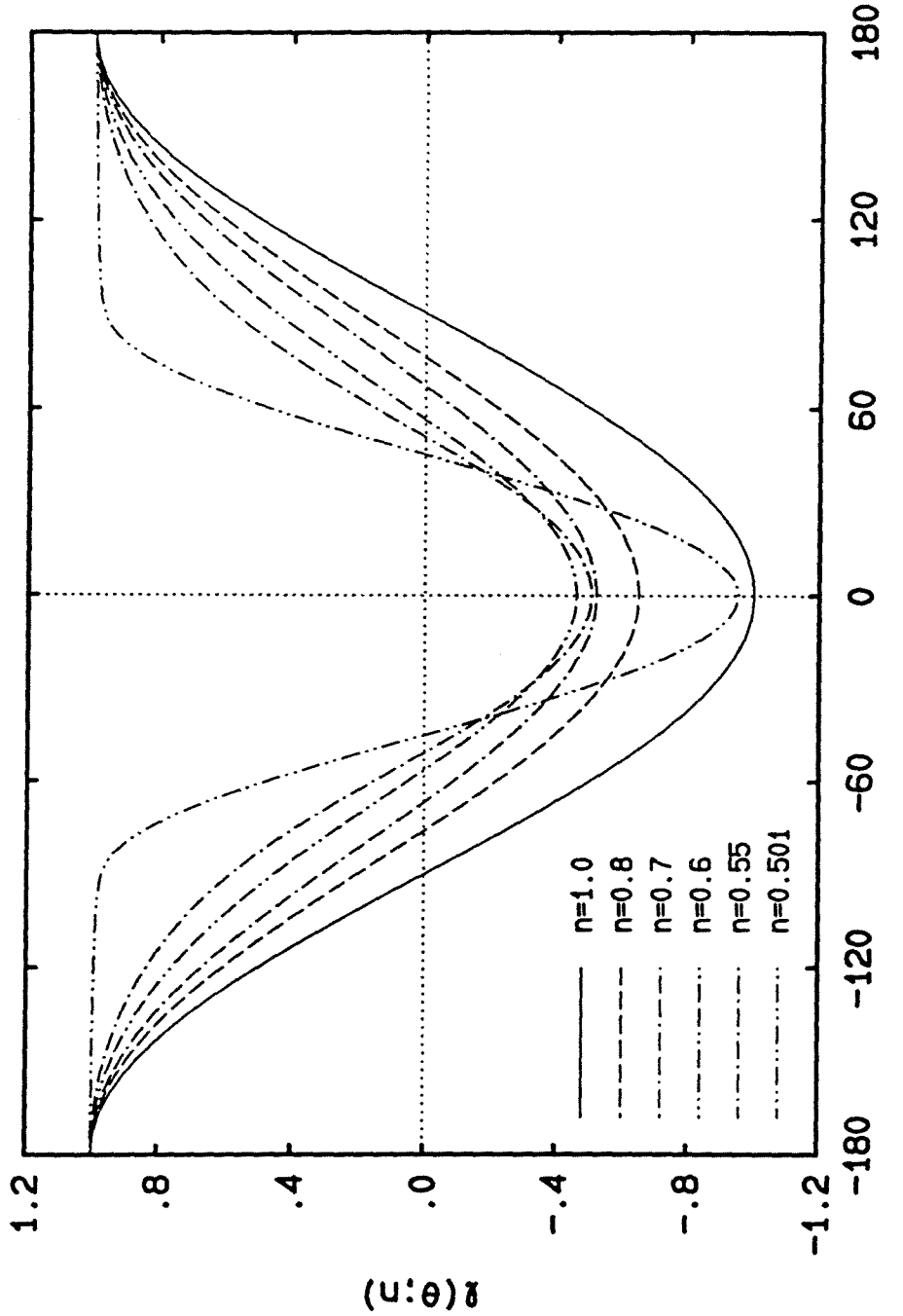

Figure 9. $I(\theta;n)$ for various values of n.

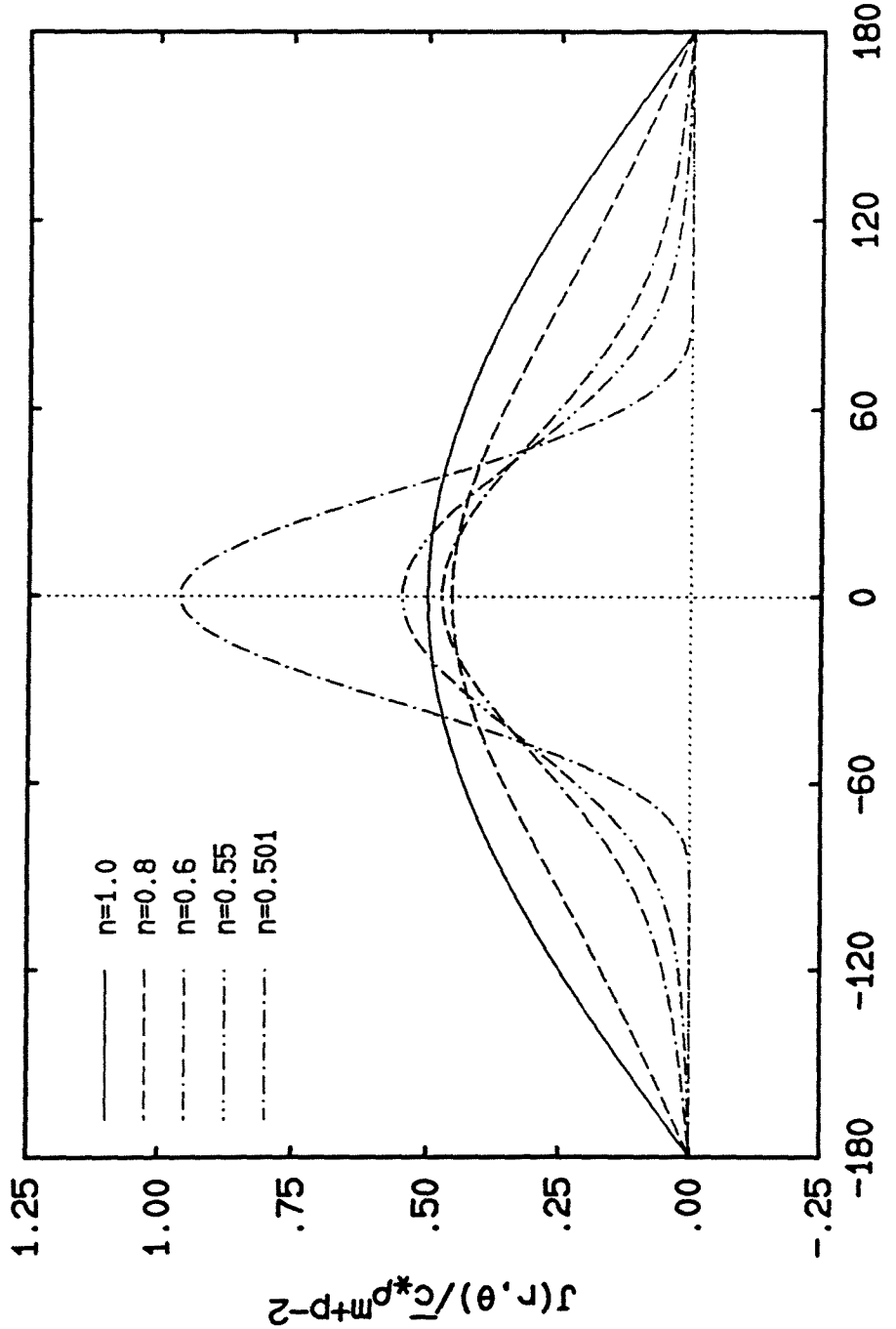

Figure 10. Angular variation of the in-plane Jacobian $J(r,\theta)/a_{\infty}r^{m+p-2}$.

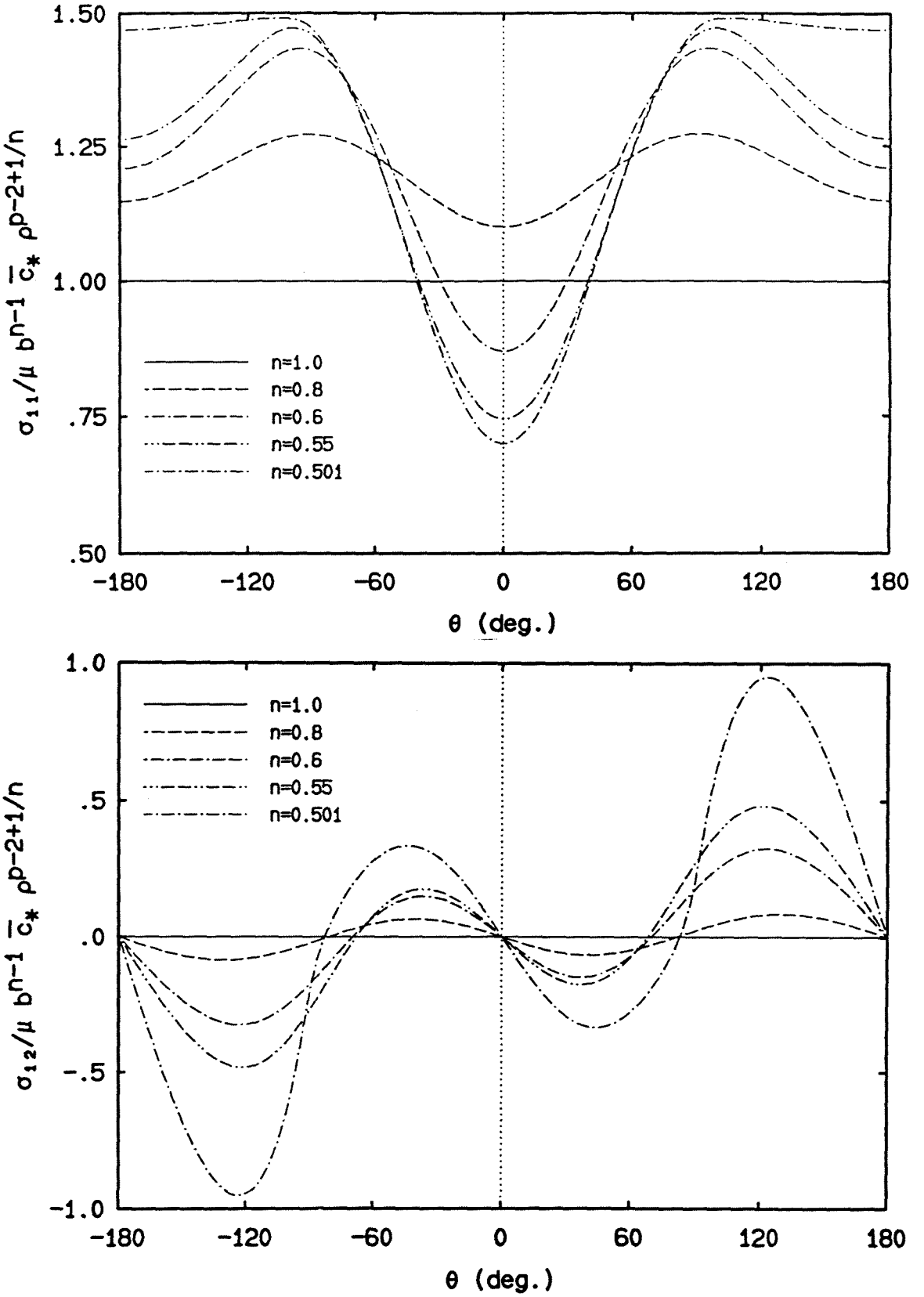

Figure 11. Angular variation of the nominal stresses $\sigma_{\alpha\beta}(r,\theta)$.

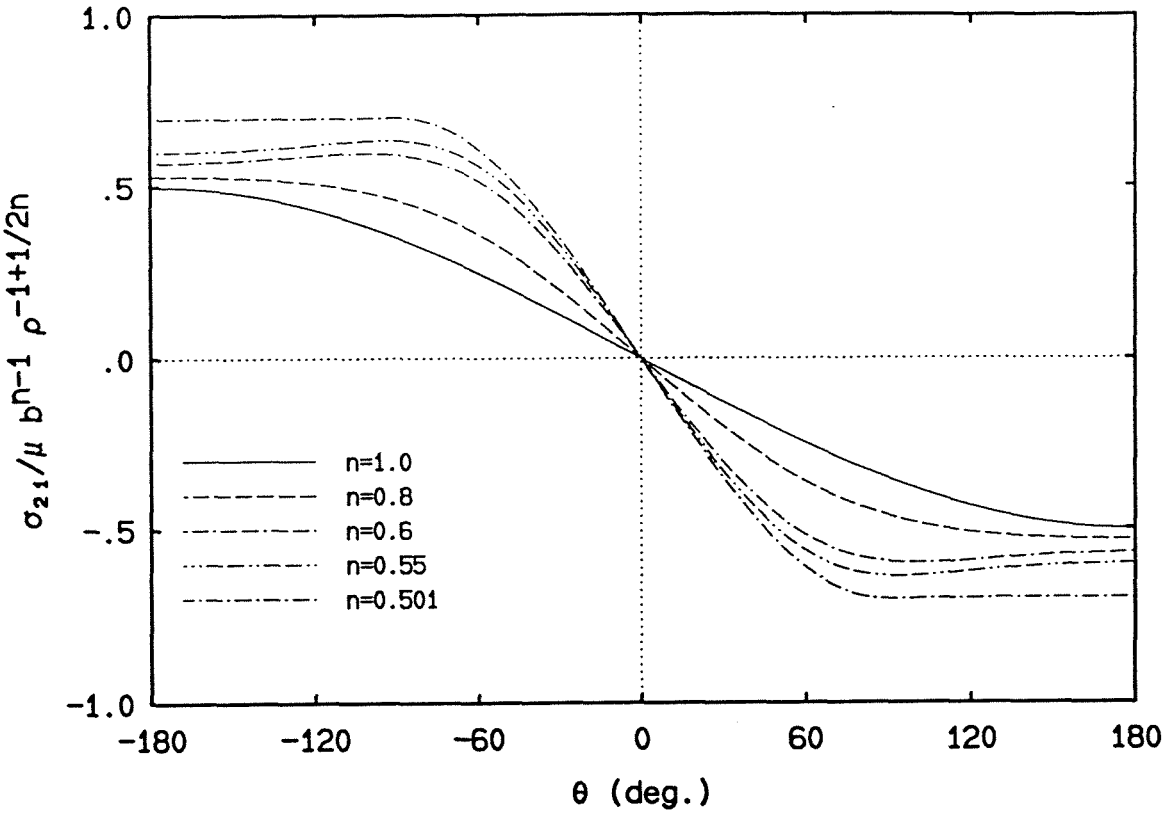

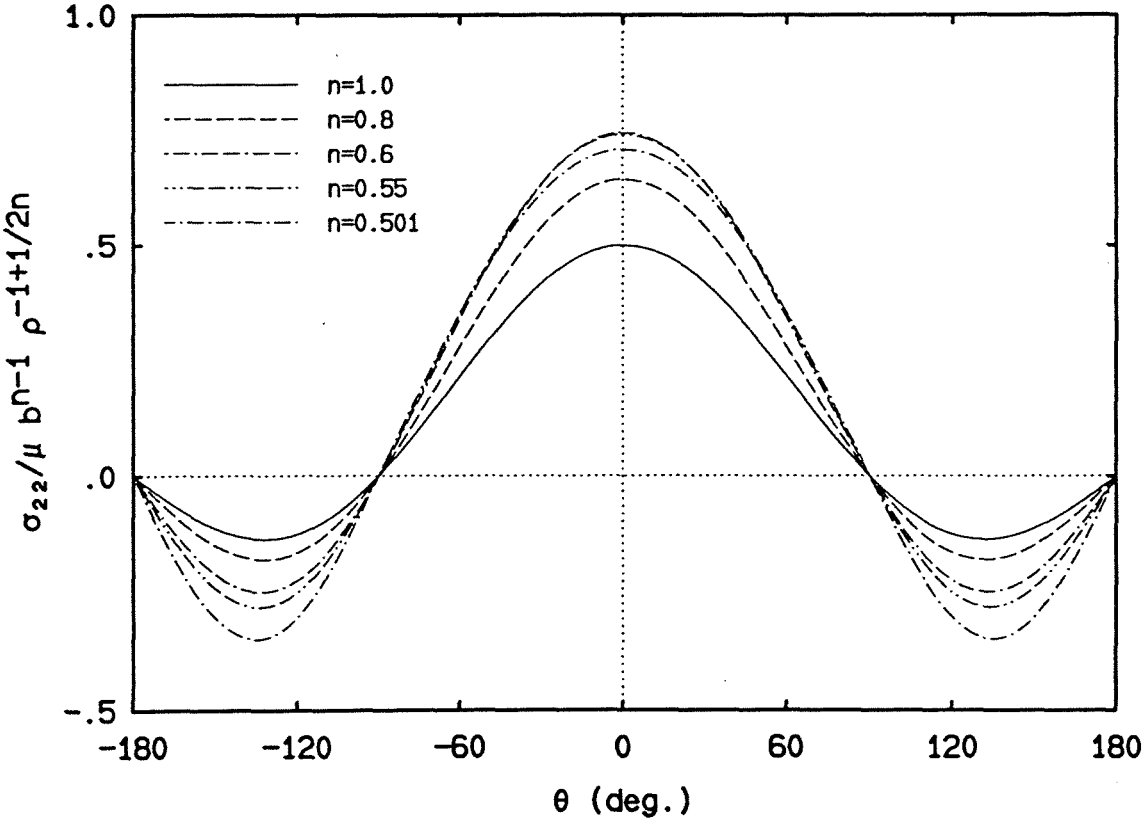

Figure 11 (Cont.). Angular variation of the nominal stresses $\sigma_{\alpha\beta}(r,\theta)$.

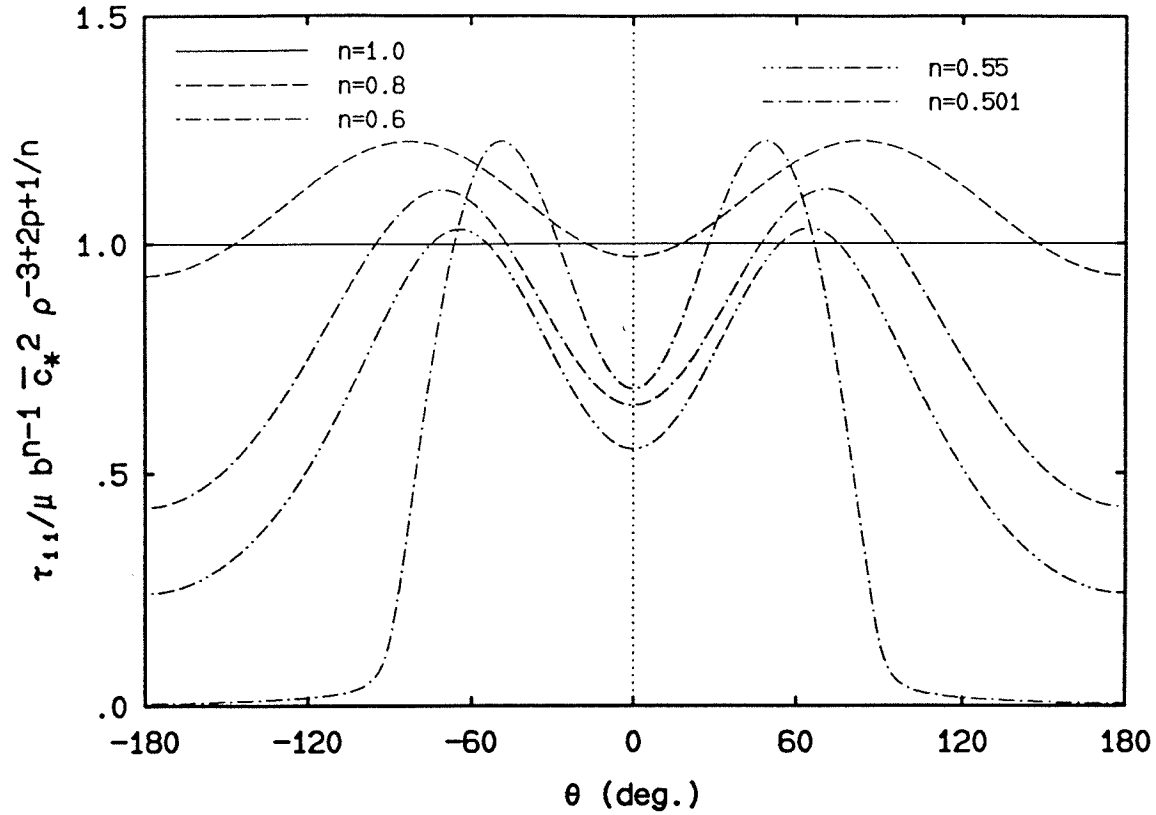

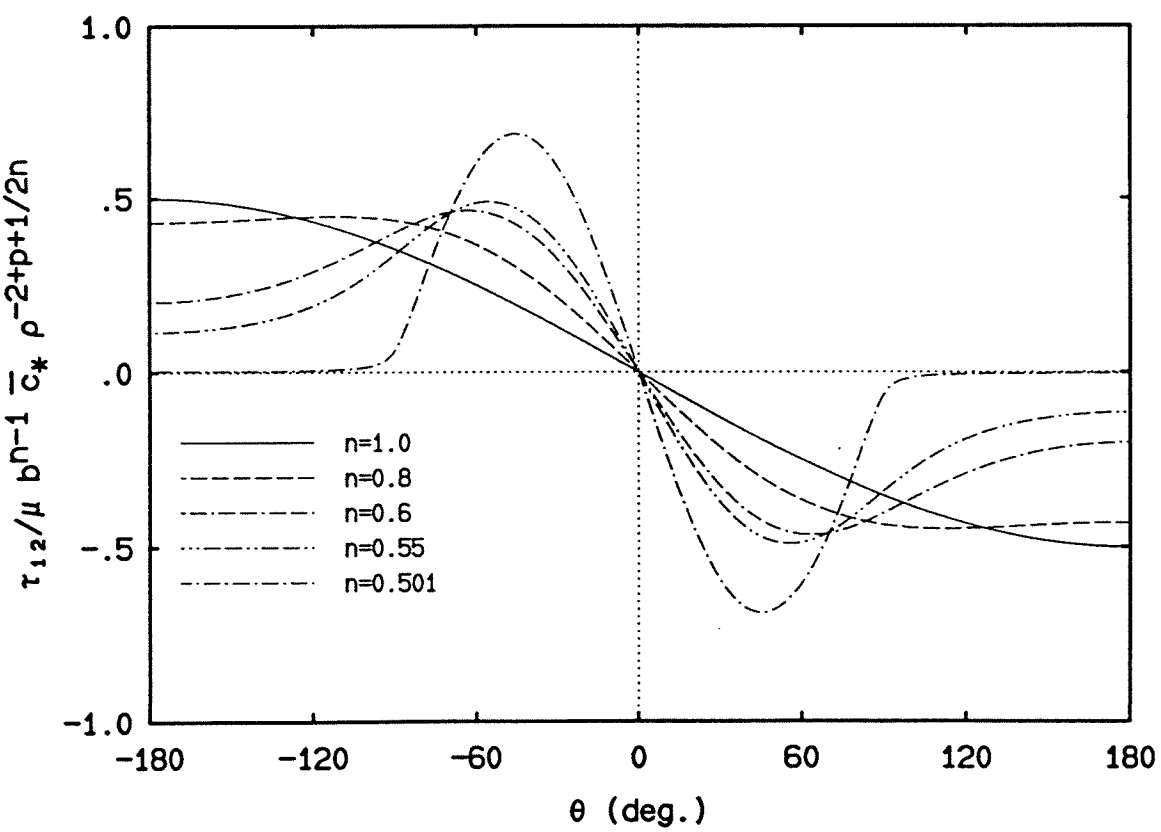

Figure 12. Angular variation of the true stresses $\tau_{\alpha\beta}(r,\theta)$.

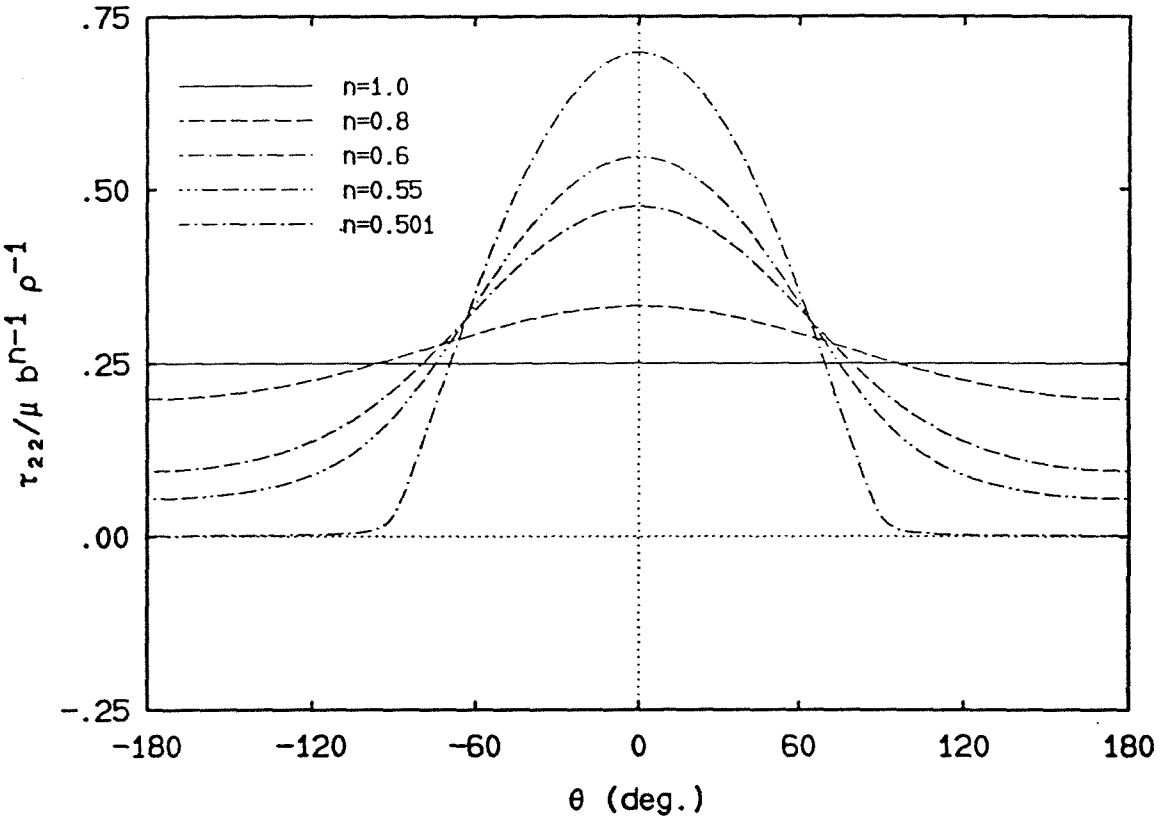

Figure 12 (Cont.). Angular variation of the true stresses $\tau_{\alpha\beta}(r,\theta)$.

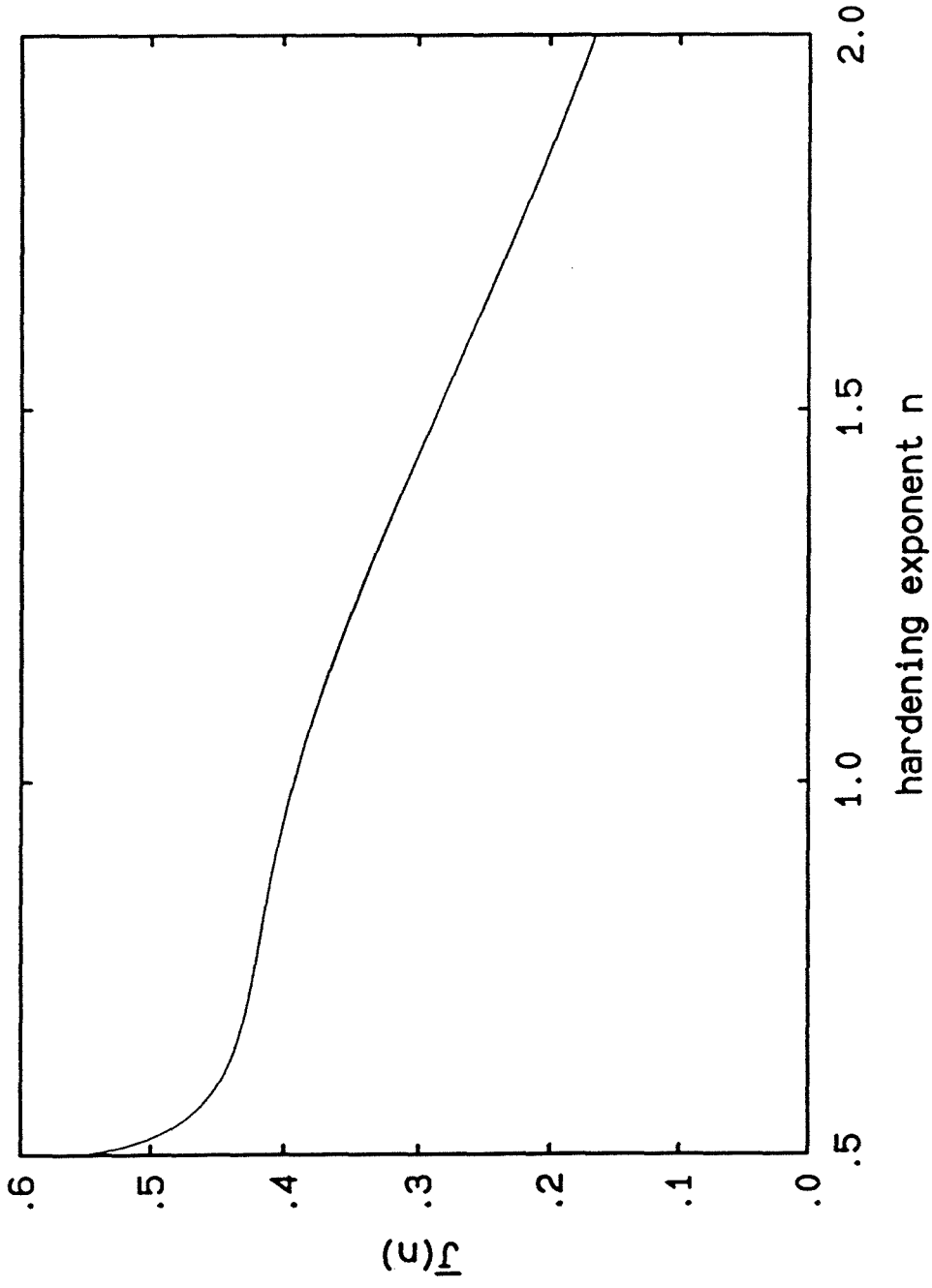

Figure 13. $\bar{J}(n)$ versus n.

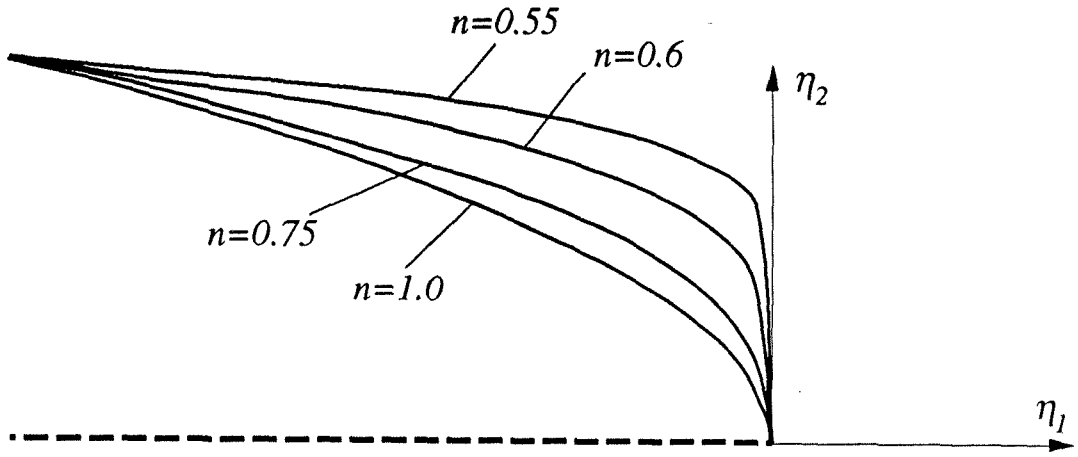

Figure 14. Deformed shape of the upper crack face - effect of n on the crack blunting.

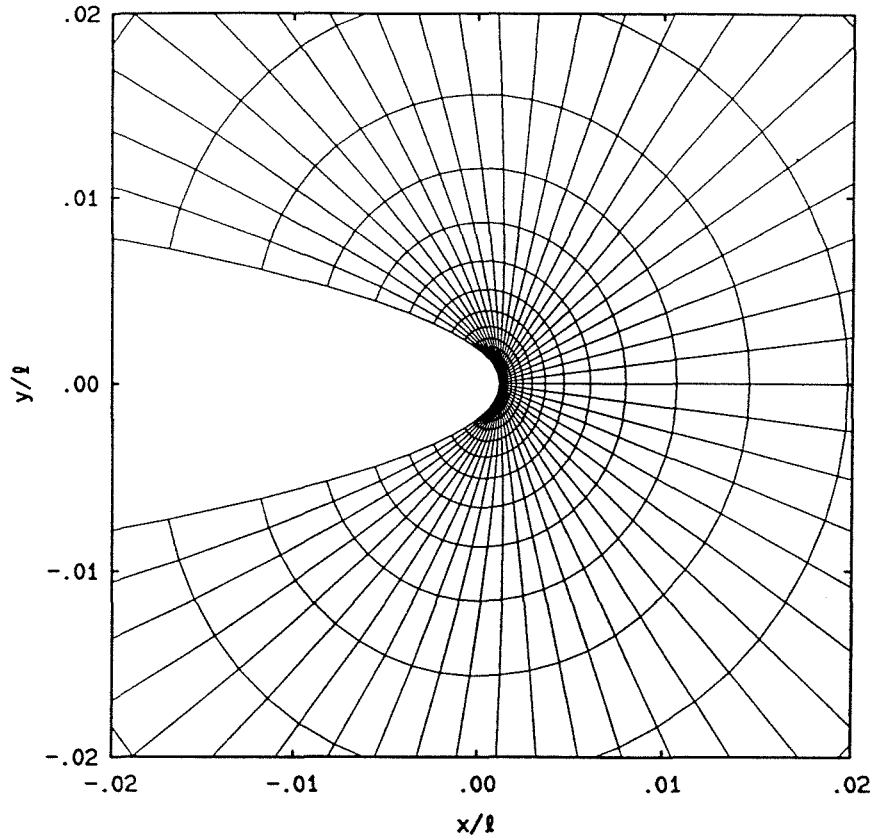

(a)

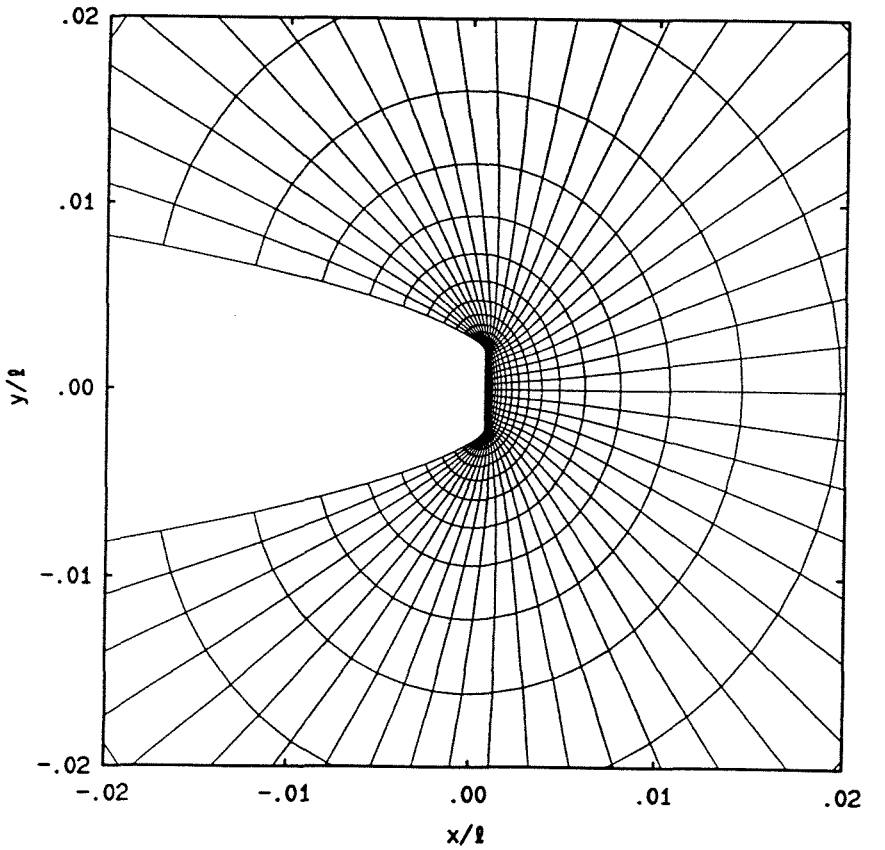

(b)

Figure 15. Crack blunting - numerical investigation : (a) *n=1.0*, (b) *n=0.55*.

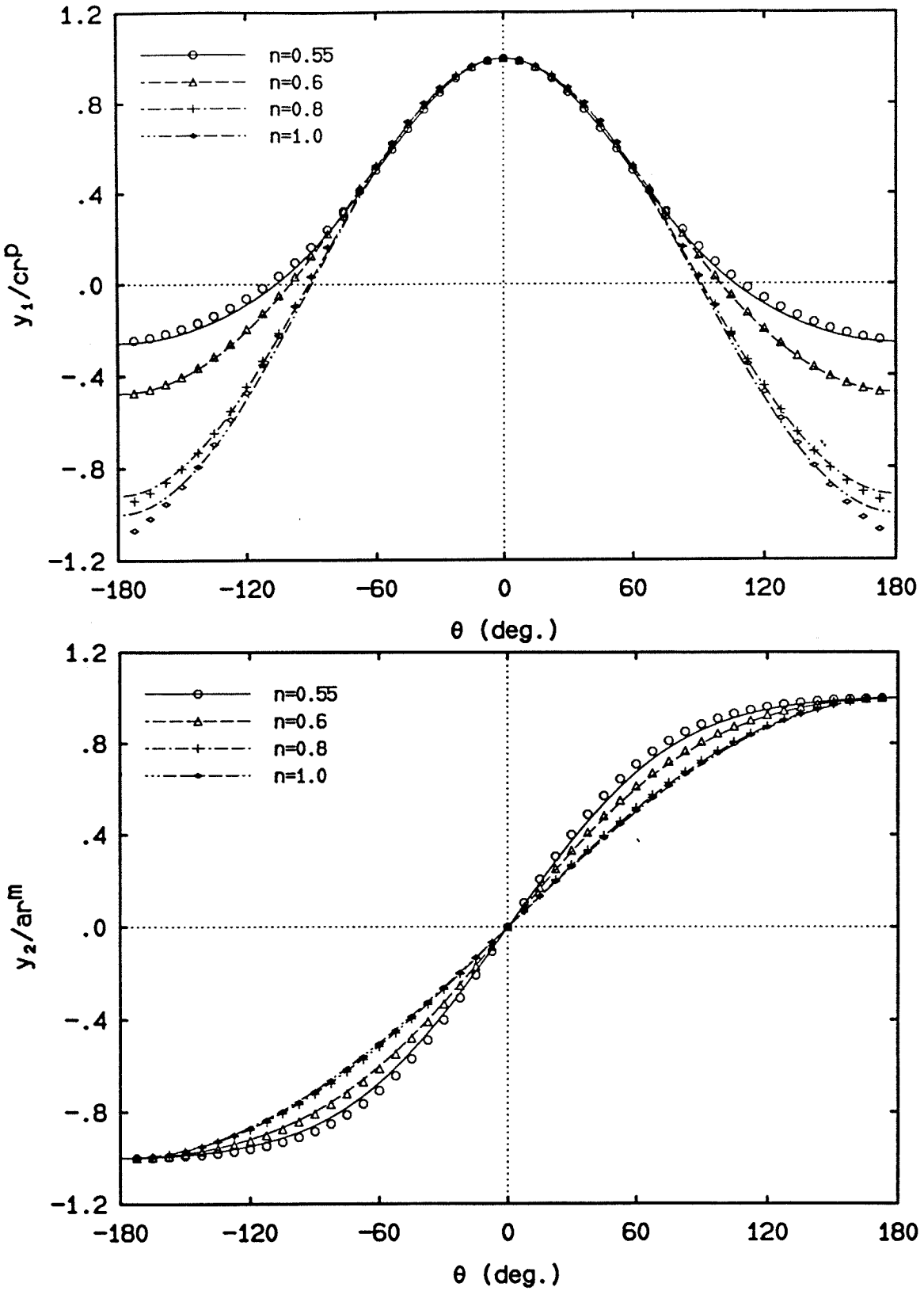

Figure 16. Comparison between asymptotics and numerics in the symmetric loading case : angular variation at $r/l = 10^{-5}$ of the deformed coordinates(a) y_1 , (b) y_2. The continuous curves correspond to the asymptotic solutions and the symbols to the numerical results.

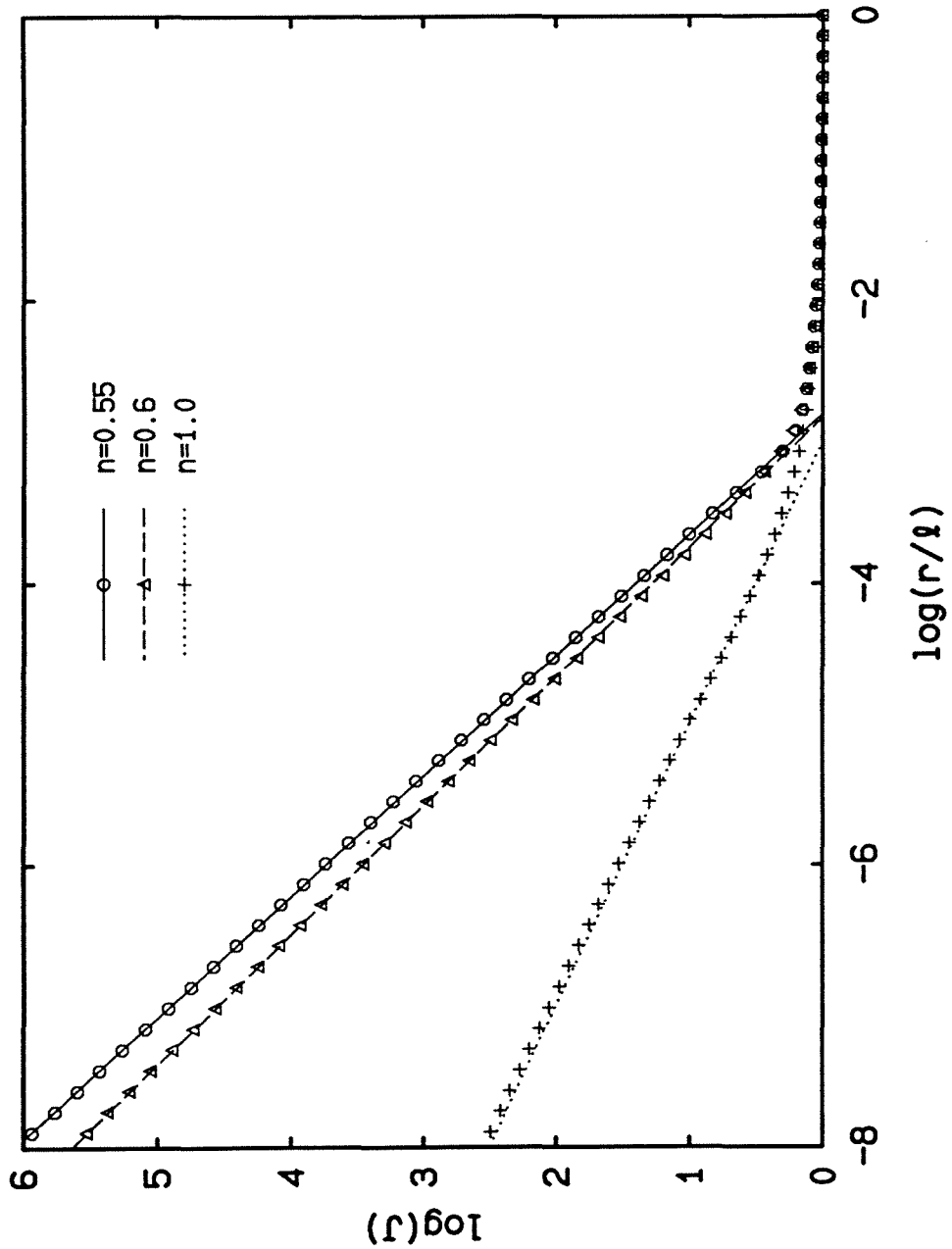

Figure 17. Radial variation of the Jacobian $J(r,\theta)$ along $\theta = 0$ in the non-symmetric loading case. The symbols represent the numerical results while the lines correspond to the analytical predictions.

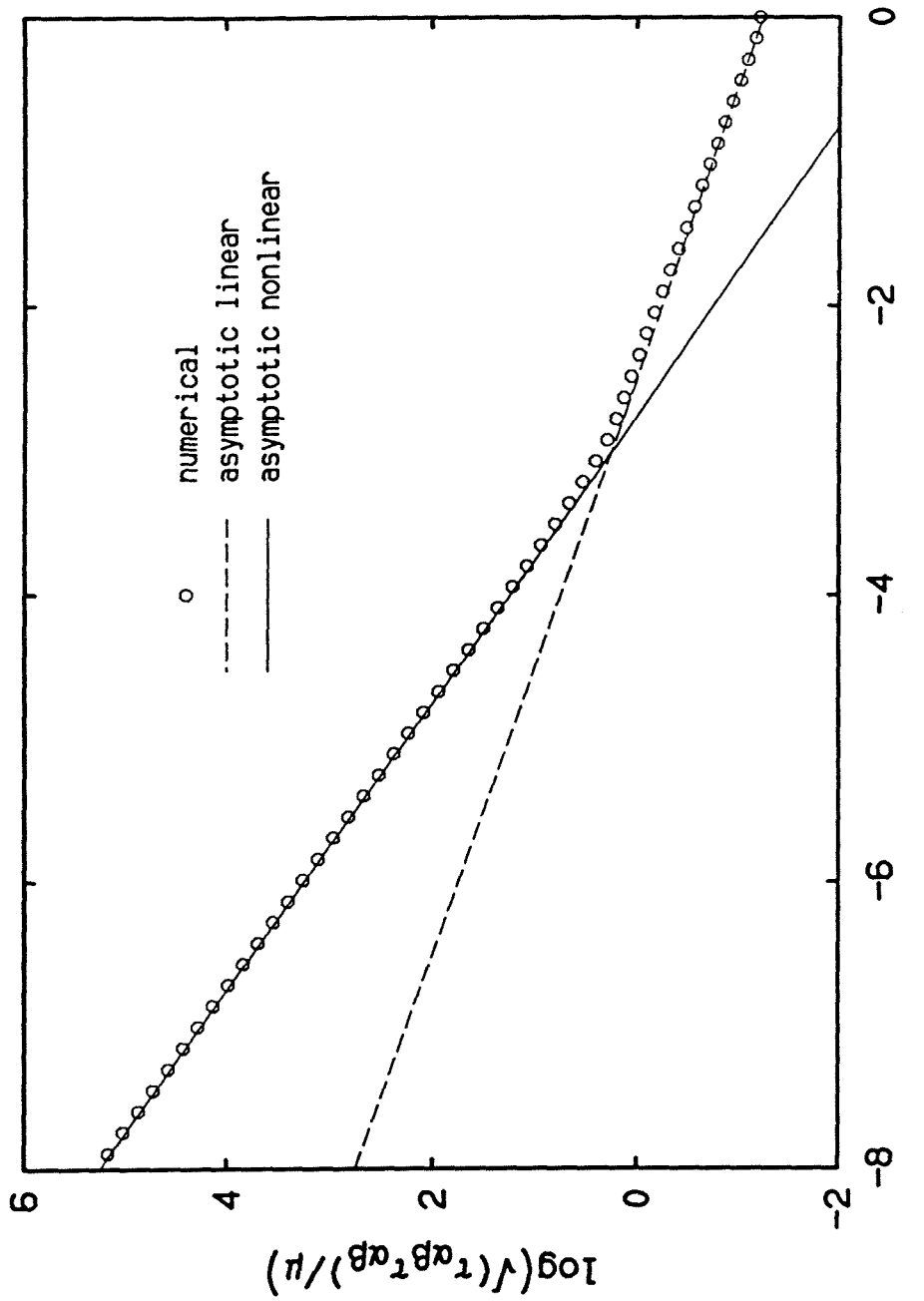

Figure 18. Determination of the size of the nonlinear zone - radial variation of $\sqrt{\tau_{\alpha\beta}\tau_{\alpha\beta}}$ along $\theta = 0$ in the mixed-mode loading case for $n=0.6$.

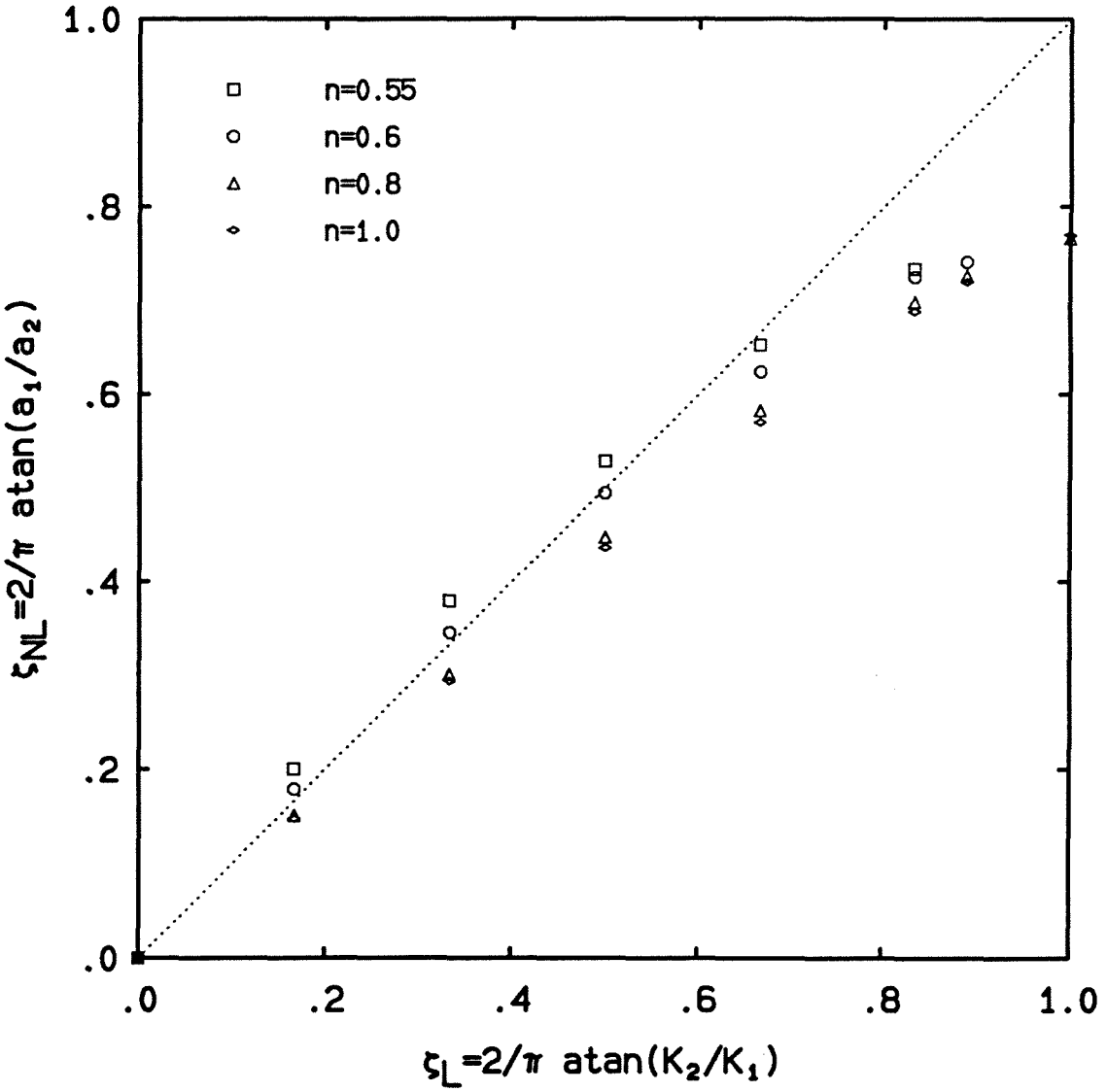

Figure 19. Relation between the linear ζ_L and nonlinear ζ_{NL} mode mixity parameters for various values of the "hardening" parameter n.

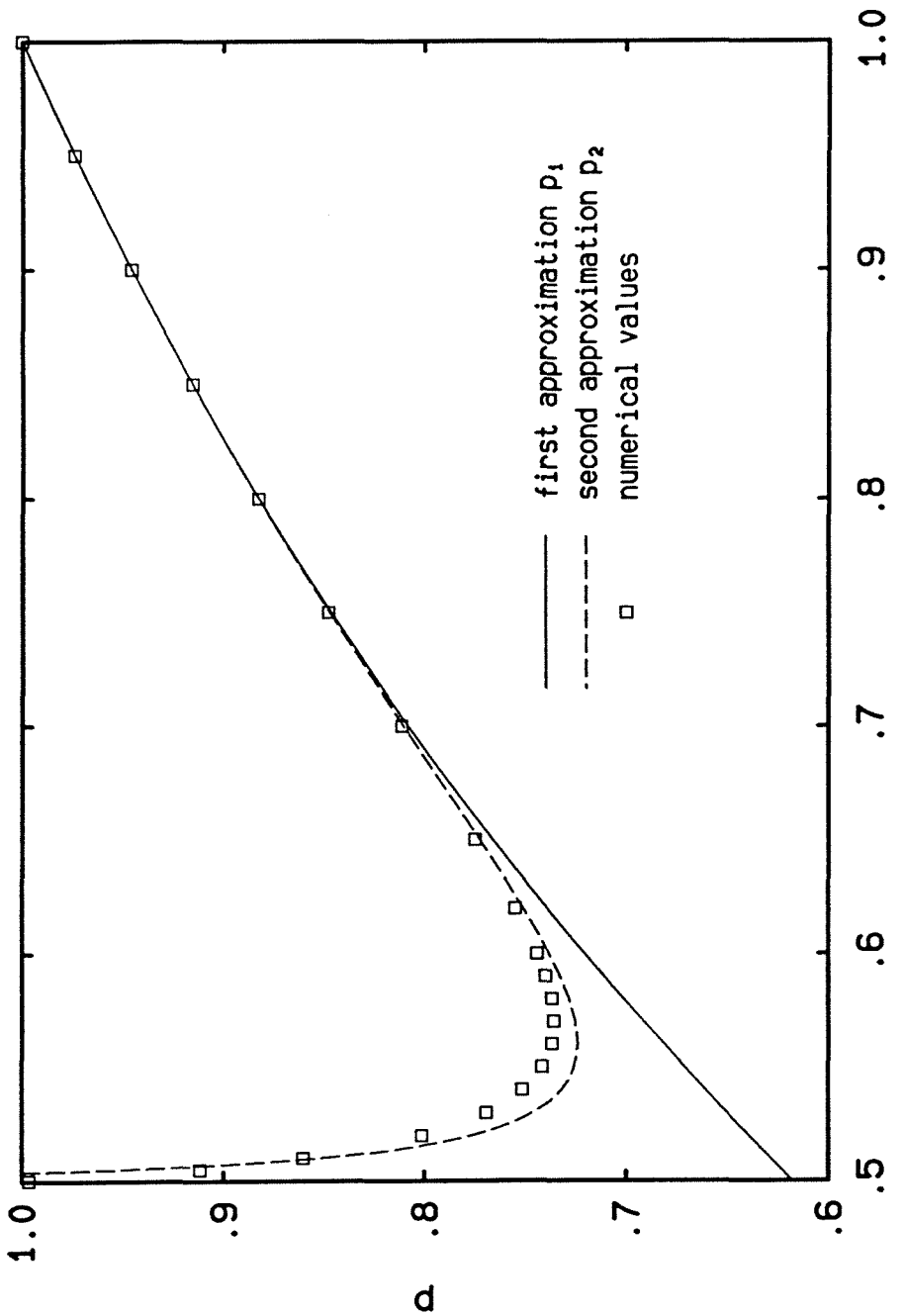

Figure A.1. WKB approximation of the eigenvalue p versus n.

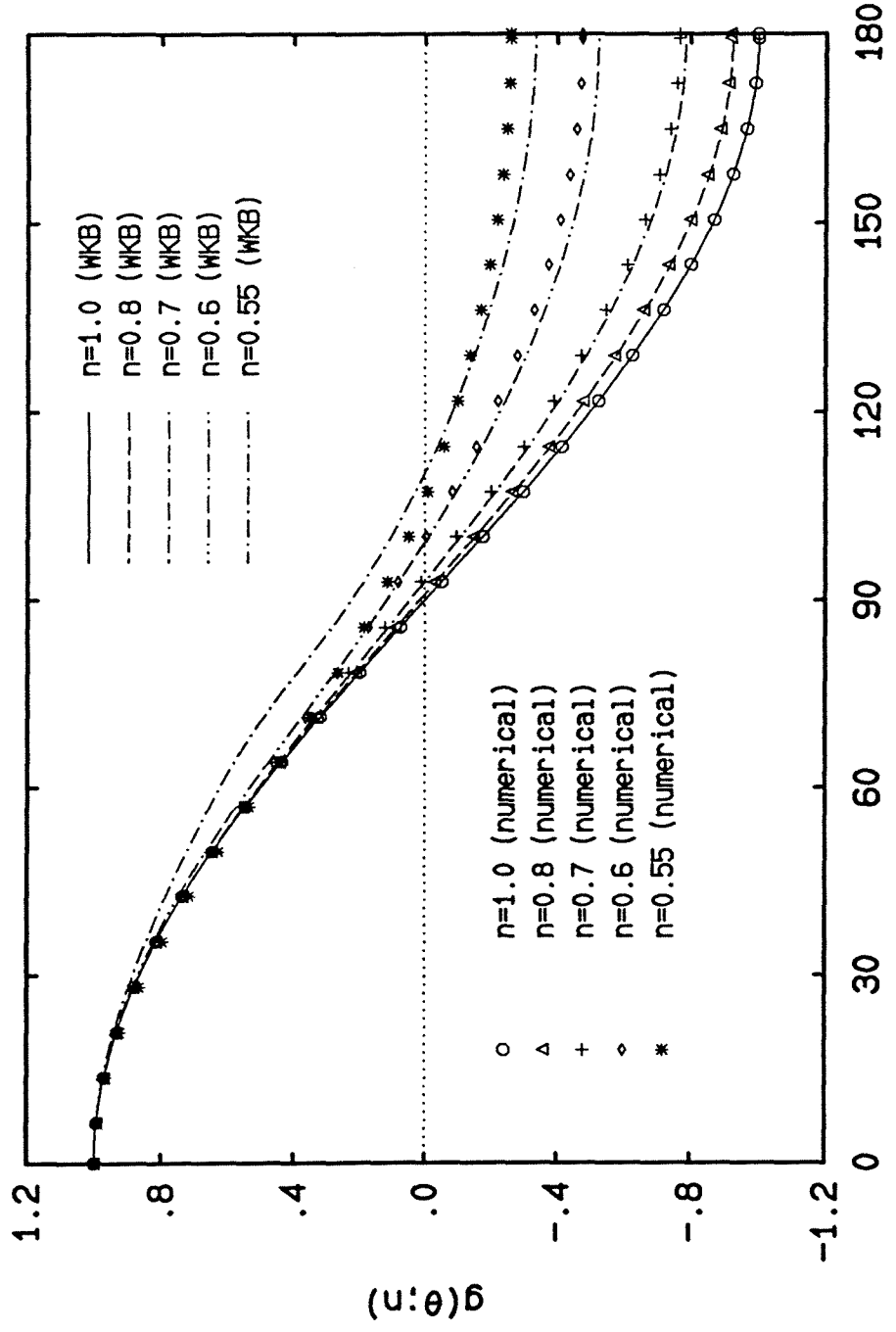

Figure A.2. WKB approximation of the eigenfunction $g(\theta;n)$ for various values of n.

Finite strain at the tip of a crack in a sheet of hyperelastic material : II. Special bimaterial cases.

Abstract.

An asymptotic analysis of the strain and stress near-tip fields for a crack in a sheet of Generalized Neo-Hookean materials is presented in this second in a series of three papers. The analysis is based on the nonlinear plane stress theory of elasticity and concerns two special cases of the interface crack problem : in the first situation both components have the same "hardening" behavior; next, we investigate the particular case of a sheet of Generalized Neo-Hookean material bonded to a rigid substrate. The transition between the two special cases is studied in detail. The analytical results are also compared with a full-field finite element solution.

1.- Introduction.

The multiplication of engineering applications involving bimaterial and multi-material components has motivated in the past decade an extensive interest in the mechanics of interfacial fracture. But this impetus has been impeded for a long time by the appearance of inconsistencies in the linearly elastic asymptotic solution to the interface crack problem : as was first noted by Williams [1] and confirmed by early work of Rice and Sih [2] and England [3], the singularity observed in the bimaterial situation is, in most cases, complex. This peculiarity has various undesirable consequences on the predicted near-tip fields : the deformation loses its consistency

(i.e., is not one-to-one), the crack faces overlap and the stress components change sign (i.e., alternate multiply from tension to compression) as the crack tip is approached, thus generating what may be called an (artificial) contact zone.

In order to cope with the presence of such a contact zone, various approaches have been suggested. The most widely used one, on which most linearly elastic analyses of bimaterial fracture are based,[1] is the so-called concept of "small-scale contact," introduced by Rice [5]. This approach suggests that the effect of the contact zone can be neglected and the bimaterial asymptotic solution accurately represents the actual near-tip fields if the size of the contact zone remains a small fraction of the zone of dominance of the asymptotic field. Another approach consists in including the influence of the contact zone on the asymptotic fields [6-9] by assuming frictionless contact between the crack faces over some portion of the crack length. Aravas and Sharma [10] showed that the two aforementioned investigations are not incompatible and that their domains of applicability depend on the relative extent of the contact zone with respect to the size of the asymptotic K-field and the length of the crack. They also demonstrated that the asymptotic solution still presents difficulties in the form of material interpenetration very close to the crack tip, even when that contact is taken into account.

Recent investigations summarized in [11] have included the effect of elastoplastic nonlinearity on the interface crack tip fields. It is shown for these small-deformation analyses that, although the near-tip fields can be characterized by a local "plastic mixity parameter" and show a fair amount of similarity with the mixed-mode homogeneous case, there is no bimaterial equivalent to the separable HRR asymptotic fields and that a nonlinear stress-strain relation mitigates but does not eliminate the inconsistencies associated with the linearly elastic solution. The extension of

[1] See, for example, the review article by Hutchinson and Suo [4].

Comninou's elastic analysis of the contact problem to the elastoplastic case has been performed by Aravas and Sharma [10,12,13] who showed, through asymptotic and numerical investigations, that a separable HRR-type solution is possible if frictionless contact is assumed between the crack faces. The domain of validity of the different asymptotic solutions is determined by the relative importance of the various characteristic lengths of the problem : geometric length scale (e.g., crack length), extent of the K-field, size of the plastic zone and of the contact zone and dimension of the large deformation/fracture process area.

The issue of the presence of inconsistencies in the near-tip fields has been also investigated by Knowles and Sternberg [14] who showed that, by relinquishing the assumption of small deformations, a smooth opening of the crack near its end is obtained. Their analysis, which has been corroborated numerically by Ravichandran and Knauss [15], focused on the effect of geometrical nonlinearities (large deformations) by investigating the case of an interface crack between two sheets of incompressible Neo-Hookean materials. Material nonlinearities have been added by Herrmann [16] who studied asymptotically the plane strain case of an interface crack between two bonded slabs of compressible hyperelastic materials, allowing for different "hardening" behaviors across the interface.

In this paper, an asymptotic and numerical analysis of the interface fracture problem within the finite strain theory of plane stress is presented for two special bimaterial situations : first, the two components are assumed to have similar "hardening" behaviors; then, we explore the case of a sheet bonded to a rigid substrate. The present work constitutes the second of a series of three papers relative to the combined effect of geometrical and material nonlinearities on the near-tip fields for a class of hyperelastic materials. The first paper [17] deals with the homogeneous case while the third one [18] concerns the general bimaterial situation for which a difference

in "hardening" behaviors is allowed for the two components. The two special cases described in the present paper have been chosen because, despite their relative simplicity compared to the general bimaterial situation, they contain most of the characteristics inherent in the nonlinear interface near-tip fields. Furthermore, the second bimaterial situation delineated in this paper, in which a sheet of hyperelastic material is bonded to a rigid substrate, cannot be obtained directly from the general problem depicted in [18] due to the presence of different types of bond conditions along the interface.

The material model used throughout these investigations is the so-called "Generalized Neo-Hookean" (GNH) model which has been discussed in some detail in the first paper. But, in order to render this paper self-contained, it appeared useful to briefly mention in the next section the main characteristics of the material model, together with a reminder of the basic relations associated with the nonlinear plane stress theory of elasticity. Sections 3 and 4 are dedicated to an asymptotic analysis of the two special bimaterial situations described above. Finally, the fifth section contains a comparison of the obtained asymptotic fields with a full-field finite element analysis, together with a discussion of the transition between the two special bimaterial cases.

2.- Basic relations of finite plane stress elastostatics - Generalized Neo-Hookean model.

This section summarizes the fundamental relations governing the nonlinear elastostatics theory of plane stress for a class of homogeneous isotropic incompressible hyperelastic materials. The details of the computation, together with a list of related references, can be found in [17]. The notations employed throughout the present paper are identical to those used in [17].

Let Π represent the undeformed mid-plane cross-section of a thin sheet of hyperelastic material and let Π^* denote the associated deformed configuration obtained through the deformation

$$\boldsymbol{y} = \hat{\boldsymbol{y}}(\boldsymbol{x}) = \boldsymbol{x} + \boldsymbol{u}(\boldsymbol{x}), \qquad \text{on } \Pi, \tag{2.1}$$

where[2] $\boldsymbol{x}$ and $\boldsymbol{y}$ are the undeformed and deformed coordinate vectors respectively and $\boldsymbol{u}$ is the displacement field. The mapping $\hat{\boldsymbol{y}}(\boldsymbol{x})$ is assumed to be twice continuously differentiable and uniquely invertible on Π. The nominal (Piola) stress field $\boldsymbol{\sigma}$ associated with the deformation satisfies, in the absence of body forces, the equilibrium equations

$$div\boldsymbol{\sigma} = \boldsymbol{0}, \qquad \text{on } \Pi. \tag{2.2}$$

The true (Cauchy) stress field is denoted by $\boldsymbol{\tau}$ and is related to the nominal stress tensor by

$$\boldsymbol{\tau} = \boldsymbol{\sigma}\boldsymbol{F}^T, \qquad \text{on } \Pi^*, \tag{2.3}$$

where $\boldsymbol{F} = \nabla \boldsymbol{y}$ is the deformation gradient tensor field. It has to be noted that, while rotational equilibrium requires that $\boldsymbol{\tau}$ be symmetric, $\boldsymbol{\sigma}$ is, in general, not symmetric. Finally, assuming that the material is hyperelastic, homogeneous and isotropic, the constitutive relations take the form

$$\boldsymbol{\sigma} = 2U_I\boldsymbol{F} + JU_J\boldsymbol{F}^{-T}, \qquad \text{on } \Pi, \tag{2.4}$$

where I and J are the scalar invariants associated with the deformations and defined by

$$\begin{aligned} I &= tr(\boldsymbol{F}\boldsymbol{F}^T) = y_{\alpha,\beta}y_{\alpha,\beta}, \\ J &= det\,\boldsymbol{F} = \lambda^{-1} = y_{1,1}y_{2,2} - y_{1,2}y_{2,1}, \end{aligned} \tag{2.5}[3]$$

---

[2] Throughout this paper, boldface quantities denote two-dimensional vectors or second-order tensors.

[3] Greek indices take the value 1 and 2 and summation on repeated index is implied, unless specified otherwise. Furthermore $y_{\alpha,\beta}$ denotes $\partial y_\alpha / \partial x_\beta$.

and where U_I and U_J are the partial derivatives of the plane stress elastic potential $U(I,J)$ with respect to I and J respectively. In (2.5), λ denotes the transverse stretch, which is equal to the inverse of the in-plane Jacobian J since the incompressibility of the material requires that the deformations be isochoric.

The material characterization which will be used throughout this analysis is the Generalized Neo-Hookean (GNH) model, first introduced by Knowles [19] to study the nonlinear effects in the antiplane shear (mode III) case. It necessitates the introduction of three material constants, a shear modulus μ, a "hardening" exponent n and a "yielding" parameter b, which define the plane stress elastic potential $U(I,J)$ as

$$U(I,J)=\frac{\mu}{2b}\left\{\left[1+\frac{b}{n}\left(I+J^{-2}-3\right)\right]^{n}-1\right\}. \tag{2.6}$$

Substituting (2.6) into (2.4) and with the aid of (2.3), we have the expression for the nominal and true stress components

$$\sigma_{\alpha\beta}=\mu A^{n-1}\{y_{\alpha,\beta}-\lambda^{3}\varepsilon_{\alpha\mu}\varepsilon_{\beta\nu}y_{\mu,\nu}\}, \tag{2.7}$$

$$\tau_{\alpha\beta}=\mu A^{n-1}\{y_{\alpha,\gamma}y_{\beta,\gamma}-\lambda^{2}\delta_{\alpha\beta}\}, \tag{2.8}$$

where λ is the transverse stretch, $\varepsilon_{\alpha\beta}$ is the two-dimensional alternator ($\varepsilon_{11}=\varepsilon_{22}=0$, $\varepsilon_{12}=-\varepsilon_{21}=1$), $\delta_{\alpha\beta}$ is the unit tensor and

$$A=1+b(I+\lambda^{2}-3)/n. \tag{2.9}$$

The equilibrium equations (2.2) is rewritten in terms of the deformed coordinates y_α as

$$A^{n-2}\left\{\frac{b(n-1)}{n}\left(\frac{\partial I}{\partial x_\beta}+\frac{\partial\lambda^{2}}{\partial x_\beta}\right)\left(y_{\alpha,\beta}-\lambda^{3}\varepsilon_{\alpha\mu}\varepsilon_{\beta\nu}y_{\mu,\nu}\right)+A\left(\nabla^{2}y_\alpha-\frac{\partial\lambda^{3}}{\partial x_\beta}\varepsilon_{\alpha\mu}\varepsilon_{\beta\nu}y_{\mu,\nu}\right)\right\}=0. \tag{2.10}$$

Note that, when $n = 1$, the GNH model reduces to the Neo-Hookean characterization which was used by Knowles and Sternberg in [14]. In this case, the equilibrium equations (2.10) reduce to

$$\nabla^2 y_\alpha = \frac{\partial \lambda^3}{\partial x_\beta} \varepsilon_{\alpha\mu} \varepsilon_{\beta\nu} y_{\mu,\nu}. \tag{2.11}$$

The physical significance of the three material parameters μ, b and n has been illustrated in section 2 of [17] through a description of the behavior of this class of hyperelastic materials under uniaxial tension (see figures 1 and 2 in [17]). It is shown there that the engineering (nominal) stress increases with the elongation as long as $n > 1/2$. It can be shown that $n = 1/2$ is the limiting value of the "hardening" exponent for which the equilibrium equations (2.10) loose their ellipticity. Throughout the present work, we will rule out non-elliptic situations, and thus assume $n > 1/2$.

In the next two sections, a local analysis of two special bimaterial fracture problems involving the class of incompressible materials described above is summarized : first, the case of an interface crack between two sheets with similar "hardening" characteristics is investigated, followed by the problem of a sheet of GNH bonded to a rigid substrate.

3.- Local analysis of the near-tip fields for an interface crack between two GNH sheets with the same "hardening" characteristics.

Problem formulation.

The bimaterial geometry on which the local analysis is performed is represented in figure 1. The mid-plane of the two bonded semi-infinite GNH sheets are denoted by $H^{(1)}$ and $H^{(2)}$. The Cartesian system is chosen such that the crack line is expressed as

$$\mathcal{L} = \{\boldsymbol{x} \mid \quad x_1 \le 0, \quad x_2 = 0\}, \tag{3.1}$$

and the interface consists of the remainder of the x_1-axis. The undeformed domain Π is the whole (x_1, x_2) plane exterior to $\mathcal{L}$. The material properties of the upper and lower sheets are $(\mu^{(1)}, b^{(1)}, n^{(1)})$ and $(\mu^{(2)}, b^{(2)}, n^{(2)})$ respectively. Our objective in this section is to obtain an asymptotic representation of the near-tip fields, in terms of the local polar coordinates (r, θ) defined in figure 1, which satisfies the equilibrium equations (2.10) together with the bond conditions

$$\begin{aligned} &y_\alpha(r, 0^+) = y_\alpha(r, 0^-), \\ &\sigma_{\alpha 2}(r, 0^+) = \sigma_{\alpha 2}(r, 0^-), \end{aligned} \qquad (r > 0), \tag{3.2}$$

and the traction-free conditions along the crack faces

$$\sigma_{\alpha 2}(r, \pm\pi) = 0, \qquad (r > 0), \tag{3.3}$$

in the special case *when the two "hardening" exponents are identical across the interface*, i.e., $n^{(1)} = n^{(2)} = n$.

In addition to the aforementioned conditions, we require that the asymptotic deformation field be non-oscillatory and that the transverse stretch λ vanish (or equivalently, the transformation Jacobian become unbounded) as the crack tip is approached in both semi-infinite sheets. The latter condition implies that not all the deformation gradient components remain bounded as $r \to 0$. Note that a vanishing value of the transverse stretch signifies that the bimaterial sheet undergoes an extreme thinning at the crack tip. Finally, the deformation field has to satisfy certain continuity requirements on each half plane which would justify the various differentiations involved in the equilibrium equations and the boundary conditions.

First-order term.

We turn now to the computation of the asymptotic term of near-tip deformation field, which is assumed to take the form

$$y_\alpha^{(k)}(r,\theta) \sim r^{m^{(k)}} v_\alpha^{(k)}(\theta), \qquad (r>0), \tag{3.4}$$[4]

where the superscript in parentheses "*(k)*" denotes the component number *(k=1,2)*. Summation over this "material index" is *never* implied. Thus (3.4) is equivalent to

$$\begin{aligned} y_\alpha^{(1)}(r,\theta) &\sim r^{m^{(1)}} v_\alpha^{(1)}(\theta), \qquad (0 \le \theta \le \pi), \\ y_\alpha^{(2)}(r,\theta) &\sim r^{m^{(2)}} v_\alpha^{(2)}(\theta), \qquad (-\pi \le \theta \le 0). \end{aligned} \tag{3.5}$$

Various considerations lead to a direct estimation of the exponents $m^{(k)}$: firstly, in order to prevent oscillations in the near-tip solution, $m^{(1)}$ and $m^{(2)}$ must be real. Furthermore, to satisfy the boundedness of the displacements at the crack tip together with the requirement on the transverse stretch λ, we impose

$$0 < m^{(k)} < 1. \tag{3.6}$$

The matching conditions along $\theta = 0$ are rewritten with the aid of (3.4) as

$$\begin{aligned} r^{m^{(1)}} v_\alpha^{(1)}(0^+) &= r^{m^{(2)}} v_\alpha^{(2)}(0^-), \\ r^{(2n-1)(m^{(1)}-1)} M_\alpha^{(1)}(0^+) &= r^{(2n-1)(m^{(2)}-1)} M_\alpha^{(2)}(0^-), \end{aligned} \tag{3.7}$$

where

$$M_\alpha(0) = \mu \left(\frac{b}{n}\right)^{n-1} \left(m^2 v_\beta(0) v_\beta(0) + \dot{v}_\beta(0)\dot{v}_\beta(0)\right) \dot{v}_\alpha(0). \tag{3.8}$$[5]

---

[4] Throughout this paper, the asymptotic equality symbol "~" has the standard meaning.

[5] Henceforth, for brevity purpose, the material index "*(k)*" will be dropped unless clarity requires it. Thus, in (3.8), $M_\alpha(\theta)$ denotes $M_\alpha^{(1)}(\theta)$ for $0 \le \theta \le \pi$ and $M_\alpha^{(2)}(\theta)$ for $-\pi \le \theta \le 0$. In the same equation, $\dot{(\,)}$ denotes differentiation with respect to θ.

Since $v_\alpha(0)$ and $M_\alpha(0)$ cannot vanish simultaneously, (3.7) yields

$$m^{(1)} = m^{(2)} = m. \tag{3.9}$$

The relation between the first asymptotic exponent m and the "hardening" parameter n can be obtained by using the conservation integral $\mathcal{J}$ [20] defined as

$$\mathcal{J} = \int_\Gamma (U n_1 - \sigma_{\alpha\beta} n_\beta y_{\alpha,1}) ds, \tag{3.10}$$

where Γ is any regular contour surrounding the crack tip and crossing the interface (figure 1), $\boldsymbol{n}$ is the unit outward normal to Γ and U is the elastic potential introduced in (2.6). An investigation of the leading order of the integrant in (3.10) leads to

$$m = 1 - \frac{1}{2n}, \tag{3.11}$$

which satisfies the inequalities (3.6).

In order to determine the angular distributions $v_\alpha^{(k)}(\theta)$ of the first asymptotic term, the leading terms of the equilibrium equations (2.10) are extracted with the aid of (3.4) and (3.11) to yield the following asymptotic form

$$(n-1)\frac{\partial I}{\partial x_\beta} y_{\alpha,\beta} + I \nabla^2 y_\alpha = 0, \qquad (r \to 0, -\pi \le \theta \le \pi), \tag{3.12}$$

where $I = y_{\gamma,\delta}\, y_{\gamma,\delta}$. By combining (3.4), (3.11) and (3.12), the system of coupled nonlinear second-order differential equations in $v_\alpha(\theta)$ is obtained as

$$B \ddot{v}_\alpha + (n-1)\dot{B}\dot{v}_\alpha + \frac{2n-1}{4n^2} B v_\alpha = 0, \tag{3.13}$$

where

$$B(\theta) = m^2 v_\gamma(\theta)\, v_\gamma(\theta) + \dot{v}_\gamma(\theta)\, \dot{v}_\gamma(\theta). \tag{3.14}$$

Note that these equations are similar to those governing the first term of the mixed-mode solution for the homogeneous problem [17]. The asymptotic form of the stress-free conditions (3.3) along the crack faces is

$$v_\alpha(\pm\pi) = 0. \tag{3.15}$$

The general solution of (3.13)-(3.15) has been obtained in [17] using previous results of Knowles and Sternberg [21] and is

$$v_\alpha^{(k)}(\theta) = a_\alpha^{(k)} f(\theta; n), \tag{3.16}$$

where $a_\alpha^{(k)}$ are four undetermined constants and $f(\theta; n)$ is given by

$$f(\theta; n) = \left[n(\omega + k\cos\theta)\right]^{\frac{n-1}{2n}} \sin\frac{\theta}{2}\left[1 - \frac{2k^2\cos^2\theta/2}{1+\omega}\right]^{1/2}, \tag{3.17}$$

with

$$\begin{aligned} k &= 1 - 1/n, \\ \omega &= [1 - k^2\sin^2\theta]^{1/2}, \end{aligned} \tag{3.18}$$

and is represented in figure 5 of [17].

Since $f^{(1)}(0^+; n) = f^{(2)}(0^-; n) = 0$, the first matching condition (3.2a) is satisfied. The continuity of tractions across the interface (3.2b) provides the following relations between $a_\alpha^{(1)}$ and $a_\alpha^{(2)}$

$$\mu^{(1)}\left[\frac{b^{(1)}}{n}\left(a_1^{(1)^2} + a_2^{(1)^2}\right)\right]^{n-1} a_\alpha^{(1)} = \mu^{(2)}\left[\frac{b^{(2)}}{n}\left(a_1^{(2)^2} + a_2^{(2)^2}\right)\right]^{n-1} a_\alpha^{(2)}, \tag{3.19}$$

which yields

$$\frac{a_1^{(1)}}{a_1^{(2)}} = \frac{a_2^{(1)}}{a_2^{(2)}} = \frac{1}{\xi}, \tag{3.20}$$

where

$$\xi = \left[\frac{\mu^{(1)}}{\mu^{(2)}} \left(\frac{b^{(1)}}{b^{(2)}} \right)^{n-1} \right]^{1/2n-1} . \tag{3.21}$$

We can thus write the first term of the asymptotic expansion as

$$y_\alpha(r,\theta) \sim a_\alpha \, j(\theta) f(\theta;n) r^m, \tag{3.22}$$

where a_α are two constants left undetermined by the present local analysis[6] and which depend on the far-field conditions, the geometry of the global crack problem and the material characteristics of the bimaterial combination; $f(\theta;n)$ and m are given by (3.17) and (3.11) respectively, while $j(\theta)$ is the step-function

$$j(\theta) = \begin{cases} 1 & \text{for } 0 \le \theta \le \pi, \\ \xi & \text{for } -\pi \le \theta \le 0, \end{cases} \tag{3.23}$$

in which ξ, defined in (3.21), is a function of the material constants $\mu^{(k)}$, $b^{(k)}$ and n.

It can readily be shown that the Jacobian J of the transformation described by (3.22) vanishes identically, which contradicts the consistency requirement of the solution and leaves the transverse stretch $\lambda = J^{-1}$ undetermined. It is therefore necessary to obtain a second term in the asymptotic expansion of the near-tip deformation field.

Second-order terms.

Motivated by the first-term analysis described above, we assume that the two-term asymptotic expansion has the form

---

[6] See the relation between a_α and the conservation integral J later in this section.

$$y_\alpha(r,\theta) \sim a_\alpha\, j(\theta) f(\theta;n) r^m + r^{s^{(k)}} w_\alpha^{(k)}(\theta), \qquad (3.24)^7$$

where $s^{(k)} > m$. An examination of the order of the various terms constituting the equilibrium equations (2.10) leads to the same asymptotic form (3.12) which, in turn, yields, with the aid of (3.24) and assuming $a_2 \neq 0$,

$$\begin{aligned} &(1+a_{12}^2)H_1^s(w_1) + 2a_{12}^2 H_2^s(w_1) + 2a_{12}H_2^s(w_2) = 0, \\ &(1+a_{12}^2)H_1^s(w_2) + 2a_{12}H_2^s(w_1) + 2\,H_2^s(w_2) = 0, \end{aligned} \qquad (3.25)$$

where $a_{12} = a_1/a_2$ and $H_\alpha^s(w)$ are two linear second-order differential operators similar to those encountered in the general (mixed-mode) homogeneous situation

$$\begin{aligned} H_1^s(w) &= B_f D_w + (n-1)(2s(m-1)B_f w + \dot{B}_f \dot{w}), \\ H_2^s(w) &= D_f E_w + (n-1)(m(m+s-2)f\,E_w + \dot{f}\,\dot{E}_w), \end{aligned} \qquad (3.26)$$

with

$$\begin{aligned} B_f &= \dot{f}^2 + m^2 f^2, & E_w &= ms\,f\,w + \dot{f}\,\dot{w}, \\ D_f &= \ddot{f} + m^2 f, & D_w &= \ddot{w} + s^2 w. \end{aligned} \qquad (3.27)$$

Note that, due to (3.20),

$$a_{12}^{(1)} = a_{12}^{(2)} = a_{12}. \qquad (3.28)$$

The traction-free boundary conditions along the crack faces are equivalently written as

$$\dot{w}_\alpha(\pm\pi) = 0. \qquad (3.29)$$

As was the case for the first asymptotic term, the matching conditions along $\theta = 0$ impose the equality of the exponents

$$s^{(1)} = s^{(2)} = s. \qquad (3.30)$$

---

[7] Recall that summation on the material index "*(k)*" is *never* implied.

Furthermore, the system of coupled differential equations (3.25) can be "decoupled" by using the linearity of the operators $H_\alpha^s(w)$ and may be rewritten as

$$\begin{aligned} H_1^s(w_1 - a_{12}w_2) &= 0, \\ H_3^s(a_{12}w_1 + w_2) &= 0, \end{aligned} \tag{3.31}$$

where $H_3^s(w) = (H_1^s + 2H_2^s)(w)$. The new form (3.31) of the equilibrium equations suggests that there are two sets of solutions of $w_\alpha(\theta)$: either we have

$$w_1 = a_{12}w_2, \qquad \text{with } H_3^s(w_2) = 0, \tag{3.32}$$

or

$$w_2 = -a_{12}w_1, \qquad \text{with } H_1^s(w_1) = 0. \tag{3.33}$$

Finally, the bond conditions impose

$$w_\alpha^{(1)}(0^+) = w_\alpha^{(2)}(0^-), \tag{3.34}$$

$$\begin{aligned} \mu^{(1)}\left(\frac{b^{(1)}}{n}\right)^{n-1} I^{n-1}(r,0^+)\left(a_\alpha j(0^+)\dot{f}(0;n) + \dot{w}_\alpha^{(1)}(0^+)\right) = \\ \mu^{(2)}\left(\frac{b^{(2)}}{n}\right)^{n-1} I^{n-1}(r,0^-)\left(a_\alpha j(0^-)\dot{f}(0;n) + \dot{w}_\alpha^{(2)}(0^-)\right), \end{aligned} \tag{3.35}$$

where $j(0^+)$ and $j(0^-)$ are equal to 1 and ξ respectively, and

$$\begin{aligned} I(r,0) = r^{2m-2}a_\beta\, a_\beta\, \dot{j}^2(0)\, \dot{f}^2(0) \;+\; 2\, j(0)\, r^{m+s-2}\dot{f}(0)a_\beta\, \dot{w}_\beta(0) \\ +\; r^{2s-2}(s^2 w_\beta(0)w_\beta(0) + \dot{w}_\beta(0)\dot{w}_\beta(0)). \end{aligned} \tag{3.36}$$

In (3.35) and (3.36), $\dot{f}(0;n)$ can be expressed in terms of the "hardening" exponent n as

$$\dot{f}(0;n) = (2n-1)^m/2n. \tag{3.37}$$

The equations (3.32) and (3.33), together with the boundary conditions (3.29), (3.34) and (3.35), constitutes two eigenvalue problems in $(s, w_\alpha^{(k)})$, the solution of which is fairly similar to the mixed-mode homogeneous case. The first four terms of the asymptotic approximation of the deformation field are

$$y_\alpha(r,\theta) \sim a_\alpha r^m j(\theta) f(\theta;n) + c\varepsilon_{\alpha\beta} a_\beta r^p g(\theta;n) + k a_\alpha r^t l(\theta;n) + d a_\alpha r^q j(\theta) h(\theta;n), \quad (3.38)$$

where $\varepsilon_{\alpha\beta}$ is the two-dimensional alternator, $j(\theta)$ is the step function defined in (3.23), c, d and k are three undetermined constants. The exponent p and the angular function $g(\theta;n)$ are the solutions of the eigenvalue problem defined by (3.29) and (3.33) with

$$\dot{w}_\alpha^{(1)}(0^+) = \dot{w}_\alpha^{(2)}(0^-) = 0. \quad (3.39)$$

The solutions have been obtained numerically and are presented in figure 2 of the present paper for p and figure 8 of [17] for $g(\theta;n)$. On the other hand, $(t, l(\theta;n))$ and $(q, h(\theta;n))$ are, respectively, the first even and first odd solutions of (3.29) and (3.32) satisfying $s > m$. They have been obtained in [17] using a transformation established by Knowles and Sternberg [22] and are given by

$$\begin{aligned} t &= (n - 1 + \sqrt{n^2 + 6n - 3})/2n, \\ l(\theta;n) &= n^t (\omega + k\cos\theta)^t (2\cos^2\zeta - 1), \end{aligned} \quad (3.40)$$

and

$$\begin{aligned} q &= (n - 1 + \sqrt{n^2 + 16n - 8})/2n, \\ h(\theta;n) &= n^q (\omega + k\cos\theta)^q (4\cos^3\zeta - 3\cos\zeta), \end{aligned} \quad (3.41)$$

with

$$\cos\zeta = \frac{1-k}{\sqrt{2}}\frac{\sqrt{1+k\sin^2\theta-\omega\cos\theta}}{\omega+k\cos\theta},$$
$$k = 1-1/n, \qquad (3.42)$$
$$\omega = (1-k^2\sin^2\theta)^{1/2}.$$

The exponents t and q are shown in figure 2 while the angular functions $l(\theta;n)$ and $h(\theta;n)$ are presented in figures 9 and 8 of [17], respectively.

As outlined in section 3 of [17], the domain of validity of (3.38) is defined by the requirement on the exponent of the higher-order terms (see figure 2)

$$s < 1+1/4n. \qquad (3.43)^8$$

Discussion of the asymptotic results.

Before discussing the structure and properties of the asymptotic field, let us non-dimensionalize (3.38) by defining as in [17]

$$\rho = \frac{r}{l_c} \quad \text{and} \quad \eta_\alpha = \frac{y_\alpha}{l_c}, \qquad (3.44)$$

where l_c is a characteristic length

$$l_c = (a_1^2 + a_2^2)^{1/2(1-m)} = a^{1/(1-m)} = a^{2n}. \qquad (3.45)$$

The asymptotic solution (3.38) is then rewritten as

$$\eta_\alpha(r,\theta) \sim \bar{a}_\alpha \rho^m j(\theta) f(\theta;n) + \bar{c}\varepsilon_{\alpha\beta}\bar{a}_\beta\rho^p g(\theta;n) + \bar{k}\bar{a}_\alpha\rho^t l(\theta;n) + \bar{d}\bar{a}_\alpha\rho^q j(\theta)h(\theta;n), \qquad (3.46)$$

where $\bar{a}_\alpha$, $\bar{c}$, $\bar{k}$ and $\bar{d}$ are dimensionless undetermined constants defined as

---

[8] Note that the lower-order term is valid for all $n>1/2$.

$$\bar{a}_\alpha = a_\alpha / a, \qquad \bar{c} = c a^{\frac{p-m}{1-m}}, \qquad \bar{k} = k a^{\frac{t-m}{1-m}}, \qquad \bar{d} = d a^{\frac{q-m}{1-m}}. \quad (3.47)$$

The characteristic length l_c can be related to the far-field conditions and the material properties through the conservation integral $\mathcal{J}$ introduced in (3.10)

$$\mathcal{J} = \mu^{(1)} b^{(1)^{n-1}} l_c (1+\xi) \bar{\mathcal{J}}(n), \quad (3.48)$$

where ξ is given by (3.21) and

$$\bar{\mathcal{J}}(n) = m^{2n-1} n^{1-n} \pi / 4 \quad (3.49)$$

is illustrated in figure 13 of [17].

As was the case for the general non-symmetric (mixed-mode) homogeneous situation,[9] it can be shown that the obtained asymptotic field (3.46) is a mere rotation of a "simpler" canonical bimaterial field $\boldsymbol{y}^*$ such that

$$\boldsymbol{y} = \boldsymbol{Q}\boldsymbol{y}^*, \quad (3.50)$$

where $\boldsymbol{Q}$ is the rotation tensor defined by the angle

$$\theta^* = tan^{-1}(-a_1/a_2) = tan^{-1}(-\bar{a}_1/\bar{a}_2), \quad (3.51)$$

and $\boldsymbol{y}^*$ is given in its dimensionless form by

$$\begin{cases} \eta_1^* \sim \bar{c}\, \rho^p g(\theta; n), \\ \eta_2^* \sim \rho^m j(\theta) f(\theta; n) + \bar{k}\, \rho^t l(\theta; n) + \bar{d}\, \rho^q j(\theta) h(\theta; n). \end{cases} \quad (3.52)$$

An important result of the asymptotic analysis developed here is to give an indication of the effect of the "hardening" parameter on the deformation distribution across the interface : as indicated by (3.21) which defines the dimensionless nonlinear modulus mismatch parameter ξ, as the "hardening" exponent n decreases, the

[9] See section 4 of [17].

mismatch in (linearly) elastic properties is amplified, tending to an infinite value when the material behavior approaches the "perfectly plastic" situation $(n \to 0.5)$. Note also through (3.21) that the mismatch in "yield stress," described by the ratio[10] $b^{(1)}/b^{(2)}$, has an effect similar to the mismatch in linearly elastic properties $\mu^{(1)}/\mu^{(2)}$. The concentration of deformations in the weaker component[11] can be illustrated by the angular distribution of the Jacobian $J(r,\theta)$ of the transformation

$$J = \lambda^{-1} \sim \bar{c}\rho^{m+p-2} j(\theta)(p\dot{f}g - mf\dot{g}), \tag{3.53}$$

which is shown in figure 3 for $\xi = 3$.

The effect of the "hardening" exponent n on the near-tip field can be analyzed by examining the shape of the deformed crack. As indicated by (3.52), the upper and lower crack faces deform as

$$\begin{aligned} \eta_1^* &= -\bar{b}\,|\eta_2^*|^{p/m}, && (\eta_2^* \geq 0), && \text{along } \theta = \pi, \\ \eta_1^* &= -\bar{b}\left|\frac{\eta_2^*}{\xi}\right|^{p/m}, && (\eta_2^* \leq 0), && \text{along } \theta = -\pi, \end{aligned} \tag{3.54}$$

where[12] $\bar{b} = |\bar{c}\,g(\pi;n)| = |\bar{c}\,g(-\pi;n)|$. The relations (3.54) are illustrated in figure 4 for the case $\mu^{(1)}/\mu^{(2)} = 1/2$ and $b^{(1)}/b^{(2)} = 1$. The corresponding values of the nonlinear mismatch parameter ξ are given in table 1

n	0.55	0.60	0.75	1.00
p/m	8.16	4.47	2.55	2.00
ξ	$9.8\ 10^{-4}$	0.0313	0.25	0.50

Table 1.- Values of ξ and p/m vs n used in figure 4.

[10] Recall that an increase of b corresponds to a decrease of the "elastic limit" or "yield stress".
[11] The lower sheet will be considered as weaker if $\xi > 1$ and stronger if $\xi < 1$.
[12] It is assumed that $\bar{c} \neq 0$.

The asymptotic representation developed above can thus capture the effect of the "hardening" exponent n on both the crack blunting process and the deformation distribution across the interface. It also confirms the result obtained by Knowles and Sternberg in the Neo-Hookean case [14] : *the finite elasticity theory does not predict any interpenetration of the crack faces which are found to open smoothly for the class of GNH materials.* The deformed interface is expressed, in the (η_1^*, η_2^*) coordinate system, as

$$\eta_2^* = \hat{b}(\eta_1^*)^{t/p}, \qquad \text{along } \theta = 0, \tag{3.55}$$

where $\hat{b} = -\bar{k}\,\bar{c}^{-t/p}(2n-1)^t$ and the variation of t/p is illustrated in figure 2.

We describe next the nominal and true stress fields derived from the canonical deformation field (3.52). The leading term of the Piola stress components $\sigma_{\alpha\beta}^*$ is given, in a dimensionless form, by

$$\begin{cases} \dfrac{\sigma_{11}^*}{\mu^{(1)}} \sim \left(\dfrac{b^{(1)}}{n}\right)^{n-1} \bar{c}\,\rho^{p+\frac{1}{n}-2}\dfrac{B_f^{n-1}}{j(\theta)}(p\cos\theta\, g - \sin\theta\, \dot{g}), \\ \dfrac{\sigma_{12}^*}{\mu^{(1)}} \sim \left(\dfrac{b^{(1)}}{n}\right)^{n-1} \bar{c}\,\rho^{p+\frac{1}{n}-2}\dfrac{B_f^{n-1}}{j(\theta)}(p\sin\theta\, g + \cos\theta\, \dot{g}), \\ \dfrac{\sigma_{21}^*}{\mu^{(1)}} \sim \left(\dfrac{b^{(1)}}{n}\right)^{n-1} \rho^{\frac{1}{2n}-1}B_f^{n-1}\left(m\cos\theta\, f - \sin\theta\, \dot{f}\right), \\ \dfrac{\sigma_{22}^*}{\mu^{(1)}} \sim \left(\dfrac{b^{(1)}}{n}\right)^{n-1} \rho^{\frac{1}{2n}-1}B_f^{n-1}\left(m\sin\theta\, f + \cos\theta\, \dot{f}\right), \end{cases} \tag{3.56}$$

where

$$B_f(\theta) = m^2 f^2(\theta) + \dot{f}^2(\theta) = m^2 n^{-1/2}(k\cos\theta + \omega)^{-1/n}, \tag{3.57}$$

with k and ω defined in (3.42). The true (Cauchy) stress components $\tau_{\alpha\beta}^*$ are given by

$$\begin{cases} \dfrac{\tau_{11}^*}{\mu^{(1)}} \sim \left(\dfrac{b^{(1)}}{n}\right)^{n-1} B_f^{n-1}\bar{c}^2 \dfrac{B_g}{j(\theta)} \rho^{2p+\frac{1}{n}-3}, \\ \dfrac{\tau_{12}^*}{\mu^{(1)}} = \dfrac{\tau_{21}^*}{\mu^{(1)}} \sim \left(\dfrac{b^{(1)}}{n}\right)^{n-1} B_f^{n-1}\bar{c}(pmfg + \dot{f}\dot{g})\rho^{p+\frac{1}{2n}-2}, \\ \dfrac{\tau_{22}^*}{\mu^{(1)}} \sim \left(\dfrac{b^{(1)}}{n}\right)^{n-1} B_f^n \, j(\theta)\, \rho^{-1}. \end{cases} \tag{3.58}$$

Note that, as was the case for the homogeneous situation, the most singular component is τ_{22}^* $(= O(\rho^{-1}))$, the singularity of which is stronger than that predicted by the linearized theory. It has to be noted also that the asymptotic solution described by (3.50)-(3.52) satisfies the continuity of displacements across the interface for all orders, while the continuity of tractions is only satisfied to the leading order (relations (3.56)). A measure of the error introduced can be obtained by examining the jump in the main traction component σ_{22}^* across the interface, the first two asymptotic terms of which are

$$\frac{\sigma_{22}^*(\rho, 0^{\pm})}{\mu^{(1)}} \sim \left(\frac{b^{(1)}}{n}\right)^{n-1} \rho^{\frac{1}{2n}-1} \dot{f}(0) \left(1 + \frac{\rho^{2(t-m)} \tilde{k}^2 t^2 l^2(0)}{j^2(0^{\pm})\, \dot{f}^2(0)}\right)^{n-1}, \tag{3.59}$$

where $j(0^+) = 1$ and $j(0^-) = \xi$. Since $t>m$ and $\rho << 1$, the second term in the right-hand-side parenthesis in (3.59) is small and the traction jump can be approximated by

$$\Delta\sigma_{22} = \frac{\sigma_{22}^*(\rho, 0^+) - \sigma_{22}^*(\rho, 0^-)}{\sigma_{22}^*(\rho, 0^+) + \sigma_{22}^*(\rho, 0^-)} = \frac{1 - 1/\xi^2}{C + 1 + 1/\xi^2}, \tag{3.60}$$

where

$$C = \frac{2\dot{f}^2(0)}{(n-1)\bar{k}^2 t^2 l^2(0)\, \rho^{2(t-m)}}. \tag{3.61}$$

The latter can be evaluated with the aid of (3.11), (3.21), (3.37), (3.40) and (3.42), and is illustrated in figure 5 for the situation where the lower-half component is much

weaker than the upper-half ($\xi = 1000$). Note from (3.60) that, as expected, no traction jump is detected in the homogeneous case ($\xi = 1$) but neither in the bimaterial situations for $n=1$ (Neo-Hookean case) and $n \to 1/2$ (limit of the "perfectly plastic" case). As indicated in figure 5, for a given value of ξ, the traction discontinuity across the interface attains a maximum for $n \approx 0.85$.

A comparison of the asymptotic solution with a full-field numerical analysis obtained through the finite element method, together with further discussion of the local results, is presented in section 5.

4.- Local analysis of the near-tip fields for an interface crack between a GNH sheet and a rigid substrate.

In this section, we summarize the results of the asymptotic analysis of the stress and deformation fields at the tip of a crack lying at the interface between a sheet of Generalized Neo-Hookean material and a rigid substrate. This case does not constitute a special limit case of the bimaterial problem described in section 3 primarily because the matching conditions along the interface do not revert to the boundary conditions for this special problem. The limiting process by which this case is obtained is somewhat more complex and is examined in detail in section 5.

Problem formulation.

Figure 6 illustrates the geometry of the bimaterial system on which the local analysis is carried out. A semi-infinite sheet of GNH material, the mid-plane of which is denoted by H, is bonded to a rigid substrate. A Cartesian coordinate system is chosen such that the crack tip is located at the origin, the rigid substrate corresponds to

the lower half plane and the interface crack line is the negative x_1-axis. Let μ, b and n denote the three material parameters characterizing the elastic potential $U(I,J)$ of the GNH sheet. The local analysis is again more conveniently performed in terms of the polar coordinates (r,θ) defined in figure 6 and can be formulated as follows : determine the asymptotic form of the near-tip fields which satisfy the equilibrium equations (2.10) together with the stress-free conditions along the crack faces

$$\sigma_{\alpha 2}(r,\pi) = 0, \tag{4.1}$$

and the bond conditions along the interface

$$u_\alpha(r,0) = 0, \tag{4.2}$$

where the displacement field $\boldsymbol{u}$ has been introduced in (2.1). Furthermore, the deformation field must be non-oscillatory and such that the transverse stretch λ defined in (2.5) vanishes as the crack tip is approached. Finally, the local field $\boldsymbol{y}$ must satisfy continuity requirements compatible with the various differentiations involved in the analysis.

First-order term.

The analysis of the first asymptotic term is very similar to the bimaterial case described in section 3. Starting from the assumed form

$$y_\alpha(r,\theta) \sim r^m v_\alpha(\theta), \qquad (0 \le \theta \le \pi), \tag{4.3}$$

one immediately deduces the expression of the exponent m through the following considerations

- the boundedness of the displacements at the crack tip imposes $m>0$.

- not all deformation gradients must be finite at the crack tip, which implies $m<1$.

- the path-independence of the conservation integral J defined in (3.10)[13] furnishes, as before,

$$m = 1 - \frac{1}{2n}, \qquad (n > 1/2). \tag{4.4}$$

The determination of the angular function $v_\alpha(\theta)$ is identical to that in the first bimaterial situation : the asymptotic equilibrium equations (3.12) yield the same system of differential equations (3.13) which, together with the asymptotic form of the stress-free boundary conditions along the crack face

$$\dot{v}_\alpha(\pi) = 0, \tag{4.5}$$

provides the same solution

$$v_\alpha(\theta) = a_\alpha f(\theta; n), \tag{4.6}$$

where $f(\theta;n)$ has been given by (3.17) and (3.18), and a_α are two constants left undetermined by the present local analysis. The solution satisfies the bond condition (4.2) since $f(0;n) = 0$ but does not constitute a one-to-one mapping of the near-tip region since the Jacobian J of the transformation (4.3) vanishes identically. The latter fact justifies the necessity of obtaining again a second term in the asymptotic expansion.

Higher-order terms.

Substituting the assumed separable form for the second term

---

[13] The only contribution to J comes from the GNH sheet by integration along the contour Γ^+ shown in figure 6.

$$y_\alpha(r,\theta) \sim a_\alpha\, f(\theta;n) r^m + r^s w_\alpha(\theta;n), \qquad (s > m), \qquad (4.7)$$

into the equilibrium equations, we obtain the same asymptotic expression (3.12) which, in turn, leads to the same system of coupled second-order differential equations (3.25).[14] The boundary conditions along the crack faces (4.1) are asymptotically equivalent to

$$\dot{w}_\alpha(\pi;n) = 0. \qquad (4.8)$$

But the bond conditions (4.2) provide a different requirement on the values of $w_\alpha(\theta)$ at $\theta = 0$: if $s \neq 1$, we have the homogeneous conditions

$$w_\alpha(0;n) = 0, \qquad \text{for } s \neq 1, \qquad (4.9)$$

while, if the exponent of the second-order term is unity, (4.2) imposes

$$w_1(0;n) = 1, \qquad w_2(0;n) = 0, \qquad \text{for } s = 1. \qquad (4.10)$$

As was the case in the first bimaterial problem, one can use the linearity property of the differential operators to uncouple the system (3.25) into

$$\begin{aligned} H_1^s(\tilde{w}_1) &= 0, \\ H_3^s(\tilde{w}_2) &= 0, \end{aligned} \qquad (4.11)$$

where

$$\begin{aligned} \tilde{w}_1 &= w_1 - a_{12} w_2, \\ \tilde{w}_2 &= a_{12} w_1 + w_2, \end{aligned} \qquad (4.12)$$

in which $a_{12} = a_1/a_2$ and the linear differential operators $H_1^s(w)$ and $H_3^s(w)$ have been defined in (3.26) and (3.31).

---

[14] As was the case before, we will assume, without loss of generality, that $a_2 \neq 0$.

The solution to the case $s \neq 1$ has been obtained earlier since the boundary conditions (4.8) and (4.9) are equivalently written in terms of $\tilde{w}_\alpha(\theta;n)$ through (4.12) as

$$\begin{aligned} \dot{\tilde{w}}_\alpha(\pi;n) &= 0, \\ \tilde{w}_\alpha(0;n) &= 0. \end{aligned} \tag{4.13}$$

The eigenvalue problem (4.11b) and (4.13) thus yields, with the aid of (4.12),

$$w_\alpha(\theta;n) = d\, a_\alpha r^q h(\theta;n), \tag{4.14}$$

where q and $h(\theta;n)$ are given by (3.41) and (3.42), and d is an undetermined constant. Note however that the second-order term described by (4.14) does not contribute to the Jacobian of the transformation and that the above solution is valid as long as the exponent q satisfies

$$q < 1 + \frac{1}{4n}. \tag{4.15}$$

The latter inequality is represented by a dotted line in figure 2.

The second-order asymptotic term which has a non-vanishing contribution to the Jacobian J, while being compatible with the bond conditions (4.10), is thus determined by the solution for which $s = 1$. Using the linearity of the uncoupled system (4.11), we define

$$\overline{w}_1(\theta;n) = \tilde{w}_1(\theta;n), \qquad \overline{w}_2(\theta;n) = a_{12}\, \tilde{w}_2(\theta;n), \tag{4.16}$$

which satisfy

$$\begin{aligned} H_1^1(\overline{w}_1) &= 0, \\ H_3^1(\overline{w}_2) &= 0, \end{aligned} \tag{4.17}$$[15]

---

[15] The differential operators $H_\alpha^1(w)$ are given by (3.26) and (3.31) with $s = 1$.

with the boundary conditions

$$\overline{w}_\alpha(\pi;n) = 0, \qquad \overline{w}_\alpha(0;n) = 1. \tag{4.18}$$

The angular functions $w_\alpha(\theta;n)$ are expressed, with the aid of (4.12) and (4.16), as

$$\begin{aligned} w_1(\theta;n) &= \frac{\overline{w}_1 + a_{12}^2 \overline{w}_2}{1 + a_{12}^2}, \\ w_2(\theta;n) &= \frac{a_{12}(\overline{w}_1 - \overline{w}_2)}{1 + a_{12}^2}. \end{aligned} \tag{4.19}$$

The solution to (4.17a) with (4.18) has been obtained numerically and the first auxiliary angular function $\overline{w}_1(\theta;n)$ is shown in figure 7 for various values of n. A closed-form expression for the other auxiliary angular function $\overline{w}_2(\theta;n)$ is found using the transformation (3.42) which turns (4.17b) into

$$W_2''(\zeta) + \frac{4n}{2n-1} W_2(\zeta) = 0, \tag{4.20}$$

where

$$W_2(\zeta) = \frac{\overline{w}_2(\theta;n)}{(\omega + k\cos\theta)}. \tag{4.21}$$

The boundary conditions (4.18) are equivalent to

$$W_2'(0) = 0, \qquad W_2(\pi/2) = \frac{1}{1+k}. \tag{4.22}$$

Solving (4.20) with (4.22) renders $\overline{w}_2(\theta;n)$ as

$$\overline{w}_2(\theta;n) = \frac{\omega + k\cos\theta}{(1+k)\cos\left(\sqrt{\frac{4n}{2n-1}}\,\frac{\pi}{2}\right)} \cos\sqrt{\frac{4n}{2n-1}}\zeta. \tag{4.23}$$

The expression (4.23), which is illustrated in figure 8 for various values of n, indicates that $\overline{w}_2(\theta;n)$ tends to infinity for particular values of the "hardening" exponent n given by

$$n = n_* = \frac{j^2}{2(j^2-2)}, \qquad (j=3,\ 5,\ 7,\ \ldots). \tag{4.24}$$

For these values of n, the asymptotic representation (4.7) of the near-tip deformation field is not valid and a different form has to be introduced. Note, however, that no difficulty arises in the particular case $a_{12} = 0$, for which one has, for all values of n,

$$w_1(\theta;n) = \overline{w}_1(\theta;n), \qquad w_2(\theta;n) \equiv 0. \tag{4.25}$$

The general situation for which $n = n_*$ with $a_{12} \neq 0$ will be examined later in this section. Note also that the Jacobian J, the expression of which is the main objective of the higher-order local analysis, does not depend on the second auxiliary angular function $\overline{w}_2(\theta;n)$ and is therefore valid for all values of $n > 1/2$

$$J(r,\theta) = y_{1,1}y_{2,2} - y_{1,2}y_{2,1} \sim a_2 r^{m-1}(\dot{f}\,\overline{w}_1 - m f \dot{\overline{w}}_1). \tag{4.26}$$

The angular variation of $J(r,\theta)$ is presented in figure 9 for various values of n.

Discussion of the asymptotic solution.

The first three terms of the asymptotic solution for the rigid substrate problem are thus

$$y_\alpha(r,\theta) \sim a_\alpha r^m f(\theta;n) + r\,w_\alpha(\theta;n) + d\,a_\alpha r^q h(\theta;n), \tag{4.27}$$

where a_α and d are undetermined constants, m is given by (4.4), $f(\theta;n)$ by (3.17) and (3.18), q and $h(\theta;n)$ are described by (3.41) and (3.42), $w_\alpha(\theta;n)$ by (4.19) and

(4.23). The first two terms are valid for all values of $n > 1/2$ while, due to (4.15), the domain of validity of the last term is limited to $1/2 < n < 41/52 \approx 0.79$. In order to facilitate the analysis of the near-tip field, it is convenient to rotate the coordinate system and rewrite (4.27) as

$$\boldsymbol{y} = \boldsymbol{Q}\,\boldsymbol{y}^*, \tag{4.28}$$

with the component of the rotation matrix $\boldsymbol{Q}$ defined as

$$\left[Q_{\alpha\beta}\right] = \frac{1}{a}\begin{pmatrix} a_2 & a_1 \\ -a_1 & a_2 \end{pmatrix} = \frac{a_2}{a}\begin{pmatrix} 1 & a_{12} \\ -a_{12} & 1 \end{pmatrix}, \tag{4.29}$$

where $a = (a_1^2 + a_2^2)^{1/2} > 0$ and $a_{12} = a_1/a_2$. The "unrotated" canonical field $\boldsymbol{y}^*$ is then

$$\begin{cases} y_1^* \sim \tilde{a}_2\, r\, \overline{w}_1(\theta;n), \\ y_2^* \sim a r^m f(\theta;n) + \tilde{a}_1\, r\, \overline{w}_2(\theta;n) + a d r^q h(\theta;n), \end{cases} \tag{4.30}$$

in which $\tilde{a}_\alpha = a_\alpha/a$ and $\overline{w}_\alpha(\theta;n)$ are the auxiliary angular functions introduced earlier.

Following the non-dimensionalization in section 3, we may write again

$$\rho = \frac{r}{l_c}, \qquad \eta_\alpha^* = \frac{y_\alpha^*}{l_c}, \qquad l_c = a^{1/(1-m)} = a^{2n}, \tag{4.31}$$

so that the reference field $\boldsymbol{y}^*$ becomes

$$\begin{cases} \eta_1^* \sim \tilde{a}_2\, \rho\, \overline{w}_1(\theta;n), \\ \eta_2^* \sim \rho^m f(\theta;n) + \tilde{a}_1\, \rho\, \overline{w}_2(\theta;n) + \tilde{d}\, \rho^q h(\theta;n), \end{cases} \tag{4.32}$$

where

$$\tilde{d} = a^{\frac{q-m}{1-m}} d. \tag{4.33}$$

The characteristic length l_c is related to the far-field conditions, the geometry of the global fracture problem and the material properties through the conservation integral $\mathcal{J}$ which is found to be

$$\mathcal{J} = \mu\, b^{n-1}\, l_c\, \bar{\mathcal{J}}(n), \tag{4.34}$$

where $\bar{\mathcal{J}}(n)$ is given by (3.48).

The effect of the "hardening" exponent n on the opening of the crack near its tip can now be studied by writing the relation governing the shape of the deformed crack

$$\eta_1^* = -\tilde{a}_2 \left|\overline{w}_1(\pi; n)\right| \eta_2^{*1/m}, \qquad \text{along } \theta = \pi. \tag{4.35}$$

The effect of a decreasing "hardening" exponent on the blunting of the crack is thus similar to that illustrated in figure 4 for the first bimaterial case. Once again, the current asymptotic solution (4.32) is found to be oscillation-free and to provide a smooth opening of the crack near its tip.

Finally, the expression of the nominal and true stress fields is similar to that found in the previous section (equations (3.55) and (3.58) with $\theta \in [0, \pi]$) except for the following components

$$\begin{aligned}
\frac{\sigma_{11}^*}{\mu} &\sim \left(\frac{b}{n}\right)^{n-1} \tilde{a}_2\, \rho^{\frac{1}{n}-1} B_f^{n-1} \left(\cos\theta\, \overline{w}_1 - \sin\theta\, \dot{\overline{w}}_1\right), \\
\frac{\sigma_{12}^*}{\mu} &\sim \left(\frac{b}{n}\right)^{n-1} \tilde{a}_2\, \rho^{\frac{1}{n}-1} B_f^{n-1} \left(\sin\theta\, \overline{w}_1 + \cos\theta\, \dot{\overline{w}}_1\right), \\
\frac{\tau_{11}^*}{\mu} &\sim \left(\frac{b}{n}\right)^{n-1} \tilde{a}_2^2\, \rho^{\frac{1}{n}-1} B_f^{n-1} \left(\dot{\overline{w}}_1^2 + \overline{w}_1^2\right), \\
\frac{\tau_{12}^*}{\mu} = \frac{\tau_{21}^*}{\mu} &\sim \left(\frac{b}{n}\right)^{n-1} \tilde{a}_2\, \rho^{\frac{1}{2n}-1} B_f^{n-1} (m f \overline{w}_1 + \dot{f}\, \overline{w}_1).
\end{aligned} \tag{4.36}$$

Special case $n = n_* = 9/14$.

As noted earlier, the asymptotic solution (4.27) of the rigid substrate problem suffers some apparent inconsistencies for some specific values (4.24) of the "hardening" exponent n, the first one being located at $n_* = 9/14 \approx 0.643$. At these values, the second auxiliary function $\overline{w}_2(\theta;n)$ described by (4.23) is unbounded. The problem arises because of the interaction between two second-order terms : as n tends to $n_* = 9/14$, for example, the exponent q of the homogeneous second-order term $r^q h(\theta;n)$ tends to 1, which makes it interact with the singularity of the nonhomogeneous term $r\overline{w}_2(\theta;n)$. Since the boundary conditions at $\theta = 0$ are not compatible ($\overline{w}_2(0;n) = 1$ versus $h(0;n) = 0$), a separable solution of the type (4.7) does not exist for these particular values. In this paragraph, we develop the modified second-order asymptotic solution for the special case $n = n_* = 9/14$. The other particular cases can be solved in a very similar way. We will assume that $a_{12} \neq 0$ since it was shown earlier (see equation (4.25)) that the particular case of $a_{12} = 0$ does not present this difficulty.

Following Knowles and Sternberg [22], the analysis starts with noticing with the aid of (4.23) that $\overline{w}_2(\theta;n)$ has a pole of order 1 at $n = n_*$, which motivates

$$\overline{w}_2(\theta;n) \sim \frac{z_2(\theta;n)}{n - n_*}, \tag{4.37}$$

where $z_2(\theta;n_*)$ is finite for all θ in $[0,\pi]$. We therefore rewrite (4.27) as

$$y_\alpha(r,\theta) \sim a_\alpha r^m f(\theta;n) + r\hat{w}_\alpha(\theta;n) + r^q \hat{h}_\alpha(\theta;n), \tag{4.38}$$

where we assume that

$$\hat{w}_\alpha(\theta;n)=\frac{\xi_\alpha(\theta;n)}{n-n_*}+\zeta_\alpha(\theta;n),$$
$$\hat{h}_\alpha(\theta;n)=-\frac{\xi_\alpha(\theta;n)}{n-n_*}+\eta_\alpha(\theta;n), \tag{4.39}$$

in which $\xi_\alpha(\theta;n)$, $\zeta_\alpha(\theta;n)$ and $\eta_\alpha(\theta;n)$ are finite at $n=n_*$. The choice of (4.39a) is motivated by (4.37) while (4.39b) is introduced to ensure a finite value of y_α at $n=n_*$.

Realizing that a term "*r lnr*" is generated by computing

$$\lim_{n\to n_*}\left(\frac{r\xi_\alpha(\theta;n)}{n-n_*}-\frac{r^q\xi_\alpha(\theta;n)}{n-n_*}\right), \tag{4.40}$$

we assume the asymptotic expansion at $n=n_*=9/14$ in the form

$$y_\alpha(r,\theta)\sim a_\alpha r^{m_*}f(\theta;n_*)+rv_\alpha(\theta)+r\ln r\,w_\alpha(\theta), \tag{4.41}$$

where $m_*=1-1/2n_*$ while $v_\alpha(\theta)$ and $w_\alpha(\theta)$ must satisfy the equilibrium equations (2.10) and the boundary conditions (4.1) and

$$v_1(0)=1, \qquad v_2(0)=w_1(0)=w_2(0)=0. \tag{4.42}$$

The stress-free conditions along the crack face (4.1) are asymptotically equivalent to

$$\dot{w}_\alpha(\pi)=\dot{v}_\alpha(\pi)=0. \tag{4.43}$$

The computation of the various terms of the asymptotic equilibrium equations (3.12) yields, for $w_\alpha(\theta)$, the relations

$$H_1^1(w_1-a_{12}w_2)=0,$$
$$H_3^1(a_{12}w_1+w_2)=0, \tag{4.44}$$

where $H_1^1(w)$ and $H_3^1(w)$ have been given in (4.17). Since the boundary conditions (4.42) and (4.43) are homogeneous for $w_\alpha(\theta)$, the solution to (4.44) is

$$w_\alpha(\theta) = d\,\tilde{a}_\alpha h(\theta; n_*), \tag{4.45}$$

where d is an undetermined constant, $\tilde{a}_\alpha = a_\alpha / a$ and $h(\theta; n)$ has been described earlier in (3.41).

The differential equations for $v_\alpha(\theta)$ are

$$\begin{aligned} H_1^I(v_1 - a_{12}v_2) &= 0, \\ H_3^I(a_{12}v_1 + v_2) &= -F(a_{12}w_1 + w_2), \end{aligned} \tag{4.46}$$

where

$$F(w) = 4(n-1)mf\dot{f}\dot{w} + 2mfD_f w + \frac{2(n^2 - n + 1)}{n} B_f w, \tag{4.47}$$

in which D_f and B_f have been defined in (3.27). Using the fact that

$$w_1 = a_{12}w_2, \tag{4.48}$$

(4.46) is rewritten, with the aid of (4.45), as

$$\begin{aligned} H_1^I(v_1 - a_{12}v_2) &= 0, \\ H_3^I(a_{12}v_1 + v_2) &= -d\,\tilde{a}_2(1 + a_{12}^2)F(h(\theta; n_*)). \end{aligned} \tag{4.49}$$

Due to the boundary conditions (4.42), a solution of the type $v_1 = a_{12}v_2$ is impossible. Introducing the definitions

$$\begin{aligned} v_1^*(\theta) &= v_1(\theta) - a_{12}\,v_2(\theta), \\ v_2^*(\theta) &= (a_{12}v_1(\theta) + v_2(\theta))/a_{12}, \end{aligned} \tag{4.50}$$

which can be inverted as

$$\begin{aligned} v_1(\theta) &= \frac{v_1^*(\theta) + a_{12}^2 v_2^*(\theta)}{1 + a_{12}^2}, \\ v_2(\theta) &= \frac{a_{12}(v_2^*(\theta) - v_1^*(\theta))}{1 + a_{12}^2}, \end{aligned} \tag{4.51}$$

the system of differential equations (4.49) and the boundary conditions (4.42)-(4.43) become

$$\begin{aligned} H_1^1(v_1^*(\theta)) &= 0, \\ H_3^1(v_2^*(\theta)) &= -c\,F(h(\theta;n_*)), \end{aligned} \tag{4.52}$$

with

$$v_\alpha^*(\pi) = 0, \qquad v_\alpha^*(0) = 1, \tag{4.53}$$

$$c = \frac{d\,\tilde{a}_2(1+a_{12}^2)}{a_{12}}. \tag{4.54}$$

The first of (4.52) and (4.53) readily yield

$$v_1^*(\theta) = \overline{w}_1(\theta;n_*), \tag{4.55}$$

where $\overline{w}_1(\theta;n)$ has been obtained numerically earlier (see figure 7). The general solution to (4.52b) can be written as

$$v_2^*(\theta) = n_*(\omega + k_* \cos\theta)(A\cos(3\zeta(\theta)) + B\sin(3\zeta(\theta))) + v_2^{*p}(\theta;c), \tag{4.56}$$

where the transformation $\zeta(\theta)$ and the function $\omega(\theta)$ have been defined in (3.42), A and B are two constants and $v_2^{*p}(\theta;c)$ is a particular solution of the non-homogeneous problem (4.52). An examination of the solution (4.56) and the boundary conditions (4.53) shows that the non-homogeneous problem has a solution for a unique value of c which is found numerically to be

$$c = c_* \approx 0.9042. \tag{4.57}$$

For that particular value of c, which, in turn, specifies the unknown constant d through (4.55), the problem has an infinite number of solutions since the scalar A in (4.56) is left undetermined by the boundary conditions. The solution is therefore expressed as

$$v_2^*(\theta) = \bar{v}_2^*(\theta) + Ah(\theta; n_*), \tag{4.58}$$

where $\bar{v}_2^*(\theta)$ is shown in figure 10[16] and corresponds to the value of c specified by (4.57) while A is left undetermined.

Through a reasoning similar to that leading to (4.28)-(4.30), one can rewrite the solution to the special case $n = n_* = 9/14$ as

$$\boldsymbol{y} = \boldsymbol{Q}\boldsymbol{y}^*, \tag{4.59}$$

where the rotation matrix $\boldsymbol{Q}$ is given by (4.29) and the "reference field" $\boldsymbol{y}^*$ is now expressed as

$$\begin{cases} y_1^*(r,\theta) \sim \tilde{a}_2 r \bar{w}_1(\theta; n_*), \\ y_2^*(r,\theta) \sim a r^m f(\theta; n_*) + a d_* r \ln r\, h(\theta; n_*) + \tilde{a}_1 r\left(\bar{v}_2^*(\theta) + Ah(\theta; n_*)\right), \end{cases} \tag{4.60}$$

with a_α and A are undetermined constants, $a = (a_\beta a_\beta)^{1/2}$ and $\tilde{a}_\alpha = a_\alpha / a$; m, $f(\theta; n)$, d_* and $h(\theta; n)$ are given by (3.17), (3.18), (3.41), (4.4), (4.54) and (4.57) while $\bar{w}_1(\theta)$ and $\bar{v}_2^*(\theta)$ are shown in figures 7 and 10 respectively. It is important to note that, if $a_1 = 0$, (4.60) yields the expected result (4.25) and that the expression of the Jacobian associated with the deformation (4.59)-(4.60) is identical to the formulation (4.26) which does not present any difficulties for any value of n.

5.- Further discussion of the local results - Numerical investigation.

The results of the local analysis of the two bimaterial problems have been discussed separately at the end of sections 3 and 4. In this section we study how the

---

[16] Note that $\bar{v}_2^*(\pi)$ has been arbitrarily chosen as 0.

transition from one solution to the other takes place as the material characteristics of the two components are varied. The transition process is investigated with the aid of the full-field solution of a finite-element analysis of two bimaterial problems. The numerical results are also compared to the asymptotic approximations.

Numerical analysis.

The finite element mesh used throughout the numerical investigation is similar to that introduced in the homogeneous problem (see section 5 of [17]). The effect of a decrease of the "hardening" parameter n on the shape of the deformed crack in both bimaterial problems are shown in the next two figures. In figure 11, the first bimaterial situation is illustrated for $n = 1.0$ and $n = 0.6$ showing an amplification of the material mismatch as n is reduced, as indicated by the value of the nonlinear mismatch parameter ξ ($\xi = 3.33$ for $n = 1.0$ and $\xi = 411.5$ for $n = 0.6$). As was qualitatively illustrated in figure 4, most deformations are concentrated in the softer material as n decreases. The second effect of the "hardening" exponent on the shape of the deformed crack, the phenomenon of crack blunting, which is somewhat apparent in figure 11b, is more clearly illustrated in figure 12, which corresponds to the rigid substrate situation for the same values of n ($n=1.0$ and $n=0.6$).

A comparison between the asymptotic results and the full-field numerical solution is shown in figure 13 which presents the angular variation of the deformed coordinates y_2 in the bimaterial case with $n = 1.0$ and $n = 0.6$. The angular variation of the in-plane Jacobian with respect to θ for various values of the "hardening" exponent n - including the special case $n = n_* = 9/14$ - is presented in figure 14 for the rigid substrate situation, showing a good agreement between the asymptotics and the numerics.

Transition from the bimaterial case to the rigid substrate case.

It is interesting to note that the asymptotic exponents appearing in the near-tip approximations (3.52) and (4.30) depend only on the value of the "hardening" exponent n. This fact explains why similar terms ($O(r^m)$ and $O(r^q)$) can be found in the solution of both problems. The first asymptotic term for the "rotated" deformed coordinate y_1^* is however different for most values of n : it is $O(r^p)$ in the first problem and $O(r)$ in the rigid substrate case. This peculiarity appears to be incompatible with the intuitively accepted notion that the rigid substrate case is a particular limit of the bimaterial situation for which $\mu^{(1)}/\mu^{(2)}$ tends to zero. The limit, or rather transition process, can however be better understood by examining the radial variation of the Jacobian of the in-plane transformation, which is $O(r^{m+p-2})$ in the bimaterial situation and $O(r^{m-1})$ in the rigid substrate case.[17] As shown in figure 15, three distinct regions can be defined : in the first one *(A)*, the deformations are large in both components and the near-tip fields can be approximated by the first asymptotic solution (3.52). In the third region *(C)*, the deformations are small in both materials and linear elasticity is applicable. In the transition region *(B)*, the deformations are small in the hard material and remain large in the soft component : as illustrated in figure 15, this situation approaches the rigid substrate case. The "gap" between the two curves in the hard and soft components in region *(A)*, and hence the extent of regions *(A)* and *(B)*, is dictated by the nonlinear mismatch parameter ξ defined in (3.21) : as ξ increases, the size of region *(A)* decreases while that of *(B)* increases and the rigid substrate situation constitutes the limiting case for which $\xi \to 0$ and the zone *(A)* is of vanishing dimension.

---

[17] Relations (3.53) and (4.26).

6.- Conclusion.

In this paper, the asymptotic analysis of the near-tip finite deformation fields in a bimaterial sheet of Generalized Neo-Hookean material has been obtained for two special cases : in the first one, the "hardening" characteristics of the two components have been assumed to be identical while the second problem relates to the problem of a crack at the interface between a GNH sheet and a rigid substrate. In both cases, at least three terms of the approximation series were computed, confirming the existence of a separable, non-oscillatory and contact-free solution near the tip of the crack, which is found to open smoothly. The asymptotic solution also allows to study the effect of the "hardening" exponent on the blunting of the interface crack and on the mismatch in material properties across the interface through the introduction of a nonlinear mismatch parameter. The latter shows that, as the "hardening" behavior of the bimaterial specimen becomes weaker and approaches the "perfectly-plastic" ("non-hardening") situation, the difference between the two components is amplified and the situation tends to the rigid substrate case. The details of the transition between the two bimaterial situations have also been studied through a full-field finite element analysis of both problems.

Acknowledgments.

The support of AFOSR (under the technical direction of Dr. C.T. Liu) and ONR (under the supervision of Dr. P. Schmidt) is gratefully acknowledged. The access of the computing facilities of the San Diego Supercomputing Center has been made possible by a grant of the National Science Foundation. The authors wish to thank Professor J.K. Knowles for his help regarding some aspects of the asymptotic analysis.

References.

1. Williams, M.L., *The stress around a fault or crack in dissimilar media.* Bull. Seismol. Soc. Am., 1959. **49**: pp. 199-204.

2. Rice, J.R. and Sih, G.C., *Plane problems of cracks in dissimilar media.* J. Appl. Mech, 1965. **32**: pp. 418-423.

3. England, A.H., *A crack between dissimilar media.* J. Appl. Mech., 1965. **32**: pp. 400-402.

4. Hutchinson, J.W. and Suo, Z., *Mixed-mode cracking in layered materials,* in *Advances in Applied Mechanics,* edited by J.W. Hutchinson and T.W. Wu. 1991, Academic Press.

5. Rice, J.R., *Elastic fracture mechanics concepts for interfacial cracks.* J. Appl. Mech., 1988. **55**: pp. 98-103.

6. Comninou, M., *The interface crack.* J. Appl. Mech., 1977. **44**: pp. 631-636.

7. Comninou, M. and Schmueser, D., *The interface crack in a combined tension-compression and shear field.* J. Appl. Mech., 1979. **46**: pp. 345-348.

8. Gautesen, A.K. and Dundurs, J., *The interface crack in a tension field.* J. Appl. Mech., 1987. **54**: pp. 93-98.

9. Gautesen, A.K. and Dundurs, J., *The interface crack under combined loading.* J. Appl. Mech., 1988. **55**: pp. 580-586.

10. Aravas, N. and Sharma, S.M., *An elastoplastic analysis of the interface crack with contact zone.* J. Mech. Phys. Solids, 1991. **39**(3): pp. 311-344.

11. Shih, C.F., *Cracks on bimaterial interfaces : elasticity and plasticity aspects.* Mat. Sc. Engng., 1991. **A 143**: pp. 77-90.

12. Sharma, S.M. and Aravas, N., *Determination of higher-order terms in asymptotic elastoplastic crack tip solutions.* J. Mech. Phys. Solids, 1991. **39**(8): pp. 1043-1072.

13. Sharma, S.M. and Aravas, N., *Plane stress elastoplastic solutions of interface cracks with contact zones.* Mech. Mater., 1991. **12**: pp. 147-163.

14. Knowles, J.K. and Sternberg, E., *Large deformations near the tip of an interface crack between two Neo-Hookean sheets.* J. Elasticity, 1983. **13**: pp. 257-293.

15. Ravichandran, G. and Knauss, W.G., *A finite elastostatic analysis of bimaterial interface cracks.* Int. J. Fracture, 1989. **39**: pp. 235-253.

16. Herrmann, J.M., *An asymptotic analysis of finite deformation near the tip of an interface crack.* J. Elasticity, 1989. **21**: pp. 227-269.

17. Geubelle, P.H. and Knauss, W.G., *Finite strains at the tip of a crack in a sheet of hyperelastic material : I. Homogeneous case.* Galcit SM Report 92-42, Caltech, 1992. Submitted to J. Elasticity.

18. Geubelle, P.H. and Knauss, W.G., *Finite strains at the tip of a crack in a sheet of hyperelastic material : III. General bimaterial case.* Galcit SM Report 92-44, Caltech, 1992. Submitted to J. Elasticity.

19. Knowles, J.K., *The finite anti-plane shear field near the tip of a crack for a class of incompressible elastic solids.* Int. J. Fracture, 1977. **13**(5): pp. 611-639.

20. Parks, J.H. and Earmme, Y.Y., *Application of conservation integrals to interfacial crack problems.* Mech. Mater., 1986. **5**: pp. 261-276.

21. Knowles, J.K. and Sternberg, E., *An asymptotic finite-deformation analysis of the elastostatic field near the tip of a crack.* J. Elasticity, 1973. **3**: pp. 67-107.

22. Knowles, J.K. and Sternberg, E., *Finite-deformation analysis of the elastostatic field near the tip of a crack : reconsideration and higher-order results.* J. Elasticity, 1974. **4**: pp. 201-233.

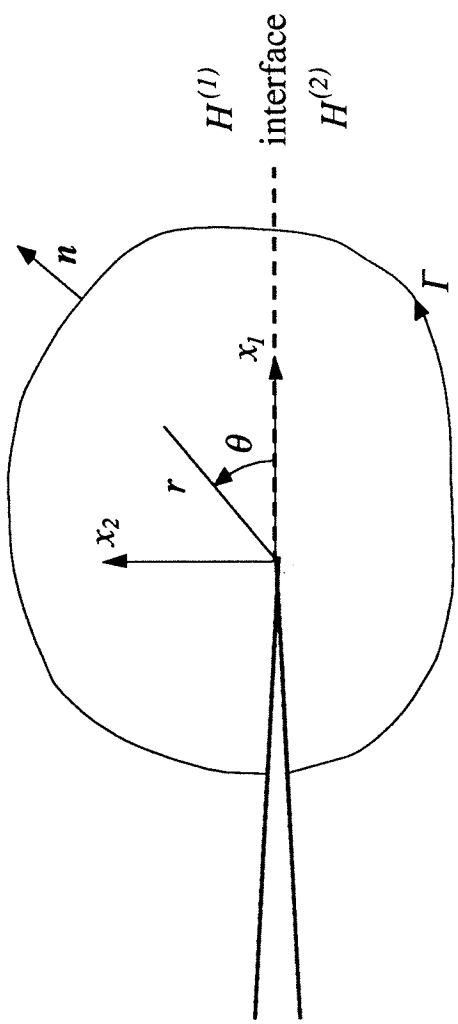

Figure 1. Geometry of the first bimaterial problem.

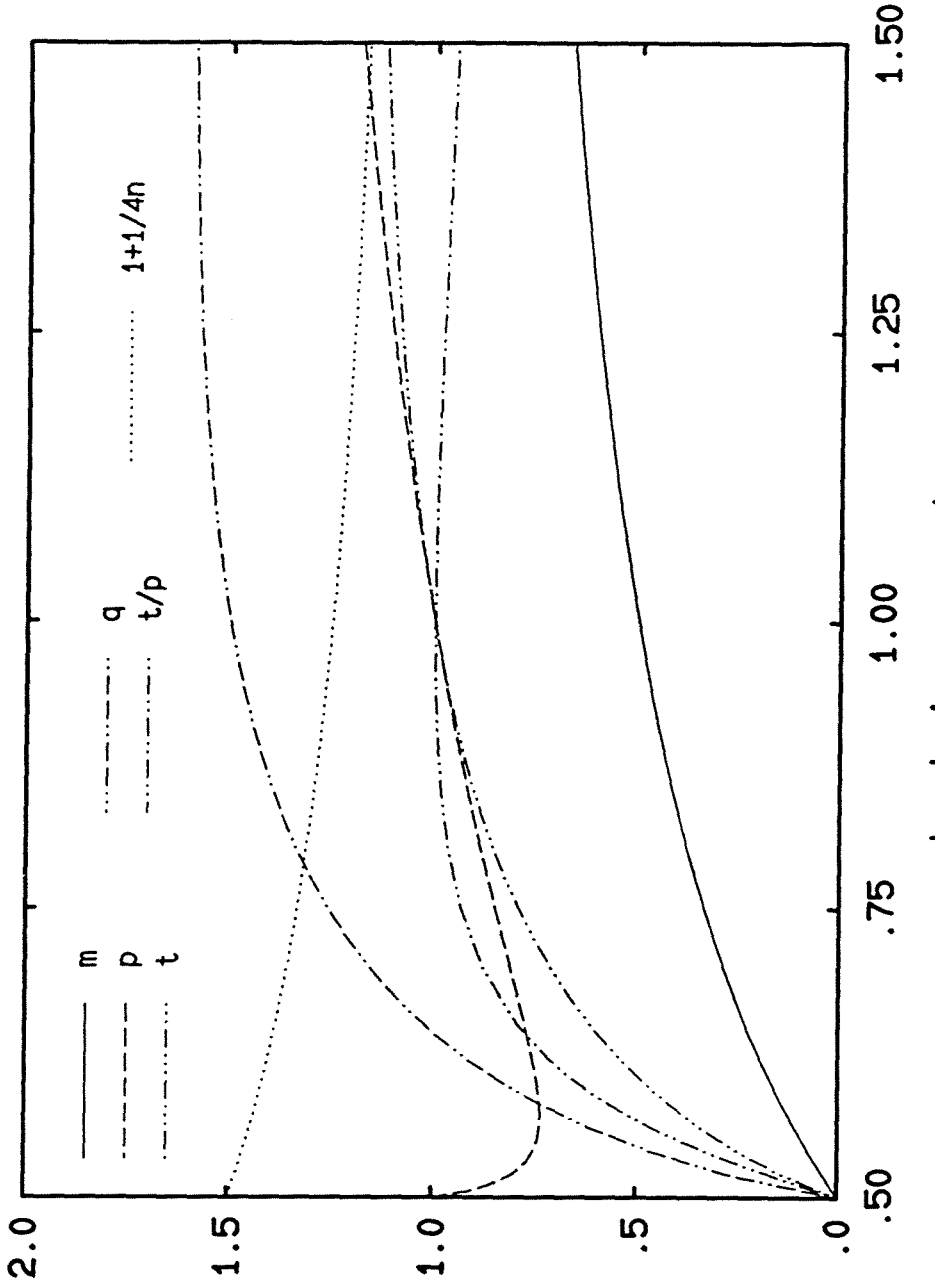

Figure 2. Variation of the asymptotic exponents with respect to the "hardening" parameter n and limit of validity of the asymptotic solution.

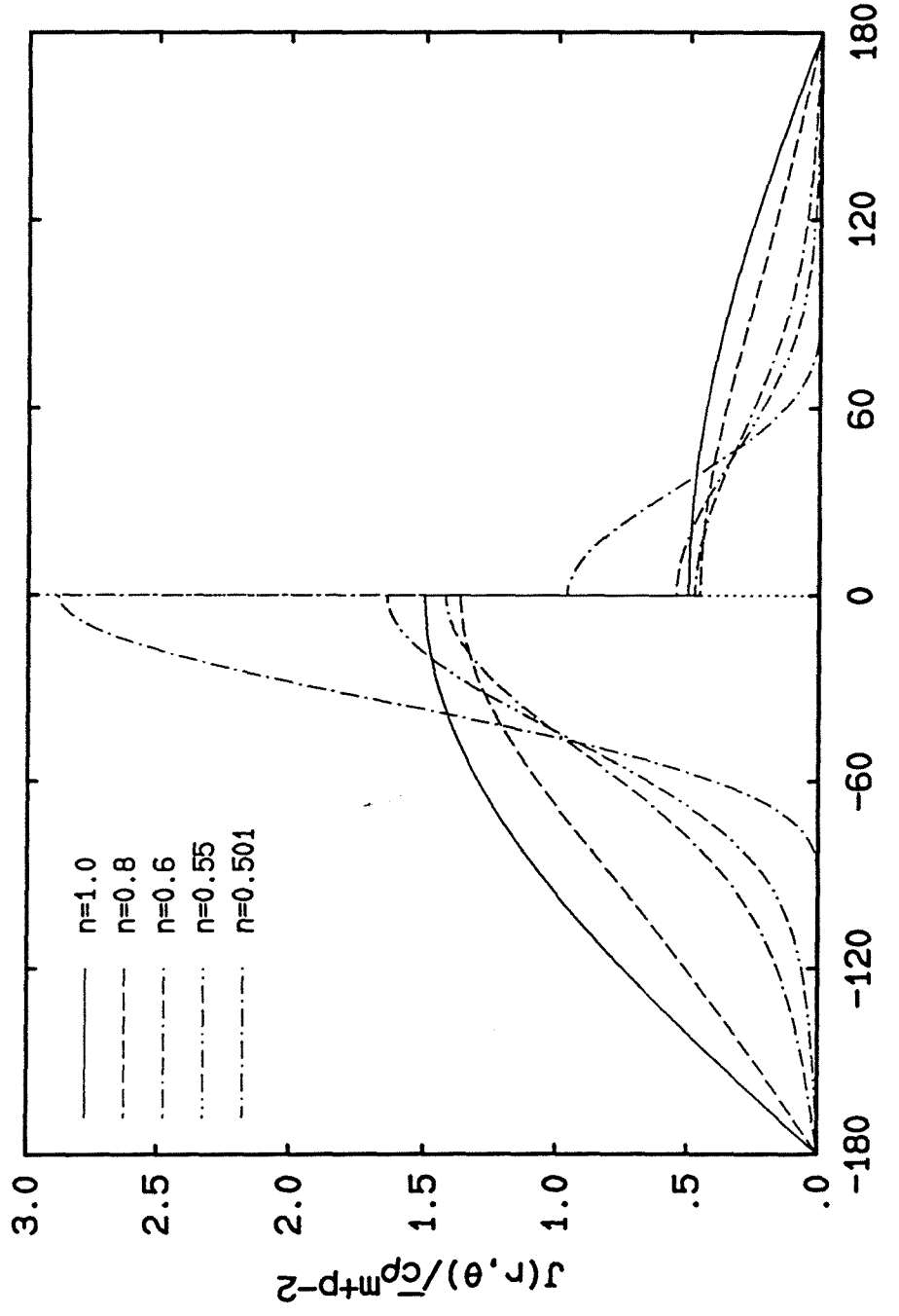

Figure 3. Angular variation of the in-plane Jacobian $J(r,\theta)$ for $\xi = 3$ for various values of n.

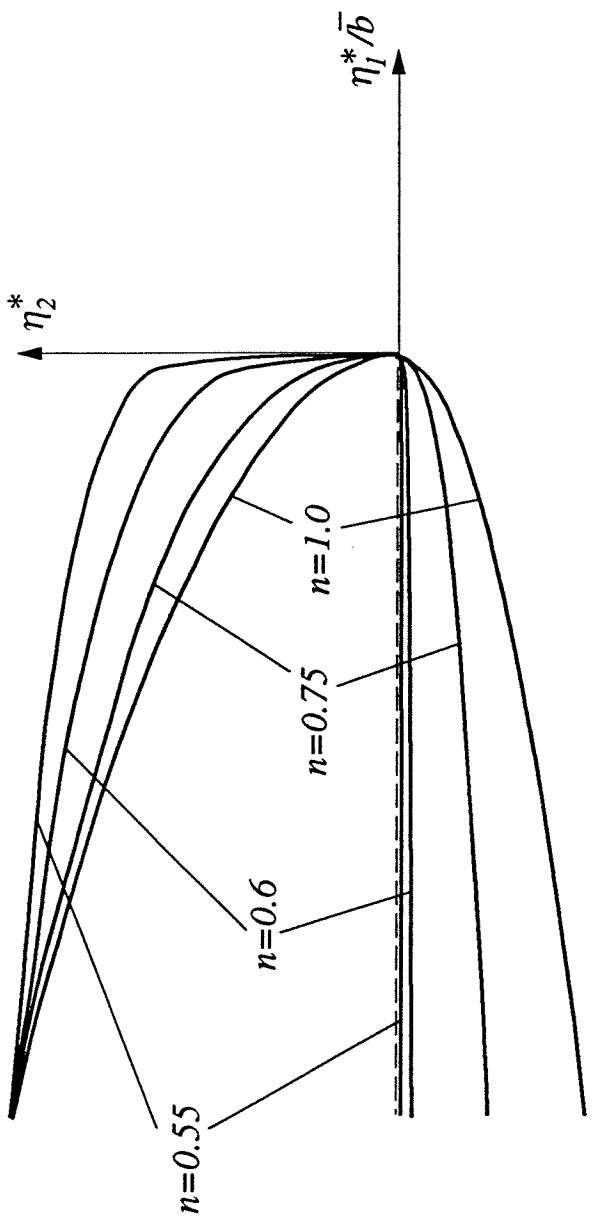

Figure 4. Effect of n on the shape of the deformed crack ($\mu^{(1)}/\mu^{(2)} = 0.5$, $b^{(1)}/b^{(2)} = 1.0$).

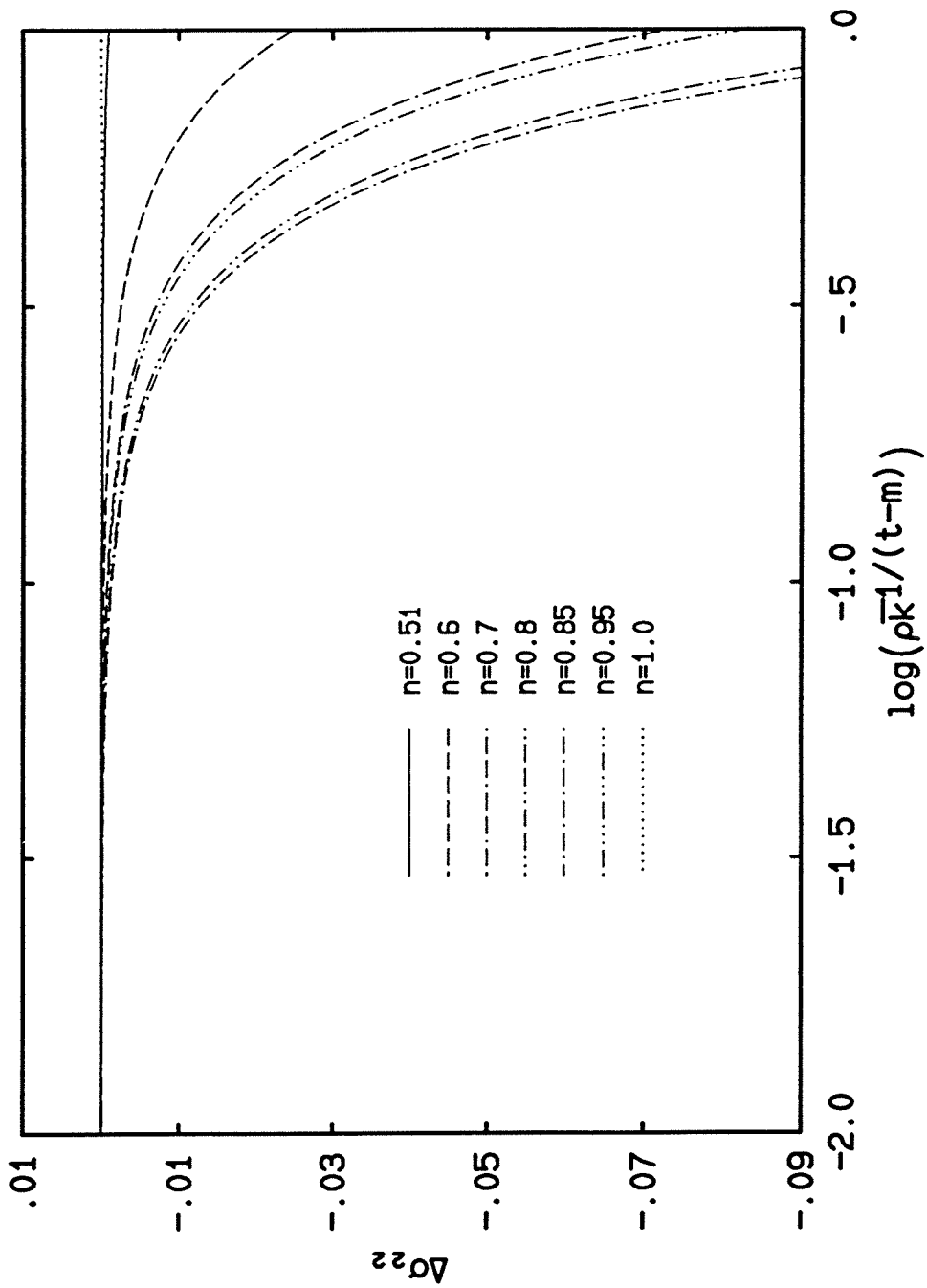

Figure 5. Traction jump across the interface $\Delta\sigma_{22}$ vs $\rho\,\bar{k}^{1/(1-m)}$ for various values of n.

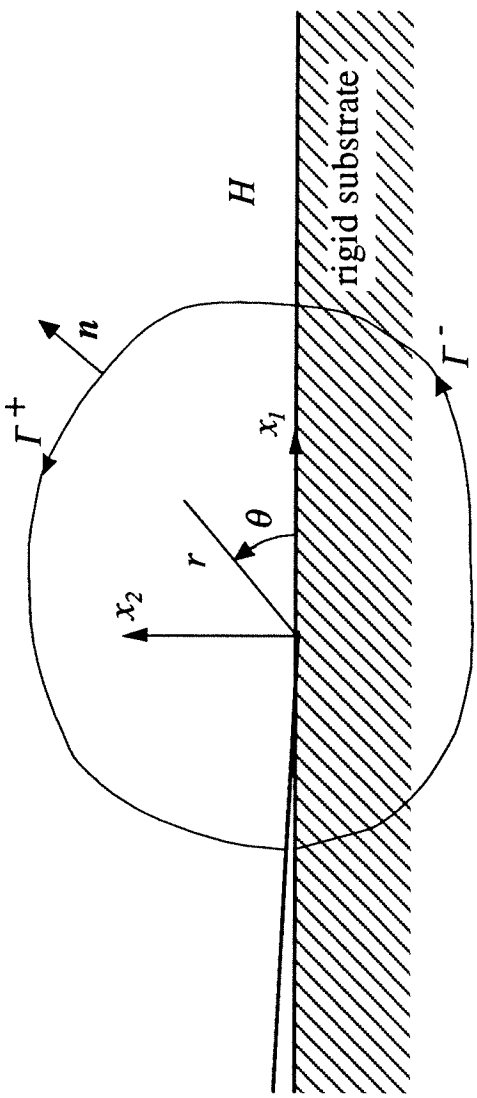

Figure 6. Geometry of the rigid substrate problem.

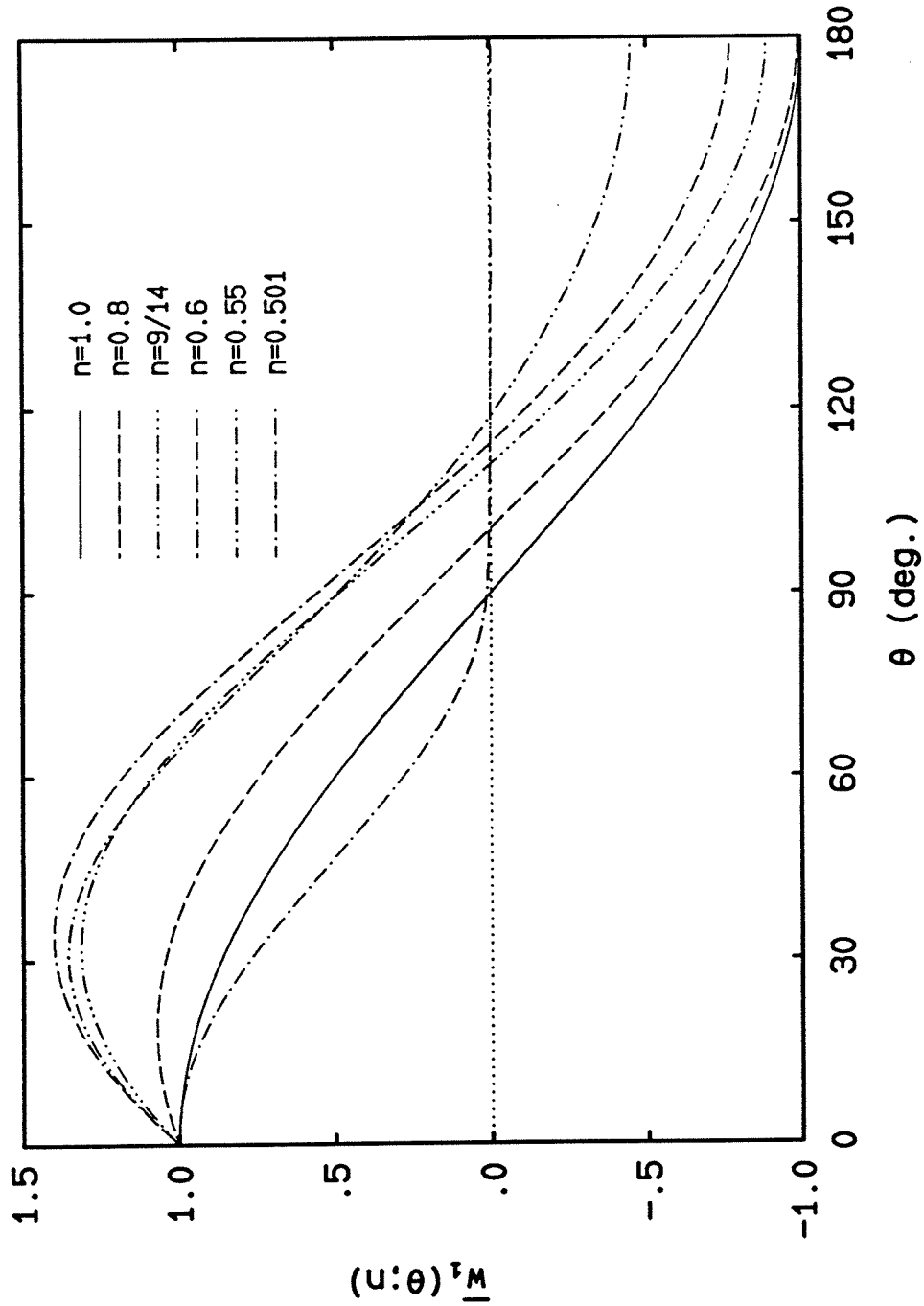

Figure 7. First auxiliary angular function $\overline{w}_1(\theta;n)$.

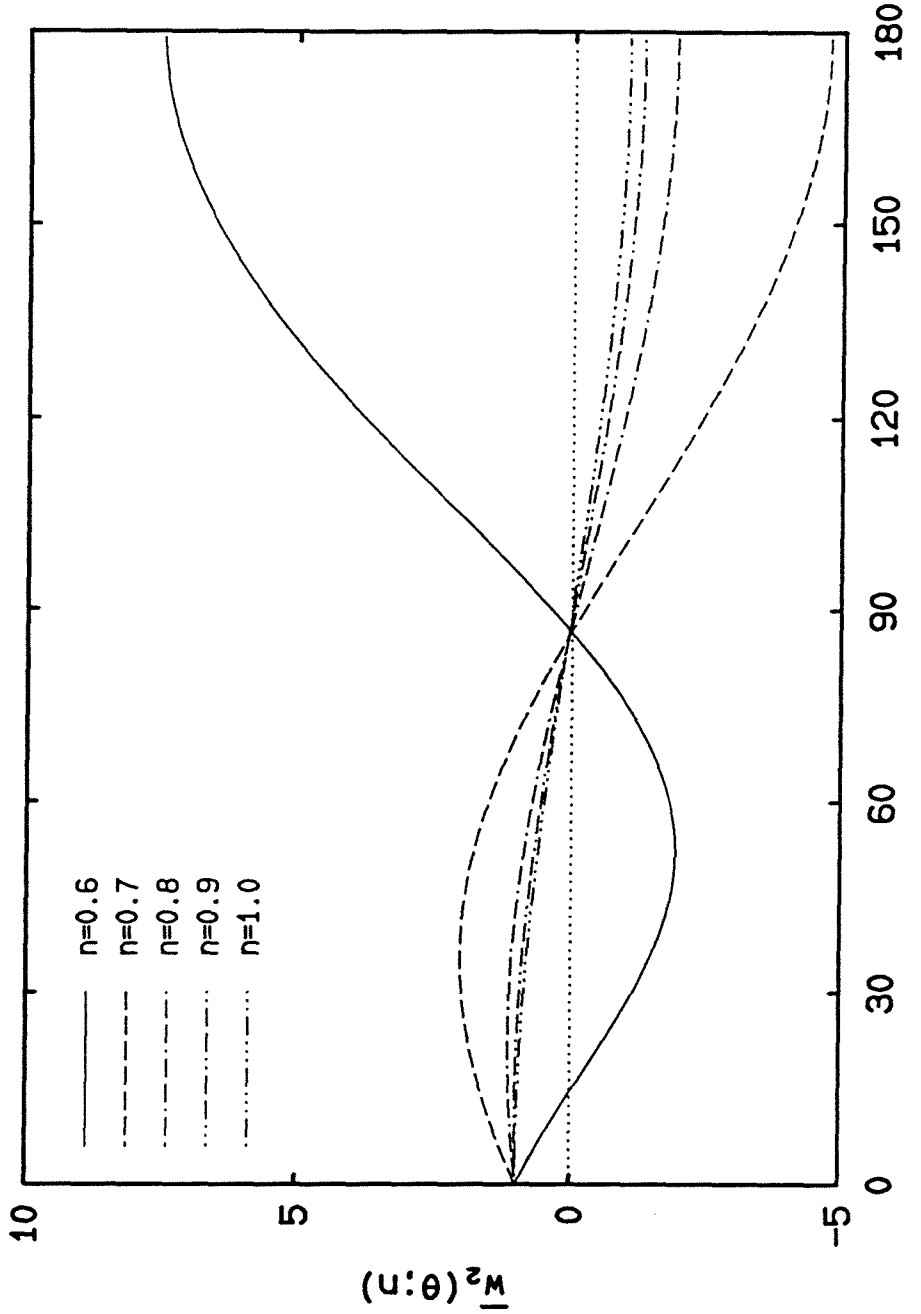

Figure 8. Second auxiliary angular function $\overline{w}_2(\theta;n)$.

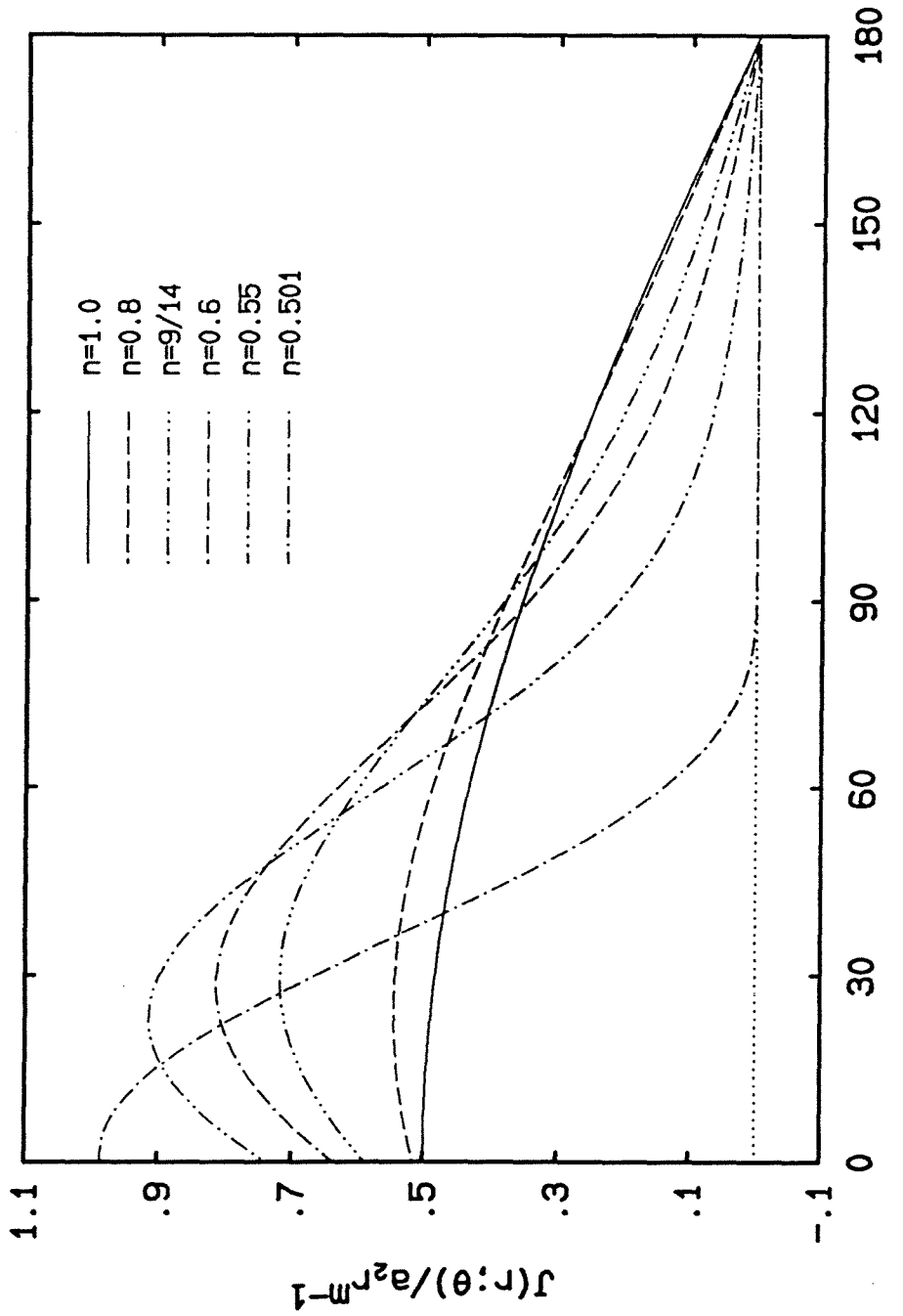

Figure 9. Angular variation of the Jacobian $J(r,\theta)$ for the rigid substrate case.

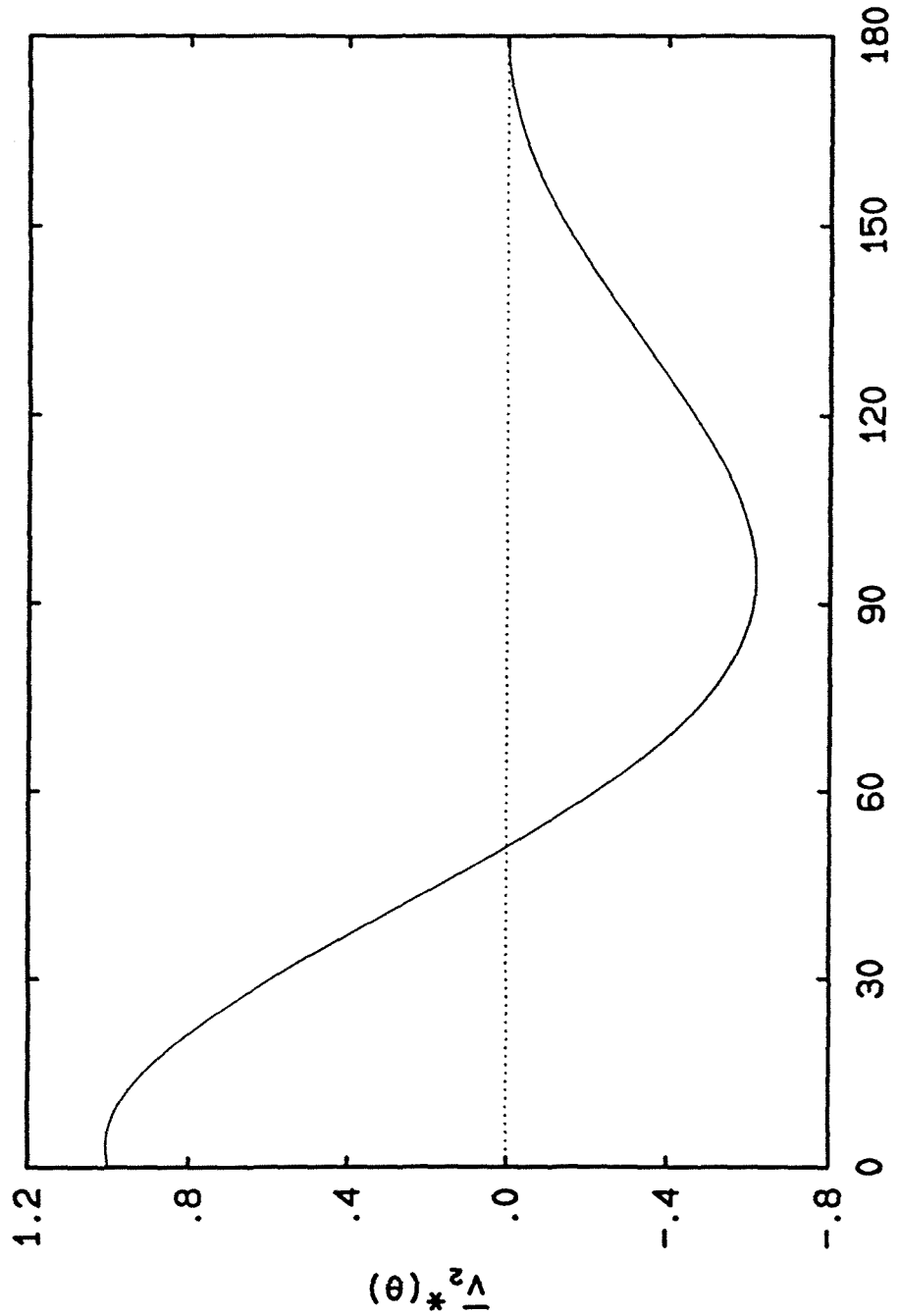

Figure 10. $\bar{v}_2^*(\theta)$.

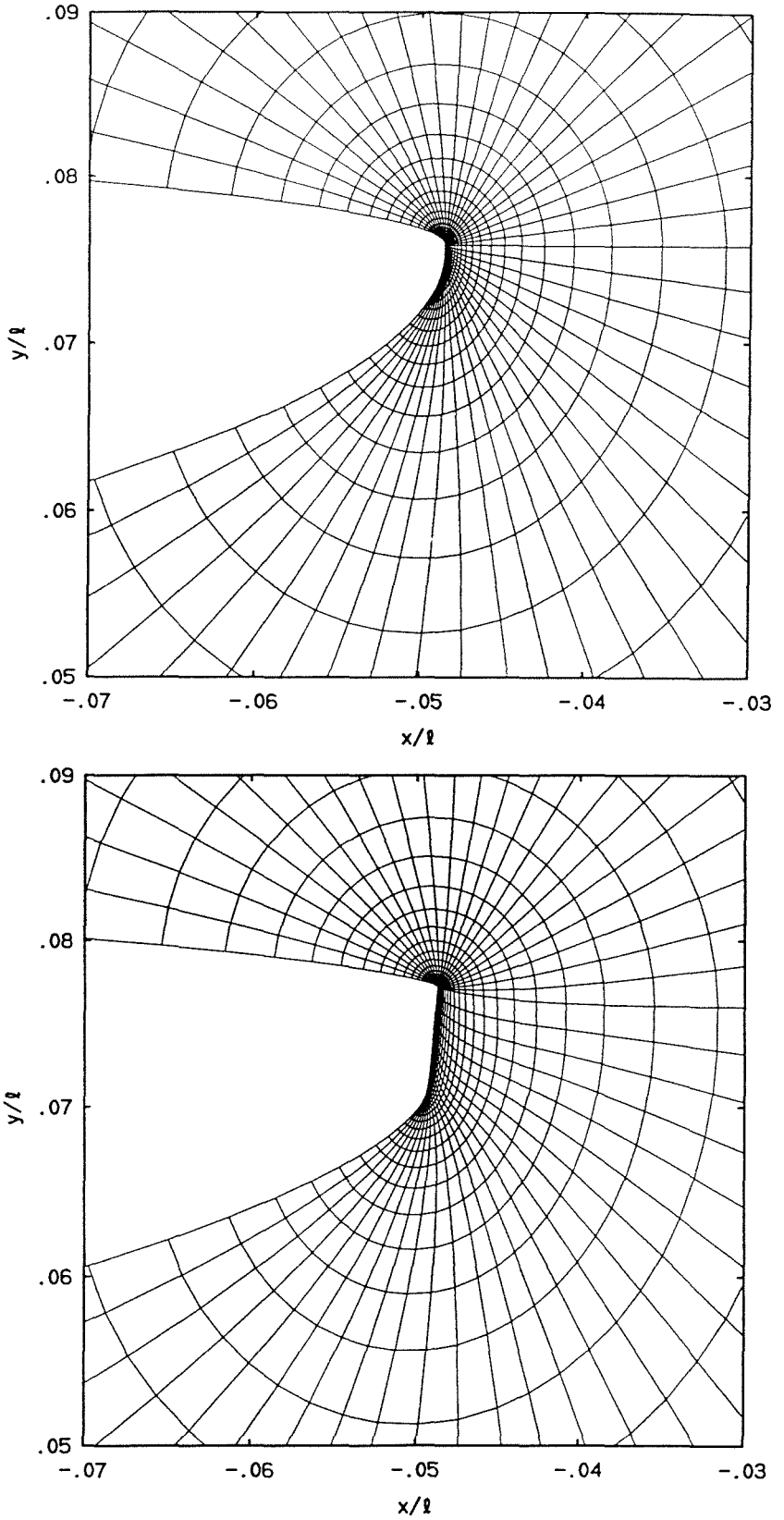

Figure 11. Effect of n on the shape of the deformed crack in the first bimaterial problem : (a) $n=1.0$, (b) $n=0.6$.

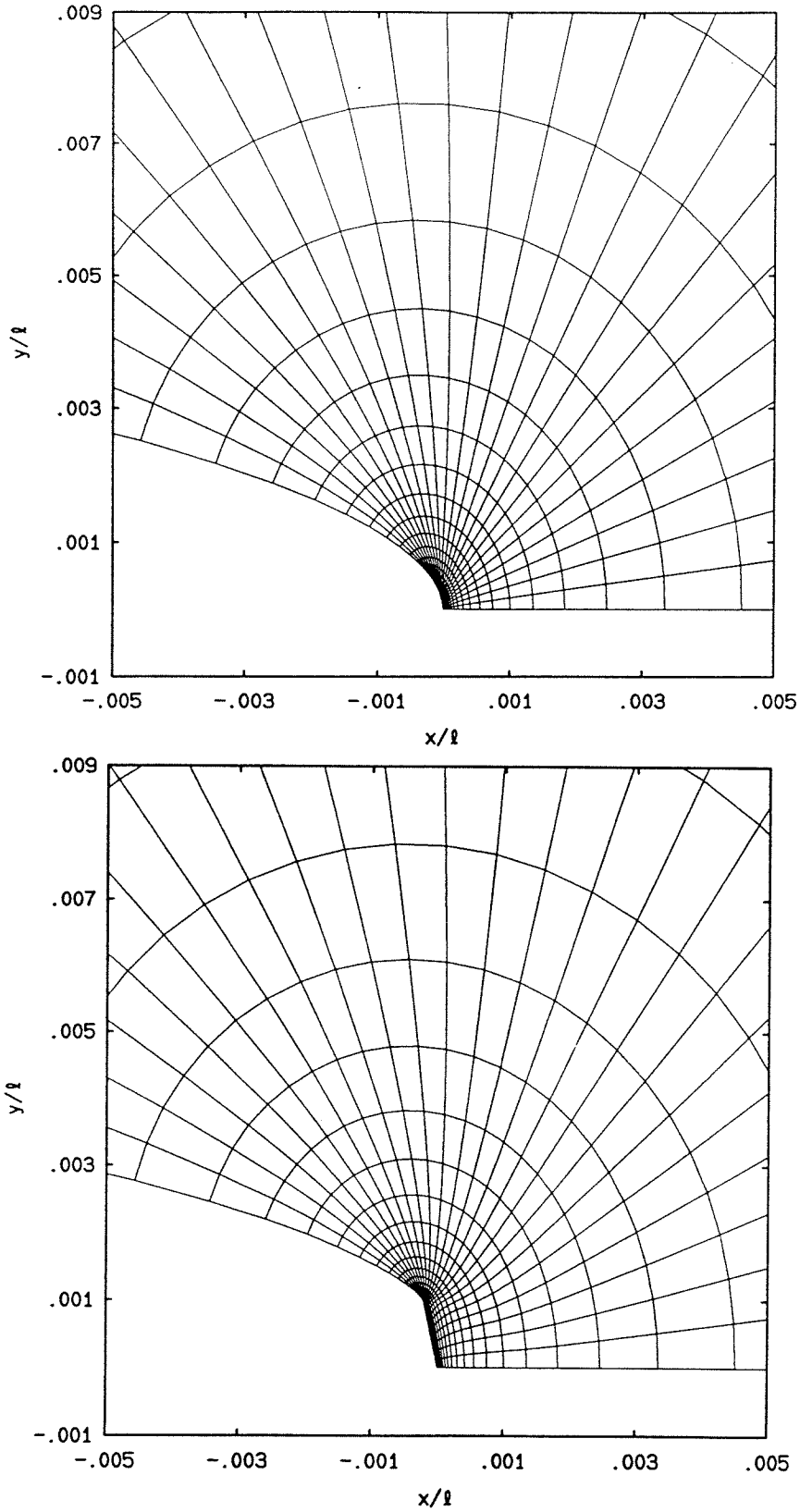

Figure 12. Effect of n on the shape of the deformed crack in the rigid substrate problem : (a) $n=1.0$, (b) $n=0.6$.

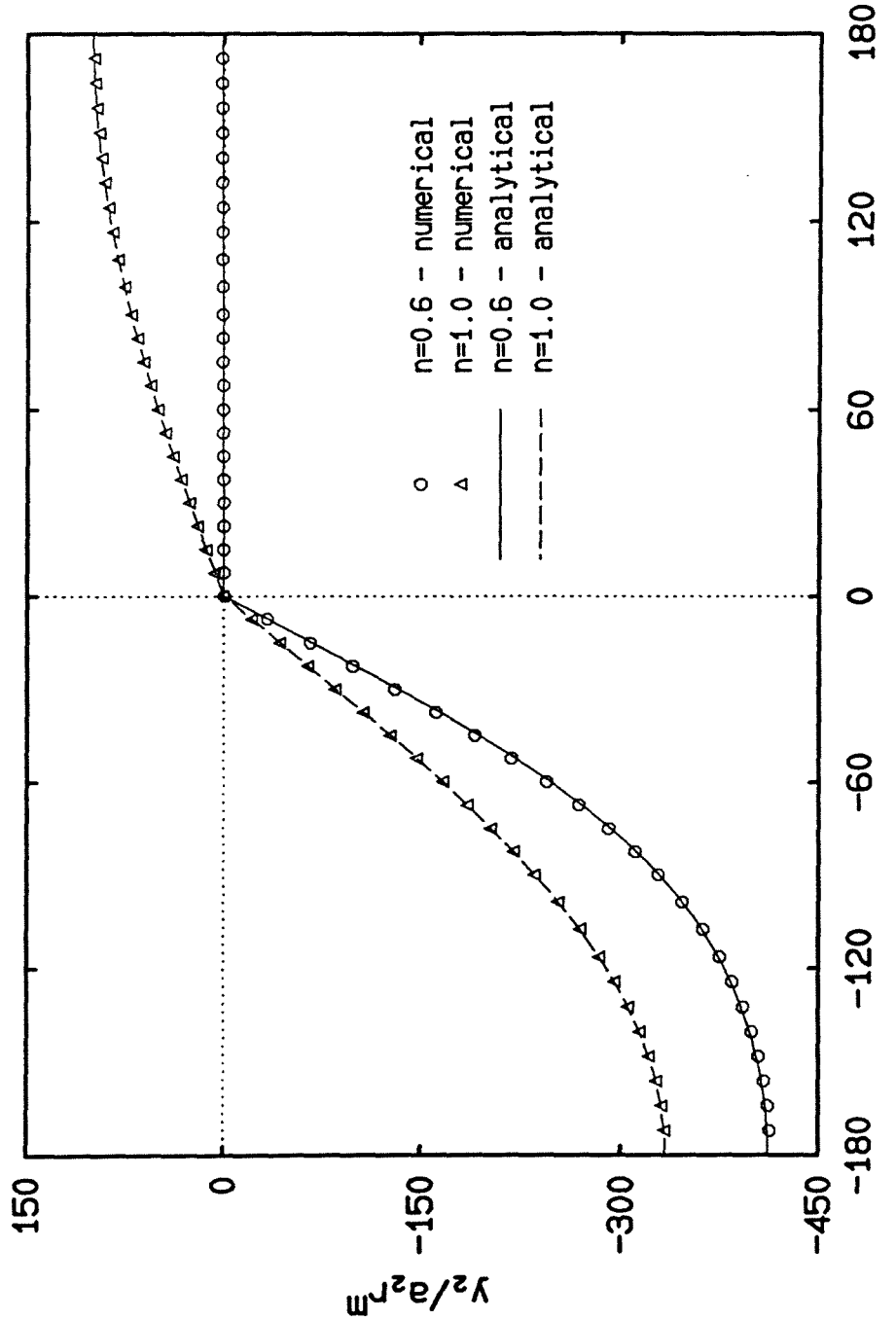

Figure 13. Angular variation of the deformed coordinate y_2 in the first bimaterial problem for $n=1.0$ and $n=0.6$: comparison between asymptotics and numerics.

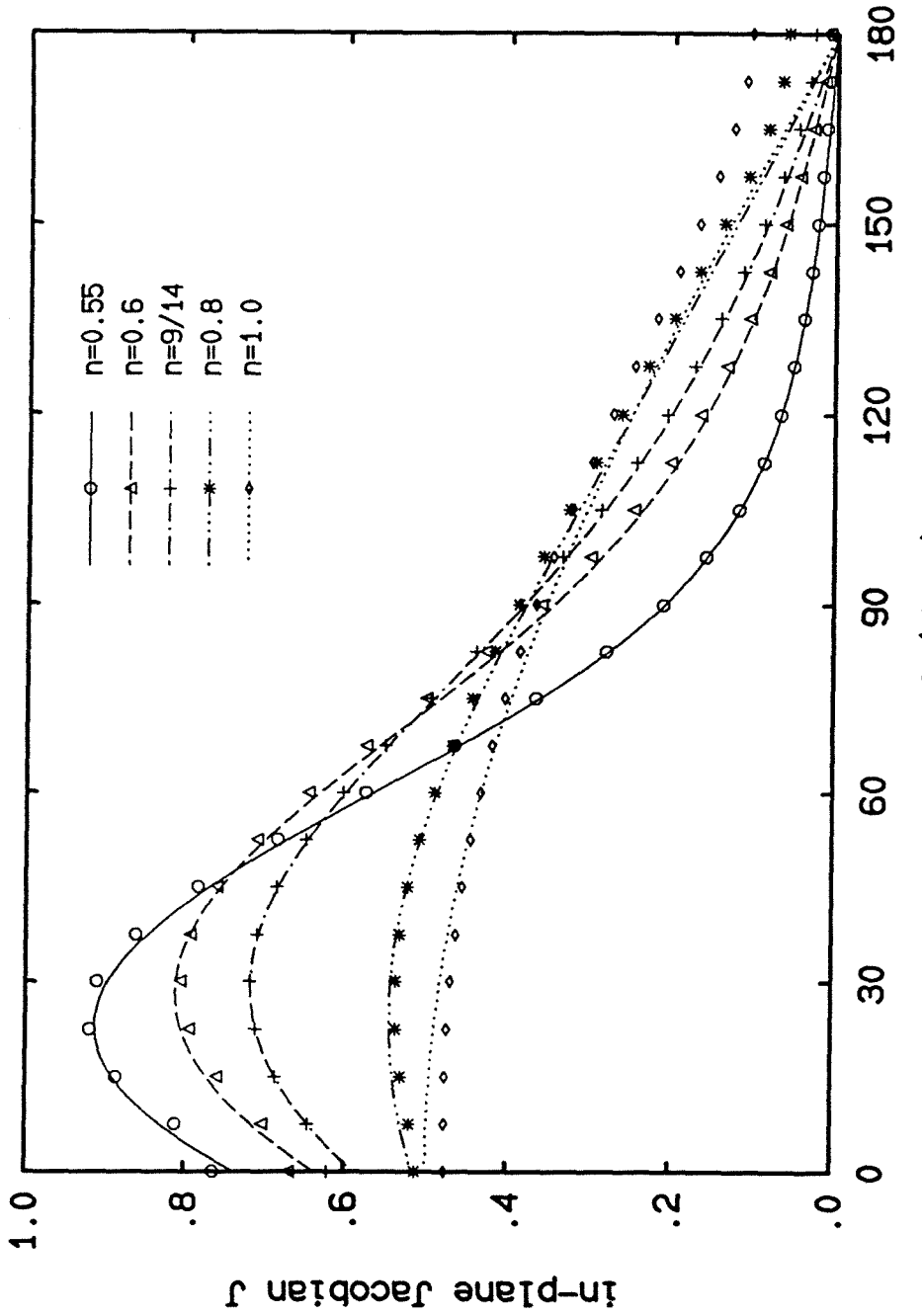

Figure 14. Angular variation of the in-plane Jacobian in the rigid substrate case for various values of n : numerical (symbols) and analytical (curves) solutions.

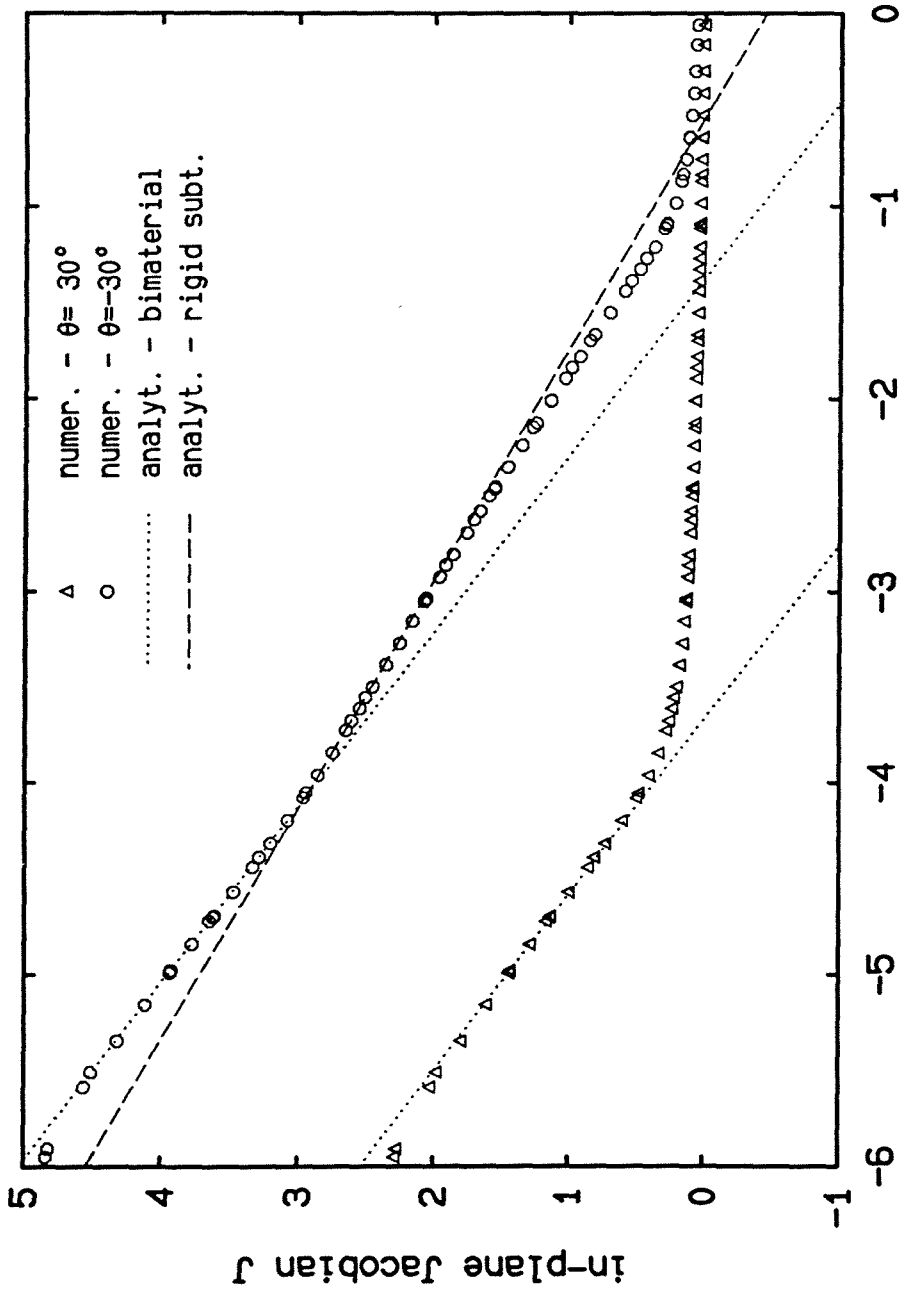

Figure 15. Transition from problem 1 to problem 2 : radial variation of the Jacobian $J(r,\theta)$ in the bimaterial case $n = 0.6$, $\mu^{(1)}/\mu^{(2)} = 3.33$, $b^{(1)}/b^{(2)} = 1.0$. The triangles and circles correspond to the full-field numerical solution in the hard and soft materials respectively. The dotted lines denote the asymptotic solution of the first bimaterial problem while the dashed line represents the near-tip approximation for the rigid substrate case.

Finite strains at the tip of a crack in a sheet of hyperelastic material : III. General bimaterial case.

Abstract.

In this last in a series of three papers, we summarize an asymptotic analysis of the near-tip stress and deformation fields for an interface crack between two sheets of Generalized Neo-Hookean materials. This investigation, which is consistent with the nonlinear elastostatic theory of plane stress, allows for an arbitrary choice, on both sides of the interface, of the three parameters characterizing this class of hyperelastic materials. The first three terms of the approximation series are obtained, showing the existence of a non-oscillatory and contact-free solution to the interface crack problem. The analytical results are compared with a full-field solution obtained numerically using the finite element method.

1.- Introduction.

Although finite-strain analysis is very successful in coping with the difficulties inherent in the linearized analysis of the interface fracture problem (such as oscillatory fields, complex singularities, crack face overlapping and wrinkling[1]), this approach has been rarely used so far in bimaterial fracture mechanics since the early work by Knowles and Sternberg [2] who, through an asymptotic analysis of the near-tip fields for a crack at the interface between two sheets of Neo-Hookean material, showed the

[1] See [1] for a more complete review of existing work.

existence of a separable, non-oscillatory and contact-free solution. The plane strain compressible situation was later investigated by Herrmann [3] for a wider class of hyperelastic materials, allowing for a different "hardening" behavior across the interface. In the present paper, we extend the plane stress incompressible analysis described in [2] by combining material and geometrical nonlinearities through the use of the Generalized Neo-Hookean model. Although it is simple enough to allow for an asymptotic analysis of the near-tip fields, the latter model presents sufficient complexity to capture a fairly wide range of material behaviors.

The present work constitutes the last of a series of three papers relative to the effect of geometrical and material nonlinearities on the stress and deformation fields near the tip of a crack in a sheet of Generalized Neo-Hookean material. The first paper [4] dealt with the symmetric (mode I) and non-symmetric (mixed-mode) cases for a homogeneous solid. In the second paper [1], two special bimaterial situations were investigated : in the first one, the "hardening" behaviors of both components were assumed to be identical, and, in the second, one component of the bimaterial sheet was considered as a rigid substrate. These two particular cases were chosen because the relative simplicity of the asymptotic solutions allowed for an easier understanding of the main aspects of the nonlinear bimaterial solution, including the effect of the "hardening" parameter on the material mismatch. Furthermore, because of an incompatibility in the interface conditions, the rigid substrate situation cannot be obtained directly as a limit from the general case and the transition process required special consideration. In the present paper, the general - and therefore more complex - bimaterial situation is examined, for which a difference in "hardening" characteristics on both sides of the interface is allowed. Although most of the basic relations have been detailed in [4] and [1], section 2 contains a brief presentation of the fundamental equations of plane stress elastostatics for the Generalized Neo-Hookean class hyperelastic materials for completeness purposes. The third section summarizes the computation of the lowest-

order asymptotic term while the next terms are derived in section 4. Then, a discussion of the asymptotic solution is presented together with a comparison of the near-tip approximation with the results of a finite element investigation of the bimaterial problem formulated on a bounded domain.

2.- Nonlinear plane stress theory and Generalized Neo-Hookean materials.

Our objective is to study the deformation of a sheet of hyperelastic, homogeneous, isotropic, incompressible material in the absence of body forces. Let Π denote the mid-plane of the sheet in the undeformed configuration and Π^* the same mid-plane in the deformed configuration, related to Π by a one-to-one, twice continuously differentiable mapping $\hat{\boldsymbol{y}}(\boldsymbol{x})$ such that

$$\boldsymbol{y} = \hat{\boldsymbol{y}}(\boldsymbol{x}) = \boldsymbol{x} + \boldsymbol{u}(\boldsymbol{x}), \qquad \text{on } \Pi, \tag{2.1}$$

where $\boldsymbol{x}$ and $\boldsymbol{y}$ are the undeformed and deformed position vectors respectively and $\boldsymbol{u}$ is the displacement field. Associated with the mapping $\hat{\boldsymbol{y}}(\boldsymbol{x})$ are the deformation tensor field $\boldsymbol{F} = \nabla \boldsymbol{y}$ and the corresponding scalar invariants I and J

$$\begin{aligned} I &= tr(\boldsymbol{F}\boldsymbol{F}^T) = y_{\alpha,\beta} y_{\alpha,\beta}, \\ J &= det\,\boldsymbol{F} = \lambda^{-1} = y_{1,1} y_{2,2} - y_{1,2} y_{2,1}, \end{aligned} \tag{2.2}$$

where λ is the transverse stretch and is, by virtue of the incompressibility of the material, equal to the inverse of the in-plane Jacobian J. Also associated with the

---

[2] A more complete description of the origin and physical significance of these relations can be found in [4]. The notations used here are identical to those used in [1] and [4]. Boldface characters represent two-dimensional vectors and matrices. Greek indices take the values (1,2) and summation over repeated indices is implied.

deformation are two stress tensor fields, the nominal (or Piola) stress tensor $\boldsymbol{\sigma}$ and the true (or Cauchy) stress tensor $\boldsymbol{\tau}$, related by

$$\boldsymbol{\tau} = \boldsymbol{\sigma}\boldsymbol{F}^{T}. \tag{2.3}$$

We also assume the existence of a plane stress elastic potential $U(I,J)$ which allows to express the stresses in terms of the deformations as

$$\boldsymbol{\sigma} = 2U_{I}\boldsymbol{F} + JU_{J}\boldsymbol{F}^{-T}, \qquad \text{on } \Pi, \tag{2.4}$$

where U_I and U_J are the partial derivatives of $U(I,J)$ with respect to I and J respectively. The equilibrium equations are

$$\begin{aligned} &div\,\boldsymbol{\sigma} = \boldsymbol{0}, \\ &\boldsymbol{\sigma}\boldsymbol{F}^{T} = \boldsymbol{F}\boldsymbol{\sigma}^{T}, \end{aligned} \qquad \text{on } \Pi. \tag{2.5}$$

Throughout this analysis, we are concerned with a special class of incompressible, homogeneous, isotropic, hyperelastic materials, the so-called Generalized Neo-Hookean (GNH) materials, characterized by the following expression of the plane-stress elastic potential

$$U(I,J) = \frac{\mu}{2b}\left\{\left[1 + \frac{b}{n}\left(I + J^{-2} - 3\right)\right]^{n} - 1\right\}. \tag{2.6}$$

The physical significance of the three material parameters μ, b and n appearing in (2.6) has been described in [4] through an examination of the uniaxial response of this class of materials. They are referred to as the shear modulus (μ), the "yielding" parameter (b) and the "hardening" exponent (n). It was shown there that the latter parameter has to be greater than *1/2* to guarantee ellipticity of the equilibrium equations which, with the aid of (2.4), (2.5) and (2.6), are written as

$$A^{n-2}\left\{\frac{b(n-1)}{n}\left(\frac{\partial I}{\partial x_\beta} + \frac{\partial \lambda^2}{\partial x_\beta}\right)\left(y_{\alpha,\beta} - \lambda^3 \varepsilon_{\alpha\mu}\varepsilon_{\beta\nu}y_{\mu,\nu}\right) + A\left(\nabla^2 y_\alpha - \frac{\partial \lambda^3}{\partial x_\beta}\varepsilon_{\alpha\mu}\varepsilon_{\beta\nu}y_{\mu,\nu}\right)\right\} = 0, \tag{2.7}$$

with I and λ defined in (2.2), $\varepsilon_{\alpha\beta}$ is the two-dimensional alternator[3] and

$$A = 1 + b(I + \lambda^2 - 3)/n. \tag{2.8}$$

Throughout the present analysis, we deal with values of n varying between the "perfectly-plastic" situation ($n \to 1/2$) and the Neo-Hookean case ($n=1$). Finally, the stress-strain relations for this class of hyperelastic materials are

$$\begin{aligned} \sigma_{\alpha\beta} &= \mu A^{n-1}\{y_{\alpha,\beta} - \lambda^3 \varepsilon_{\alpha\mu}\varepsilon_{\beta\nu} y_{\mu,\nu}\}, \\ \tau_{\alpha\beta} &= \mu A^{n-1}\{y_{\alpha,\gamma} y_{\beta,\gamma} - \lambda^2 \delta_{\alpha\beta}\}, \end{aligned} \tag{2.9}$$

A and λ having been introduced in (2.8) and (2.2), respectively, and $\delta_{\alpha\beta}$ is the unit tensor.

3.- Lower-order asymptotic analysis of the near-tip fields for an interface crack between two GNH sheets.

In this section, we present the analysis leading to the first term of the asymptotic approximation of the deformation field near the tip of an interface crack between two sheets of GNH materials. The work summarized in this section followed an earlier analysis by Herrmann [3] of the bimaterial fracture problem : although the latter concerned the compressible plane strain case for a completely different class of hyperelastic materials, it happens that the relations leading to the first asymptotic term are similar to the present situation.

---

[3] i.e., $\varepsilon_{11} = \varepsilon_{22} = 0$, $\varepsilon_{12} = -\varepsilon_{21} = 1$.

Problem formulation.

The local analysis of the interface fracture problem is carried out on the bimaterial geometry illustrated in figure 1 and which consists of two bonded half-planes $H^{(1)}$ and $H^{(2)}$. A Cartesian coordinate system is chosen in the mid-plane of the bimaterial sheet such that the interface lies along the positive x_1-axis while the semi-infinite crack line is represented by the negative x_1-axis, the crack tip being located at the origin. Let $(\mu^{(k)}, b^{(k)}, n^{(k)})$[4] denote the material parameters characterizing the two GNH sheets $H^{(k)}$. The local polar coordinates (r,θ), defined in figure 1, are used throughout the present analysis which aims at obtaining an asymptotic approximation of the near-tip fields, consistent with the equilibrium equations (2.7), the constitutive relations (2.9), the matching conditions along the interface

$$\begin{aligned} &y_\alpha(r,0^+) = y_\alpha(r,0^-), \\ &\sigma_{\alpha 2}(r,0^+) = \sigma_{\alpha 2}(r,0^-), \end{aligned} \qquad (r>0), \tag{3.1}$$

and the traction-free boundary conditions along the crack faces

$$\sigma_{\alpha 2}(r,\pm\pi) = 0, \qquad (r>0). \tag{3.2}$$

As was the case in the investigation of the special bimaterial situations reviewed in [1], we look for a solution such that the asymptotic field be non-oscillatory and singular, i.e., that the Jacobian of the in-plane transformation be unbounded as the crack tip is approached from either side of the interface. Finally, the solution must satisfy certain continuity requirements on each half-plane $H^{(k)}$ in order to justify the differentiations appearing in the equilibrium equations and the boundary conditions.

---

[4] As was the case in [1], the superscript "*(k)*" written in parentheses corresponds to the upper *(1)* and lower *(2)* materials and is *never* summed over.

The procedure used to determine the first asymptotic term consists of studying each half-plane independently and then connecting the asymptotic solutions through the bond conditions (3.1). Since the computation of the first asymptotic term has been detailed in [3], the next subsections only review the main steps of the lower-order analysis.

Solution for each half-plane $H^{(k)}$.

Starting from the following assumed separable form of the deformation field

$$y_\alpha^{(k)}(r,\theta) \sim r^{m^{(k)}} v_\alpha^{(k)}(\theta), \qquad \text{on } H^{(k)} \ (k=1,2), \qquad (3.3)^5$$

where the exponents $m^{(k)}$ must be real to avoid the appearance of oscillations and satisfy the inequalities

$$0 < m^{(k)} < 1, \qquad (3.4)$$

in order to ensure bounded displacements but admit unbounded gradients at the crack tip.

Examination of the order of each term appearing in the equilibrium equations (2.7) leads to the asymptotic relations

$$(n-1)\frac{\partial I}{\partial x_\beta} y_{\alpha,\beta} + I\nabla^2 y_\alpha = 0, \qquad (r \to 0, -\pi \le \theta \le \pi), \qquad (3.5)^6$$

where the scalar invariant I has been defined in (2.2). Substituting (3.3) into (3.5), the system of coupled nonlinear second-order differential equations results

---

[5] Recall that no summation on the material superscript "*(k)*" is implied. The symbol "~" conventionally represents the asymptotic equality.

[6] In order to avoid cumbersome notations, the material index "*(k)*" will henceforth be omitted unless needed for clarity.

$$B\ddot{v}_\alpha + (n-1)\dot{B}\dot{v}_\alpha + m(2(n-1)(m-1)+m)Bv_\alpha = 0, \tag{3.6}$$

where $(\dot{\ })$ denotes $d(\ )/d\theta$ and

$$B(\theta) = m^2 v_\gamma(\theta)\, v_\gamma(\theta) + \dot{v}_\gamma(\theta)\, \dot{v}_\gamma(\theta). \tag{3.7}$$

The stress-free boundary conditions (3.2) are equivalently written, with the aid of (2.9) and (3.3), as

$$\dot{v}_\alpha(\pm\pi) = 0. \tag{3.8}$$

The solution to (3.6)-(3.8) is expressed as

$$v_\alpha^{(k)}(\theta) = a_\alpha^{(k)} f^{(k)}(\theta; n^{(k)}, m^{(k)}), \tag{3.9}$$

where $a_\alpha^{(k)}$ are four undetermined constants and $f^{(k)}(\theta; n^{(k)}, m^{(k)})$ satisfy

$$G^{m^{(k)}}(f^{(k)}) = 0, \tag{3.10}$$

in which the differential operator G^m is

$$G^m(f) = \ddot{f} + m^2 f + (n-1)\left(2m(m-1)f + \frac{\dot{B}_f}{B_f}\dot{f}\right), \tag{3.11}$$

with

$$B_f(\theta) = m^2 f^2(\theta) + \dot{f}^2(\theta). \tag{3.12}$$

The boundary conditions (3.8) are rewritten as

$$\dot{f}^{(1)}(\pi; n^{(1)}, m^{(1)}) = 0, \quad \dot{f}^{(2)}(-\pi; n^{(2)}, m^{(2)}) = 0. \tag{3.13}$$

The solution to (3.10)-(3.13) on each half-plane has been found by Herrmann [3] using a transformation into the phase plane suggested by Knowles and Sternberg

[5]. Without loss of generality, we henceforth assume that the lower component has a weaker "hardening" behavior than the upper-half material, i.e.,

$$n^{(2)} \leq n^{(1)}. \tag{3.14}$$

It is possible to show (see [3]) that the corresponding asymptotic exponents satisfy a similar inequality

$$m^{(2)} \leq m^{(1)}. \tag{3.15}$$

Furthermore, the first asymptotic exponent of the lower-half sheet can be determined following the reasoning already used in [1] and [4] : the conservation of the $\mathcal{J}$-integral defined by

$$\mathcal{J} = \int_{\Gamma} (U n_1 - \sigma_{\alpha\beta} n_\beta y_{\alpha,1}) ds, \tag{3.16}$$

in which Γ is a regular contour of outward normal $\boldsymbol{n}$ surrounding the crack tip (figure 1) and U is the plane stress elastic potential introduced in (2.5), yields, with the aid of (2.6), (2.9) and (3.3), the familiar result

$$m^{(2)} = 1 - 1/2n^{(2)}, \tag{3.17}$$

which satisfies (3.4). The solution to (3.10)-(3.13b) in the lower-half plane is found to be

$$f(\theta; n, m) = \left[n(\omega + k\cos\theta)\right]^{\frac{n-1}{2n}} \sin\frac{\theta}{2}\left[1 - \frac{2k^2\cos^2\theta/2}{1+\omega}\right]^{1/2}, \tag{3.18}$$

where $n = n^{(2)}$, $m = m^{(2)}$ is given by (3.17) and

$$\begin{aligned} k &= 1 - 1/n, \\ \omega &= [1 - k^2 \sin^2\theta]^{1/2}. \end{aligned} \tag{3.19}$$

The solution in the upper half plane has the form

$$f(\theta;n,m) = K\cos\psi(\theta)\left|1-\frac{2(n-1)}{m(2n-1)}\cos^2\psi(\theta)\right|^{\frac{1}{2(m-1)}}, \qquad (3.20)$$

where the transformation $\psi(\theta)$ is implicitly given by

$$\pi-\theta = \psi - \frac{m-1}{m}\kappa\tan^{-1}(\kappa\tan\psi), \qquad (3.21)$$

with $n = n^{(1)}$, $m = m^{(1)}$ and

$$\kappa = \left(\frac{m(2n-1)}{(m-1)(2n-1)+1}\right)^{1/2}. \qquad (3.22)$$

The constant K in (3.20) is chosen such that $f(\pi;n^{(1)},m^{(1)}) = 1$, i.e.,

$$K = \left|1-\frac{2(n^{(1)}-1)}{m^{(1)}(2n^{(1)}-1)}\right|^{\frac{1}{2(1-m^{(1)})}}. \qquad (3.23)$$

Application of the bond conditions along the interface.

The continuity conditions (3.1) across the interface yield an expression for the asymptotic exponent $m^{(1)}$ and a relation between the undetermined scalars[7] $a_\alpha^{(k)}$

$$m^{(1)} = \frac{4n^{(2)}n^{(1)} - 4n^{(2)} + 1}{2n^{(2)}(2n^{(1)}-1)}, \qquad (3.24)$$

and

$$a_\alpha^{(2)} = \xi\,(a_\beta^{(1)}a_\beta^{(1)})^{\frac{n^{(1)}-n^{(2)}}{2n^{(2)}-1}}\,a_\alpha^{(1)}, \qquad (3.25)$$

where the constant ξ depends on the six material parameters $(\mu^{(k)},b^{(k)},n^{(k)})$ through

[7] See [3] for the details of the computation leading to (3.24) and (3.25).

$$\xi^{2n^{(2)}-1} = \frac{\mu^{(1)}}{\mu^{(2)}}\left[\frac{b^{(1)}}{n^{(1)}}\right]^{n^{(1)}-1}\left[\frac{b^{(2)}}{n^{(2)}}\right]^{1-n^{(2)}} \left(\dot{f}^{(2)}(0^-;n^{(2)},m^{(2)})\right)^{1-2n^{(2)}} \dot{f}^{(1)}(0^+;n^{(1)},m^{(1)}) \bullet$$
$$\bullet\left(m^{(1)^2} f^{(1)^2}(0^+;n^{(1)},m^{(1)}) + \dot{f}^{(1)^2}(0^+;n^{(1)},m^{(1)})\right)^{n^{(1)}-1}, \tag{3.26}$$

with $f(0^{\pm};n,m)$ and $\dot{f}(0^{\pm};n,m)$ determined from (3.18) and (3.20). The relations (3.17) and (3.24) are illustrated in figure 2 for $1/2 < n^{(2)} \le n^{(1)} \le 2$. It is important to note that combining (3.14), (3.17) and (3.24) yields

$$m^{(2)} = 1 - \frac{1}{2n^{(2)}} \le 1 - \frac{1}{2n^{(1)}} \le m^{(1)}, \tag{3.27}$$

and that the equalities hold if and only if $n^{(1)} = n^{(2)} = n$. Note also that in the latter case[8] the first term of the asymptotic expansion reduces to

$$m^{(1)} = m^{(2)} = m = 1/2n, \tag{3.28}$$

$$y_\alpha(r,\theta) \sim a_\alpha\, j(\theta) f(\theta;n) r^m, \tag{3.29}$$

where $f(\theta;n)$ is described by (3.18) and the angular step function $j(\theta)$ takes the value

$$j(\theta) = \begin{cases} 1 & \text{for } 0 \le \theta \le \pi, \\ \xi & \text{for } -\pi \le \theta \le 0. \end{cases} \tag{3.30}$$

In (3.30), the nonlinear mismatch parameter ξ takes then the simple form

$$\xi = \left[\frac{\mu^{(1)}}{\mu^{(2)}}\left(\frac{b^{(1)}}{b^{(2)}}\right)^{n-1}\right]^{1/2n-1}. \tag{3.31}$$

Note finally that, if $n^{(1)} \neq n^{(2)}$, (3.25) indicates that the relation between $a_\alpha^{(1)}$ and $a_\alpha^{(2)}$ depends on the "intensity of loading," since it may be written as

---

[8] The special bimaterial case for which both components have identical "hardening" behaviors has been detailed in section 3 of [1].

$$a_\alpha^{(1)} = \xi^{\frac{2n^{(2)}-1}{1-2n^{(1)}}} (a_\beta^{(2)} a_\beta^{(2)})^{\frac{n^{(2)}-n^{(1)}}{2n^{(1)}-1}} a_\alpha^{(2)}. \tag{3.32}$$

The second factor on the right-hand side of (3.32) can, in turn, be related to the value of the $\mathcal{J}$-integral defined in (3.16)

$$\mathcal{J} = \mu^{(2)} b^{(2)n^{(2)}-1} (a_\beta^{(2)} a_\beta^{(2)})^{n^{(2)}} \bar{\mathcal{J}}(n^{(2)}, m^{(2)}), \qquad (n^{(1)} > n^{(2)}), \tag{3.33}$$[9]

where

$$\bar{\mathcal{J}}(n,m) = m^{2n-1} n^{1-n} \pi/4. \tag{3.34}$$

Thus, with the aid of (3.33), (3.32) is equivalent to

$$a_\alpha^{(1)} = \xi^{\frac{1-2n^{(2)}}{2n^{(1)}-1}} \left(\frac{\mathcal{J}}{\mu^{(2)} (b^{(2)})^{n^{(2)}-1} \bar{\mathcal{J}}(n^{(2)}, m^{(2)})} \right)^{\frac{n^{(2)}-n^{(1)}}{n^{(2)}(2n^{(1)}-1)}} a_\alpha^{(2)}. \tag{3.35}$$

Note that (3.35) reduces to (3.29)-(3.31) when $n^{(1)} = n^{(2)}$ since the factor involving the $\mathcal{J}$-integral then tends to unity. The angular functions $f^{(k)}(\theta; n^{(k)}, m^{(k)})$ of the first asymptotic term are shown in figure 3 for $n^{(2)}$=*0.51*, *0.6* and *0.8*, together with the corresponding values of the asymptotic exponents $m^{(1)}$ and $m^{(2)}$.

It is worth noting that the continuity of displacements is ensured across the interface to the leading order only since

$$f^{(2)}(0^-; n^{(2)}, m^{(2)}) = 0. \tag{3.36}$$

But, as shown in figure 3, if $n^{(1)} > n^{(2)}$, one has

$$f^{(1)}(0^+; n^{(1)}, m^{(1)}) \neq 0, \tag{3.37}$$

---

[9] Note that, since $U^{(1)} = o(1/r)$ for $\theta \geq 0$ when $n^{(1)} > n^{(2)}$, the upper-half sheet does not contribute to the value of the $\mathcal{J}$-integral.

and additional higher-order terms in the lower-half sheet have to be introduced in order to guarantee displacement continuity along $\theta = 0$. This fact constitutes a first motivation in obtaining other terms in the near-tip approximation series. But the main reason to justify the computation of additional asymptotic terms is the fact that the Jacobian of the in-plane transformation defined by (3.3) vanishes identically on both sheets, leaving the transverse stretch λ[10] undetermined by the present lower-order analysis.

4.- Higher-order terms of the near-tip approximation of the deformation field.

We summarize next the local analysis leading to higher-order terms of the asymptotic series which approximates the near-tip fields for the interface crack. Motivated by (3.3), we assume the following separable form for the deformed coordinates y_α

$$y_\alpha^{(k)}(r,\theta) \sim a_\alpha^{(k)}\, r^{m^{(k)}} f^{(k)}(\theta; n^{(k)}, m^{(k)}) + r^{p^{(k)}} w_\alpha^{(k)}(\theta), \qquad (4.1)$$

where $m^{(k)}$ have been given by (3.17) and (3.24),[11] $f^{(k)}(\theta; n^{(k)}, m^{(k)})$ by (3.18) and (3.20) and the relation between the scalars $a_\alpha^{(1)}$ and $a_\alpha^{(2)}$ has been expressed by (3.25) and (3.26). In (4.1), we require that the exponents $p^{(k)}$ of the higher-order term be real and satisfy

$$p^{(k)} > m^{(k)}, \qquad (4.2)$$

---

[10] defined in (2.2).

[11] As was the case for the first asymptotic term, we will -without loss of generality- only consider the situation for which $n^{(1)} \geq n^{(2)}$.

while the angular functions $w_\alpha^{(k)}(\theta)$ are twice continuously differentiable on their respective domains. Furthermore, both a_α cannot vanish simultaneously in (4.1).[12] Therefore, and without loss of generality, we assume that $a_2^{(k)} \neq 0$. Substituting (4.1) into the asymptotic equilibrium equations (3.5), there results a system of coupled second-order linear differential equations

$$\begin{aligned} &(1+a_{12}^2)\, H_1^p(w_1)+2a_{12}^2\, H_2^p(w_1)+2a_{12}\, H_2^p(w_2)=0,\\ &(1+a_{12}^2)\, H_1^p(w_2)+2a_{12}\, H_2^p(w_1)+2\, H_2^p(w_2)=0, \end{aligned} \tag{4.3}$$[13]

where we have introduced the scalar $a_{12} = a_1/a_2$[14] and the differential operators

$$\begin{aligned} H_1^p(w) &= B_f D_w + (n-1)(2p(m-1)B_f w + \dot{B}_f \dot{w}),\\ H_2^p(w) &= D_f E_w + (n-1)(m(m+p-2)f\, E_w + \dot{f}\, \dot{E}_w), \end{aligned} \tag{4.4}$$

in which

$$\begin{aligned} B_f(\theta) &= \dot{f}^2(\theta)+m^2 f^2(\theta), & E_w(\theta) &= m\,p\,f(\theta)\; w(\theta)+\dot{f}(\theta)\; \dot{w}(\theta),\\ D_f(\theta) &= \ddot{f}(\theta)+m^2 f(\theta), & D_w(\theta) &= \ddot{w}(\theta)+p^2 w(\theta). \end{aligned} \tag{4.5}$$

As was the case in [1] and [4], the linearity of the operators $H_\alpha^p(w)$ turns (4.3) into

$$\begin{aligned} &(1+a_{12}^2)\, H_1^p(w_1 - a_{12}w_2)=0,\\ &(1+a_{12}^2)\, H_3^p(a_{12}w_1 + w_2)=0, \end{aligned} \tag{4.6}$$

where

$$H_3^p(w) = (H_1^p + 2H_2^p)(w). \tag{4.7}$$

The stress-free boundary conditions (3.2) are asymptotically equivalent to

$$\dot{w}_\alpha^{(1)}(\pi) = 0, \qquad \dot{w}_\alpha^{(2)}(-\pi) = 0. \tag{4.8}$$

---

[12] See (3.25) and (3.32).

[13] The system is identical to that encountered in the homogeneous case [4], but, due to the presence of different boundary conditions, it will yield a different solution.

[14] Note that, due to (3.35), $a_{12}^{(1)} = a_{12}^{(2)} = a_{12}$.

The continuity conditions across the interface provide the additional information necessary to determine the asymptotic exponents $p^{(k)}$. It has been shown in the analysis of the first asymptotic term that, if $n^{(1)} \neq n^{(2)}$, the continuity of displacements across the interface is satisfied to first order only.[15] The mismatch in "hardening" properties therefore suggests the appearance of higher-order terms necessary to ensure complete displacement continuity across $\theta = 0$. This first type of additional terms, referred to as "hardening mismatch terms," is not present in the simpler case investigated independently in [1] where $n^{(1)} = n^{(2)}$.

Other higher-order terms, which appear "independently," satisfy the displacement continuity along the interface. As shown later, only these "independent" terms contribute to the in-plane Jacobian which was left undetermined by the lower-order local analysis presented above in section 3. The computation of the two sets of higher-order terms is summarized in the next two subsections.

"Hardening mismatch" higher-order terms.

As mentioned in the introductory remark, the lower-order analysis of the deformations in the upper-half plane generates a non-vanishing displacement along the interface

$$y_\alpha^{(1)}(r, 0^+) \sim a_\alpha^{(1)}\, r^{m^{(1)}} f^{(1)}(0^+; n^{(1)}, m^{(1)}), \tag{4.9}$$

where $m^{(1)}$ has been given by (3.24) and $f^{(1)}(0^+; n^{(1)}, m^{(1)})$, computed through (3.20), vanishes if and only if $n^{(1)} = n^{(2)}$. Therefore, the terms described in the present subsection do not appear when the "hardening" characteristics of the two components of the bimaterial specimen are identical. We thus assume here that $n^{(1)} > n^{(2)}$, which by

[15] See the remark at the end of section 3.

(3.27) implies $m^{(1)} > m^{(2)}$. In order to compensate the non-vanishing displacement (4.9) along the interface by the first local term of the upper-half plane, the second lower-order asymptotic term of the lower-half sheet must be chosen such that

$$p^{(2)} = m^{(1)}, \tag{4.10}$$

and

$$w_\alpha^{(2)}(0^-) = a_\alpha^{(1)}\, f^{(1)}(0^+; n^{(1)}; m^{(1)}). \tag{4.11}$$

Note with the aid of (3.27) and (4.10), that the asymptotic exponent $p^{(k)}$ satisfies the requirement (4.2). Relations (4.9) and (4.10), combined with (4.6)-(4.8), allow to solve for the angular functions $w_\alpha^{(2)}(\theta)$ of the second-order mismatch term in the lower-half plane. Defining the auxiliary angular functions $\tilde{w}_\alpha^{(2)}(\theta)$ as

$$\begin{aligned} \tilde{w}_1^{(2)}(\theta) &= w_1^{(2)}(\theta) - a_{12}^{(2)} w_2^{(2)}(\theta), \\ \tilde{w}_2^{(2)}(\theta) &= a_{12}^{(2)} w_1^{(2)}(\theta) + w_2^{(2)}(\theta), \end{aligned} \tag{4.12}$$

which can be inverted as

$$\begin{aligned} w_1^{(2)}(\theta) &= \frac{\tilde{w}_1^{(2)}(\theta) + a_{12}^{(2)} \tilde{w}_2^{(2)}(\theta)}{1 + (a_{12}^{(2)})^2}, \\ w_2^{(2)}(\theta) &= \frac{\tilde{w}_2^{(2)}(\theta) - a_{12}^{(2)} \tilde{w}_1^{(2)}(\theta)}{1 + (a_{12}^{(2)})^2}, \end{aligned} \tag{4.13}$$

one can rewrite the system (4.6) as

$$\begin{aligned} H_1^{p^{(2)}}(\tilde{w}_1^{(2)}) &= 0, \\ H_3^{p^{(2)}}(\tilde{w}_2^{(2)}) &= 0, \end{aligned} \qquad \text{on } [-\pi, 0], \tag{4.14}$$

with the boundary conditions

$$\dot{\tilde{w}}_\alpha^{(2)}(-\pi) = 0, \tag{4.15}$$

$$\tilde{w}_1^{(2)}(0^-) = a_1^{(1)} f^{(1)}(0^+) - a_{12}^{(2)} a_2^{(1)} f^{(1)}(0^+) = 0,$$
$$\tilde{w}_2^{(2)}(0^-) = a_{12}^{(2)} a_1^{(1)} f^{(1)}(0^+) + a_2^{(1)} f^{(1)}(0^+) = a_2^{(1)}(1 + a_{12}^2) f^{(1)}(0^+). \quad (4.16)^{16}$$

The first equations of (4.14)-(4.16) yield

$$\tilde{w}_1^{(2)}(\theta) \equiv 0, \qquad \text{on } [-\pi, 0], \quad (4.17)$$

while $\tilde{w}_2^{(2)}(\theta)$ can be solved analytically with the aid of a transformation introduced by Knowles and Sternberg [6] and previously used in [1] and [4]

$$\tilde{W}_2^{(2)}(\zeta) = (\omega + k\cos\theta)^{-p^{(2)}} \tilde{w}_2^{(2)}(\theta),$$
$$\cos\zeta(\theta) = \frac{1-k}{\sqrt{2}} \frac{\sqrt{1 + k\sin^2\theta - \omega\cos\theta}}{\omega + k\cos\theta}, \quad (4.18)$$

where k and ω have been defined in (3.19) and $p^{(2)}$ is given by (3.24) and (4.10). Through (4.18), the differential equation (4.14b) is transformed into

$$\frac{d^2\tilde{W}_2^{(2)}(\zeta)}{d\zeta^2} + \frac{4n^{(2)}p^{(2)}(n^{(2)}p^{(2)} - n^{(2)} + 1)}{2n^{(2)} - 1} \tilde{W}_2^{(2)}(\zeta) = 0, \quad (4.19)$$

while the boundary conditions (4.15) and (4.16b) become

$$\frac{d}{d\zeta}\tilde{W}_2^{(2)}(0) = 0,$$
$$\tilde{W}_2^{(2)}(\pi/2) = (1+k)^{-p^{(2)}} a_2^{(1)}(1 + a_{12}^2) f^{(1)}(0^+). \quad (4.20)$$

Defining

$$j^2 = \frac{4n^{(2)}p^{(2)}(n^{(2)}p^{(2)} - n^{(2)} + 1)}{2n^{(2)} - 1}, \quad (4.21)$$

the solution to (4.19) and (4.20) results as

---

[16] Recall that $a_{12}^{(1)} = \frac{a_1^{(1)}}{a_2^{(1)}} = a_{12}^{(2)} = \frac{a_1^{(2)}}{a_2^{(2)}} = a_{12}$.

$$\tilde{W}_2^{(2)}(\zeta) = \frac{(1+k)^{-p^{(2)}} a_2^{(1)} (1+a_{12}^2) f^{(1)}(0^+)}{\cos j\frac{\pi}{2}} \cos j\zeta. \qquad (4.22)$$

The auxiliary angular function $\tilde{w}_2^{(2)}(\theta)$ is then obtained by combining (4.18), (4.21) and (4.22). Note that the solution (4.22) becomes invalid as the pair $(n^{(1)}, n^{(2)})$ tends to values such that the parameter j in (4.21) is equal to an odd integer, as represented in figure 4. A similar problem has been encountered in the rigid substrate situation analyzed in section 4 of [1]. It was shown there that the separable form (4.1) for the second term of the near-tip approximation series is not valid and that a different form of the asymptotic deformation field (containing a logarithmic singularity) has to be introduced. Similar treatment of the second-order term would be necessary here for these special values of $(n^{(1)}, n^{(2)})$. However, since, as shown later, the "hardening mismatch terms" do not contribute to the expression of the in-plane Jacobian, which is the prime motivation for investigating higher-order terms in the near-tip expansion, such treatment will not be attempted here.

The near-tip approximation series, including the "hardening mismatch" lower-order term, is thus far, for the lower-half plane, (when $n^{(1)} > n^{(2)}$)

$$y_\alpha^{(2)}(r,\theta) \sim a_\alpha^{(2)} r^{m^{(2)}} f^{(2)}(\theta; n^{(2)}, m^{(2)}) + r^{m^{(1)}} w_\alpha^{(2)}(\theta), \qquad \text{on } [-\pi, 0], \qquad (4.23)$$

where $a_\alpha^{(2)}$ are two undetermined constants,[17] $m^{(2)} = 1 - 1/n^{(2)}$, $m^{(1)}$ is given by (3.24), $f^{(2)}(\theta)$ is described in (3.18) and the angular functions $w_\alpha^{(2)}(\theta)$ are obtained by combining (4.13), (4.17), (4.18) and (4.22) as

$$w_\alpha^{(2)}(\theta) = a_\alpha^{(1)} \overline{w}^{(2)}(\theta), \qquad (4.24)$$

where

---

[17] Related to the value of the J-integral through (3.33).

$$\overline{w}^{(2)}(\theta) = \left(\frac{\omega + k\cos\theta}{1+k}\right)^{p^{(2)}} \frac{f^{(1)}(0^+)}{\cos j\frac{\pi}{2}} \cos\left(j\zeta(\theta)\right), \tag{4.25}$$

with j, k, ω and $\zeta(\theta)$ defined in (4.21), (3.19) and (4.18b). As was mentioned before, the mismatch term ensures displacement continuity across the interface, in combination with the first term of the approximation series for the upper sheet. However, it also creates a traction discontinuity along $\theta = 0$ which has to be compensated for by a higher-order "hardening mismatch" term in the upper-half plane

$$y_\alpha^{(1)}(r,\theta) \sim a_\alpha^{(1)} r^{m^{(1)}} f^{(1)}(\theta; n^{(1)}, m^{(1)}) + r^{p^{(1)}} w_\alpha^{(1)}(\theta), \qquad \text{on } [0,\pi]. \tag{4.26}$$

The details of the computation of this additional mismatch term are given in appendix A. We only mention here that the higher-order asymptotic exponent $p^{(1)}$ is such that

$$p^{(1)} = 2m^{(1)} - m^{(2)}. \tag{4.27}$$

Note once again that the higher-order mismatch terms appearing in (4.23) and (4.26) exist only if $n^{(1)} \neq n^{(2)}$ and are introduced in order to ensure displacement and traction continuity across the interface. Another objective of the introduction of higher-order terms in the near-tip asymptotic series was to obtain an estimation of the in-plane Jacobian, left undetermined by the lower-order local analysis. It is interesting to note that the additional term in (4.23)[18] does not contribute to the expression of the Jacobian since the latter is expressed in the lower-half plane, with the aid of (4.23) and (4.24), by

$$J(r,\theta) \sim (a_1^{(2)} a_2^{(1)} - a_2^{(2)} a_1^{(1)}) (m^{(2)} f^{(2)} \dot{\overline{w}}^{(2)} - p^{(2)} \dot{f}^{(2)} \overline{w}^{(2)}) r^{m^{(2)} + p^{(2)} - 2}. \tag{4.28}$$

---

[18] A similar result is obtained for the upper-half plane : as shown in appendix A, the additional "mismatch term" appearing in (4.26) leads to a vanishing value of the in-plane Jacobian.

The first multiplicative term in (4.28) is identically equal to zero since $a_{12}^{(1)} = a_{12}^{(2)}$. As shown in the next subsection, an estimation of the Jacobian can only be obtained by introducing another type of higher-order terms, referred to as "independent terms."

"Independent" higher-order terms.

In addition to the mismatch terms described in the previous subsection, the system (4.3) has another set of solutions of similar separable form

$$y_\alpha \sim a_\alpha \, r^m \, f(\theta; n, m) + r^p \, w_\alpha(\theta), \qquad (4.29)^{19}$$

with $p > m$. As suggested by the equivalent uncoupled system (4.6), there are two possible sets of solutions $(p, w_\alpha(\theta))$: the first one is such that

$$w_1 = a_{12} w_2, \qquad \text{with } H_3^p(w_2) = 0, \qquad (4.30)$$

while the second set of solutions is given by

$$w_2 = -a_{12} w_1, \qquad \text{with } H_1^p(w_1) = 0. \qquad (4.31)$$

It can be shown that the latter solution only contributes to the Jacobian of the in-plane transformation[20] and is therefore the focus of the present subsection. The two-term expansion of the near-tip deformation field is thus

$$y_\alpha(r, \theta) \sim a_\alpha \, r^m f(\theta; n, m) + c \, \varepsilon_{\alpha\beta} \, a_\beta \, r^p \, g(\theta; n, m), \qquad (4.32)$$

where c is an undetermined constant, $\varepsilon_{\alpha\beta}$ is the two-dimensional alternator and $(p^{(k)}, g^{(k)}(\theta))$ is the solution of

---

[19] Recall that the material index "*(k)*" *(k=1,2)* is omitted unless required for clarity purposes.

[20] The solution corresponding to (4.30) is presented in Appendix B.

$$H_1^{p^{(k)}}(g^{(k)}) = 0, \qquad \text{on } [-\pi,\pi], \tag{4.33}$$

$$\dot{g}^{(1)}(\pi) = \dot{g}^{(2)}(-\pi) = 0. \tag{4.34}$$

The additional relations necessary to determine the asymptotic exponents $p^{(k)}$ are provided by the continuity conditions (3.1). In order to satisfy the continuity of displacements across the interface, we impose

$$p^{(1)} = p^{(2)} = p, \tag{4.35}$$

together with

$$c^{(1)}a_\alpha^{(1)}g^{(1)}(0^+) = c^{(2)}a_\alpha^{(2)}g^{(2)}(0^-). \tag{4.36}$$[21]

With the aid of (2.3), (2.11) and (4.32), the tractions along the interface are expressed as

$$\begin{aligned}\sigma_{\alpha 2}(r,\theta=0^+) &= A_\alpha^{(1)} r^{s^{(1)}}(1 + C_\alpha^{(1)} r^{p-m^{(1)}} + o(r^{p-m^{(1)}})),\\ \sigma_{\alpha 2}(r,\theta=0^-) &= A_\alpha^{(2)} r^{s^{(2)}}(1 + C_\alpha^{(2)} r^{p-m^{(2)}} + o(r^{p-m^{(2)}})),\end{aligned} \qquad \text{(no sum on } \alpha\text{)}, \tag{4.37}$$[22]

where

$$\begin{aligned} A_\alpha &= \mu\left(\frac{b}{n}\right)(a_\gamma a_\gamma)^{n-1}\, B_f^{(n-1)}(0)\; a_\alpha\, \dot{f}\,(0),\\ s &= (m-1)\,(2n-1),\\ C_\alpha &= c\,\varepsilon_{\alpha\beta}\frac{a_\beta}{a_\alpha}\frac{\dot{g}(0)}{\dot{f}(0)}, \qquad \text{(no sum on } \alpha\text{)}, \end{aligned} \tag{4.38}$$

with $B_f(\theta)$ defined in (4.5). Since it was assumed that $m^{(1)} \geq m^{(2)}$ and since we require that $p > m^{(1)}$, we have

$$0 < p - m^{(1)} \leq p - m^{(2)}. \tag{4.39}$$

---

[21] Note that (4.36) constitutes only one relation since, by (3.35), $a_{12}^{(1)} = a_{12}^{(2)}$.

[22] Note that the first asymptotic term satisfies the continuity of tractions across $\theta = 0$ since $A_\alpha^{(1)} = A_\alpha^{(2)}$ and $s^{(1)} = s^{(2)}$.

Therefore, in order to minimize the jump in tractions across $\theta = 0$, $g^{(1)}(\theta)$ has to be chosen such that $C_\alpha^{(1)} = 0$, i.e.,

$$\dot{g}^{(1)}(0^+) = 0. \tag{4.40}$$

Thus $(p, g^{(1)}(\theta))$ is the solution of the eigenvalue problem (4.33) with the boundary conditions (4.34a) and (4.40) and under the restriction $p > m^{(1)}$. Once p is determined, $g^{(2)}(\theta)$ is computed for $-\pi \le \theta \le 0$ by solving (4.33) once more with (4.34b) as boundary condition.[23] The eigenvalue problem for $(p, g^{(1)}(\theta))$ and the differential equation in $g^{(2)}(\theta)$ have been solved numerically. The variation of the asymptotic exponent p with respect to $(n^{(1)}, n^{(2)})$ is illustrated in figure 5. Note that, when $n^{(1)} = n^{(2)}$, the solution coincides with the solution described in section 3 of [1].[24] The angular functions $g^{(1)}(\theta)$ and $g^{(2)}(\theta)$ are plotted in figure 6, for $n^{(2)} = 0.51, 0.6$ and 0.8. It is interesting to note that, as the "softer" (bottom) material tends to the "perfectly-plastic" or "non-hardening" case $(n^{(2)} \to 0.5)$, the higher-order exponent p approaches the lower-order exponent $m^{(1)}$ when $n^{(1)} > n^{(2)}$, as can be seen by comparing figures 2 and 5. A detailed asymptotic analysis, summarized in Appendix C, actually shows that, in the limit case for which $n^{(2)} \to 0.5$ with $n^{(1)} > n^{(2)}$, the angular function of the second asymptotic term for the top material $g^{(1)}(\theta)$ approaches that of the first asymptotic term $f^{(1)}(\theta; n^{(1)}, m^{(1)})$ introduced in (3.20).

In the next section, the near-tip deformation fields are discussed and compared to the results of a full-field finite element analysis.

---

[23] For normalization purpose, we set $g^{(1)}(0^+) = g^{(2)}(0^-) = 1$.

[24] See figure 2 of [1] for the variation of p with respect to the "hardening" exponent n.

5.- Discussion of the asymptotic results and numerical investigation.

We start by summarizing the asymptotic solution developed in the previous two sections. For $n^{(1)} \geq n^{(2)}$, we obtained

$$\begin{aligned} y_\alpha^{(1)}(r,\theta) \sim\ & a_\alpha^{(1)} r^{m^{(1)}} f^{(1)}(\theta; n^{(1)}, m^{(1)}) + a_\alpha^{(1)} r^{2m^{(1)}-m^{(2)}} \overline{w}^{(1)}(\theta) \\ & + c^{(1)} \varepsilon_{\alpha\beta}\, a_\beta^{(1)} r^p\, g^{(1)}(\theta; n^{(1)}, m^{(1)}) + k^{(1)} a_\alpha^{(1)} r^t\, l^{(1)}(\theta; n^{(1)}, m^{(1)}), \end{aligned} \tag{5.1}$$

$$\begin{aligned} y_\alpha^{(2)}(r,\theta) \sim\ & a_\alpha^{(2)} r^{m^{(2)}} f^{(2)}(\theta; n^{(2)}, m^{(2)}) + a_\alpha^{(1)}\, r^{m^{(1)}}\, \overline{w}^{(2)}(\theta) \\ & + c^{(2)} \varepsilon_{\alpha\beta}\, a_\beta^{(2)} r^p\, g^{(2)}(\theta; n^{(2)}, m^{(2)}) + k^{(2)} a_\alpha^{(2)} r^t\, l^{(2)}(\theta; n^{(2)}, m^{(2)}), \end{aligned} \tag{5.2}$$

where $\varepsilon_{\alpha\beta}$ is the two-dimensional alternator, $m^{(k)}$ are given by (3.17) and (3.24), $f^{(k)}(\theta)$ by (3.18) and (3.20), $\overline{w}^{(2)}(\theta)$ by (4.25), $\overline{w}^{(1)}(\theta)$ is described in Appendix A, p and $g^{(k)}(\theta)$ are shown in figures 5 and 6 respectively, t and $l^{(k)}(\theta)$ are given in Appendix B, and $a_\alpha^{(k)}$, $c^{(k)}$ and $k^{(k)}$ are undetermined constants related to the far-field loading conditions, the geometry of the global crack problem, the mechanical properties of the bimaterial specimen and to each other through (3.35), (4.36), (B.6) and (B.13). The deformation fields (5.1) and (5.2) may be rewritten as a rotation of a "reference field" defined by

$$\boldsymbol{y} = \boldsymbol{Q}\,\hat{\boldsymbol{y}}, \tag{5.3}$$

where the rotation matrix depends on the "mode-mixity" of the first asymptotic term

$$\left[Q_{\alpha\beta}\right] = \begin{pmatrix} \tilde{a}_2 & \tilde{a}_1 \\ -\tilde{a}_1 & \tilde{a}_2 \end{pmatrix}, \tag{5.4}$$

and

$$\begin{cases} \hat{y}_1^{(1)}(r,\theta) \sim c^{(1)}\, a^{(1)}\, r^p\, g^{(1)}(\theta), \\ \hat{y}_2^{(1)}(r,\theta) \sim a^{(1)}\, r^{m^{(1)}} f^{(1)}(\theta) + a^{(1)}\, r^{2m^{(1)}-m^{(2)}}\, \overline{w}^{(1)}(\theta) + k^{(1)}\, a^{(1)}\, r^t\, l^{(1)}(\theta), \end{cases} \tag{5.5}$$

$$\begin{cases} \hat{y}_1^{(2)}(r,\theta) \sim c^{(2)}\, a^{(2)}\, r^{p}\, g^{(2)}(\theta), \\ \hat{y}_2^{(2)}(r,\theta) \sim a^{(2)}\, r^{m^{(2)}}\, f^{(2)}(\theta) + a^{(1)}\, r^{m^{(1)}}\, \overline{w}^{(2)}(\theta) + k^{(2)}\, a^{(2)}\, r^{t}\, l^{(2)}(\theta), \end{cases} \tag{5.6}$$

with

$$\begin{aligned} a^{(k)} &= (a_\gamma^{(k)} a_\gamma^{(k)})^{1/2}, \\ \tilde{a}_\alpha &= \frac{a_\alpha^{(1)}}{a^{(1)}} = \frac{a_\alpha^{(2)}}{a^{(2)}}. \end{aligned} \tag{5.7}$$

The asymptotic solution of the general bimaterial problem is somewhat more complex than the approximation series found in [1] for the special case $n^{(1)} = n^{(2)}$ due to the presence of terms associated with the mismatch in "hardening" properties of the two sheets, which makes the discussion of the structure of the asymptotic field more difficult. However, most of the conclusions reached in [1] are still applicable in the general bimaterial situation.

The most important result of the present analysis is the confirmation of the existence of an oscillation-free, contact-free field near the tip of the interface crack, first demonstrated by Knowles and Sternberg [2] in the particular Neo-Hookean case and confirmed by Herrmann [3] in the compressible plane strain situation. The asymptotic solution also predicts a smooth opening of the crack

$$\begin{aligned} \hat{y}_2^{(1)}(r,\pi) &\sim \tilde{b}^{(1)} \left| \hat{y}_1^{(1)}(r,\pi) \right|^{m^{(1)}/p}, \\ \hat{y}_2^{(2)}(r,-\pi) &\sim -\tilde{b}^{(2)} \left| \hat{y}_1^{(2)}(r,-\pi) \right|^{m^{(2)}/p}, \end{aligned} \tag{5.8}$$

where $\tilde{b}^{(k)}$ are two positive constants. The relations (5.8) also allow to study the blunting effect of the "hardening" parameters $n^{(1)}$ and $n^{(2)}$ on the shape of the deformed crack. Since $m^{(1)}/p \geq m^{(2)}/p$, the blunting effect is stronger in the softer (bottom) material, the strongest effect being detected when the two hardening exponents are similar or close to each other.

The nonlinearly elastic asymptotic solution is also characterized by the appearance of more than one singular term, unlike in the linearized theory. The strongest singularity $(O(r^{m^{(2)}}))$, which occurs in the softer material, is independent of the "hardening" characteristics of the other sheet while all other asymptotic exponents are function of the "hardening" parameters of both components of the bimaterial sheet.

Substituting the asymptotic expansions (5.1) and (5.2) into (2.2), the leading-order expression of the Jacobian of the in-plane transformation (and, therefore, of the transverse stretch λ) is obtained as

$$J(r,\theta) \sim c\,(a_1^2 + a_2^2)\,(p\dot{f}g - mf\dot{g})\,r^{m+p-2}. \tag{5.9}$$

The angular distribution of the Jacobian is illustrated in figure 7 for various values of $(n^{(1)}, n^{(2)})$.

The asymptotic results presented in previous sections have been compared with the results of a full-field finite element investigation of the bimaterial problem. The finite element mesh is similar to that used in the homogeneous case (see section 5 of [4]). In the numerical example discussed below, the only material mismatch between the two GNH sheets concerns the "hardening" parameters $n^{(k)}$ (i.e., $\mu^{(1)} = \mu^{(2)}$ and $b^{(1)} = b^{(2)}$). The far-field loading conditions correspond to a purely symmetric (mode I) case. Figure 8 presents the shape of the deformed crack for two combinations of the "hardening" exponents $n^{(k)}$. Although the far-field loading is symmetric, a slight mismatch in "hardening" parameters introduces a mixity in the near-tip deformation field. This fact is further illustrated in figure 9 in which the nonlinear mixity parameter a_{12} is plotted versus $n^{(1)}$ (with $n^{(2)} = 0.6$).

The angular variation of the deformed coordinate y_2 is shown in figure 10, for the case $n^{(2)} = 0.6$ and $n^{(1)} = 0.6, 0.65, 0.8$ and 1.0. The agreement between the numerical and analytical solutions is very good for the bottom (softer) material where

the deformations are especially large, while it is not as satisfactory in the top (harder) material where the strains are more limited and where the asymptotic exponents of the higher-order terms have values that are similar to that of the first term (for example, when $n^{(1)} = 0.8$, one has $m^{(2)} = 0.375$, $m^{(1)} = 0.722$ and $p = 0.800$) and thereby introduce a more significant correction to the near-tip field. In figure 11, the radial variation of the Jacobian $J(r,\theta)$ is presented on a logarithmic scale for various bimaterial combinations and compared with the corresponding predicted value of the asymptotic exponent. Note that the size of the "zone of agreement" between the analytical and numerical solutions is much smaller in the bimaterial case ($n^{(2)} = 0.6$, $n^{(1)} = 0.8$ and 1.0) than in the homogeneous situation[25] ($n^{(1)} = n^{(2)} = 0.6$). Finally, the angular variation of $J(r,\theta)$ along a circle defined close to the crack tip is presented in figure 12, showing a satisfactory agreement, especially in the lower (softer) material where most of the deformations are concentrated. As the ratio $n^{(1)}/n^{(2)}$ increases, the strains distribute in a more uneven fashion across the interface explaining why, as was the case in figure 10, the agreement between the numerical and analytical results diminishes in the harder material.

The analysis of the special bimaterial case in [1] for which both components have the same "hardening" characteristics ($n^{(1)} = n^{(2)} = n$) has shown how, as n decreases, a mismatch in the linearly elastic properties ($\mu^{(1)}/\mu^{(2)}$) or in the "yielding" properties ($b^{(1)}/b^{(2)}$) is amplified, as indicated by the expression of the nonlinear mismatch parameter ξ in (3.31). This trend is also applicable in the general case where $n^{(1)} \neq n^{(2)}$, as quantified by (3.26) and illustrated in figure 13 which presents the angular variation of the deformed coordinate y_2 in the case $\mu^{(1)}/\mu^{(2)} = 2$, $b^{(1)}/b^{(2)} = 1$ and for two combinations of the "hardening" exponents $(n^{(1)}, n^{(2)}) = (0.6, 0.6)$ and $(1.0, 0.6)$. The concentration of strains in the lower material, which is already present in the first case (for which $a^{(2)}/a^{(1)} = 32$) is amplified in the second situation. But, as

[25] Represented by the circles and the continuous line in figure 11.

shown in (3.35), the "deformation gap" between the upper and the lower sheets also increases as the "intensity of loading," denoted by the value of the conservation integral J, increases. Thus, as the softer material approaches the "perfectly plastic" situation, the bimaterial problem tends toward the situation of a GNH sheet bonded to a rigid substrate. The latter special case has been investigated in section 4 of [1] and the transition process from the bimaterial problem to the rigid substrate case has been detailed in section 5 of the same paper.

6.- Conclusion.

An asymptotic analysis of the near-tip deformation fields for an interface crack between two sheets of Generalized Neo-Hookean materials of arbitrary properties has been presented. The investigation has been carried out according to the nonlinear elastostatic theory of plane stress for isotropic, hyperelastic materials. The asymptotic solution shows no sign of oscillation or contact close to the crack tip, confirming thereby the result obtained by Knowles and Sternberg [2] in the particular case of two sheets of Neo-Hookean materials and by the authors [1] in special bimaterial problems involving GNH sheets. The analysis presented in this paper has focused on the effect of a mismatch in the "hardening" characteristics across the interface on the structure of the near-tip fields. It has been shown that such a mismatch generates the emergence of additional terms in the near-tip approximations, which are introduced in order to satisfy the displacement and traction continuity conditions along the interface. The mismatch in "hardening" behavior also accentuates the disparity in strain distribution across the interface. The asymptotic results have been compared with those of a detailed full-field numerical investigation, showing that sufficiently refined numerical analyses can give reasonably close results.

Acknowledgments.

The present work has been supported by AFOSR (contract F04611-88-K-0024) under the supervision of Dr. C.T. Liu with additional support from ONR (grant N00014-91-J-1427) under the technical monitoring of Dr. P. Schmidt. The computational part has been performed on the Cray YMP of the San Diego Supercomputing Center, the access of which has been made possible through a NSF grant.

Appendix A.

In this appendix, the higher-order asymptotic term for the upper-plane, associated with the mismatch in "hardening" characteristics ($n^{(1)} > n^{(2)}$) and introduced in equation (4.26), is presented. As mentioned in section 4, this higher-order term has, for objective, to compensate for the traction discontinuity across the interface arising from the mismatch in "hardening" exponents. The approximation series in the lower half-plane, defined by (4.23)-(4.25), introduces, along $\theta = 0^-$, the tractions

$$\sigma_{\alpha 2}^{(2)}(r,\theta = 0^-) = C_\alpha^{(2)} r^{s^{(2)}} (1 + D_\alpha^{(2)} r^{p^{(2)} - m^{(2)}} + o(r^{p^{(2)} - m^{(2)}})), \quad \text{(no sum on } \alpha), \text{(A.1)}$$

where

$$C_\alpha^{(2)} = \mu^{(2)} \left(\frac{b^{(2)}}{n^{(2)}} \right)^{n^{(2)} - 1} a_\alpha^{(2)} \left(\dot{f}^{(2)}(0^-) \right)^{2n^{(2)} - 1} (a_\beta^{(2)} a_\beta^{(2)})^{n^{(2)} - 1}, \tag{A.2}$$

$$D_\alpha^{(2)} = \left(2 (n^{(2)} - 1) \frac{a_\beta^{(1)} a_\beta^{(2)}}{a_\gamma^{(2)} a_\gamma^{(2)}} + \frac{a_\alpha^{(1)}}{a_\alpha^{(2)}} \right) \frac{\dot{\overline{w}}_2^{(2)}(0^-)}{\dot{f}^{(2)}(0^-)}, \quad \text{(no sum on } \alpha), \tag{A.3}$$

$$s^{(2)} = (m^{(2)} - 1)(2n^{(2)} - 1), \tag{A.4}$$

with $f^{(2)}(\theta)$ and $\overline{w}_2^{(2)}(\theta)$ defined in (3.18) and (4.25), respectively. Note that, with the aid of (3.17), (3.24) and (4.10),

$$p^{(2)} - m^{(2)} = \frac{n^{(1)} - n^{(2)}}{n^{(2)}(2n^{(1)} - 1)} > 0. \tag{A.5}$$

On the other hand, the approximation (4.26) in the upper-half plane leads to the interface tractions

$$\sigma_{\alpha 2}^{(1)}(r,\theta = 0^+) = C_\alpha^{(1)} r^{s^{(1)}} (1 + D_\alpha^{(1)} r^{p^{(1)} - m^{(1)}} + o(r^{p^{(1)} - m^{(1)}})), \quad \text{(no sum on } \alpha), \tag{A.6}$$

where

$$C_\alpha^{(1)} = \mu^{(1)} \left(\frac{b^{(1)}}{n^{(1)}} \right)^{n^{(1)}-1} a_\alpha^{(1)} \dot{f}^{(1)}(0^+) \left(m^{(1)^2} f^{(1)^2}(0^+) + \dot{f}^{(1)^2}(0^+) \right)^{n^{(1)}-1} (a_\beta^{(1)} a_\beta^{(1)})^{n^{(1)}-1}, \quad \text{(A.7)}$$

$$D_\alpha^{(1)} = 2(n^{(1)}-1) \frac{\left(m^{(1)} p^{(1)} f^{(1)}(0^+)\, a_\beta^{(1)} w_\beta^{(1)}(0^+) + \dot{f}^{(1)}(0^+)\, a_\beta^{(1)} \dot{w}_\beta^{(1)}(0^+) \right)}{\left(a_\beta^{(1)} a_\beta^{(1)} \right) \left(m^{(1)^2} f^{(1)^2}(0^+) + \dot{f}^{(1)^2}(0^+) \right)} + \frac{\dot{w}_\alpha^{(1)}(0^+)}{a_\alpha^{(1)} \dot{f}^{(1)}(0^+)}, \quad \text{(A.8)}^{26}$$

$$s^{(1)} = (m^{(1)}-1)(2n^{(1)}-1), \quad \text{(A.9)}$$

with $f^{(1)}(\theta)$ defined by (3.20). The choice of $m^{(1)}$ in (3.24) and the relations (3.32) between the scalars $a_\alpha^{(1)}$ and $a_\alpha^{(2)}$ ensure the continuity of tractions to the leading order (i.e., $s^{(1)} = s^{(2)}$ and $C_\alpha^{(1)} = C_\alpha^{(2)}$). The unknown asymptotic exponent $p^{(1)}$ and the angular functions $w_\alpha^{(1)}(\theta)$ are therefore determined such as to minimize the traction jump across the interface to the second-order. With the aid of (A.1) and (A.6), one obtains

$$p^{(1)} = m^{(1)} + p^{(2)} - m^{(2)} = 2m^{(1)} - m^{(2)}. \quad \text{(A.10)}$$

Combining (4.6), (4.7), (A.3) and (A.8), and realizing that $D_1^{(2)} = D_2^{(2)}$, one rewrites the differential system in $w_\alpha^{(1)}(\theta)$ as

$$w_\alpha^{(1)}(\theta) = a_\alpha^{(1)}\, \overline{w}^{(1)}(\theta), \quad \text{(A.11)}$$

$$H_3^{p^{(1)}}(\overline{w}^{(1)}) = 0, \quad \text{(A.12)}$$

$$\overline{c}_1 \overline{w}^{(1)}(0^+) + \overline{c}_2 \dot{\overline{w}}^{(1)}(0^+) = \overline{b}, \quad \text{(A.13)}$$

$$\dot{\overline{w}}^{(1)}(\pi) = 0, \quad \text{(A.14)}$$

where

$$\overline{c}_1 = \frac{2(n^{(1)}-1)\, m^{(1)}\, p^{(1)}\, f^{(1)}(0^+)}{B_{f^{(1)}}(0^+)}, \quad \text{(A.15)}$$

---

[26] No sum on α.

$$\bar{c}_2 = \frac{2(n^{(1)} - 1)\,\dot{f}^{(1)}(0^+)}{B_{f^{(1)}}(0^+)} + \frac{1}{\dot{f}^{(1)}(0^+)}, \tag{A.16}$$

$$\bar{b} = \frac{a_2^{(1)}}{a_2^{(2)}}(2n^{(2)} - 1)\frac{\dot{\bar{w}}^{(2)}(0^-)}{\dot{f}^{(2)}(0^-)}, \tag{A.17}$$

in which $a_2^{(1)}/a_2^{(2)}$ can be expressed through (3.35), $\bar{w}^{(2)}(\theta)$ has been introduced in (4.25) and

$$B_{f^{(1)}}(\theta) = m^{(1)^2}\, f^{(1)^2}(\theta) + \dot{f}^{(1)^2}(\theta). \tag{A.18}$$

Note that this higher-order mismatch term vanishes when $n^{(1)} = n^{(2)}$ and that, due to (A.11), it does not contribute to the expression of the Jacobian of the in-plane transformation.

Appendix B.

The second appendix focuses on the computation of the higher-order asymptotic terms corresponding to the relations (4.29) and (4.30), i.e., of the form

$$y_\alpha(r,\theta) \sim a_\alpha r^m f(\theta;n,m) + a_\alpha r^t w(\theta), \tag{B.1}$$

where $t > m$ and $w(\theta)$ satisfies

$$H_3^t(w) = 0, \qquad \text{on } [-\pi,\pi], \tag{B.2}$$

with the linear second-order differential operator $H_3^s(w)$ defined in (4.7). The traction-free boundary conditions along the crack faces are equivalent to

$$\dot{w}^{(1)}(\pi) = \dot{w}^{(2)}(-\pi) = 0. \tag{B.3}$$

As was suggested in section 4, the continuity of displacements along $\theta = 0$ requires that the asymptotic exponents $t^{(k)}$ be equal on both sides of the interface, i.e.,

$$t^{(1)} = t^{(2)} = t > m^{(1)} \geq m^{(2)}. \tag{B.4}$$[27]

The displacement continuity condition also imposes that

$$a_\alpha^{(1)} w^{(1)}(0^+) = a_\alpha^{(2)} w^{(2)}(0^-), \tag{B.5}$$

which, in view of (3.35), can be rewritten as

$$w^{(2)}(0^-) = \xi^{\frac{1-2n^{(2)}}{2n^{(1)}-1}} \left(\frac{\mathcal{J}}{\mu^{(2)} (b^{(2)})^{n^{(2)}-1} \bar{\mathcal{J}}(n^{(2)}, m^{(2)})} \right)^{\frac{n^{(2)}-n^{(1)}}{n^{(2)}(2n^{(1)}-1)}} w^{(1)}(0^+), \tag{B.6}$$

where $\mathcal{J}$ is the conservation integral introduced in (3.16) while ξ and $\bar{\mathcal{J}}(n,m)$ have been defined in (3.26) and (3.34) respectively.

---

[27] Recall that it has been assumed that $n^{(1)} \geq n^{(2)}$.

The tractions along the interface are

$$\sigma_{\alpha 2}(r,0) \sim A_\alpha r^{(m-1)(2n-1)}(1+Mr^{t-m}), \tag{B.7}$$

where A_α are given by (4.37) and

$$M = \frac{\dot{w}(0)}{\dot{f}(0)} + \frac{2(n-1)(m\,t\,f(0)w(0)+\dot{f}(0)\dot{w}(0))}{m^2 f^2(0)+\dot{f}^2(0)}. \tag{B.8}$$

Since

$$0 < t-m^{(1)} \le t-m^{(2)}, \tag{B.9}$$

we choose $(t, w^{(1)}(\theta))$ such that $M^{(1)} = 0$. The traction continuity condition yields, in terms of $w^{(1)}(\theta)$,

$$c_1 \dot{w}^{(1)}(0^+) + t c_2 w^{(1)}(0^+) = 0, \tag{B.10}$$

where the constants c_1 and c_2 depend on the material properties as

$$\begin{aligned} c_1 &= m^{(1)^2} f^{(1)^2}(0^+) + (2n^{(1)}-1)\, \dot{f}^{(1)^2}(0^+), \\ c_2 &= 2m^{(1)}(n^{(1)}-1)\, f^{(1)}(0^+)\, \dot{f}^{(1)}(0^+). \end{aligned} \tag{B.11}$$

Note that, if $n^{(1)} = n^{(2)}$, $f^{(1)}(0^+) = 0$ and (B.10) reduces to

$$\dot{w}^{(1)}(0^+) = 0. \tag{B.12}$$

In that case, one also has $m^{(1)} = m^{(2)}$ and $w^{(1)}(\theta) \equiv w^{(2)}(\theta)$.[28] In the general situation $(n^{(1)} \ge n^{(2)})$, one has thus to solve the eigenvalue problem in $(t, w^{(1)}(\theta))$ on $[0,\pi]$ constituted of (B.2), (B.3a) and (B.10) under the restriction (B.4). The latter has been solved numerically and the variation of the eigenvalue t with respect to $(n^{(1)}, n^{(2)})$ is shown in figure B.1.

---

[28] See the analysis of the special case $n^{(1)} = n^{(2)}$ in section 3 of [1].

The angular function of the corresponding lower-order asymptotic term has the form

$$w(\theta) = k\, l(\theta; n, m), \tag{B.13}$$[29]

where $k^{(1)}$ and $k^{(2)}$ are undetermined constants related to each other through (B.6) and $l(\theta; n, m)$ is shown in figure B.2 for some values of the $(n^{(1)}, n^{(2)})$. Note that $l^{(2)}(\theta)$ can be obtained analytically using the transformation introduced by Knowles and Sternberg [6] and already used in section 4

$$l^{(2)}(\theta) = \left(\frac{\omega + (1 - 1/n)\cos\theta}{2 - 1/n}\right)^{t} \frac{\cos(j\zeta(\theta))}{\cos j\frac{\pi}{2}}, \tag{B.14}$$

where $\zeta(\theta)$ is given in (4.18) and j is described by

$$j^2 = \frac{4n^{(2)}\, t\, (n^{(2)} t - n^{(2)} + 1)}{2n^{(2)} - 1}. \tag{B.15}$$

Finally, note that, due to its form (B.1), the higher-order term presented in this appendix has no effect on the leading order of the Jacobian of the in-plane transformation.

---

[29] $l^{(1)}(\theta)$ and $l^{(2)}(\theta)$ are normalized such that $l^{(1)}(\pi) = l^{(2)}(-\pi) = 1$.

Appendix C.

We study here the behavior of the higher-order solution described in figures 6 and 7 in the limiting situation in which the "softer" material approaches the "perfectly plastic" situation. Our objective is to show that, when $n^{(2)} \to 0.5$ and $n^{(1)} > n^{(2)}$, the value of the second asymptotic exponent p tends to that of the first one $m^{(1)}$ (as indicated by the "well" appearing in figure 5 in the neighborhood of $n^{(2)} = 1/2$) and the angular function $g^{(1)}(\theta)$ approaches $f^{(1)}(\theta)$, which has been introduced in (3.18). We also show how this limit process takes place. Let

$$n^{(2)} = \frac{1}{2} + \varepsilon, \tag{C.1}$$

where $0 < \varepsilon << 1$. Assuming that $n^{(1)} > n^{(2)}$, one finds, with the aid of (3.24), that

$$m^{(1)} = 1 - \frac{2\varepsilon}{2n^{(1)} - 1} + O(\varepsilon^2). \tag{C.2}$$

By combining (3.20)-(3.22), (C.1) and (C.2), $\dot{f}^{(1)}(0^+)$ is approximated by

$$\dot{f}^{(1)}(0^+) = \frac{2\pi\varepsilon}{\sqrt{2n^{(1)} - 1}} + O(\varepsilon^2). \tag{C.3}$$

The latter relation shows that as $n^{(2)}$ tends to $1/2$ the boundary conditions for $f^{(1)}(\theta)$ approach those for $g^{(1)}(\theta)$. Since the differential equations for the two angular functions (3.10) and (4.33) are similar, the corresponding solutions will tend to each other. In order to analyze the limit process, we write

$$g(\theta) = f(\theta) + \varepsilon \tilde{g}(\theta), \qquad (0 \le \theta \le \pi), \tag{C.4}$$

and

$$p^{(1)} = m^{(1)} + \delta\varepsilon. \tag{C.5}$$

Substituting (C.4) and (C.5) into (4.33) yields, for the leading order,

$$H_1^{m^{(1)}}(\tilde{g}) = -2\,\delta\,(m^{(1)} + (n^{(1)} - 1)(m^{(1)} - 1))\,f^{(1)}, \tag{C.6}$$

where the differential operator $H_1^p(w)$ has been defined in (4.4).

The boundary conditions, expressed in terms of the auxiliary function $\tilde{g}(\theta)$, are, with the aid of (C.3) and (C.4),

$$\begin{aligned} &\dot{\tilde{g}}(0) = -\frac{1}{\varepsilon}\dot{f}(0) = -\frac{2\pi}{\sqrt{2n^{(1)} - 1}}, \\ &\dot{\tilde{g}}(\pi) = 0. \end{aligned} \tag{C.7}$$

The eigenvalue problem (C.6)-(C.7) in $(\delta, \tilde{g}(\theta))$ has been solved numerically. The variation of δ with respect to the "hardening" parameter of the upper material $n^{(1)}$ is presented in figure C.1 for various values of ε which appears in the differential equation (C.6) through $n^{(1)}$ and $m^{(1)}$ (relations (C.1) and (C.2)). As expected, the analysis is not valid as the upper material approaches the "perfectly plastic" limit too, since $\delta \to \infty$ as $n^{(1)} \to 1/2$. Let us recall at this point that the present analysis is valid only when[30] $n^{(1)} > n^{(2)}$. Note that $\tilde{g}(\theta)$ is not uniquely determined for a given pair $(n^{(1)}, \varepsilon)$. It can be written as

$$\tilde{g}(\theta) = \bar{g}(\theta) + A\,\hat{g}(\theta), \tag{C.8}$$

where A is an undetermined constant, $\bar{g}(\theta)$ satisfies (C.6), (C.7) and has a specified value at a given value of θ ($\theta = 0$, for example) while $\hat{g}(\theta)$ satisfies

$$H_1^{m^{(1)}}(\hat{g}) = 0, \qquad \text{on } [0, \pi], \tag{C.9}$$

together with

$$\dot{\hat{g}}(0) = \dot{\hat{g}}(\pi) = 0, \qquad \hat{g}(0) = 1. \tag{C.10}$$

---

[30] The analysis loses its validity as early as (C.2) when $n^{(1)} = n^{(2)}$.

Note also that, since it was shown that $p^{(1)} \to m^{(1)}$, $\hat{g}(\theta)$ tends to $g^{(1)}(\theta)$ described in section 4. Note finally that, since the eigenvalue δ appears in the forcing function in (C.6), the particular choice of $\bar{g}(0)$ or $\bar{g}(\pi)$ has an influence on the obtained value of δ. This influence is however of second-order, as confirmed by the analysis of the special case for which the upper sheet is made of Neo-Hookean material (i.e., $n^{(1)} = 1$). In this particular case, (C.6) and (C.7) reduce to

$$\ddot{\bar{g}} + m^{(1)^2}\bar{g} = -2\delta \cos(m^{(1)}(\pi - \theta)), \tag{C.11}$$

with

$$\dot{\bar{g}}(0) = -2\pi, \qquad \dot{\bar{g}}(\pi) = 0. \tag{C.12}$$

Specifying the value at $\theta = 0$ as

$$\bar{g}(0) = \bar{g}_0, \tag{C.13}$$

one finds

$$\delta = 2 + (2\pi - 2 + \bar{g}_0)\varepsilon, \tag{C.14}$$

which shows that the effect of $\bar{g}_0$ on the eigenvalue δ vanishes as $\varepsilon \to 0$.

Some examples of angular functions $\bar{g}(\theta)$ for typical values of $n^{(1)}$ are presented in figure C.2, for $\varepsilon = 0.001$ and $\bar{g}_0 = 0$.

References

1. Geubelle, P.H. and Knauss, W.G., *Finite strains at the tip of a crack in a sheet of hyperelastic material : II. Special bimaterial cases.* Galcit SM Report 92-43, Caltech, 1992. Submitted to J. Elasticity.

2. Knowles, J.K. and Sternberg, E., *Large deformations near the tip of an interface crack between two Neo-Hookean sheets.* J. Elasticity, 1983. **13**: pp. 257-293.

3. Herrmann, J.M., *An asymptotic analysis of finite deformation near the tip of an interface crack.* J. Elasticity, 1989. **21**: pp. 227-269.

4. Geubelle, P.H. and Knauss, W.G., *Finite strains at the tip of a crack in a sheet of hyperelastic material : I. Homogeneous case.* Galcit SM Report 92-42, Caltech, 1992. Submitted to J. Elasticity.

5. Knowles, J.K. and Sternberg, E., *An asymptotic finite-deformation analysis of the elastostatic field near the tip of a crack.* J. Elasticity, 1973. **3**: pp. 67-107.

6. Knowles, J.K. and Sternberg, E., *Finite-deformation analysis of the elastostatic field near the tip of a crack : reconsideration and higher-order results.* J. Elasticity, 1974. **4**: pp. 201-233.

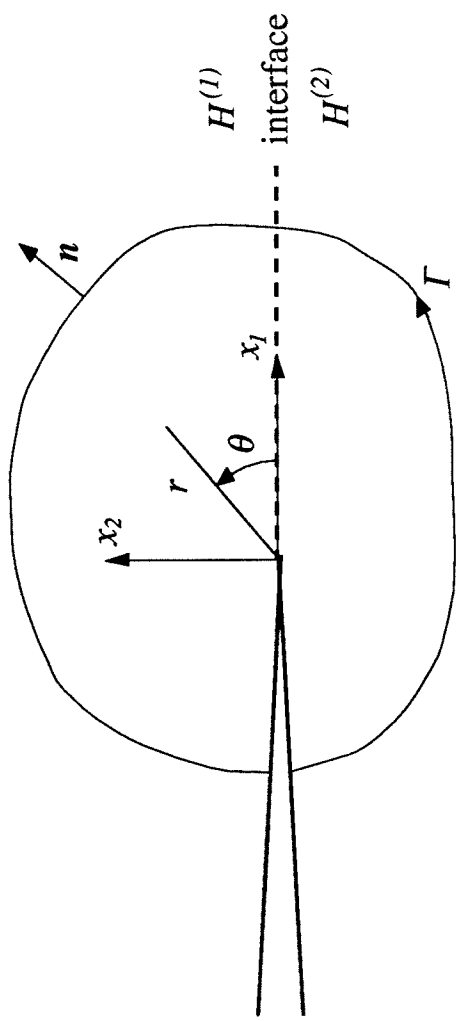

Figure 1. Geometry of the bimaterial interface problem.

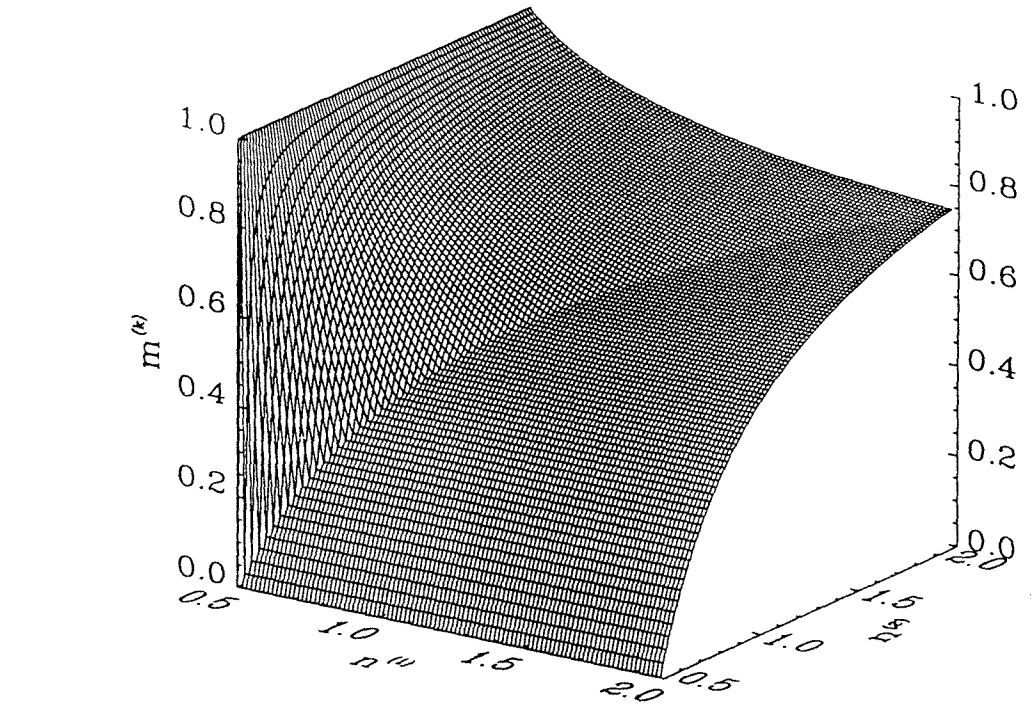

(a)

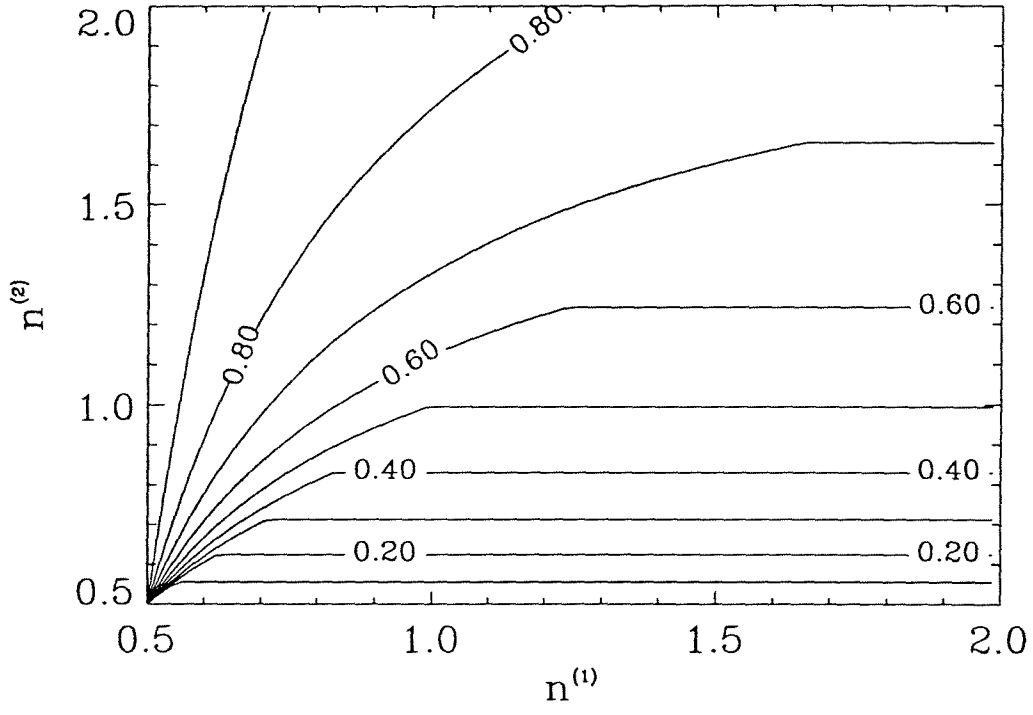

(b)

Figure 2. First asymptotic exponents $m^{(k)}$ versus $(n^{(1)}, n^{(2)})$ for $0.5 < n^{(2)} \leq n^{(1)} \leq 2$: $m^{(1)}$ (3.24) is represented in the triangle $(n^{(1)} < n^{(2)})$ while $m^{(2)}$, which is independent of $n^{(1)}$ (3.17), is represented in the triangle $(n^{(1)} > n^{(2)})$: (a) three-dimensional view and b) contour plot.

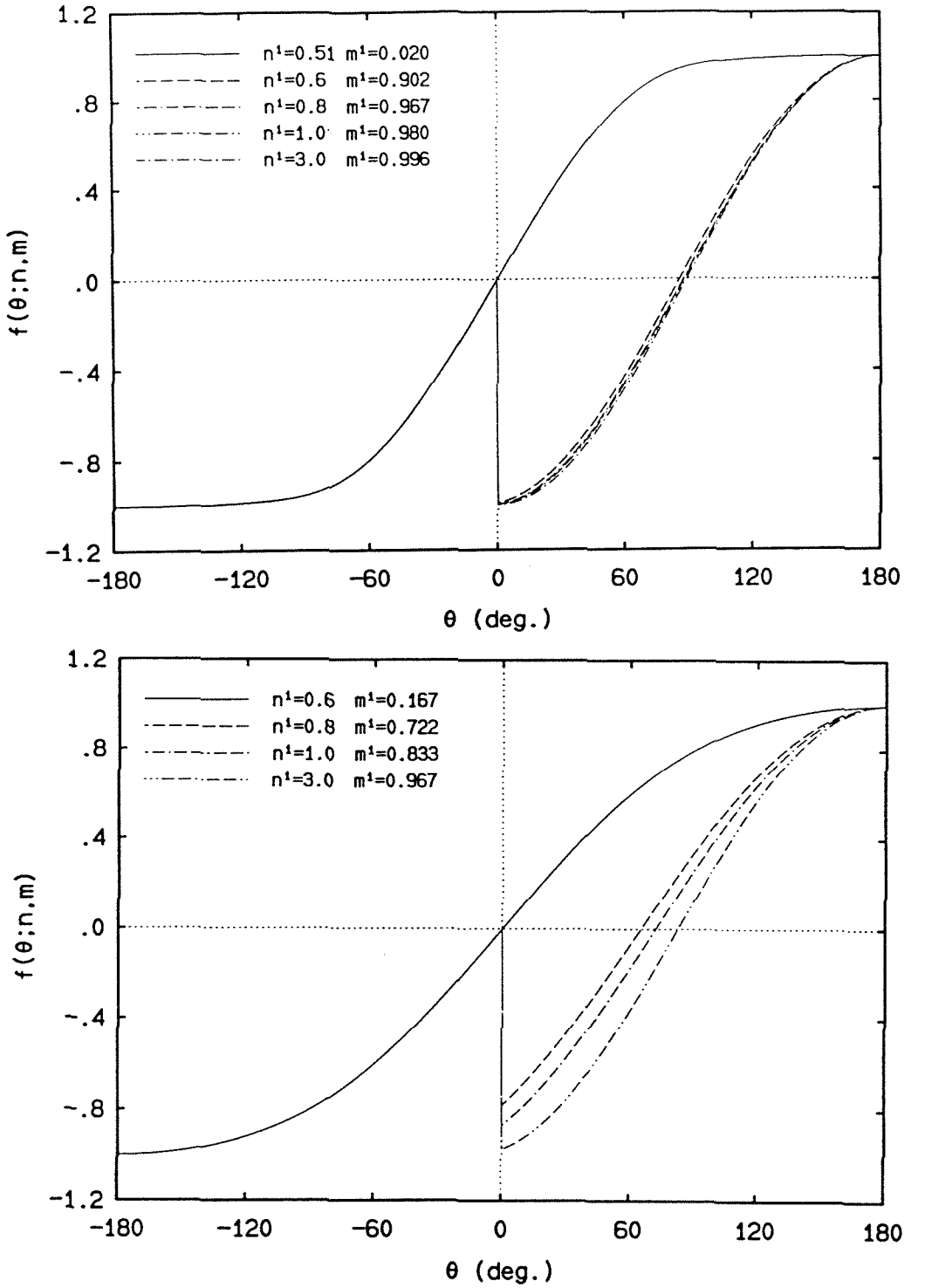

Figure 3. Angular variation of the first asymptotic term $f^{(k)}(\theta; n, m)$ with corresponding values of the exponents $m^{(k)}$: (a) $n^{(2)} = 0.51$ $(m^{(2)} = 0.0196)$, (b) $n^{(2)} = 0.6$ $(m^{(2)} = 0.167)$, (c) $n^{(2)} = 0.8$ $(m^{(2)} = 0.375)$. Note that, since $f^{(2)}(\theta)$ depends on $n^{(2)}$ only, all curves are superposed for $-\pi \leq \theta \leq 0$.

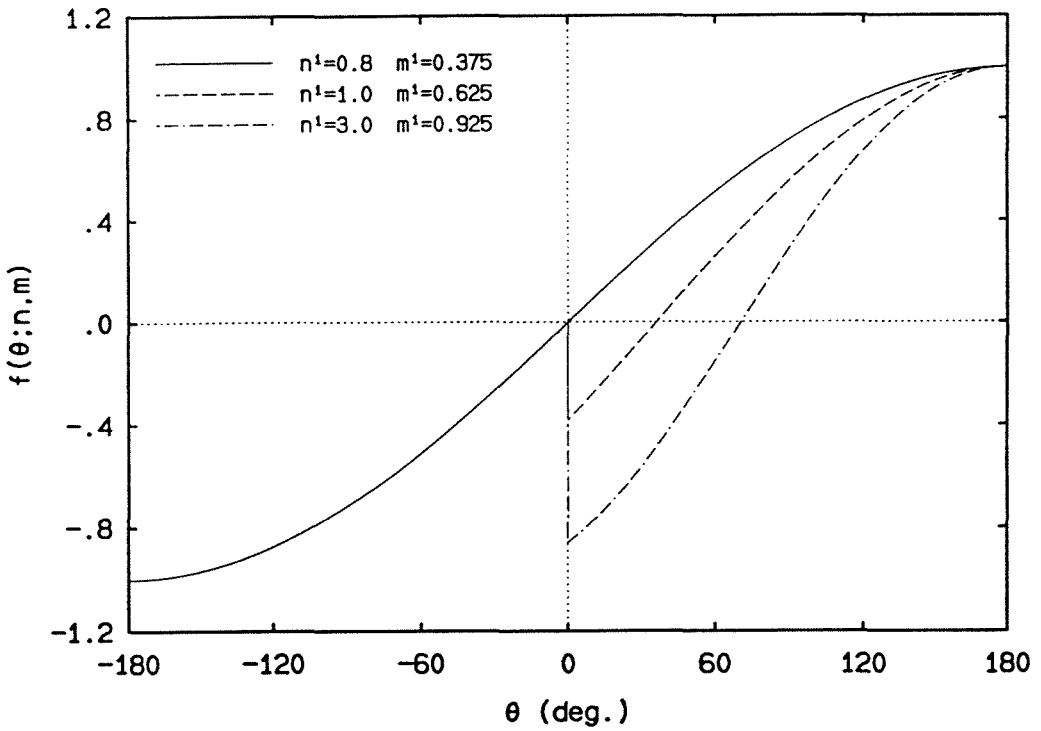

(c)

Figure 3 (Cont.).

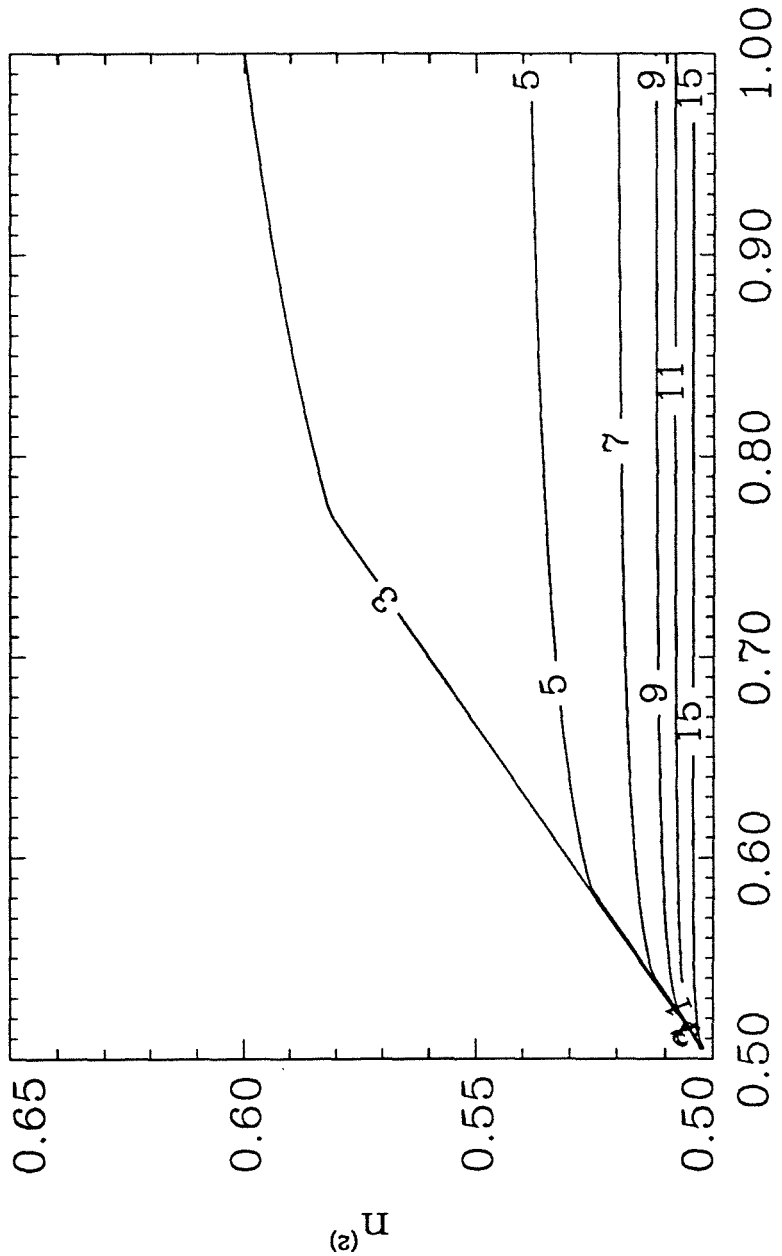

Figure 4. Contour plot of j (4.21) in the $(n^{(1)}, n^{(2)})$-plane for the case $n^{(2)} < n^{(1)}$. The contours represent the values of $(n^{(1)}, n^{(2)})$ for which the two-term asymptotic representation (4.23)-(4.25) is not valid.

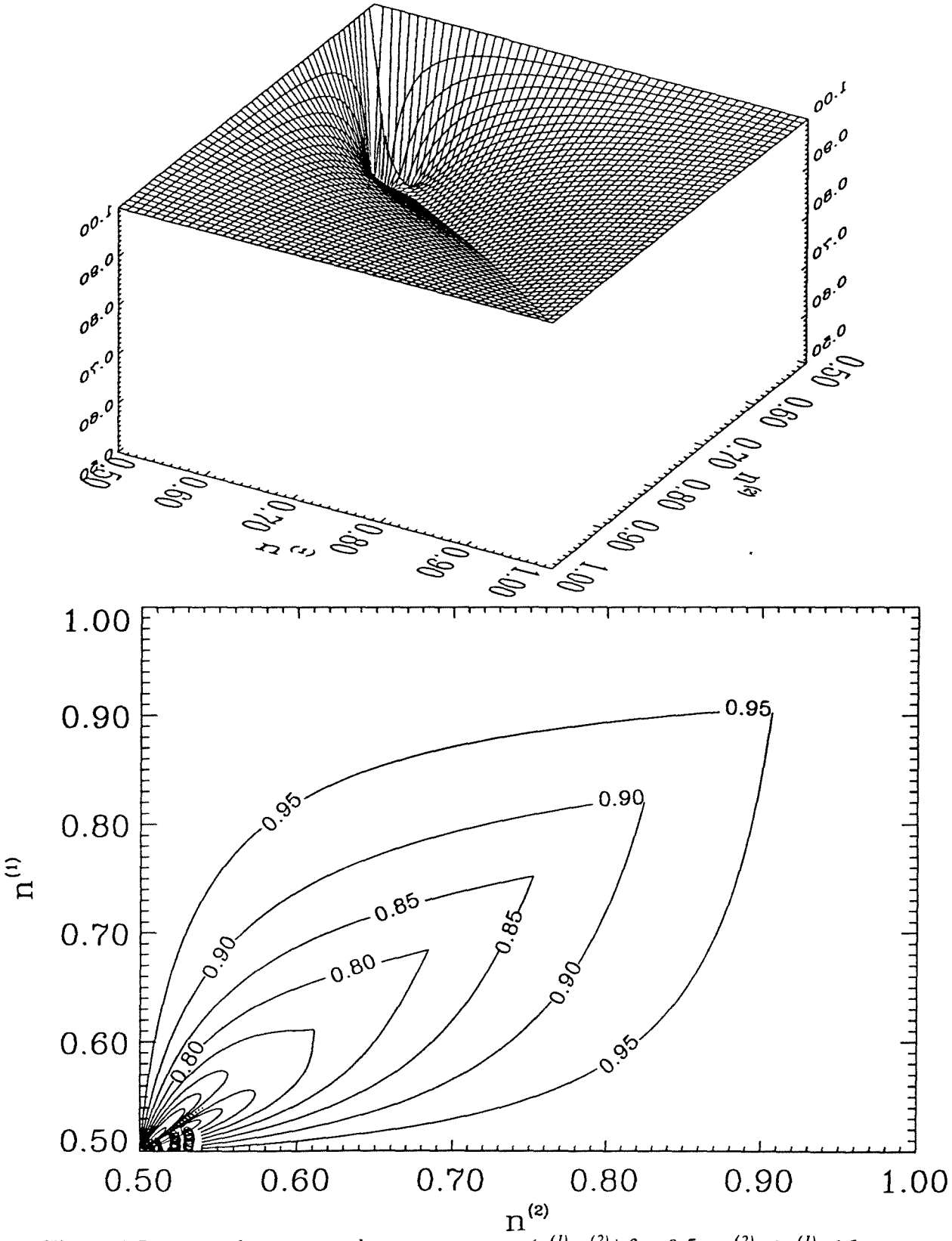

Figure 5. Lower-order asymptotic exponent p vs. $(n^{(1)},n^{(2)})$ for $0.5 < n^{(2)} \leq n^{(1)} \leq 1$: a) three-dimensional view and b) contour plot. For visualization purpose, the values of p have been repeated symmetrically with respect to the axis $n^{(1)} = n^{(2)}$.

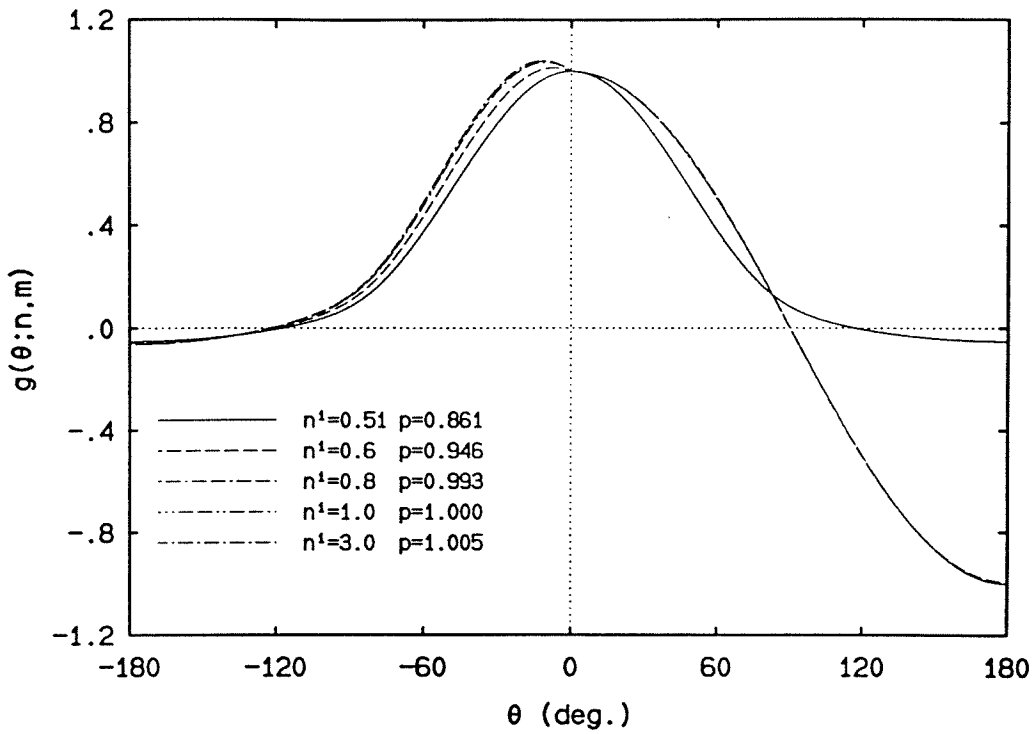

(a)

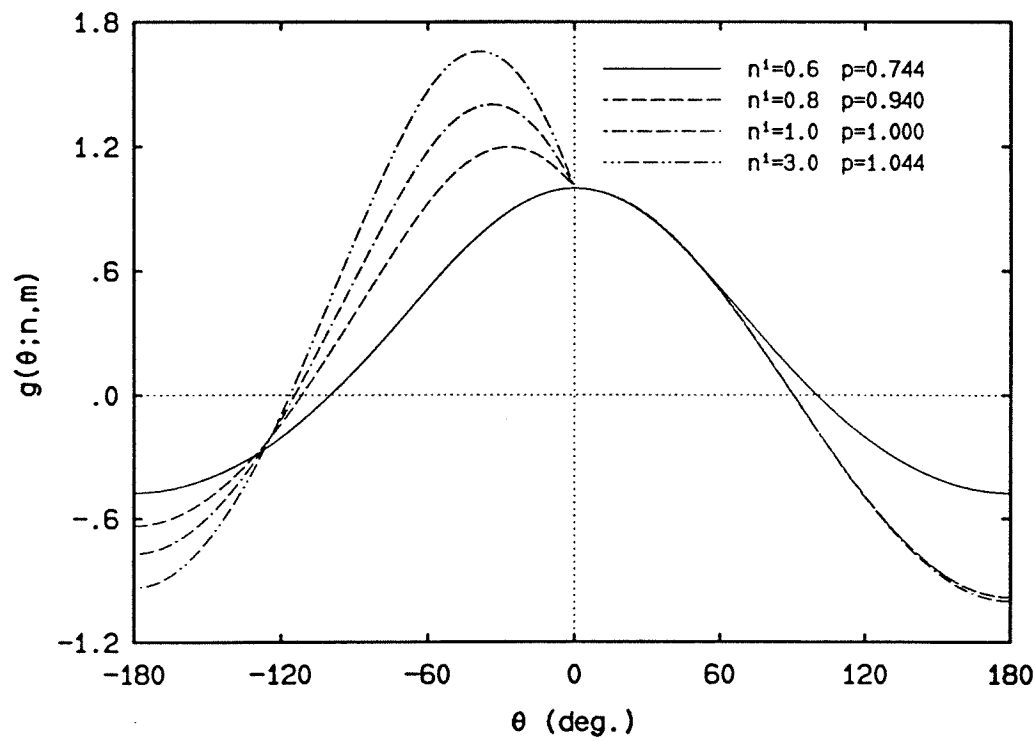

(b)

Figure 6. Angular variation of the lower-order asymptotic term $g^{(k)}(\theta; n, m)$ with corresponding values of the exponent p : (a) $n^{(2)} = 0.51$, (b) $n^{(2)} = 0.6$, (c) $n^{(2)} = 0.8$.

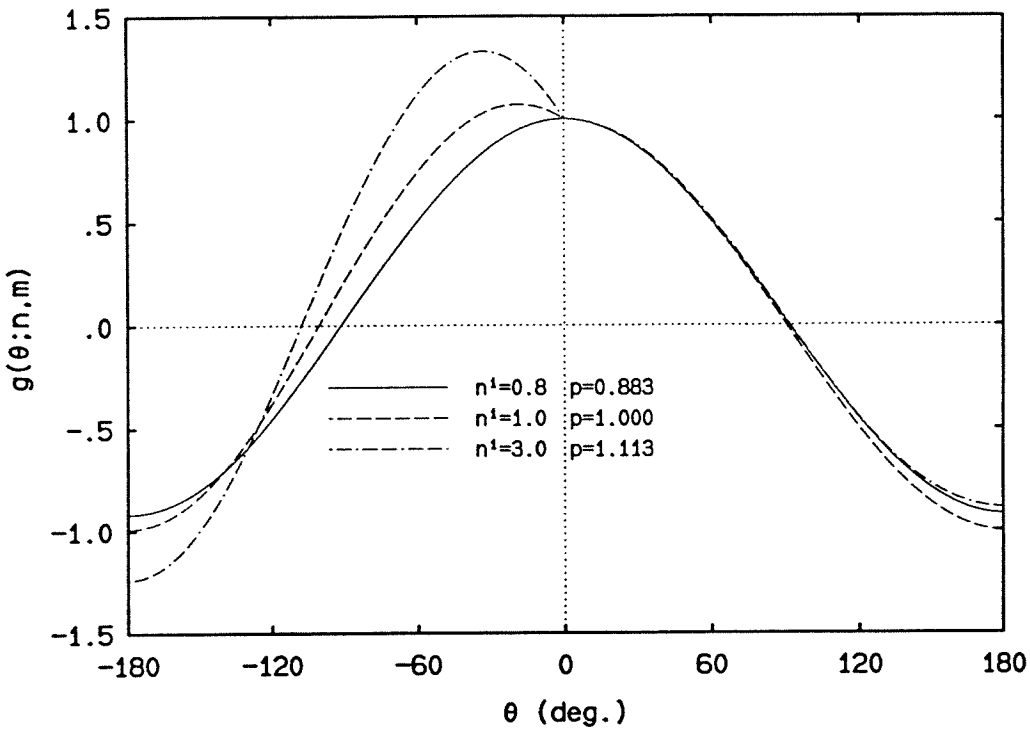

(c)

Figure 6 (Cont.).

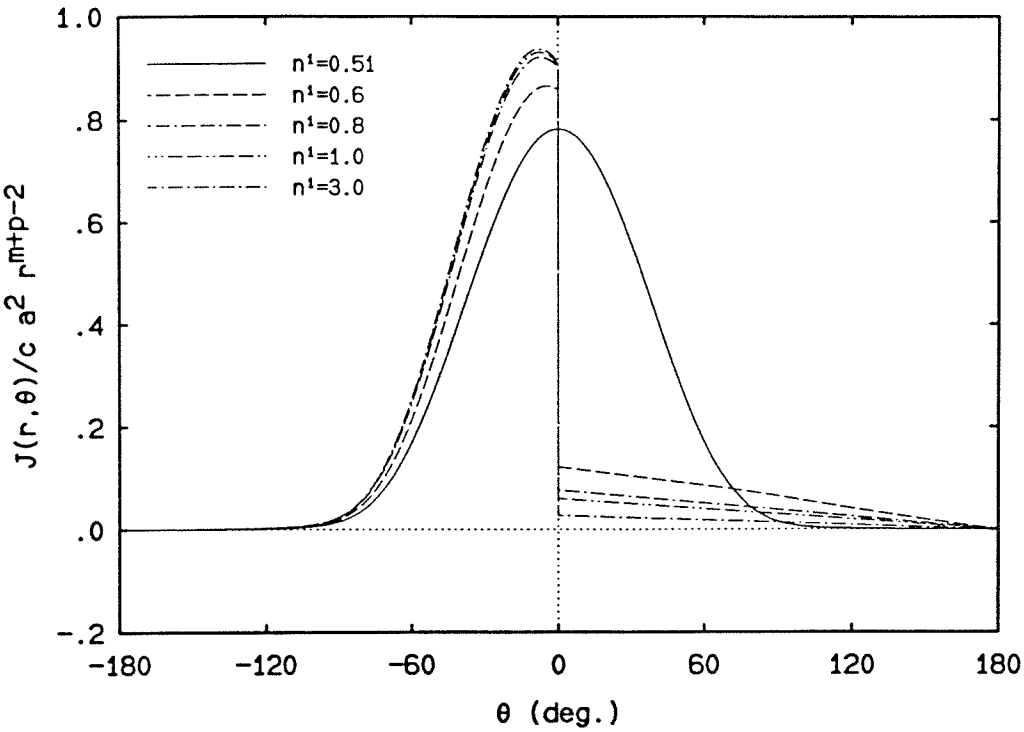

(a)

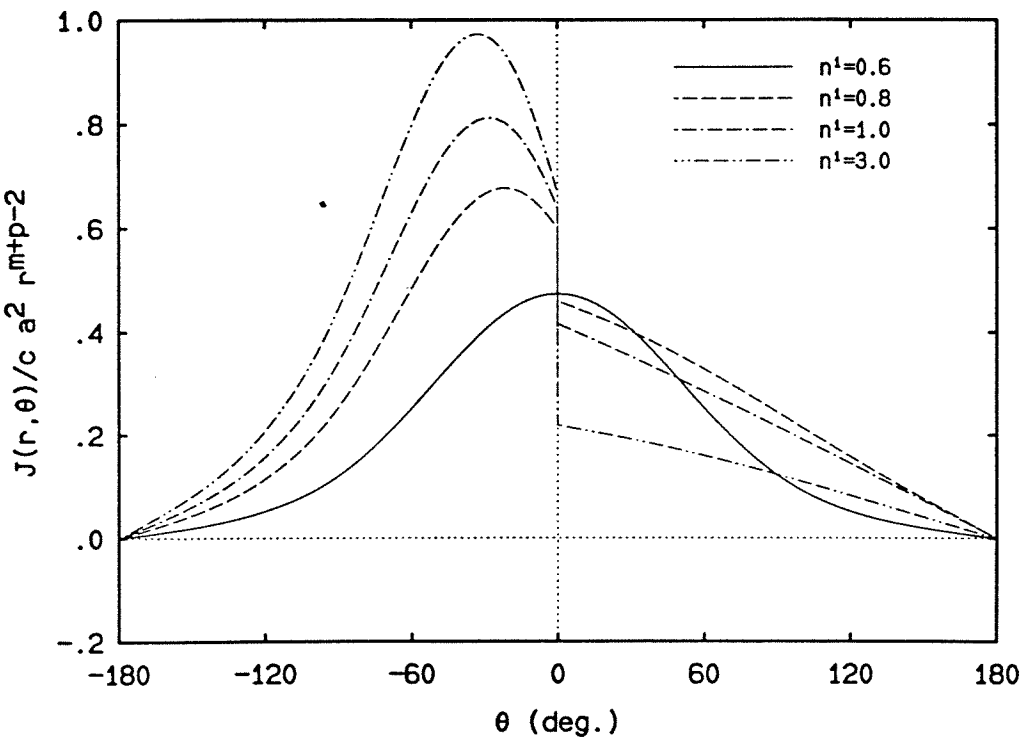

(b)

Figure 7. Angular variation of the in-plane Jacobian $J(r,\theta)$ for the same $(n^{(1)},n^{(2)})$ combinations as in figures 2 and 6 : (a) $n^{(2)} = 0.51$, (b) $n^{(2)} = 0.6$, (c) $n^{(2)} = 0.8$.

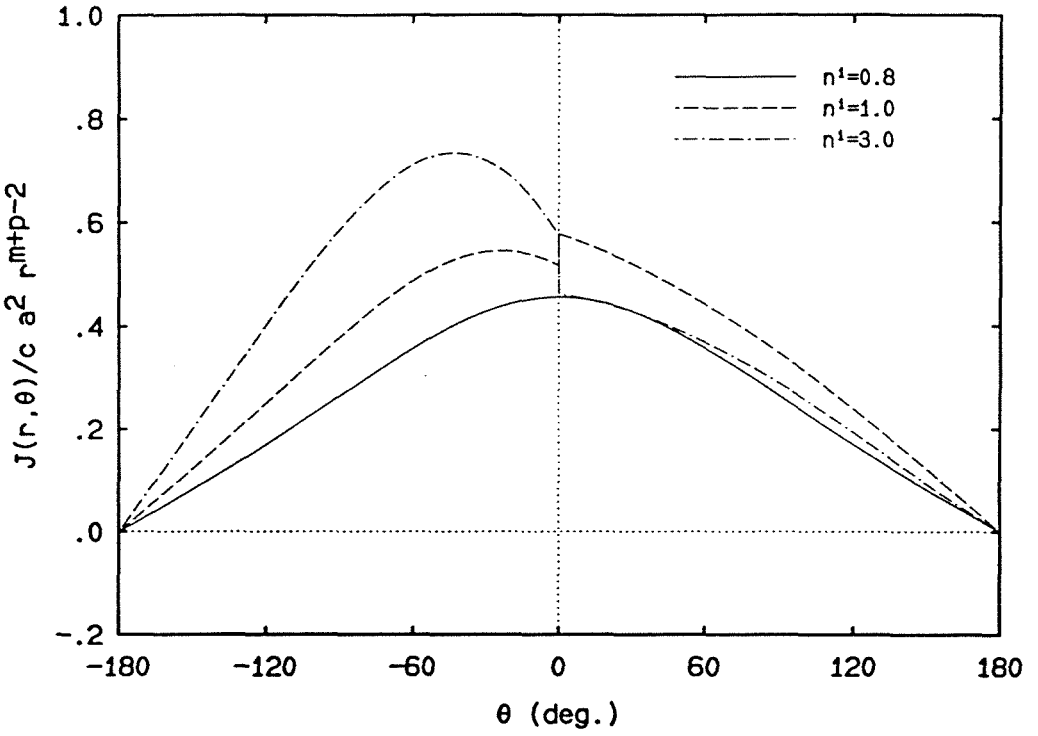

(c)

Figure 7 (Cont.).

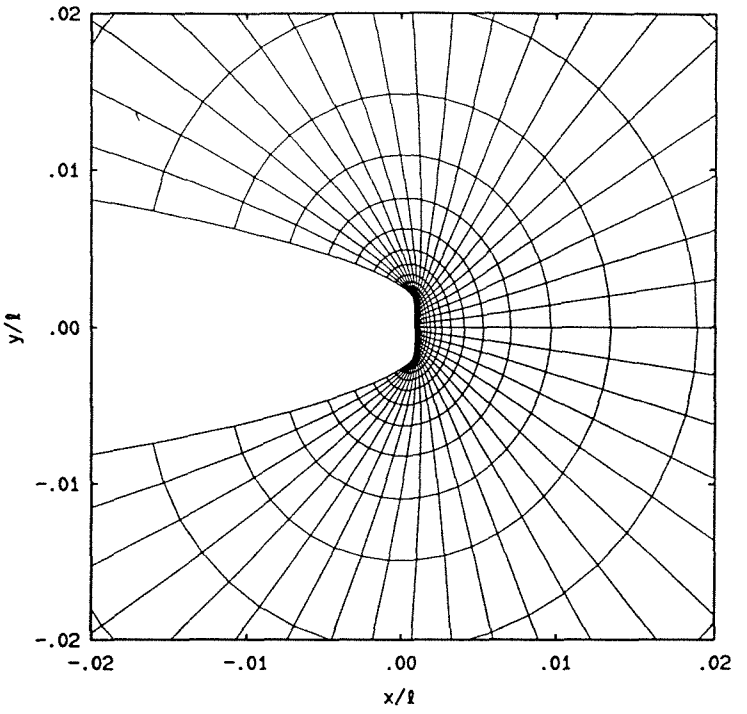

(a)

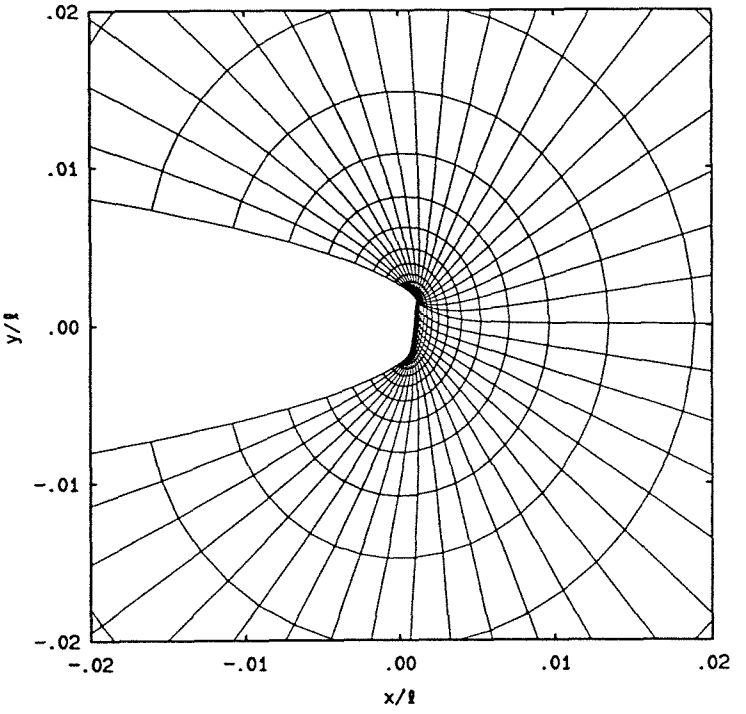

(b)

Figure 8. Effect of the mismatch in "hardening" parameter of the near-tip strain field : deformed mesh under symmetric (mode I) far-field loading for (a) $n^{(1)} = n^{(2)} = 0.6$ and (b) $n^{(2)} = 0.6$ and $n^{(1)} = 1.0$. The length scale l corresponds to the radius of the circular domain along the boundary of which the symmetric (mode I) boundary conditions are applied.

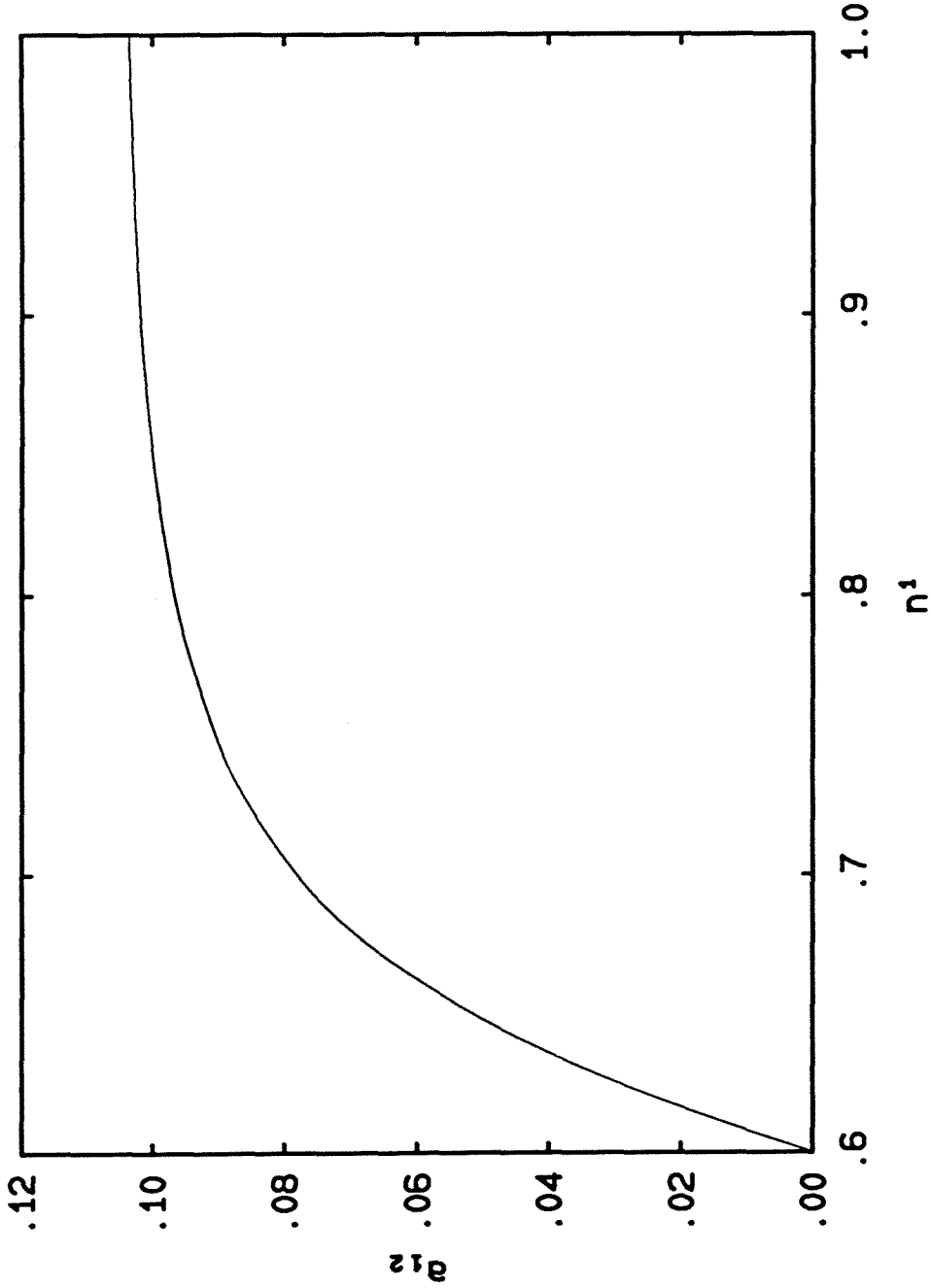

Figure 9. Mode-mixity associated with the mismatch in "hardening" characteristics : nonlinear mode-mixity parameter a_{12} versus $n^{(1)}$ (with $n^{(2)} = 0.6$) corresponding to a symmetric far-field loading.

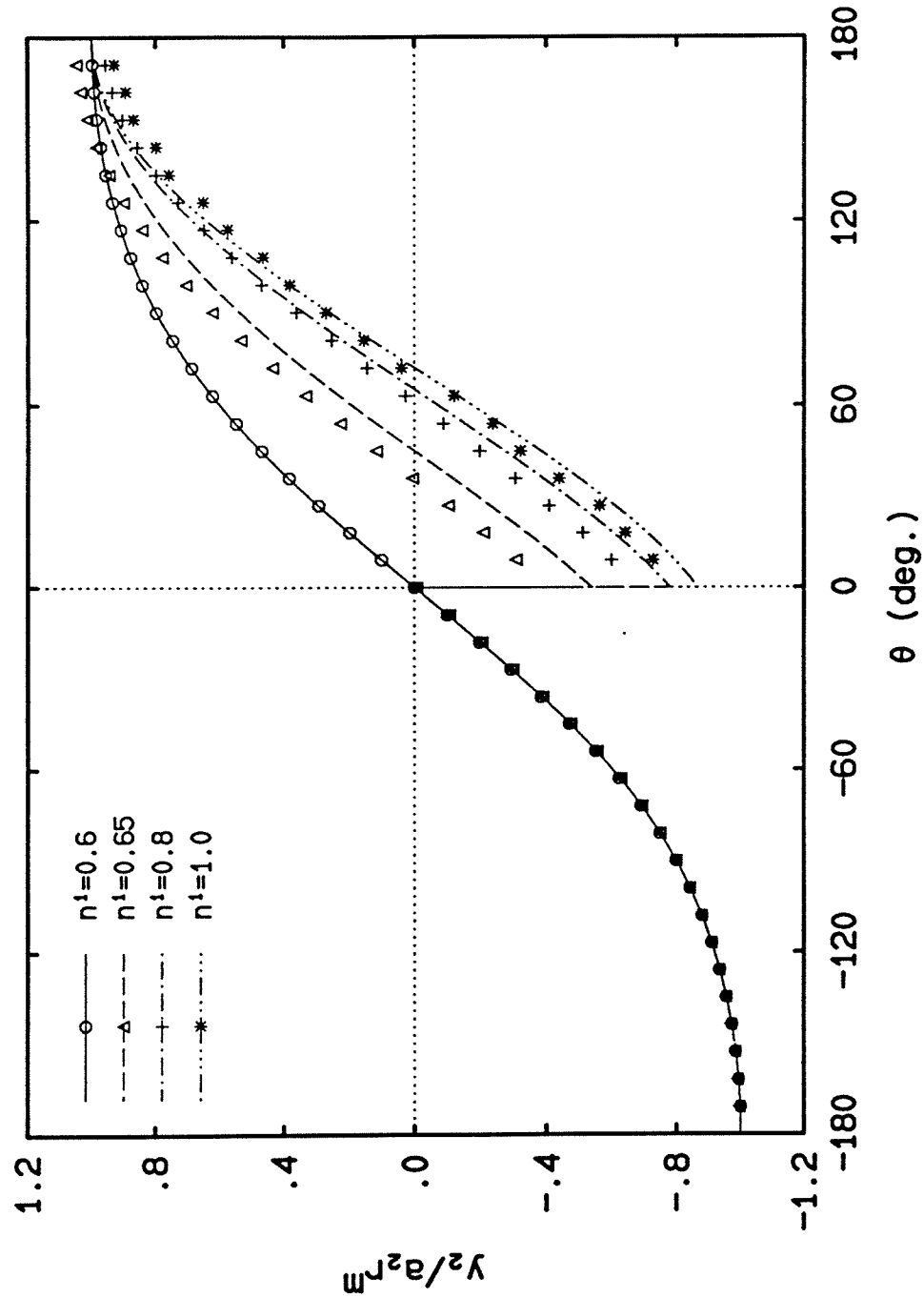

Figure 10. Angular variation of the deformed coordinate y_2 for $n^{(2)} = 0.6$, $n^{(1)} = 0.6$, *0.65*, *0.8* and *1.0* (with $\mu^{(1)} = \mu^{(2)}$, $b^{(1)} = b^{(2)}$) : numerical (symbols) and analytical (curves) results.

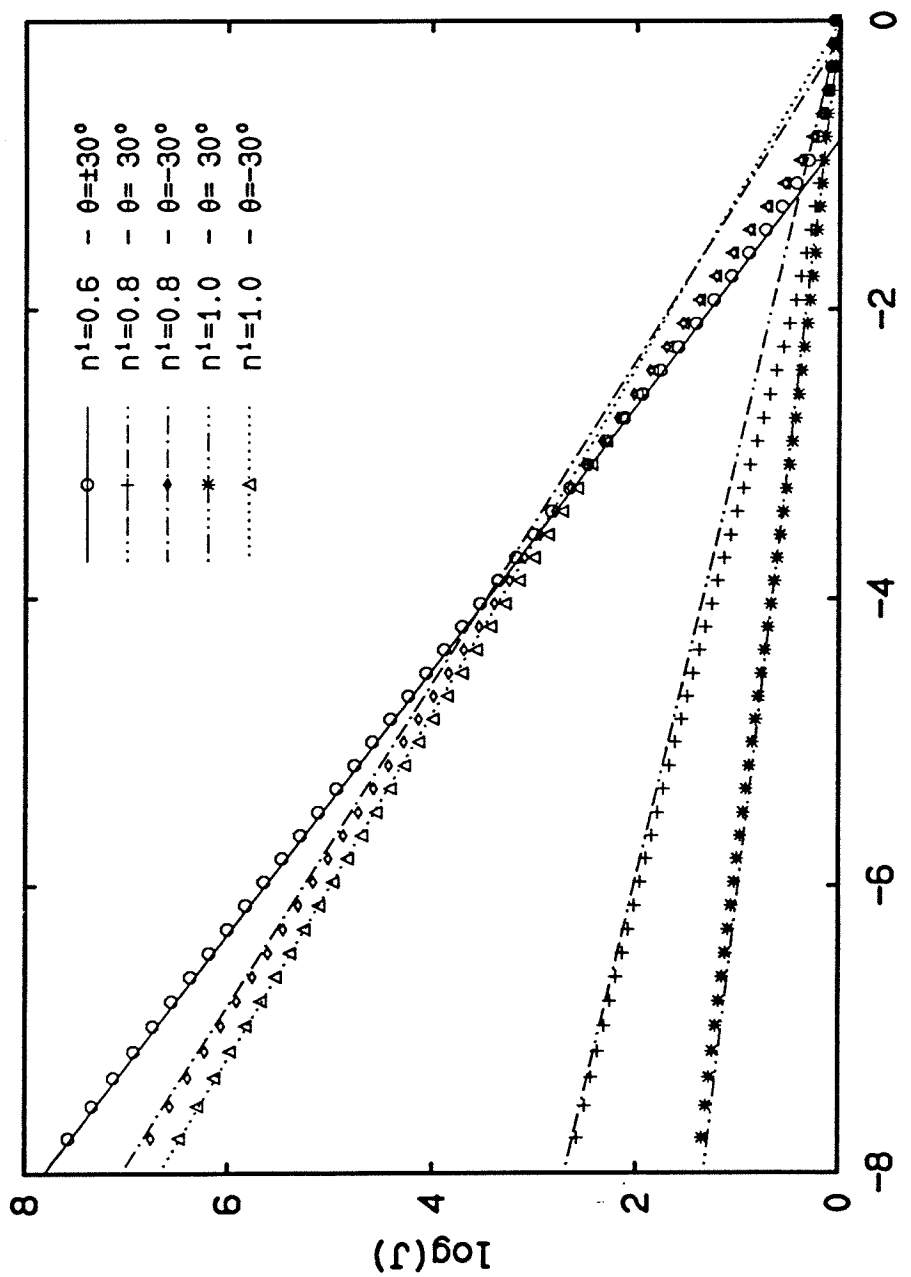

Figure 11. Comparison between asymptotics and numerics : radial variation of the Jacobian along $\theta = \pm 30^\circ$ for the same values of the material parameters as in figure 10. The asymptotic predictions are denoted by lines while the symbols correspond to the numerical values.

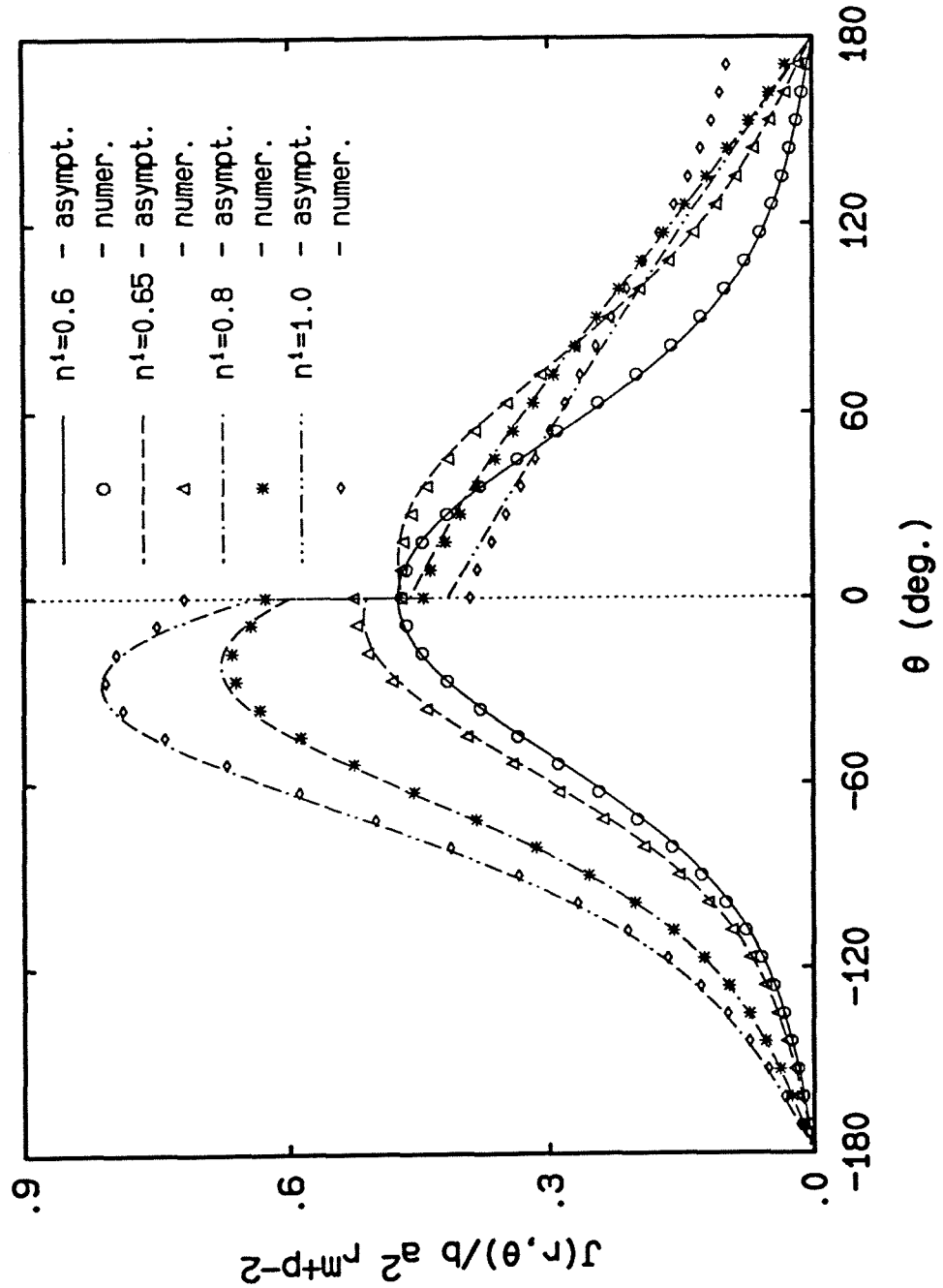

Figure 12. Angular variation of the in-plane Jacobian for $n^{(2)} = 0.6$ and four different values of $n^{(1)}$ (with $\mu^{(1)} = \mu^{(2)}$, $b^{(1)} = b^{(2)}$) : comparison between full-field and approximate solutions.

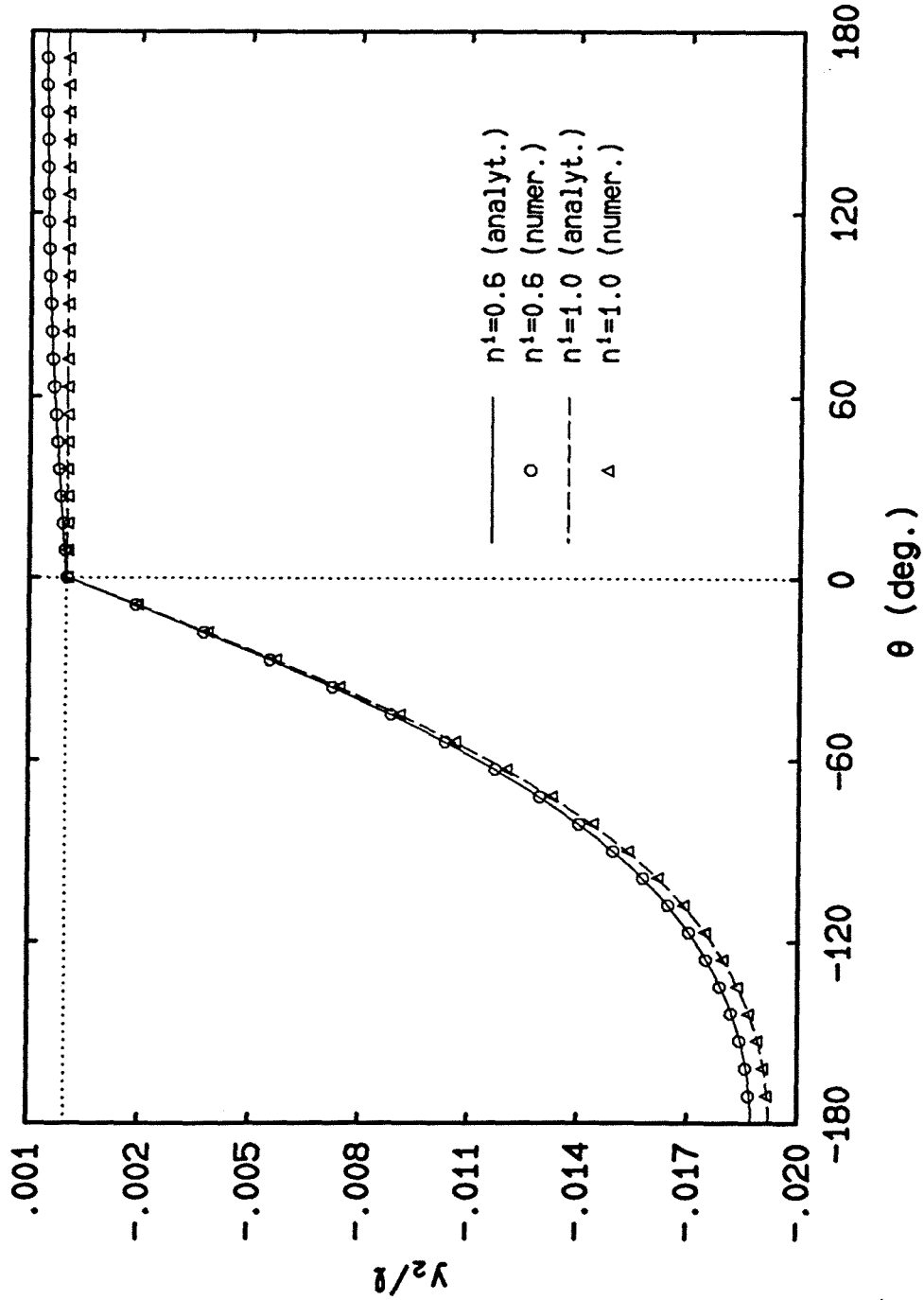

Figure 13. Angular variation of the deformed coordinate y_2 at $r/l = 10^{-6}$ in the bimaterial case $\mu^{(1)}/\mu^{(2)} = 2$, $b^{(1)}/b^{(2)} = 1$ and $(n^{(1)}, n^{(2)}) = (0.6, 0.6)$ and $(1.0, 0.6)$, showing the concentration of the deformations in the lower-half material.

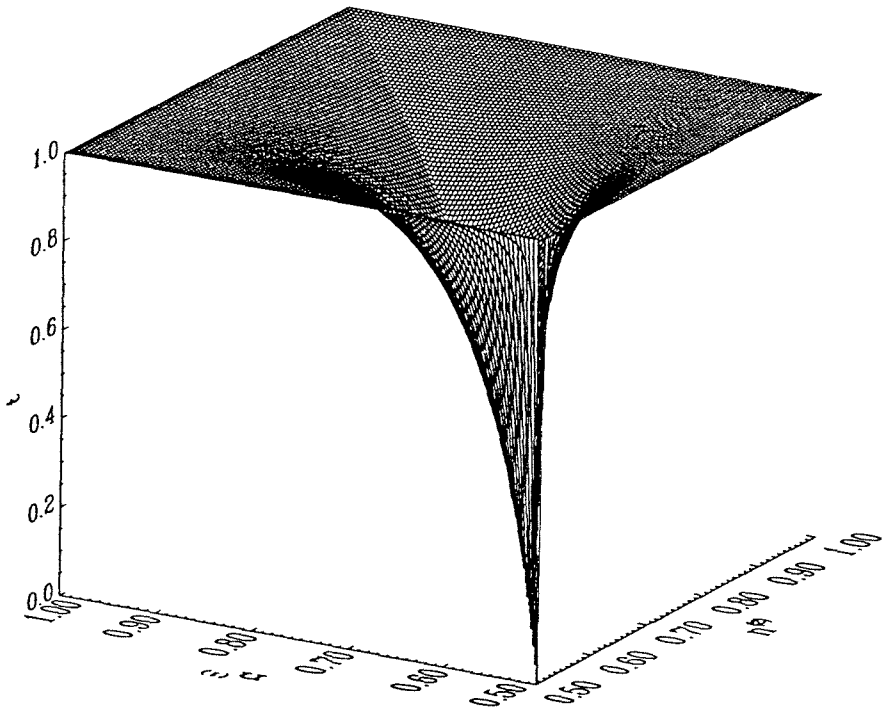

(a)

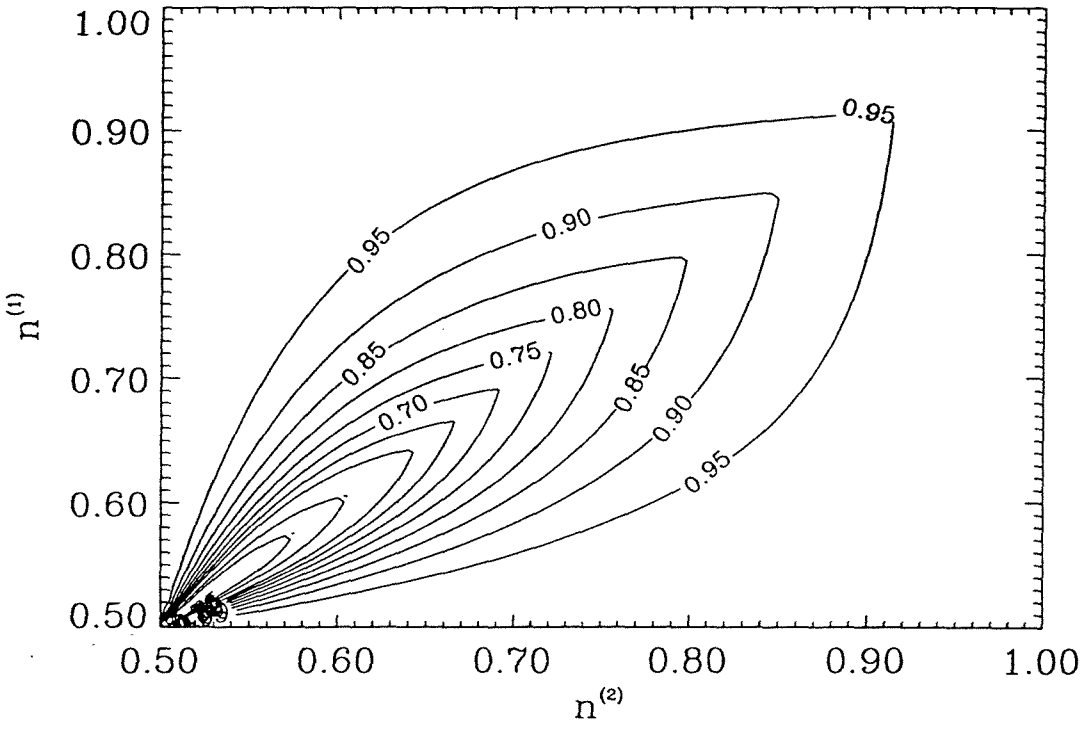

(b)

Figure B.1. Higher-order asymptotic exponent t vs. $(n^{(1)},n^{(2)})$ for $0.5 < n^{(2)} \le n^{(1)} \le 1$: a) three-dimensional view and b) contour plot. To enhance the visualization, the values of t have been repeated symmetrically with respect to the axis $n^{(1)} = n^{(2)}$.

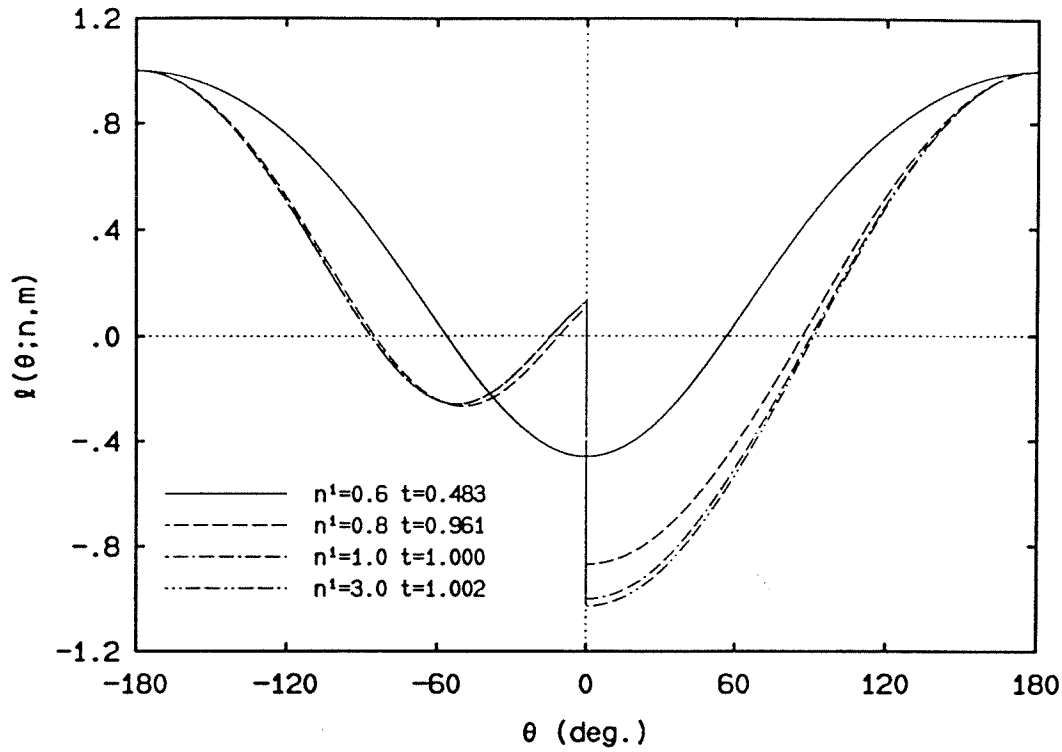

(a)

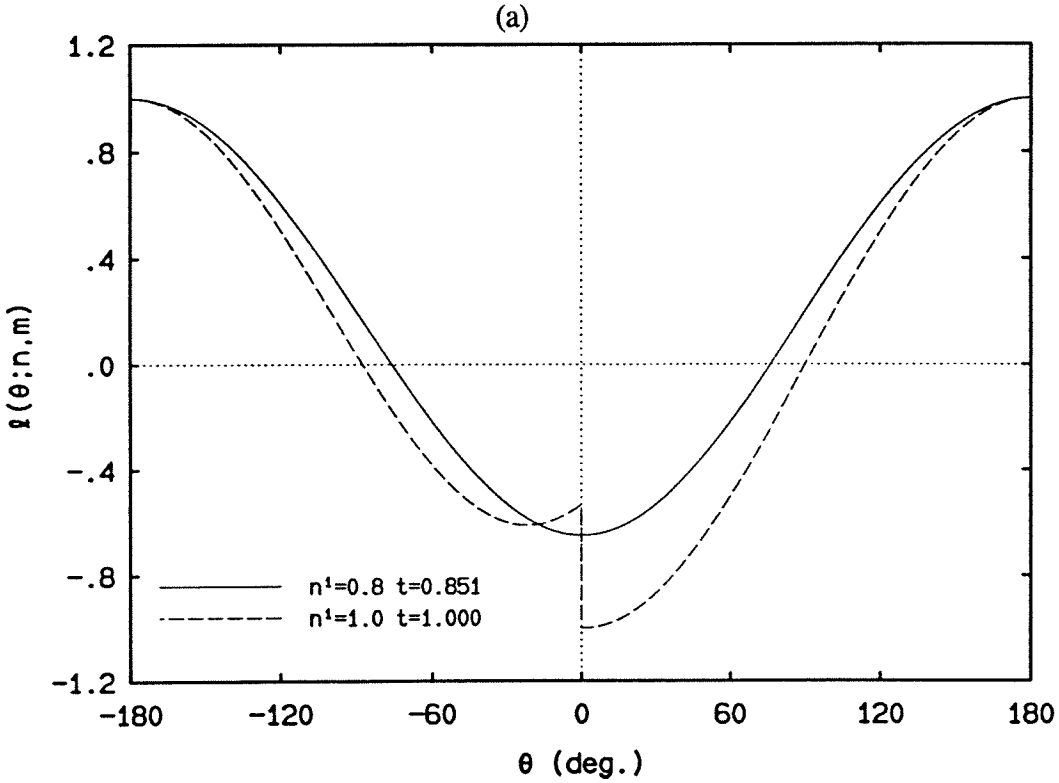

(b)

Figure B.2. Angular variation of the lower-order asymptotic term $l^{(k)}(\theta; n, m)$ with corresponding values of the exponent t : for (a) $n^{(2)} = 0.6$, (b) $n^{(1)} = 0.8$.

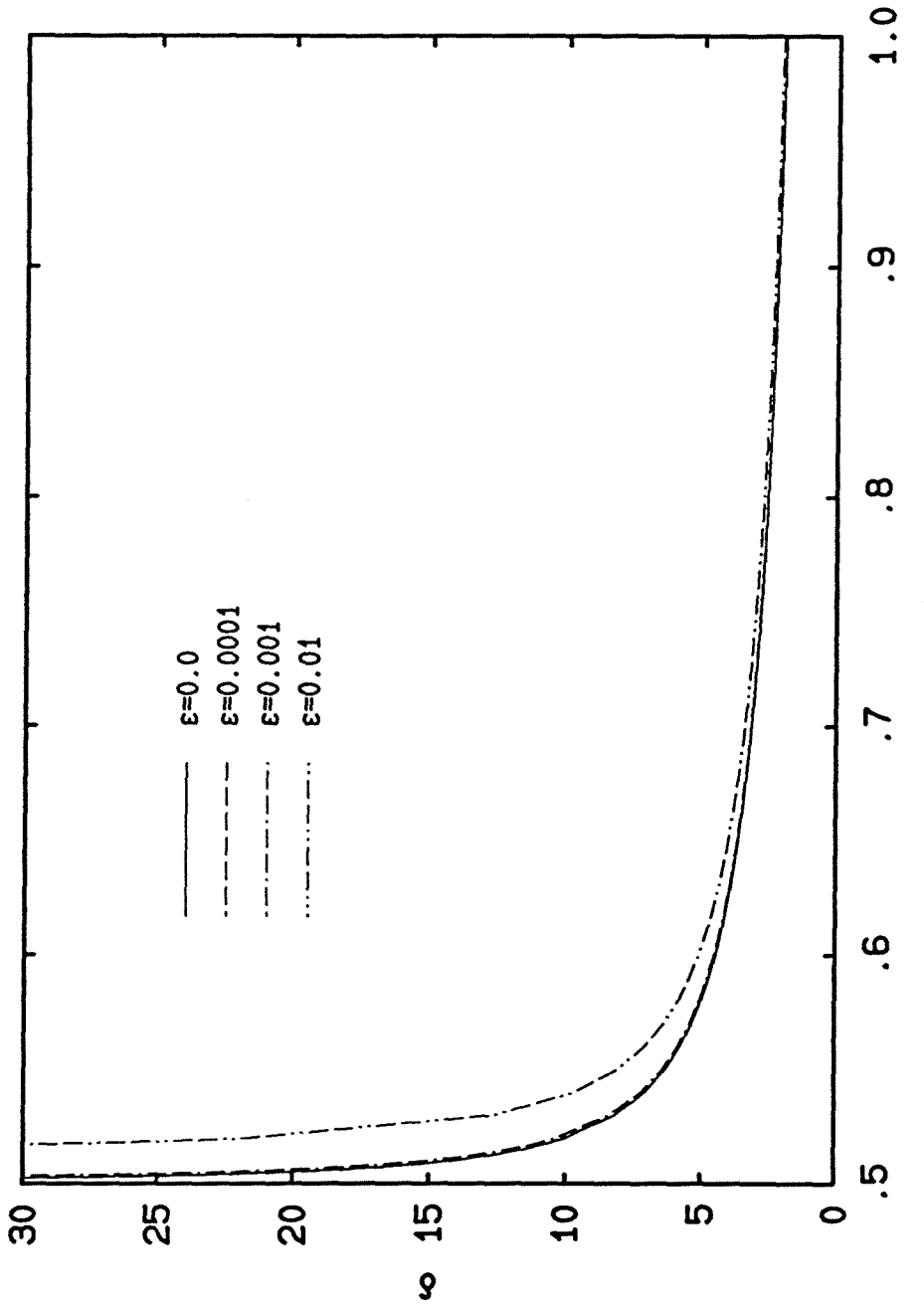

Figure C.1. Variation of the eigenvalue δ with respect to $n^{(1)}$ for various values of ε.

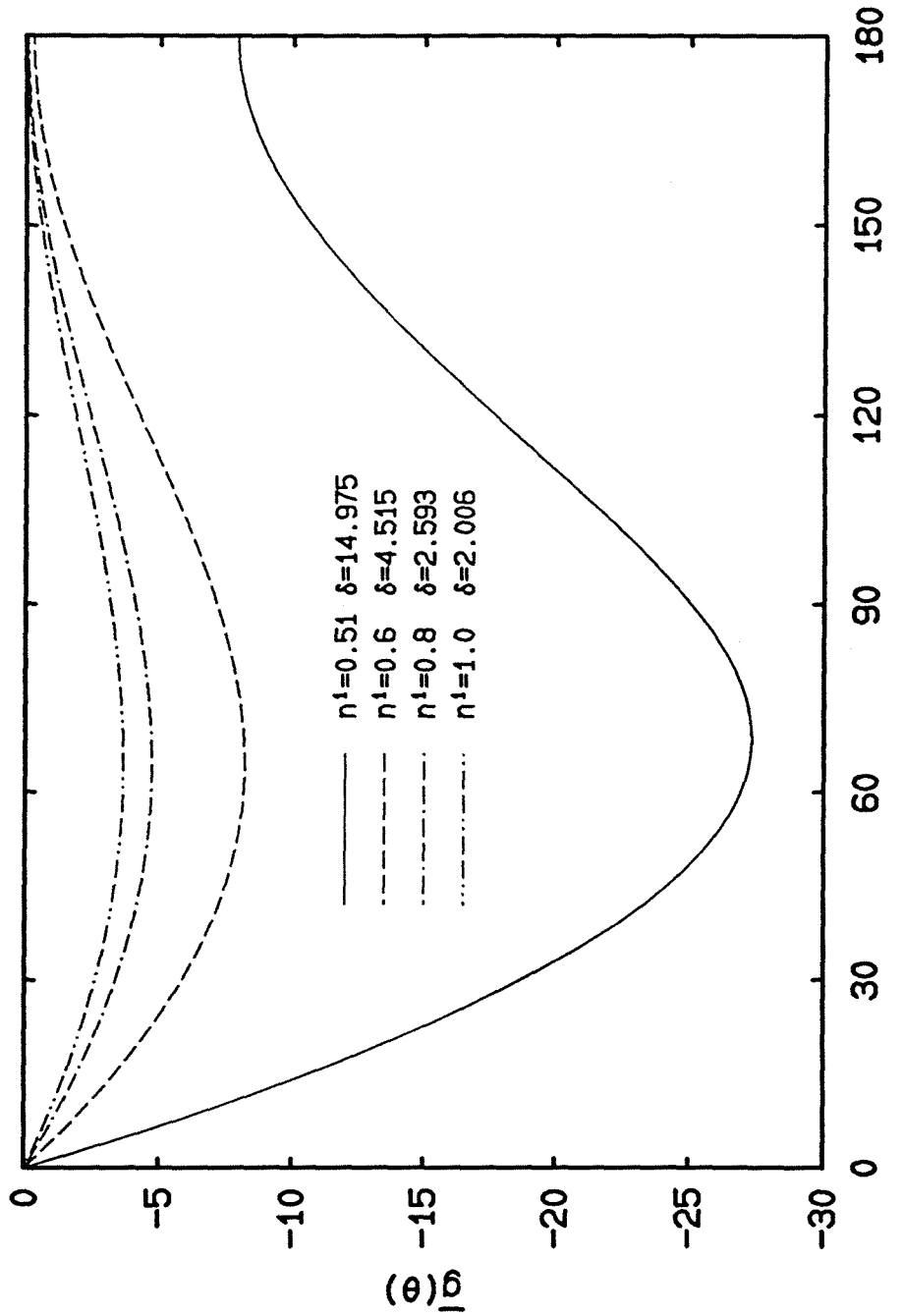

Figure C.2. Auxiliary angular function $\bar{g}(\theta)$ for various values of $n^{(1)}$ ($\varepsilon = 0.001$ and $\bar{g}_0 = 0$).